

Spray Water Control of a Boiler Superheater Outlet Temperature

Hans-Jürgen Gadinger



Report submitted in partial fulfilment of a Research Project for the degree Masters in Engineering in the Department of Electrical and Electronic Engineering at the University of Stellenbosch.

Study Leader: Professor W.H. Steyn

April 2019

Acknowledgements:

I would like to acknowledge and thank my family for their support during the work carried out in conducting this research. I would also like to acknowledge my supervisor for the support and guidance given, without which I would not have been able to complete this project. To all my colleagues at Komati Power Station that have supported this research effort, and have made it possible, I thank you for the support and assistance.

Declaration of Own Work:

I, the undersigned, hereby declare that, unless indicated otherwise through citation, the work contained in this report is my own original work completed for the sole purpose of completion of this research project. The work has been carried out within the prescribes of Stellenbosch University's policy on plagiarism.

Author:

Hans-Jürgen Gadinger

Date:

April 2019

Copyright © 2019 Stellenbosch University
All rights reserved

Abstract

This thesis investigates Fuzzy and MPC control techniques for use in superheated steam temperature control through spray water quenching. The techniques are evaluated against the PID controller currently in operation on a specific generating unit at Komati Power Station. These techniques are specifically developed to compensate for plant non-linearity associated with the large thermal inertia that varies with changes in the steam throughput of the superheater.

An MPC controller is constructed based on minimising a cost function of the system's modelled response. It is further developed and shown that, by using a variable sample time in the discrete controller, the model dependency on the steam flow rate can be reduced. The Takagi-Sugeno-Kang Fuzzy control architecture is also developed to compensate for operations at the extreme ends of the operating envelope. The steam flow rate and acceleration are used to construct the rule base for the controller while operating at a fixed sample time.

The two controllers are evaluated through the simulation of the controller and the plant model and comparing the results to that of the actual PID controller currently in operation. The simulation indicated a significant improvement in response with both Fuzzy and MPC based controllers over the PID controller, with the Fuzzy controller showing the best result. The MPC controller succeeded in preventing the two trip scenarios simulated. In general, The MPC controller reduced the standard temperature deviation from setpoint to 46 %, and reduces the peak positive transient responses to as little as 51 % of the PID controlled response. The Fuzzy controller performed even better by reducing the standard deviation to 43 % of the PID controller's deviation and reducing the peak positive transient response to as little as 50 %.

The controllers were also tested on an independent operations training simulator commissioned for the station. Although the emulated plant model is perturbed compared to the specific unit used for simulation and modelling, it provides a good validation of the controllers' robustness. The MPC controller performed on par with the PID controller on the operations simulator while the Fuzzy controller continued to provide a significant performance increase despite the perturbation. It is recommended that the Fuzzy controller be field tested to assist with higher efficiency in operating the generating unit, as well as reducing component wear and fatigue due to temperature excursions.

Table of Contents

| | |
|---|-------|
| Acknowledgements: | i |
| Declaration of Own Work: | ii |
| Abstract..... | iii |
| Table of Contents | iv |
| List of Figures..... | vii |
| List of Tables..... | x |
| List of Equations..... | xii |
| Abbreviations | xvi |
| Definitions | xvii |
| Symbols | xviii |
| Chapter 1 Introduction | 1 |
| 1.1. Project Description | 1 |
| 1.2. Problem Statement..... | 2 |
| 1.3. Plant Description..... | 3 |
| 1.4. Literature study | 6 |
| 1.4.1. Background..... | 6 |
| 1.4.2. Research on the Subject..... | 7 |
| 1.4.3. Project Support Documentation | 16 |
| Chapter 2 System Analysis | 18 |
| 2.1. Process Description..... | 18 |
| 2.1.1. Combustion and Flue Gas | 18 |
| 2.1.2. Water/Steam Closed Cycle..... | 21 |
| 2.1.3. Process Measurement and Control | 23 |
| 2.1.4. Final Superheater Outlet Steam Temperature Control | 28 |
| 2.2. Operating Envelope | 34 |
| 2.3. Disturbance Analysis | 35 |
| 2.3.1. Failed Mill Start..... | 36 |
| 2.3.2. Over-Firing of a Furnace | 39 |
| 2.3.3. Less Notable Disturbances | 41 |
| 2.4. Methodology | 41 |
| 2.4.1. Modelling | 41 |
| 2.4.2. Control | 42 |
| 2.4.3. Simulation..... | 42 |
| 2.4.4. Evaluation..... | 42 |
| Chapter 3 System Identification and Modelling | 44 |

| | | |
|-----------|--|-----|
| 3.1. | Description of Plant Disturbances and Dynamics | 44 |
| 3.2. | State Space Model | 45 |
| 3.2.1. | Thermodynamic Principles of a Superheater | 46 |
| 3.2.2. | Model Development | 48 |
| 3.3. | Model Parameter Determination..... | 54 |
| 3.4. | Firing Prefilter..... | 56 |
| 3.5. | Iterative Least Squares Regression | 58 |
| 3.5.1. | Sudden Steam Flow Rate Swing | 65 |
| 3.5.2. | Machine Deloading and Mill Outage | 70 |
| 3.5.3. | Steam Flow Rate Cycling while Deloading | 73 |
| 3.5.4. | Various Load Changes | 75 |
| 3.5.5. | Introduction of Mill and Load Increase..... | 77 |
| 3.5.6. | Scenario Sample Summary..... | 80 |
| 3.6. | Final Discrete State Space Model..... | 80 |
| Chapter 4 | Controller Design | 82 |
| 4.1. | State Space Model with a variable sample time | 82 |
| 4.2. | MPC Control Strategy | 84 |
| 4.2.1. | Augmented System model..... | 84 |
| 4.2.2. | Predicted Output Variables..... | 86 |
| 4.2.3. | Cost Function..... | 88 |
| 4.2.4. | MPC Control Parameter Calculation..... | 90 |
| 4.2.5. | Reduced Order Observer – MPC Controller | 91 |
| 4.2.6. | MPC Controller | 92 |
| 4.3. | Fuzzy Control Strategy | 94 |
| 4.3.1. | Membership Functions | 95 |
| 4.3.2. | Rules | 97 |
| 4.3.3. | TSK Fuzzy Control Law Calculation | 98 |
| 4.3.4. | Reduced Order Observer – Fuzzy Controller | 105 |
| 4.3.5. | TSK Fuzzy Controller | 106 |
| Chapter 5 | Simulation and Evaluation | 109 |
| 5.1. | Simulation Strategy and Evaluation Criteria | 109 |
| 5.2. | MPC Control Strategy | 110 |
| 5.2.1. | Case Study Analysis for MPC Controller..... | 110 |
| 5.2.2. | MPC Performance Evaluation | 114 |
| 5.2.3. | MPC Avoidance of Failed Mill Start Trip..... | 117 |
| 5.2.4. | MPC Avoidance of Over-Firing Trip..... | 119 |

| | | |
|--------------|---|-----|
| 5.3. | Fuzzy Control Strategy | 120 |
| 5.3.1. | Case Study Analysis for Fuzzy Controller | 120 |
| 5.3.2. | TSK Fuzzy Performance Evaluation | 124 |
| 5.3.3. | TSK Fuzzy Avoidance of Failed Mill Start Trip..... | 127 |
| 5.3.4. | TSK Fuzzy Avoidance of Over-Firing Trip | 128 |
| 5.4. | High Fidelity Operations Simulator Results | 129 |
| 5.4.1. | Mill C Trip Simulation | 129 |
| 5.4.2. | Rapid Pressure Raising Simulation | 135 |
| 5.5. | Holistic Evaluation of Various Results..... | 138 |
| 5.5.1. | Direct MPC and Fuzzy Performance Comparison | 138 |
| 5.5.2. | Practical Implications and Considerations | 142 |
| Chapter 6 | Conclusions and Recommendations..... | 144 |
| 6.1. | Summary | 144 |
| 6.2. | Recommendations..... | 147 |
| 6.3. | Conclusion | 150 |
| Appendix A | Performance Evaluation Extended Tables | 157 |
| Appendix A.1 | Standard Temperature Error Deviation | 157 |
| Appendix A.2 | Mean Temperature Error | 158 |
| Appendix A.3 | Maximum Temperature Error | 160 |
| Appendix A.4 | Temperature Error Total Span..... | 161 |
| Appendix A.5 | Peak Response Time Reduction | 162 |
| Appendix B | Simulation Code | 164 |
| Appendix B.1 | Initial Iterative Model Fitting | 164 |
| Appendix B.2 | Simultaneous Iteration of Scenarios | 170 |
| Appendix B.3 | Iterative Tuning of Fuzzy Control Steam Flow Acceleration Feedback Gains 173 | |
| Appendix B.4 | MPC Controller Simulation..... | 178 |
| Appendix B.5 | Fuzzy Controller Performance | 182 |

List of Figures

| | |
|---|----|
| Figure 1: General Pressure Part Arrangement..... | 4 |
| Figure 2: General Pressure Part Arrangement..... | 19 |
| Figure 3: Single Line Process Flow..... | 24 |
| Figure 4: Current PID Control Strategy (Variable parameter indicated by arrows) | 30 |
| Figure 5: Variable Gain and Filter Time Constant..... | 31 |
| Figure 6: Failed Mill-Start and Trip at Low Steam Flow Rate | 36 |
| Figure 7: Process and Control Response to Failed Mill Start | 37 |
| Figure 8: Over-Firing with No Corresponding Steam Flow Rate Increase..... | 39 |
| Figure 9: Process and Control Response to Over Firing | 40 |
| Figure 10: Prefiltered Firing Input Calculation (15 second sample time)..... | 56 |
| Figure 11: Model Response $N=1, J=2.37$ °C | 61 |
| Figure 12: Model Response $N=2, J=1.88$ °C | 61 |
| Figure 13: Model Response $N=3, J=1.81$ °C | 61 |
| Figure 14: First Model Estimation Process Measurements | 62 |
| Figure 15: Steady State Modelling Error..... | 64 |
| Figure 16: Sudden Steam Flow Rate Swing – Flow Rate and Superheater Inlet Temperature..... | 67 |
| Figure 17: Sudden Steam Flow Rate Swing – Mill, Fuel Oil Firing and Steam Pressure..... | 67 |
| Figure 18: Sudden Steam Flow Rate Swing – Modelled Output | 68 |
| Figure 19: Sudden Steam Flow Rate Swing – Model Inputs | 69 |
| Figure 20: Sudden Steam Flow Rate Swing – Non-Normalised Firing Parameters | 70 |
| Figure 21: Machine Deloading and Mill Outage – Modelled Output | 71 |
| Figure 22: Machine Deloading and Mill Outage – Flow Rate and Superheater Inlet Temperature | 72 |
| Figure 23: Machine Deloading and Mill Outage – Mill, Fuel Oil Firing and Steam Pressure | 73 |
| Figure 24: Machine Deloading and Mill Outage – Model Inputs | 73 |
| Figure 25: Steam Flow Cycling while Deloading – Modelled Output..... | 74 |
| Figure 26: Steam Flow Cycling while Deloading – Flow Rate and Superheater Inlet Temperature | 75 |
| Figure 27: Steam Flow Cycling while Deloading – Mill, Fuel Oil Firing and Steam Pressure..... | 75 |

| | |
|--|-----|
| Figure 28: Steam Flow Cycling while Deloading – Model Inputs..... | 75 |
| Figure 29: Various Load Changes – Modelled Output | 76 |
| Figure 30: Various Load Changes – Flow Rate and Superheater Inlet Temperature..... | 76 |
| Figure 31: Various Load Changes – Mill, Fuel Oil Firing and Steam Pressure..... | 77 |
| Figure 32: Various Load Changes – Model Inputs | 77 |
| Figure 33: Introduction of Mill and Load Increase – Modelled Output..... | 78 |
| Figure 34: Introduction of Mill and Load Increase – Flow Rate and Superheater Inlet Temperature..... | 79 |
| Figure 35: Introduction of Mill and Load Increase – Mill, Fuel Oil Firing and Steam Pressure .. | 79 |
| Figure 36: Introduction of Mill and Load Increase – Model Inputs..... | 79 |
| Figure 37: MPC Controller..... | 93 |
| Figure 38: TSK Fuzzy Steam Flow Rate Membership Functions..... | 95 |
| Figure 39: TSK Fuzzy Steam Flow Rate Derivative Membership Functions | 96 |
| Figure 40: Estimated Flow Rate Per Rule | 101 |
| Figure 41: Fuzzy Controller Gain Mesh Representation..... | 105 |
| Figure 42: Fuzzy Logic Controller | 106 |
| Figure 43: Sudden Steam Flow Rate Swing – MPC Control Response..... | 110 |
| Figure 44: Machine Deloading and Mill Outage – MPC Control Response..... | 111 |
| Figure 45: Steam Flow Rate Cycling while Deloading – MPC Control Response..... | 112 |
| Figure 46: Various Load Changes – MPC Control Response | 113 |
| Figure 47: Introduction of Mill and Load Increase – MPC Control Response | 114 |
| Figure 48: Failed Mill Start Trip – MPC Control Response | 118 |
| Figure 49: Over-Firing Trip – MPC Control Response..... | 119 |
| Figure 50: Sudden Steam Flow Rate Swing – Fuzzy Control Response | 120 |
| Figure 51: Machine Deloading and Mill Outage – Fuzzy Control Response | 121 |
| Figure 52: Steam Flow Rate Cycling while Deloading – Fuzzy Control Response..... | 122 |
| Figure 53: Various Load Changes – Fuzzy Control Response..... | 123 |
| Figure 54: Introduction of Mill and Load Increase – Fuzzy Control Response..... | 124 |
| Figure 55: Failed Mill Start Trip – Fuzzy Control Response..... | 127 |
| Figure 56: Over-Firing Trip – Fuzzy Control Response | 128 |
| Figure 57: Simulator Mill C Trip – Firing Parameters..... | 130 |

| | |
|---|-----|
| Figure 58: Simulator Mill C Trip – Steam Parameters..... | 130 |
| Figure 59: Simulator Mill C Trip – MPC Control Response | 131 |
| Figure 60: Simulator Mill C Trip – Model versus Simulator Response..... | 133 |
| Figure 61: Simulator Mill C Trip – Fuzzy Control Response | 134 |
| Figure 62: Simulator Rapid Pressure Raising – Firing Parameters | 135 |
| Figure 63: Simulator Rapid Pressure Raising – Steam Parameters..... | 135 |
| Figure 64: Simulator Rapid Pressure Raising – MPC Control Response | 136 |
| Figure 65: Simulator Rapid Pressure Raising –Fuzzy Control Response | 137 |

List of Tables

| | |
|---|-----|
| Table 1: Nomenclature for PID Controller..... | 30 |
| Table 2: Nomenclature for Thermodynamic Heat Transfer Equations | 46 |
| Table 3: Nomenclature for System State Differential Equation..... | 49 |
| Table 4: Nomenclature continuous state space model..... | 53 |
| Table 5: Nomenclature for Continuous Time State Space Model..... | 55 |
| Table 6: Nomenclature for Firing Prefilter..... | 57 |
| Table 7: Model Performance Summary | 80 |
| Table 8: Nomenclature for Non-Augmented Discrete Time Model..... | 81 |
| Table 9: Nomenclature for Digital Domain Model with Variable Sample Time..... | 84 |
| Table 10: Nomenclature for Augmented Discrete Time Model..... | 86 |
| Table 11 : Nomenclature for Predicted Output Variable Equations..... | 87 |
| Table 12: Nomenclature for MPC cost function | 88 |
| Table 13: Precalculated MPC Controller Parameters..... | 91 |
| Table 14: Nomenclature for Final MPC Controller | 93 |
| Table 15: TSK If-Then Rules Grid..... | 97 |
| Table 16: TSK Peak Rule Membership..... | 101 |
| Table 17: Nomenclature for Predicted Output Variable Equations for Fuzzy Controller..... | 102 |
| Table 18: Parameters for Initial Fuzzy Controller Gain Calculation..... | 102 |
| Table 19: TSK Fuzzy Controller Parameters, Rule 1 – 3..... | 104 |
| Table 20: TSK Fuzzy Controller Parameters, Rule 4 – 6..... | 104 |
| Table 21: Reduced Order Observer – Fuzzy Controller Parameters | 106 |
| Table 22: Nomenclature for Final Fuzzy Controller | 107 |
| Table 23: MPC Standard Temperature Error Deviation and Mean Temperature Error Performance Evaluation..... | 115 |
| Table 24: MPC Minimum and Maximum Temperature Bounds Performance Evaluation..... | 116 |
| Table 25: MPC Response Time Performance Evaluation | 117 |

| | |
|--|-----|
| Table 26: Fuzzy Standard Temperature Error Deviation and Mean Temperature Error Performance Evaluation | 125 |
| Table 27: Fuzzy Minimum and Maximum Temperature Bounds Performance Evaluation | 126 |
| Table 28: Fuzzy Response Time Performance Evaluation..... | 127 |
| Table 29: Scenario Description index | 138 |
| Table 30: Standard Temperature Error Deviation | 139 |
| Table 31: Mean Temperature Error | 139 |
| Table 32: Maximum Temperature Error | 140 |
| Table 33: Temperature Error Total Span..... | 141 |
| Table 34: Peak Response Time Reduction | 142 |

List of Equations

| | | |
|------|---|----|
| (1) | PT1 First Order Filter Transfer Function | 32 |
| (2) | First Order Low Pass Filter | 32 |
| (3) | s to z-Domain PT1 Filter Transform | 33 |
| (4) | Finite Difference Derivative With Transfer Function With Gain | 33 |
| (5) | Tube Wall Energy Conservation Equation | 47 |
| (6) | Tube Wall Energy Conservation Equation Reordered | 47 |
| (7) | Tube Wall Energy Conservation Equation Derivative | 47 |
| (8) | Tube Wall Energy Conservation Equation Derivative Assuming Stiff Coupling | 47 |
| (9) | Steam Thermodynamic Relationship Equations (Steam Tables) | 47 |
| (10) | Tube Wall final Energy Conservation Equation | 47 |
| (11) | Steam Energy Conservation Equation | 47 |
| (12) | Conservation of Mass Equation Assuming Constant Volume | 48 |
| (13) | Steam Energy Conservation Equation Expanded | 48 |
| (14) | Combined Steam Energy and Mass Conservation Equation | 48 |
| (15) | Combined Steam Energy and Mass Conservation Equation Reordered | 48 |
| (16) | Final Steam Enthalpy State Equation | 48 |
| (17) | Implicit Quasi-Steady-State Model | 49 |
| (18) | Simplified State Equation | 51 |
| (19) | State Equations Constants | 51 |
| (20) | State Space Model \mathbf{A}_m Matrix | 52 |
| (21) | State Space Model \mathbf{B}_m Matrix | 53 |
| (22) | State Space Model \mathbf{c}_m Matrix | 53 |
| (23) | Continuous Model State and Input Matrix Definitions | 53 |
| (24) | Continuous Model State Equation | 53 |
| (25) | Continuous Model Output Equation | 53 |
| (26) | Model Parameter Identification \mathbf{A}_m Matrix | 55 |

| | |
|---|----|
| (27) Model Parameter Identification \mathbf{B}_m Matrix..... | 55 |
| (28) Model Parameter Identification \mathbf{c}_m Matrix..... | 55 |
| (29) Model Parameter Identification \mathbf{d}_m Matrix | 55 |
| (30) Cost Function for Model Training Evaluation Based on Standard Deviation of Error | 59 |
| (31) Recursive Kalman Filter Equation..... | 63 |
| (32) Kalman Filter Gain Equation | 63 |
| (33) Kalman Filter Error Covariance Matrixes..... | 63 |
| (34) Observer Gain Vector for Removal of Steady State Offset During Training..... | 63 |
| (35) Model State Equation With Observer | 63 |
| (36) Normalisation of Firing Input Against Steam Flow Rate | 81 |
| (37) Normalisation of Firing Derivative Input Against Steam Flow Rate | 81 |
| (38) Normalisation of Steam Pressure Derivative Input Against Steam Flow Rate..... | 81 |
| (39) Final Discrete-Time Model State Equation..... | 81 |
| (40) Final Discrete-Time Model Output Equation | 81 |
| (41) State Space \mathbf{A}_m Matrix Conversion from Continuous to Digital Domain matrix \mathbf{F}_m | 82 |
| (42) State Space \mathbf{B}_m Matrix Conversion from Continuous to Digital Domain matrix \mathbf{G}_m | 82 |
| (43) Substitution of Sample Time and \mathbf{A}_m Matrix Based on Steam Flow Rate..... | 83 |
| (44) Steam Flow Rate Invariant \mathbf{F}_m matrix after substitution..... | 83 |
| (45) Substitution of Sample Time and \mathbf{B}_m Matrix Based on Steam Flow Rate | 83 |
| (46) Integration Substitution for \mathbf{B}_m Matrix Conversion | 83 |
| (47) Steam Flow Rate Invariant \mathbf{G}_m matrix after substitution | 83 |
| (48) Augmented Model Delta State Manipulation | 85 |
| (49) Augmented Model State Equation | 85 |
| (50) Augmented Model Output Equation | 85 |
| (51) Augmented Model Parameterised \mathbf{F} Matrix..... | 85 |
| (52) Augmented Model Parameterised \mathbf{G} Matrix | 85 |
| (53) Augmented Model Parameterised \mathbf{c} Matrix | 86 |
| (54) Augmented Model Parameterised \mathbf{d} Matrix..... | 86 |

| | |
|---|-----|
| (55) Future Dynamic Predicted Response Matrix | 87 |
| (56) Initial Condition Predicted Free Response Matrixes | 87 |
| (57) Input Predicted Impulse Response Matrixes..... | 87 |
| (58) MPC Cost Function..... | 88 |
| (59) MPC General Control Sequence | 88 |
| (60) MPC Common Gain term | 89 |
| (61) MPC General Control Law First Response Element | 89 |
| (62) Setpoint Reference Vector | 89 |
| (63) MPC Setpoint Reference Gain Equation..... | 89 |
| (64) MPC State Feedback Gains Equation | 89 |
| (65) MPC Input Feedforward Gains Equation..... | 90 |
| (66) Firing Input Control Horizon Vector | 90 |
| (67) Firing Gradient Input Control Horizon Vector | 90 |
| (68) Pressure Gradient Input Control Horizon Vector..... | 90 |
| (69) MPC Control Law Immediate Responce | 90 |
| (70) Reduced Order State Observer..... | 92 |
| (71) Reduced Order State Observer Error | 92 |
| (72) MPC Control Law | 93 |
| (73) MPC Observer Intermediate $\Delta'h_1$ State Calculation..... | 93 |
| (74) MPC Observer $\Delta\hat{h}_1$ State Calculation..... | 93 |
| (75) Disturbance Input And Plant State Definitions..... | 93 |
| (76) Flow Rate Progression Transfer Function..... | 100 |
| (77) Modified Initial Condition Predicted Free Response Matrixes..... | 102 |
| (78) Modified Input Predicted Impulse Response Matrixes..... | 102 |
| (79) Cost Function for Steam Flow Accelartion Feedback Gain Calculation | 103 |
| (80) Fuzzy Control Law Immediate Responce | 104 |
| (81) Fuzzy Controller Rules | 108 |
| (82) Fuzzy Observer Rules | 108 |

(83) Controller Comparison Function for Percentage Minimum and Maximum Peak Error.... 116

Abbreviations

CV – Controlled Variable

DCS – Distributed Control System (Refers to the Siemens SPPA T3000 Automation System)

DV – Disturbance Variables

FPPI – Fuzzy Predictive PI

HP – High Pressure (Often referring to the first turbine stage)

HMI – Human Machine Interface

LMI – Linear Matrix Inequality

LP – Low Pressure (Often referring to the last turbine stage)

MPC – Model Predictive Controller

MRAC – Model Reference Adaptive Control

MV – Manipulated Variable

PDC – Parallel Distributed Compensation

PF – Pulverised Fuel

P&ID – Piping and Instrumentation Drawing

PID – Proportional Integral and Differential control (Variation *PI* Excludes Differential Control)

PLC – Programmable Logic Controller

PT1 – T3000 System Block Representing a First Order Filter Transfer Function

SH – Superheater

SISO – Single Input Single Output

SP – Setpoint

SV – State Variable

TSK – Takagi-Sugeno-Kang (Some authors reference only TS or Sugeno-type)

ZOH – Zero Order Hold

Definitions

The Department – Refers to the Electric and Electronic department of the university

The Station – Refers to Eskom’s Komati Power Station Situated in Mpumalanga

The University – Refers to the University of Stellenbosch

Grid Separation – Refers to the industrial term Unplanned Automatic Grid Separation. This is defined as an unplanned automatic trip function that initiates a sequence of events to separate the generator from the national grid. It has the sole purpose of avoiding damage to the machine and to ensure the safety of personnel and plant. This results in a disruption of electrical supply of the particular unit to the grid.

Attemperation – To regulate. Specific to the context regulation through mixing and blending. Attemperation of steam, in this context, involves the introduction of atomised water with steam vapor which, after sufficient mixing, produces a final vapor at a lower temperature.

Symbols

| Symbol | SI Unit | Description |
|--|------------------------|---|
| a_{Burners} | | Mill A fuel oil support burners in service |
| a_{Level} | [%] | Mill A Fuel level measurement |
| a_{Load} | [kg/s] | Mill A coal loading rate |
| $\mathbf{A}_m, \mathbf{B}_m, \mathbf{c}_m, \mathbf{d}_m$ | | Continuous time state space matrixes |
| b_{Burners} | | Mill B fuel oil support burners in service |
| b_{Level} | [%] | Mill B fuel level measurement |
| b_{Load} | [kg/s] | Mill B coal loading rate |
| c_{Burners} | | Mill C fuel oil support burners in service |
| c_{Level} | [%] | Mill C fuel level measurement |
| c_{Load} | [kg/s] | Mill C coal loading rate |
| c_m | [J/(kg · K)] | Specific heat capacity of tube metal |
| \mathbf{E} | | Predictive free impulse response from initial state |
| err_{avg} | [°C/min] | Average rate of model departure from measurement |
| err_{max} | [°C/min] | Highest rate of model departure from measurement |
| $fire_{\text{in}}$ | [J/s ²] | Normalised firing rate derivative input |
| $\mathbf{F}, \mathbf{G}, \mathbf{c}, \mathbf{d}$ | | Augmented digital domain state space matrixes |
| $fire_{\text{in}}$ | [J/s] | Normalised firing rate input |
| $\mathbf{F}_m, \mathbf{G}_m, \mathbf{c}_m, \mathbf{d}_m$ | | Digital domain state space matrixes |
| f_{oil} | | Fuel oil burners firing gain |
| $\mathbf{F}_p, \mathbf{G}_p$ | | Resampled augmented digital domain state space matrixes at future index p |
| $\mathbf{g}_{p*,g}$ | | Column reference to the \mathbf{G}_p matrix |
| $\mathbf{g}^{*,g}$ | | Column reference to the \mathbf{G} matrix |
| \mathbf{h} | [J/kg] | Generic continuous time model enthalpy states |
| \mathbf{h}_m | [J/kg] | Continuous time model enthalpy states |
| h_i | [J/kg] | Continuous time model subsection states |
| h_{in} | [J/kg] | Specific enthalpy of final superheater steam inlet |
| $h_{\text{out}}(t)$ | [J/kg] | Specific enthalpy of final superheater steam outlet |
| $H_{\text{diff}}(z)$ | | Finite difference derivative transfer function |
| $h_{c_{\text{out}}}$ | [J/kg] | Continuous time model specific steam enthalpy |
| $h_{m_{\text{out}}}$ | [J/kg] | Discrete time model specific steam enthalpy |
| $H_{\text{pt1}}(z)$ | | PT1 filter transfer function |
| J_{avg} | [°C] | Average absolute model error per sample |
| J_{max} | [°C] | Maximum absolute model error |
| J_{mpc} | [(J/kg) ²] | MPC cost function |
| J_{TSK} | [°C] | TSK Fuzzy controller cost function |
| \mathbf{k}_{ff} | | Input feedforward gains |
| \mathbf{k}_{ff_x} | | Input feedforward gains for rule x of Fuzzy controller |
| $k_{\dot{m}_{\text{in}}}$ | | Linearization factor based on \dot{m}_{in} |
| k_{dm_x} | | Steam flow rate change gain for rule x of Fuzzy controller |
| k_{fire} | | Final firing gain |

| Symbol | SI Unit | Description |
|------------------------------------|--------------------------|--|
| \mathbf{k}_{phi} | | Common MPC gain term |
| k_{pid} | | Final PID controller gain |
| k_{ref_x} | | Reference feedback gain for rule x of Fuzzy controller |
| k_i | | Sample index at time of prediction |
| k_{ref} | | Reference feedback gain |
| $\mathbf{k}_{\text{state}}$ | | State feedback gains |
| $\mathbf{k}_{\text{state}_x}$ | | State feedback gains for rule x of Fuzzy observer |
| l_{sat_0} | [%] | Saturation limiter lower limit for a zero output |
| l_{sat_1} | [%] | Saturation limiter upper limit for a unity output |
| m | | Reduced order filter gain |
| \dot{m}_{in} | [kg/s] | Mass flow rate of steam from inlet to outlet |
| m_{m} | [kg] | Mass of tube section |
| \dot{m}_{out} | [kg/s] | Mass flow rate of steam at outlet |
| m_{pfA} | | Row A pulverised fuel burner relative firing gain |
| m_{pfB} | | Row B pulverised fuel burner relative firing gain |
| m_{pfC} | | Row C pulverised fuel burner relative firing gain |
| N | | Specific number of superheater subsections |
| N_c | | Control horizon |
| N_i | | Ignored initial samples |
| N_p | | Prediction horizon |
| p | [Pa] | Pressure of final superheater steam |
| \dot{p}_{in} | [Pa/s] | Normalised pressure rate of change input |
| q_{rad} | [J/s] | Heat flux through radiation from furnace firing |
| q_s | [J/s] | Heat flux from tube metal inner surface to steam |
| r_{limit} | [J · s ⁻²] | Rate limiter allowed value change per second |
| \mathbf{r}_s | [J/kg] | Setpoint reference vector over control horizon |
| $r_s(k)$ | [°C] <i>or</i> [J/kg] | Final steam temperature setpoint |
| r_u | | Control effort cost tuning constant |
| $T_{\text{in}}(k)$ | [°C] | Final superheater inlet temperature |
| T_{m} | [°C] | Temperature of tube wall |
| $T_{\text{out}}(k)$ | [°C] | Final steam temperature |
| T_s | [°C] | Temperature of steam |
| $t_{\text{s-mpc}}$ | [s] | Variable digital domain system sample time |
| $u(k)$ | [°C] <i>or</i> [J/kg] | Final superheater inlet temperature setpoint |
| \mathbf{u}_{m} | | Continuous state space model inputs |
| V | [m ³] | Volume of inner tube section and steam |
| $\mathbf{x}(k_i)$ | [J/kg] | System states at time of prediction k_i |
| y_{m} | [J/kg] | System output state |
| \mathbf{y}_{p} | [J/kg] | Predicted output states |
| $\Delta \mathbf{fire}_{\text{in}}$ | [J/s] | Vector of DV deltas across the control horizon |
| $\Delta fire_{\text{in}}$ | [J/s] | Normalised delta firing rate input |
| $\Delta \mathbf{fire}_{\text{in}}$ | [J/s ²] | Vector of DV deltas across the control horizon |

| Symbol | SI Unit | Description |
|--------------------------------|----------------------|--|
| $\Delta \dot{f}_{ire_{in}}$ | [J/s ²] | Normalised delta firing rate derivative input |
| Δh_1 | [J/kg] | First superheater section intermediate observer state |
| $\Delta h_{1_rule_x}$ | [J/kg] | Intermediate observer state for rule x of Fuzzy observer |
| Δh_1 | [J/kg] | First superheater section enthalpy state |
| $\Delta \hat{h}_1$ | [J/kg] | First superheater section observed enthalpy state |
| Δh_2 | [J/kg] | Second superheater section enthalpy state |
| $\Delta \mathbf{h}_{in}$ | [J/kg] | Vector of CV deltas across the control horizon |
| Δh_{in} | [J/kg] | Specific delta enthalpy of final superheater steam inlet |
| $\Delta h_{in_rule_x}$ | [J/kg] | Control law output for rule x of Fuzzy observer |
| $\Delta \dot{\mathbf{p}}_{in}$ | [Pa/s] | Vector of DV deltas across the control horizon |
| $\Delta \dot{p}_{in}$ | [Pa/s] | Normalised pressure rate of change input |
| ρ | [kg/m ³] | Density of steam |
| τ_{fire} | [s] | Time constant for firing rate PT1 low pass filter |
| τ_{pt1} | [s] | Variable response time constant |
| Φ_g | | Predictive impulse responses for input changes |

Chapter 1

Introduction

This project will focus on examining the performance of spray water control of a boiler superheater main steam outlet temperature. This report will start by giving a description and background of the problem. An objective will be formulated to form the basis for evaluating solution performance. Literature on previous work done in this field will be examined and documented along with supporting design information.

A thorough system analysis will form the basis for system identification and the modelling methodology. Controller design will be conducted based on the objectives for this study. A comparison between the current and designed control solutions will be made through system response simulations. The report will conclude with future recommendations as well as the author's summary of contributions made through the project.

1.1. Project Description

Eskom is the largest producer of electricity in South Africa, with the majority of its generation capacity being coal fired. The energy mix in South Africa is slowly diversifying, but coal fired power stations still form the bulk of electricity production in the country [1] [2]. Coal based production is still expanding to keep up with the country's energy demand. With the turn of the century, and an electricity shortage in the country, power stations preserved in the 1980s were returned to service. This has led to a variety of generation technologies being operational across the industry. There is a need to optimise the plant performance as it is comparatively less efficient due to age and technological advancements. Komati Power Station use to operate before the widespread use of fully integrated digital control systems.

This study will apply to Komati Power Station, built in the 1960s, mothballed in the late 1980s, with its return to service starting in 2008. Komati has 9 units recommissioned with 5x100 MW and 4x125 MW generating units. Komati was recommissioned with sophisticated digital control systems. These units are a unique combination of old and new technologies in a single plant.

1.2. Problem Statement

Spray water based temperature control of boiler outlet steam is essential in keeping within the turbine steam inlet design specification. Keeping the unit in continuous generation requires operation within an operational envelope, designed to protect the turbine from damage. Exceeding the safe operational envelope at any time will result in the protection system initiating a unit trip to prevent exceeding physical limits that would result in damage to the plant.

The control system should be capable of operating under a wide range of conditions. This includes, manual operator interventions, interconnected process influences, as well as disturbances. Few input process parameters are exclusively used for control or monitoring of the final steam temperature. It is essential that the controller works in harmony with other control systems that maintain different process parameters through shared measurements and actuating devices. The advanced integrated digital control environment used on all units, the Siemens SPPA-T3000, and associated steam temperature controller, does not currently utilise more than the most direct of process measurements to perform control. The control system, although distributed, is integrated across different processes. It is capable of accessing and utilising measurements from many other processes and incorporate them into the final steam temperature control system.

Less than optimal performance can, and has, caused unit trips in the past. Such a trip sequence involves an electrical grid separation, immediate shutoff of all fuel and air supplies to the furnace, and the closing of steam inlet valves to the turbine. This does not only result in loss of generating capacity, and therefore revenue, but also expenses incurred to return the unit to service. The cost of firing the boiler on fuel oil, while starting up, and supporting firing until stable coal combustion is achieved, quickly escalates to a loss well in the hundreds of thousands of Rands. Based on historical data and cost estimates from [3] and [4], more than 30 tons of additional oil (@ R6 000/ton) is used in the process until stable Pulverised Fuel (PF) combustion is achieved. In excess of 120 tons of coal (@ R450/ton) is burnt, with a typical 8-9-hour light-up period. During this time, 500 MW·h less revenue is made for the same amount of raw coal used. The fully integrated control system allows for the use of many, already measured, process inputs for

control purposes. The intent is to investigate and test at least two sophisticated control techniques to improve performance and prevent avoidable grid separations.

Advanced control techniques exist that are capable of utilising many process parameters to compensate for the intricacies of superheater dynamics, and are able to prevent and save the cost of avoidable grid separations. This will increase the electricity availability to the grid.

1.3. Plant Description

Before delving into a literature review of the relevant subject matter, a brief description of the plant is shared here. A more thorough analysis will follow, in *2.1 Process Description*, of the next chapter.

This study focusses specifically on unit 5 of Komati Power Station for the purposes of this research. Generally, each station strives to achieve a level of standardisation that renders all units near identical in construction. Komati Power Station, due to its age and history, does not have this luxury. As a starting point, unit 5 is chosen to be focused on as it presented sufficient historical final steam temperature control related events. Sufficient similarity exists that the research may be easily applied to the other units with some minor alterations. Direct compatibility of design, system identification, and data gathered is not assumed in this study. The descriptions that follow will describe the process with reference to *Figure 1*.

Unit 5 is a drum type sub-critical boiler with a nominal load of 100 MW. Coal is pulverised by three tube type mills with a throughput of 2.5 kg/s to 6 kg/s of coal each. Each mill delivers pulverised coal at a different height in the furnace area, through 4 burners per mill. Fuel oil is also supplied at these burners to support combustion when required. *Figure 1* shows a side view of the boiler. The 4 burners are not indicated separately, but are equally spaced on the height indicated for each mill along the rear wall of the furnace.

Chapter 1 Introduction

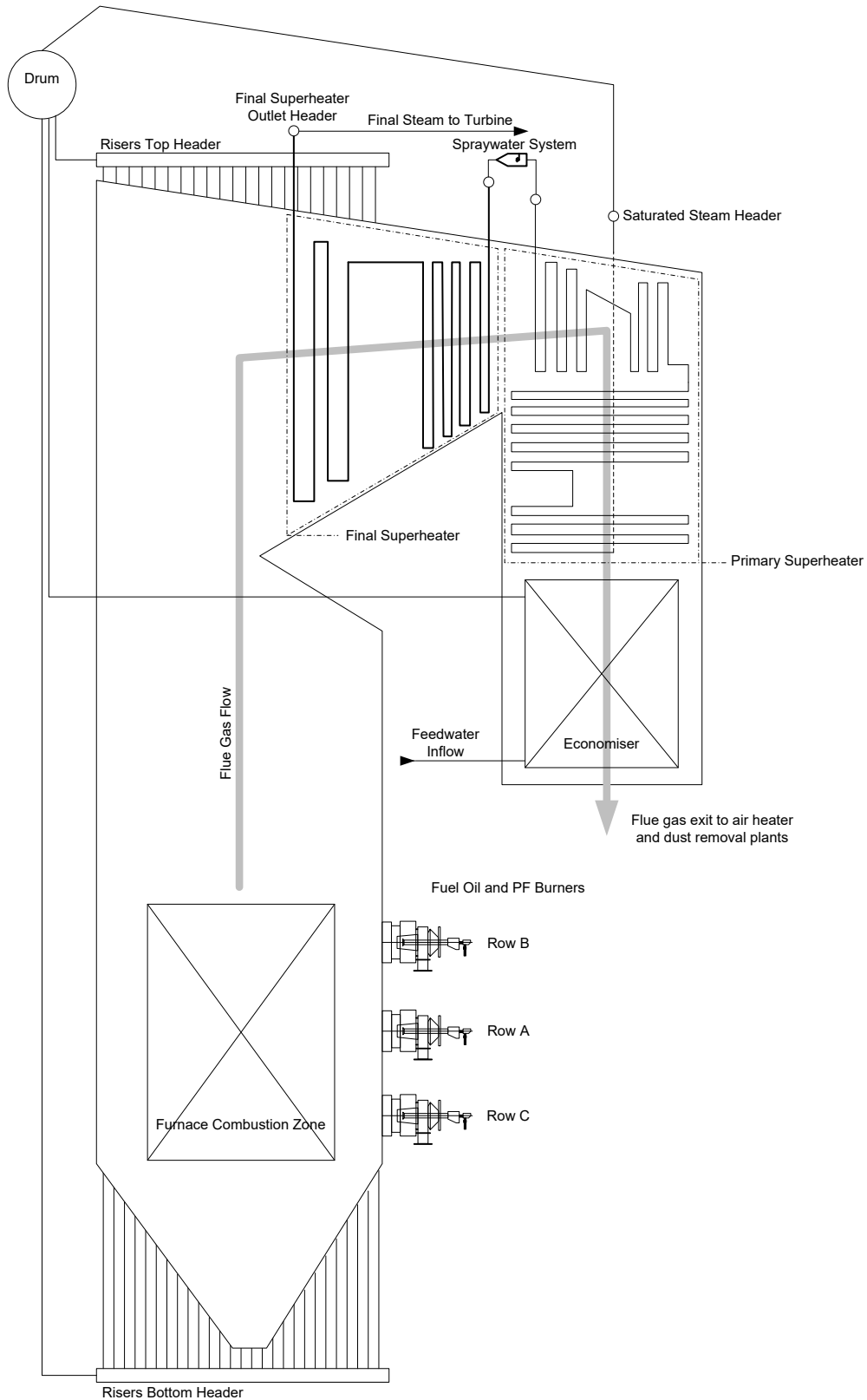


Figure 1: General Pressure Part Arrangement

Chapter 1 Introduction

The water and steam cycle in the boiler consist of heat exchangers, a boiler drum, and the attemperation system. Feedwater is introduced into the economiser where it is heated before entering the boiler drum. The drum is responsible for circulating the water through the riser tubes to reach saturation, and then separating the steam for superheating. Superheating is done in a primary and a final superheater, each subdivided between the left- and right-hand halves of the boiler. In *Figure 1* the side view is shown hiding the fact that the boiler is subdivided between left and right. In the figure the front of the boiler is on the left and the rear is on the right.

The spraywater system is situated between the primary and final superheater stages. The purpose of the spraywater system is to maintain the temperature of the steam, leaving the boiler for the turbine, to a manipulatable reference. Atomised feedwater is sprayed in with the steam before the final superheater stage. This reduces the inlet steam temperature, while ensuring sufficient residence time of the mixture to allow full evaporation. This prevents water droplets being carried to the turbine in the steam, which can pit and damage the turbine blades. This also requires a control interlock preventing inlet steam temperature saturation, which occurs at around 300 °C at 8 MPa. Manipulating the spray water control valve controls the outlet temperature, but is subject to some control lag due to thermal inertia and transportation delays related to the position of injection.

The main operating envelope of the system is determined by the required steam properties for safe steam admission to the turbine, and the units loading requirements. Steam pressure is usually maintained around 8 MPa, while safety valves will start lifting if it approaches the 9 MPa. Steam temperature is optimal for turbine admission at 510 °C, with several protection circuits that will decouple the machine from the grid if triggered. In the industry this is referred to as an unplanned automatic grid separation. In very simple terms there is a protection circuit for exceeding 525 °C for extended periods, or 530 °C instantaneously. There is also another protection circuit that activates with an excessively negative steam temperature gradient. These will be discussed in more detail when analysing previous trip events.

For the purpose of this research an unplanned automatic grid separation can be considered to constitute the tripping of the boiler, turbine and generator, practically simultaneously. Komati is not equipped with bypass systems, as with other power plants that allow boiler operation without

turbine operation other than at start up. The turbine can also not run without the boiler in service. Some power stations are capable of short turbine operating periods, without boiler operation, under the correct conditions. When the unit in question suffers a grid separation due to any of the protection functions described in this study, it necessarily means all flames are taken out of the boiler and the subsequent plants will trip. This requires a complete system purge and restart, starting with the boiler, then the turbine, and finally the generator.

The last parameter in question is the steam flow rate. This is very closely related to the loading of the machine. Load [MW] and steam flow rate [kg/s] is tightly coupled, but will change with respect to steam pressure and temperature. Each one of the left-hand and right-hand superheater sections contribute about 60 kg/s of steam to the turbine, delivering a total nominal load of 100MW at the generator. Archive data shows that temperature control is consistently required for loads from 30MW and upward. Occasionally spraywater may be applied at loads as low as 10MW, but this is very bad practice, and points to the incorrect operation of the plant. Incorrect operation is not limited to human interventions. Plant defects and deviations in concurrent processes may also contribute to early spraywater activation.

1.4. Literature study

1.4.1. Background

Advanced control techniques take some time to be adopted in certain industries. The power generation industry prefers proven and robust control techniques. Boiler outlet steam temperature on steam generators affect turbine efficiency, and are constrained by safe operating limits. There exist control techniques that could significantly increase performance, maintain constrained parameters, compensate for significant process lag, while not compromising robustness. There are advanced control applications in literature being used in this and other industries. The following literature study will look at superheater control system applications in general. The literature study then continues into MPC and Fuzzy control techniques and applications, that are not strictly limited to superheater control systems.

1.4.2. Research on the Subject

Control Applications on Superheaters in Literature

Naturally there are quite a few articles dedicated to showing the performance benefits of different control techniques over more traditional, usually cascade PID, control techniques in steam generators. However, much of the research was conducted around different boiler types. This section will review literature around the control of superheater systems.

In [5] the performance of a twin lead-lag PID cascade controller is evaluated, with practical application to a superheater system at a power plant. Here it is also noted that the better the employed control technique performance is, the closer the superheater can be allowed to run to the maximum allowable temperature. This will improve turbine thermal efficiency [6, p. 142] as well as reduce wear on low pressure (LP) turbine blades, while not reducing the main steam pipework long term health and life expectancy. The PID controller's performance in the article is quite remarkable. This might be due to the application seemingly suffering significantly less process lag, compared to the superheater at Komati Power Station. This could not be verified since only output responses are shown, with no input response curve during transients.

If there is comparatively less process lag, this could be the result of a higher boiler rating or superheater sizing. This controller was reported to achieve an error between ± 2 °C for controlled load ramps of about 60 MW executed over 10 mins. A [+ 3, - 9] °C error was achieved on a mill trip disturbance, translating to a step disturbance of -70 MW. The difference is quite important as it indicates that the performance gets worse in situations where combustion energy coming in and heat energy in steam going out is unequal through the transient. With load changes, usually heat in and heat out are ramped at the same rate, making the control effort significantly easier. With a mill trip for instance, an instant loss of heat energy to the furnace is already a large disturbance on its own. The fact that the turbine loading will settle to a new capability limited load setpoint, over a period of time, only adds to the transient condition. There is an energy imbalance to control for, as well as settling to a new process state. This new state is not linearly related to the previous process state, due to steam flow rate changes. This highlights the importance of ensuring controllers are optimised, not just for controllable load changes, but also uncoordinated load operations. This can be ensured by including these events in the training and evaluation datasets.

Chapter 1 Introduction

In [7] it is shown that PID control can be fitted to this application easily, and perform robustly. Special focus is given to the estimation error of dead-time, and in applying a simplified model. No improvements are however suggested for this technique and the research is not discussed in much detail here. The technique in [5] also showed no adaptation of the control parameters to compensate for changing conditions, as suggested in the difference in disturbance responses. In [8] and [9] the use of model reference adaptive control (MRAC), is proposed to compensate for changing plant parameters on superheater systems. In [8] only improvements in the step response is reported, which were shown to be significant. The only parameter to be adjusted was the controller gain. It should be noted here that other disturbances to the system might also interact with the reference model, and will not only affect the overall gain, but also dead-time and settling time. The system presented can be seen from the step response to have no dead time. Dead-time will mean that rule-based tuning of the reference model will have to be slow enough to prevent instability. This is an important finding as the control system cannot respond faster than the dead-time, as is already common knowledge. Measured or at least estimated disturbances can be responded to in time to avoid excessive transient conditions. This is not explored further in [8].

In [9], quite an old study, some interesting techniques are applied. An MRAC controller with two estimated load dependent parameters was implemented and tested. The results were comparable to [5], showing that the control effort is not increased to obtain performance improvements. Interestingly the parameter estimation is put on hold if there is no “Persistent Excitation”, as well as a backup parallel PID controller to safeguard the unit during controller testing. This technique can be employed on future work based on this study as well, to ensure that testing and commissioning of the proposed technique does not put the plant at risk.

In [9], the controller is also subjected to a variable sample time, to compensate for slower and faster process responses, as operating load changes. It is not discussed more in the article, but there are a number of complexities associated with this. The discrete time controller is dependent on the sampling time. If the sampling time is adjusted, it should be done in conjunction with updating the transfer function and control law. One could argue that for an adaptive technique this might be taken care of if changing the sampling time is in line with the expected change in the transfer function. This will be investigated in the research to come, for feasibility. It would be

Chapter 1 Introduction

dependent on the control technique chosen as well as the limitations of the control system implementation environment.

The application of artificial neural networks is explored in [10] through the approximate inverse dynamic process model developed for various super heater stages. This method succeeds in compensating the controller for the multitude of inputs affecting a superheater outlet temperature, and the nonlinearities related to the response. An approximate inverse model is obtained through training of the neural network off-line. A PID compensating circuit is added to ensure zero tracking error. It is noted that only variations in load are used for the training sets. This data does not include the recorded responses of other process inputs. No data is gathered relating to any other type of process changes that might excite the process inputs in a way not associated with just variations in load. It seems that the benefit of more intelligent control techniques exceeds those presented in [5] and [7]. The first tests conducted consisted of a 10 % (30 MW) reduction in load ramping at 5 MW/min. Two tests followed, dropping a further 10% load each, with settling time in between the tests. Although this technique does not require frequent retraining according to the author, it must be noted that most engineers and technicians would find it difficult to maintain and do fault finding of this control system. Maintainability and fault finding are important to this study and for that reason this technique will not be explored any further.

When process knowledge is incorporated into a control technique, larger and earlier control responses can be made to improve disturbance rejection. In the process environment disturbances sometimes coincide. Adequately rejecting known disturbances could potentially reduce the peak transient condition where more than one disturbance coincides. Predictive adaptive modelling improved disturbance rejection significantly in [11] and it is the first article reviewed that shows disturbance rejection during a wider range of disturbances, like sootblowing and mill loss. The significance of the time delay on the system, and the fact that it is load dependent, is clearly illustrated. The dead time remains the same, regardless of the control technique. Recovery after a disturbance is much faster for both Fuzzy and predictive adaptive techniques that were evaluated. Although the Fuzzy controller performed worse than the predictive adaptive controller, this was attributed to the differences in the model used, explicit versus implicit. Furthermore, it was shown that Fuzzy control succeeded in reducing the disturbance reaction overshoot by 1 °C, and the model-based control by a further 1 °C, compared to the PI controller. The article did not

Chapter 1 Introduction

regard Fuzzy control to be preferential for superheater control, compared to the PI and model-based approaches, when considering commissioning and resource demands. Although the performance improvement is clear it is mentioned that due to the many degrees of freedom of the Fuzzy controller, commissioning is resource intensive. This is also true for routine maintenance, where often more simplistic techniques are preferred. Often the skill and resources are no longer available to assist with maintaining and fault finding the system once commissioned.

Finally, [11] also discusses the feed forward control to be included based on pyrometer or other flue gas temperature measurements. This is in line with the proposal of this study and validates the expected performance increase. With early detection of process parameter changes and feed forward control, control demand is not necessarily more aggressive, but is initiated earlier. Reacting earlier in some sense negates the more aggressive control demand, especially with dead-time processes. The controller reacts before the process output shows much of a response, resulting in a much milder disturbance after the dead time has passed, with a possible smaller net response needed. Flue gas process parameters will have to be estimated largely from combustion parameters.

The work in [12] investigates multivariable constrained predictive control on the superheater of an ultra-supercritical boiler. Simulated results look promising, except that only load ramp disturbances were tested. The error compared to the PID controller was halved for load ramps of 100 MW or less. Disturbance error at constant load was also reduced from ± 0.5 °C to ± 0.3 °C. Interestingly a single model predictive controller (MPC) is applied over all superheater stages simultaneously, rather than dividing each section. This will increase computational effort as model order would increase as well as the prediction horizon, but could also give better performance. For the boiler under discussion only one superheater stage needs to be considered. In [12] there is no need to constrain control to maintain the inlet steam temperature higher than saturation, since the boiler is an ultra-supercritical type.

In [13], a hybrid MPC implementation was simulated using piecewise affine models across operational load ranges. Essentially the author created a gap metric to determine the “distance” of locally linearized models from load ranges between 50 %-100 % nominal load. From the results 7 models were chosen for 7 load ranges to be used in the hybrid MPC implementation. Each range

is chosen to ensure accuracy of the nominal model across its range as well as a sufficient distance between the nominal models of different ranges. It shows the dominance of this hybrid MPC controller over a cascade PI controller. Over a load ramp of 50 % nominal load the MPC controller error was never more than 0.3 °C, while the PI controller error went in excess of 2 °C. This article gives an alternative to the computationally intensive non-linear MPC implementation; linearizing across certain load ranges means that matrix inversion and other calculations used in MPC implementation can be done off-line, reducing computational complexity significantly.

Fuzzy control and non-linear MPC are not found readily in superheater steam temperature control applications. Two articles, [14] and [15], covered proposals for improvements of these techniques. Although MPC is not the simplest control technique, it sufficiently addresses the needs of this study to warrant a certain amount of complexity. Non-linear MPC will not be explored further since this will add unnecessary complexity, while MPC should be sufficient to address the needs of this study.

In [15] a Fuzzy-PI controller replaces the adaptive cascaded PI controller of a once-through boiler superheater steam temperature controller. Although the performance is stated to have improved on the previous controller, results are not given. The article does cover the optimisation of the Fuzzy controller that was implemented, and the improvement gained in the process. A total of 9 linguistic variables were used, with triangular membership functions, and the centre of area method for defuzzification. Optimization was then done using a minimisation criterion over the error, across a 50 % downward load step. Two parameter sets were obtained through two variations of the optimisation technique. Secondly, an upward gradual load ramp was simulated, and the Fuzzy controller was optimised, starting from the parameters optimised for the step change optimisation. A compromise then had to be made to insure adequate response to both types of disturbances. Simulation results show that the optimised controller delivered a very good performance. The temperature was maintained to within 2 °C for a 50 % load step decrease. A 50 % load ramp from 50 % to 100 % nominal load was also performed over a period of 12 minutes. During the load ramp the temperature was maintained to within 1 °C. The superheaters in this article do not seem to be severely affected by a large dead-time, and consist of 3 stages, each with actuating elements that allow more accurate control. The effects of dead-time on the Fuzzy controller will have to be evaluated.

One of the biggest challenges if the system to be controlled is the large dead-time associated with the process. This is largely due to heat capacity relating to the many lengths of boiler tube metal, compounded by the rate of transfer of steam from the superheater inlet to the outlet. There are many techniques capable of robust control of processes with large dead-time. These include predictive and intuitive techniques like, MPC, Smith predictor, Fuzzy control, neural networks, etc. [16], [17], [18], [19], [20], [21], [22], [23], [24]. Not all of these references were found to be directly relevant to the study at hand and are not discussed further. Those found to be relevant are discussed in the next section.

Fuzzy Control in Literature

Up to this point several articles and journal entries relating to MPC and Fuzzy control techniques have been discussed. This section, and the next, will review literature covering Fuzzy and MPC control techniques that are not necessarily linked to superheater system control.

Fuzzy control is perhaps the most intuitive of the adaptive control techniques. Fuzzy control is often likened to a human response, due to its ability to adjust its reaction based on certain operating parameters or rules. It does however lack some of the inherent features of MPC, most notably process variable constraints. Certain constrained behaviours can alternatively be achieved through specific rule creation for the Fuzzy controller. Fuzzy control will be discussed in more detail, as it might be able to achieve similar performance improvements without adding too much complexity. Fuzzy based controllers are very flexible solutions to the control of non-linear plants, uncertainty in plant behaviour, and capturing of operator like responses, where other techniques might fall short.

In [18], Lam and Leung investigate the performance and stability of a Fuzzy controller for time-delay systems of a non-linear nature. It comprises of a Fuzzy plant model as well as a sampled-data Fuzzy controller. They make use of a Takagi-Sugeno Fuzzy (TSK see abbreviation for disambiguation) model that incorporates a state-space model and a delayed state response in each rule. Any plant non-linearity can then be captured, based on the rule-set formulation. The sampled data Fuzzy controller gives a feedback gain rule based on the Fuzzy model state space for each of its rules. The inferred controller output is then characterised by the weighted sum of the membership of each rule and its feedback gain. The system stability is then established by

Chapter 1 Introduction

using linear matrix inequality (LMI) based stability conditions, based on the Lyapunov method. Lastly this control strategy is applied to a delayed and nonlinear response of a reversing truck trailer. This article showed the ease with which Fuzzy controllers can deal with non-linear plants, and with as few as two rules for the plant model and the controller. The time delay in question is still modest and does not address larger or time variant time delays.

Yordanova, and Tashev investigate a similar approach in [24]. They apply parallel distributed compensation on a TSK Fuzzy controller of a non-linear time delayed plant. Each Fuzzy plant model rule identifies a sub-domain of the plant where it can be seen as locally linear, with the same premise for the controller model. The plant considered in [24] is a first order plant with variable coefficients (including gain), and time delay terms. The non-linearity is linked to the plant output operating point. The controller is simply stated to be the inverse of the nominal plant model, with the time delay removed, filtered to make it a proper transfer function, and linearized around the chosen sub-domains. It also has a local internal model for control that feeds back the output error w.r.t the internal model to the controller reference. In an application for an air temperature controller, 3 sub-domains are determined, and give rise to three Fuzzy rules. Compared to a well-tuned PI controller, the Fuzzy internal model controller performs similarly, but is very robust compared to the PI controller. [24] also concludes stating that for each sub-domain the worst-case plant parameters are the deciding factor in tuning the controller filter, chosen to satisfy the minimum robust stability or robust performance criterion. This highlights the fact that when designing a Fuzzy controller with local internal models, the worst-case characteristics need to be incorporated into modelling and control design. Sub-domains therefore need to include the extreme ends of the operating range.

In [25], variations on a Fuzzy PI controller is used to address plants with large time delays. Due to a simplistic choice in membership functions, the control region could easily be divided into 20 distinct incremental control regions. These form a two-dimensional grid, based on the error and its differential. The control law was then inferred for each of the 20 regions. A Fuzzy predictor is used to infer the best prediction horizon to be used for the pure prediction component, which is not explained in more detail in the article. Three plants each with a higher order and larger time delay than the previous were then simulated and compared against PI, predictive PI, Fuzzy PI, and Fuzzy predictive PI solutions (FPPI). Although not all the details of the other control

techniques were covered, [25] reports very promising results for systems up to 3rd order and a time delay of up to 14 seconds that used the FPPI technique. In conclusion the technique is reported to be cumbersome and requires many trails in order to find the optimal tuning parameters.

Often, Fuzzy controllers have a high degree of freedom, with a need to train the controller to achieve the desired performance, but there are also many techniques where this has been reduced, like the Fuzzy PI controller where there are only a few tuning parameters, and that results in a PI controller like behaviour. Fuzzy controllers are often combined with predictive controllers, either more directly or in a cascade, or supervisory configuration. It seems clear that Fuzzy control systems are very suitable for nonlinear and uncertain plants. Time delayed systems still seem best controlled if a predictor is incorporated into the Fuzzy controller. One advantage seems to be the robustness of a properly tuned Fuzzy controller, even if this requires more effort to tune. The plant to be controlled in this study suffers from large dead time and inertia, as well as having non-linear responses to process inputs. The heat transfer of boiler superheater tubes has been studied quite extensively, but results in a very high order model. By far the most crippling characteristic of this plant is the dead time and inertia in the system response. A TSK Fuzzy model could then prove to give a very good response over the entire plant operating range. To compensate for large time delays a predictor would possibly still be preferred but can be incorporated into the Fuzzy model and control law for each of the Fuzzy rules, or sub-domains.

MPC in Literature

MPC has shown to be a very appropriate control technique for this application. From [16] it is noted that MPC can be used to incorporate many of the challenges associated with this system. It also allows constraints to be included into the control law. This can be used to prevent additional trip conditions from occurring. This process has trip conditions defined for high outlet temperature, and rate of change in a downward direction. A high negative rate of change in the final steam temperature is an precursor of possible water carry over to the turbine. Besides the actuator stroke limits, the inlet temperature must never be controlled too close to the steam's saturation point. Steam that becomes saturated will no longer be only vapor, but will also contain water in liquid form. It is also noted that dead-time is intrinsically modelled in the process, while it can be excluded when minimising the cost function as part of MPC design. This allows the

Chapter 1 Introduction

controller to focus only on the process response after dead-time, while still including the effects of previous inputs during the dead-time period (free response). Setpoint changes occur infrequently and, when they do, are limited in rate of change. In this case MPC can allow the system to follow a specific trajectory to a new setpoint as a future consideration.

The implementation platform of the control problem at hand is somewhat different from sequential programming. Although a programmable logic controller (PLC) based system is used, programming of an MPC solution will need to be done through a distributed control system (DCS). Computation will have to be implemented using the standard sequential function chart components used by the DCS. As can be seen in [26], MPC relies on many matrix computations and some iterative solutions when constraints are concerned. However, there are means of reducing computational effort, like pre-inverting of certain matrixes, through the choice in prediction horizon, and the plant model order. Computational effort should be kept low where possible since this control algorithm will reside on one of 8 distributed PLCs which itself is responsible for several other process automation and control functions.

In [27], Eitelberg, and Boje have evaluated the performance of a proposed implicit quasi steady state modelling technique. In their evaluation, the same model order reduction is achieved as with the singular perturbation modelling technique, while including both faster and slower dynamics of the strongly coupled tube wall and steam temperatures. This technique will be evaluated again during modelling of a superheater section. When employing MPC, the ability of the model to facilitate a stable control solution, is valued higher than a complete and fully accurate model. The exact ratio of radiative and convective heat transfer of the superheater in question is not known. The flue gas heat energy is also not measured directly in the applicable section of the boiler, which would also hinder further modelling of convective heat transfer. This and possible other solutions will be discussed in more detail.

It is also sometimes noted that MPC cannot be switched on (from manual to auto) with a bumpless transition due to the free response based on previous inputs that needs to settle. For this study, as soon as the system is on line, it can remain on and create the illusion of bumpless switching, by not turning off when switching to manual. Instead the input is set to track the actual manual commands, allowing the model and observer to continue to keep track of the system

states. This is largely due to the scale and complexity of the entire plant and its redundant PLC configuration and always running state. It is not subject to restarting while in operation that would cause it to lose its internal states. By the time this controller is required to be activated in the process, several hours of process operation has passed resulting in internal states having stabilised. This internal state stabilisation is based on [26], where the manipulated variable of the ideal single input single output (SISO) system response was limited before being fed back to the controller, based on the actuating element amplitude constraint.

The final superheater steam inlet temperature is controlled by an inner loop that accepts a reference from the outer control loop. Feeding back the actual measured valve response to the outer control loop can also compensate for deviations in the spray water control valve operating profile. If, for instance, the MPC controller output is to achieve a desired temperature after the spray water valve, and a PI controller is used to actuate the valve to achieve the setpoint, any deviations can be fed back in the same way, to reflect the plant's actual response. If the valve response has changed, because of wear or the feedwater temperature unexpectedly changes, the actual implemented control response (i.e. the temperature after the control valve) can be sent to the MPC controller so that it can be compensated for in the next control response. There are a multitude of conditions relating to the actuating element that can be mitigated if they occur only temporarily. Some examples are: Actuator trips and resets, feedwater temperature change, partially passing valves, etc.

1.4.3. Project Support Documentation

Since Komati Power Station boilers were designed to a certain specification, construction drawings, piping and instrumentation diagrams (P&IDs) are available. They contain much of the design information, however, the refurbishment has led to some changes. This information will be used to get a starting point for system identification and modelling, since tube masses, material and lengths are known. Operating parameters are also known for the energy rating of each of the plants involved. Operating philosophies will also serve as a guide as to what evaluation parameters will be used to compare different solutions, since they place constraints on the control system operations.

Chapter 1 Introduction

The DCS control system, is well documented in terms of its capabilities [28]. It is also integrated with a human machine interface (HMI) system and provides the ability to archive any measured process parameter that is required for data extraction. It also logs any operating interventions implemented through the plant interface. A key aspect, discovered through literature study, is the importance of accurate modelling. To achieve this, it is important that data gathering is not done specifically for situations that the researcher would like to control for. Training data should cover all real-world scenarios, which necessarily will include disturbances as a result of plant failures, maloperation, and operation at the extreme ends of the normal operational envelope. This type of scenario data can easily be obtained from the large data archive [3].

Chapter 2

System Analysis

2.1. Process Description

The boilers at Komati are drum type boilers, as opposed to the supercritical, once through type boilers that have become widespread in the industry. A full description of the boiler operation, construction and process flow will not be given here. The process will only be described in as far as it relates to boilers in general, and the final superheater stage in particular, which is the focus of the control application. For a general overview of power station design, [6] is a good reference to consult. It will also be used to justify industry specific statements and practices in the following sections.

2.1.1. *Combustion and Flue Gas*

It can be seen from *Figure 2: General Pressure Part Arrangement* on page 19 that the boiler consist of several heat exchange phases. This drawing is a simplification of the general pressure part arrangement drawing available internally [29]. Flue gas is the product after combustion of pulverised coal and fuel oil with sufficient oxygen. Fuel and air are introduced through burners, referred to in terms of rows A, B and C, on various firing levels. The coal, oil, and air mix as they enter the furnace combustion zone where they combust and produce heat. The flue gas, the product after combustion, mostly consists of O_2 , CO_x , NO_x , SO_x and ash. Combustion generally occurs around a temperature of $1100\text{ }^\circ\text{C}$. In general, the data used for this research has been sourced from the plant operations data archives, [3], kept for the station design life. Specific values of particular operating points are generally drawn from this source, including scenario data that will be discussed as part of the research effort. The data archive is very detailed and store a compressed format, of all relevant process parameters, for all units in operation.

Chapter 2 System Analysis

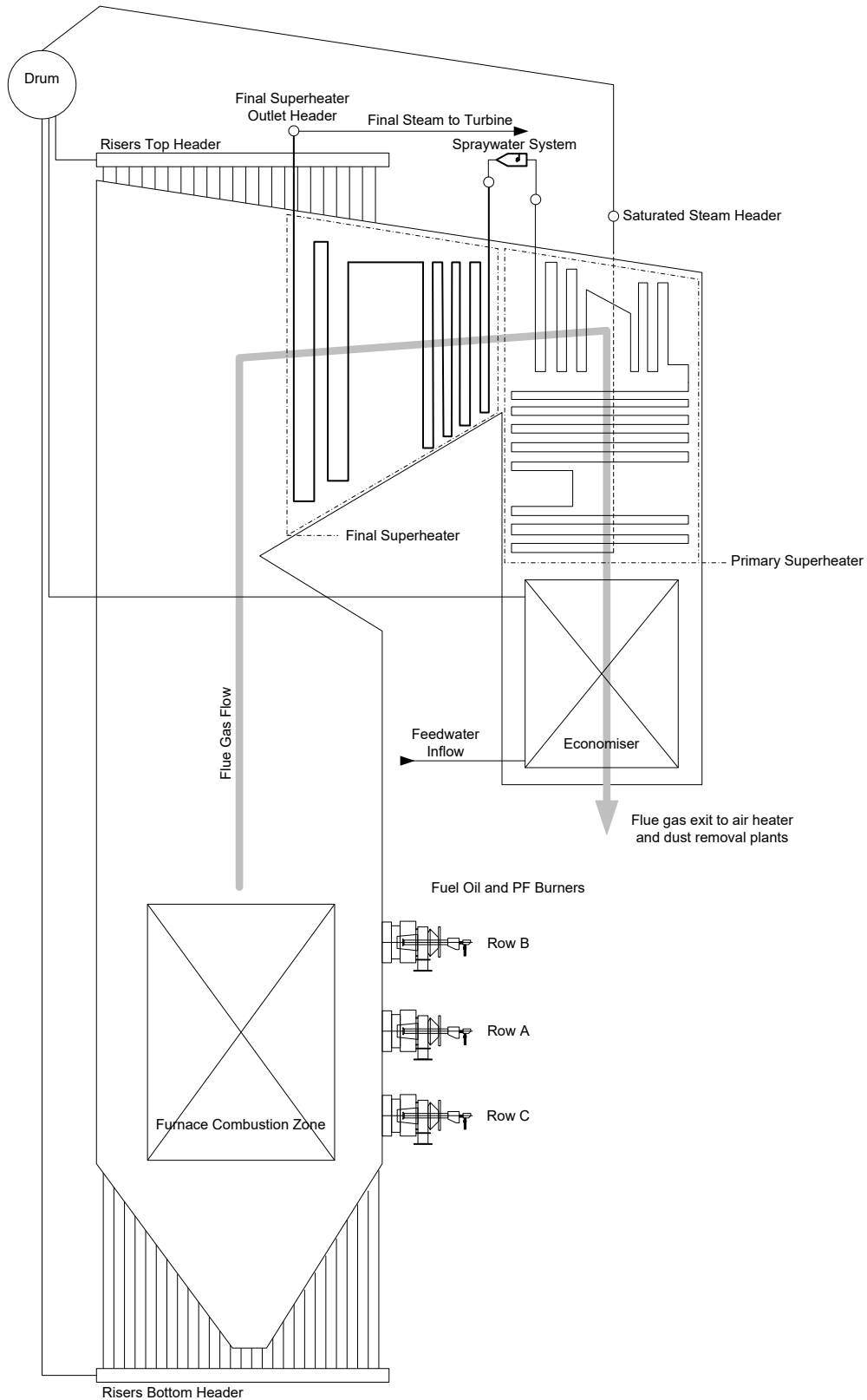


Figure 2: General Pressure Part Arrangement

Chapter 2 System Analysis

Burner firing levels are arranged in order B, A then C from top to bottom. Burners are specifically referred to in this order due to the varying effect they have on heat transfer as a result of their position in the furnace. In short, mills lower down contribute slightly more to pressure raising occurring in the first stages of heating. Higher up mills contribute more to superheating of steam in the final stages of the boiler. This will be discussed more in later sections. The unusual mill order, B, A and then C, is the combined result of numbering convention and physical design. The physical milling equipment is numbered sequentially based on location from left to right. The piping design, that transports the processed fuel from the milling equipment to the boiler, dictate the firing level. Minimising the mill to furnace pipe length plays a role in this design and therefore the resultant firing configuration.

Flue gas heat and radiative heat from combustion represents all the energy supplied to the process. It is essential that as much heat as possible is transferred through heat exchangers. All heat engines are already limited in efficiency through the fundamental laws of thermodynamics. Complex cycles and heating stages have over time been used in the industry to improve on the basic Rankine cycle efficiency. Many sources, including [30], claim overall efficiency to be in the region of 30 % to 40 % for sub-critical boilers as with Komati Power Station. The precise figure will be time variable and will be dependent on the system design, operating conditions and maintenance.

The entire boiler flue gas-pass is under a slight vacuum induced by fans and therefore induces a flow in the direction indicated on *Figure 2*. The flue gas temperature lowers as it exchanges heat with the various water and steam pressure parts. After exiting the boiler, the flue gas is transported to an air heater that further utilises some remaining heat energy to heat up combustion air. From there it proceeds to the dust removal plant, before being exhausted to atmosphere. Water and steam pressure parts are discussed next. A general rule for most heat exchange stages is: Heat exchangers transporting comparatively colder water or steam should be situated in colder boiler flue gas pass sections in order to facilitate maximum total heat transfer and efficiency. Steam will therefore be separated and superheated in some of the hottest furnace sections, while water will be pre-heated in the last and coldest sections. The flue gas flows at a cross flow to heat exchangers, not parallel to them. Furnace wall tubes are an exception to these statements. The

furnace wall tubes essentially form a wall around the combustion area in the main furnace column. Furnace wall tubes and the water/steam cycle will be discussed in the next section.

2.1.2. Water/Steam Closed Cycle

The boiler consists of the following water and steam heating areas: Economiser, boiler drum, furnace wall, primary and final superheater stages. Water passes through these stages in this order, absorbing heat energy along its path, and eventually reaching the superheated steam phase needed by the turbo-generator to generate electricity.

Economiser

The process of feedwater entering the boiler drum as part of the closed system starts at the Economiser, in the coldest section of the flue gas pass. This is a finned type tube heat exchanger, heated by a crossflow of flue gasses. The water in the economiser is heated to just before boiling point at about 290 °C. Boiling point for demineralised water is about 300 °C at 8 MPa. There are other heat exchangers external to the boiler before this phase that already heat the feedwater to a temperature of around 190 °C. This is not discussed further as this heating is done primarily using some steam that is bled off from various turbine stages.

Boiler Drum

The main purpose of the drum is to act as a steam separation vessel [6, p. 82]. The boiler drum has 4 entry and exit points: A feedwater inlet, an inlet and outlet point used for recirculation of water, and a steam outlet. For steam to be generated the water in the drum is recirculated through “down-comers” that are not exposed to the furnace, and back upward through furnace wall tubes (sometimes called risers).

Benson type boilers do not have a boiler drum since they operate past the critical pressure on demineralised water. No boiling occurs in the vessel as water turns directly to steam. This higher pressure allows boilers to be designed with a much higher nominal load rating. The Benson type boilers also suffer from significantly less lag since no boiling occurs, and has no need for a steam separation vessel. The boiler drum in subcritical boilers therefore introduces lag into the system as well as acts as an energy store due to the water capacity in the drum that can store heat energy. The boiling occurring in subcritical boilers are also subject to specific disturbances. Sudden

Chapter 2 System Analysis

changes in pressure and heat energy transfer can severely affect boiling and also the water level in the drum.

Some boiler types are able to harness this heat store during a loss of fire in the boiler for short periods of time. The heat energy is usually only enough to sustain the turbine and generator to maintain in-house electrical demand while returning the boiler to full operation. This type of operation is not available at Komati due to the relatively small sizing of the boiler drum.

Furnace Wall Natural Circulation

The water in the furnace wall tubes, or risers, is continuously boiling and therefore at a lower density compared to water in the “down-comers”. They are connected with a water header at the bottom of the boiler. The density gradient causes natural circulation to occur with the boiling water flowing upwards in the furnace wall tubes and back into the boiler drum [6, p. 87]. The steam is separated from the water in the boiler drum. The remaining water along with feedwater pumped into the drum, continues to recirculate. The steam exits the drum to the Saturated Steam Header after which superheating of steam begins.

Primary Superheater

From the saturated steam header, the steam goes through the primary superheater where it is heated to well in excess of 450 °C. After this point the spray water system introduces atomised feedwater directly mixed in with the superheated steam, in order to control the final steam temperature. As it might be guessed, this will affect thermal efficiency, but the loss is designed to be small for the required control at this point of the process. At this point the steam legs also cross to opposing sides in the boiler to counteract possible heat imbalances. This is a common arrangement [6, p. 134], In this thesis each leg will be treated as a straight section with no distinction made between left- and right-hand sides, or where they cross.

Final Superheater

After the final superheater stage, the temperature should be at 510 °C and goes to the turbo-generator to produce power. Some steam is also tapped off along the line, and at various turbine stages, for heating and deaeration of feedwater amongst other things. After most of the usable heat has been extracted from the steam in the turbine, the steam is condensed and will eventually

Chapter 2 System Analysis

make its way through the condenser and pre-heating stages, back to feedwater supplied to the economiser. This completes the closed cycle of demineralised water.

As per the codification convention used on site, the term condensate is used while being preheated at a low pressure and until entering the deaeration storage vessel. From the deaeration vessel up to the economiser the term feedwater is used. The feedwater pressure can be as high as 12 MPa as it is pumped through several more pre-heating stages and up to the economiser inlet.

Efficiency

There are two major contributors to energy losses. Condensing the steam wastes a large fraction of the added heat in the steam. The vacuum this consequently creates in the condenser, due to the steam contracting as it turns to water, this adds to the overall cycle efficiency. The other large contributor to wasted heat energy is in the form of exhaust flue gas. Only about a 1/3 of the total added heat energy is left as a very rough estimate. There have been several improvements to the Rankine cycle, over the years, that attempt to recover some waste energy.

2.1.3. Process Measurement and Control

Figure 3 below is a simplified process flow single line diagram with irrelevant systems removed for clarity. They can also be divided into controlled variables (CV), manipulated variable (MV), setpoint reference, and disturbance variables (DV) to the process. The measurements available to the researcher are:

- Primary superheater outlet steam temperature (TT1)
- Final superheater inlet steam temperature – MV (TT2)
- Final superheater outlet steam temperature – CV (TT3)
- Steam flow rate (FT1)
- Furnace energy input calculated from the various fuel sources (Calc1)
- Feedwater temperature (TT4)
- Steam pressure (PT1)
- Boiler drum saturation limit temperature
- Final steam temperature setpoint – SP

Chapter 2 System Analysis

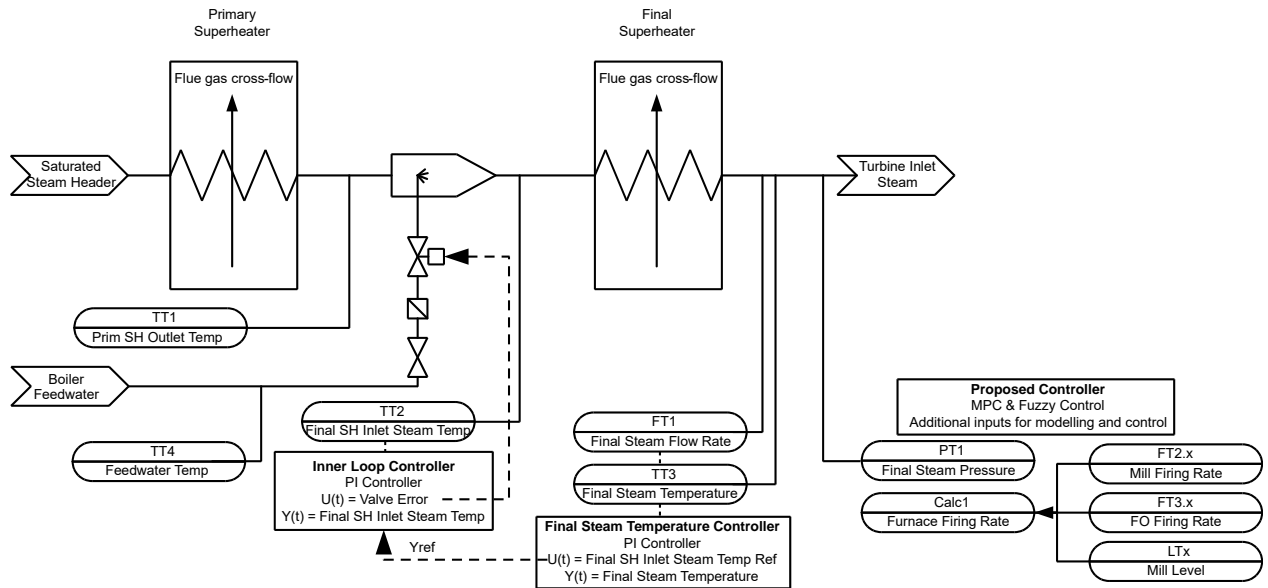


Figure 3: Single Line Process Flow

Steam flow rate and fuel firing rate and the other unmarked measurements are inputs to the process and will be discussed in more detail in section 2.3 *Disturbance Analysis*. They are considered measurable disturbances with regard to the final steam temperature controller, since they cannot be used for control of this process. The main reason for this is that these parameters cannot be separated from other parallel processes and controllers easily. Manipulating these variables will destabilise the control of other processes.

Primary Superheater Outlet Steam Temperature

Similar to the final superheater outlet steam temperature, the primary superheater outlet steam temperature is manipulated through firing conditions and dependent on the mechanical construction of the boiler. Final steam temperature control is achieved by having process measurements and a manipulated variable in between the two sequential processes.

Final Steam Flow

The final steam flow rate can be controlled more directly through the use of governor valves. Governor valves and steam flow rate are controlled for the direct purpose of governing electrical power generation. The governor controller will take precedence over final steam temperature control as per design. In some cases, the steam flow rate and machine load will be sacrificed in order to maintain steam pressure, but never for the purpose of steam temperature control.

Chapter 2 System Analysis

The detail of the interaction between these controllers can be best analysed when looking at a non-trivial sequence of events that lead to uncommon interactions. The effects of this precedence of control is discussed in more detail in section 3.5.1 with an appropriate example. Under stable running conditions the unit would be able to run at a set load, on any of the coordinated control modes. There are two coordinated controllers, the pressure controller and the load controller. These controllers, control how the boiler and turbine loads are coordinated.

If conditions are stable, the coordinated load controller is the preferred operating mode. In this control mode the turbine and boiler are coordinated to the same load setpoint. It allows for about ± 5 MW actual load variation, serving as a margin for governor control valves manipulation to actively control for small pressure deviations from setpoint. This operating mode is preferred in order to have a predictable output onto the grid and to comply to the supply requirements set out by the National Grid Code. The National Grid Code consisting of amongst others, The Network Code [31] and The System Operation Code [32]. Amongst other things, The Network Code [31] requires a governor response with respect to frequency control of the grid. This means that the grid will also dictate steam flow changes in certain situations that supersede operational requirements. The Network Code may also require emergency load operation. This System Operator Code [32] sets out regulation & load following requirements. In this mode of operation, the System Operator can coordinate and control all units on the national grid, that are not exempt, within a given margin to maintain stable grid operation.

Under slightly perturbed conditions that are still mostly stable, the coordinated pressure controller can be preferred. In this mode of operation, the turbine governors actively control to maintain a steady turbine inlet steam pressure, regardless of what the resultant generated load will be. The boiler is still given a load setpoint and should, in steady state, result in the turbine and generator settling to the same load setpoint.

The boiler also has an additional master pressure controller that will regulate boiler firing concurrently with the unit coordinator controllers, to maintain turbine inlet steam pressure. The master pressure controller's gain is scheduled based on the coordinated controller that is currently active. In coordinated pressure control mode, the master pressure controller's gain is reduced.

Chapter 2 System Analysis

It can be seen that final steam flow rate is critical for the coordinated load control of the turbine and generator. The alternative, coordinated pressure control mode, also provides at least some assurance that, in steady state, a certain load setpoint can be maintained. Since the steam flow rate is the only manipulatable parameter available to control the generator's load, it cannot be used for control of the final steam temperature.

Furnace Energy Input

Furnace energy input is calculated from the various fuel sources used in the furnace. Fuel admission control is governed by a unit coordinator, a multi-tiered controller. It is closely interlinked to the electrical load controller in order to continuously match energy in versus energy out. Importantly, it is responsible for safety critical operation of the boiler in order to prevent explosive combustion conditions. Final steam temperature control can therefore not be allowed to manipulate firing conditions. Within the multi-tier control configuration, the three mills can be fired in a coordinated mode, following identical setpoints, or manually based on an individual setpoint.

Feedwater Temperature

Feedwater temperature affects the process in two ways: 1) Feedwater is fed into the boiler drum through the economiser at the start of the boiler heating process; 2) Feedwater is used as the source for attemperation of superheated steam. Feedwater temperature is affected mostly by plant availability and, critically, affects the entire plants capability limit and thermal efficiency. As a source of attemperation, it is still significantly cooler than superheated steam. Feedwater temperature deviation from normal operating temperatures can affect the inner control loop stability. The actuator error command is the MV for the inner loop of control. Although the water flow rate and the actuator position are measured, none are used for control of the final superheater inlet temperature. They are however used for condition monitoring that warn against abnormal behaviour. This loop is much faster than the outer loop and will be discussed in more detail later.

Steam Pressure

Steam pressure is also controlled by the previously mentioned unit coordinator. It is considered to be more stable than other parameters, but does influence the process in a few ways. Two major

process variables that affect boiler steam pressure are combustion energy and steam flow rate. Boiler steam pressure, in some ways, represents energy storage in between the continuous supply and demand of energy. These variables represent the input and output energy balance required for sustained boiler and turbine operation. Mismatches in these process variables cause boiler steam pressure to deviate from its normal operating level. Higher energy demand versus supply will result in the energy store being depleted, and causes the pressure to decay. The inverse is true for excess energy supply. Deviations in steam pressure can occur as a result of rapid changes in the steam flow rate, both of which can be measured directly. A sudden and large steam demand can result in a momentary boiler steam pressure reduction, until the balance of energy is supplied through additional firing in the furnace. Uncorrected and prolonged mismatches over time will also result in significant steady state deviation from the normal operating level. This may lead to a significant effect on the boiler drum steam temperature saturation limit that is discussed next.

Boiler Drum Saturation Limit Temperature

The boiler drum saturation limit temperature is the point where steam starts to superheat. While superheated it is considered “dry” when using industry jargon. This term references the fact that a boiling water and steam mixture is measured to be at its thermodynamic boiling point. This operating point is influenced by, amongst other things, the steam pressure [33, p. 115]. Water is supplied into the boiler drum at below boiling point. During natural circulation the water is heated and will reach boiling point in the risers. While boiling, latent heat is being added to the water and steam mixture in the riser tubes. This turns more water to steam in the liquid and vapor mixture. Steam can only be superheated or become “dry” if there is no more liquid in the mixture. By separating the steam from the water in the drum cycle, it may pass on to the boiler superheating stage. The remaining water will continue to recirculate and be heated. Should the steam temperature drop to the boiling point at any time, some steam will condense back to a liquid state. This is called the steam saturation point, and is actively avoided in all superheater stages. Water droplets forming in the steam flow path to the turbine can significantly damage its blades and thereby reduce the turbine life expectancy. Once the boiling point is reached, the steam temperature does not change. The temperature will only start changing once all the steam has condensed back to water and stops boiling, or if it returns to being superheated once sufficient latent heat is supplied.

Chapter 2 System Analysis

This saturation limitation will limit the spray water controllable range. Maintaining steam pressure is therefore crucial for proper functioning of the spray water controller. Since steam pressure control lies outside the spray water controller's influence it is crucial that this control limit be constrained even at a cost of approaching other protection limits. Steam temperature measurements are conducted at certain points in the system. The steam temperature will drop due to losses as it is being transported and will drop again as it is transferring its energy in the turbine. Two scenarios are constrained and protected against:

1. Prevent steam being quenched to its boiling point by limiting the spray water controller. (measured at spray water discharge)
2. Prevent saturated steam delivery to the turbine by means of a turbine trip. (measured at turbine inlet)

A third tripping scenario exists that will prevent inadvertent supply of saturated steam to the turbine. This protection is, however, more closely related to preventing metal fatigue. Metal fatigue can occur due to a sudden rapid decline in metal temperatures in both the turbine and boiler metal components, also called thermal shock. This protection and acceptable limits are discussed in more detail in section 5.2.3.

3. Tripping of the turbine if steam temperature rate of change exceeds acceptable limits. (measured at turbine inlet)

It might be considered that condition 2 would be sufficient to prevent reaching the saturation limit. Condition 1 is required, nonetheless, due to the fact that larger water droplets may be formed if the spray water is not atomised well when injected into the superheated steam flow. The steam might not technically be in saturation as a whole, but locally the water droplet requires sufficient residence time to fully evaporate and superheat. Providing sufficient travel distance for mixing, and by limiting the spray water being injected, the steam can confidently be considered "dry" when it reaches the turbine.

2.1.4. Final Superheater Outlet Steam Temperature Control

The current control strategy can be described as follows: An actuated valve is used to spray atomised water, taken from the boiler feedwater supply, into the superheated steam. This takes

place at the primary superheater exit, before entering the final superheater. The control cascades such that the final superheater inlet steam temperature setpoint is controlled by the outer loop. This controlled reference consequently controls the final superheater outlet (also the boiler outlet) steam temperature to a setpoint. This is a more complex control objective, as the most severe process dynamics occur across the final superheater stage, and not across the actuating device.

Cascade Configuration

In *Figure 3* these two cascade controllers can be seen. The inner loop controls the spray water valve actuator to control the final superheater inlet steam temperature. This controller will remain unchanged and is considered to settle within one sample time of the proposed control techniques. The controller under investigation is the final steam temperature controller that supplies an inlet temperature reference to the inner loop. There are some recommendations made for improvements to the inner loop in a later section of this study. Both loops are currently implemented as two cascading PID controllers with only limited compensation based on the measurable disturbance characteristics.

This cascade type of configuration works well for the control of superheater steam temperatures. The use of an MPC controller as the outer loop for controlling a faster inner loop is also seen in the chemical processing industry as outlined in [34], where it is also noted that acceptance and success of this type of technology has become widespread. This cascade type of control for non-linear subprocesses is also investigated and summarised in [35, p. 280] where PID controllers are often supervised by a higher order controller in the power industry. The inner loop of control is considered faster, specifically in references to the differences in settling times between the two sub-systems. The inner control loop can generally be faster since there is no significant lag in the sub-process it controls. It is however assumed that it is optimally tuned for all operating ranges, and therefore stable. This prevents thermal cycling and valve wear.

The outer loop control system, as shown in *Figure 4*, uses the temperature before and after the final superheater as inputs. The controller does limited gain compensation based on the machine's loading. This compensation addresses the dead time and large settling time in the response, due to thermal inertia. Not shown in *Figure 4* is the variable parameter graphs for the final gain, discrete filtered derivative time constant, and time in the discrete first order filters.

Chapter 2 System Analysis

These will be discussed in the following sections. Where variable parameters are used the arrows indicate what value is applied. The transfer functions are discussed in the next section.

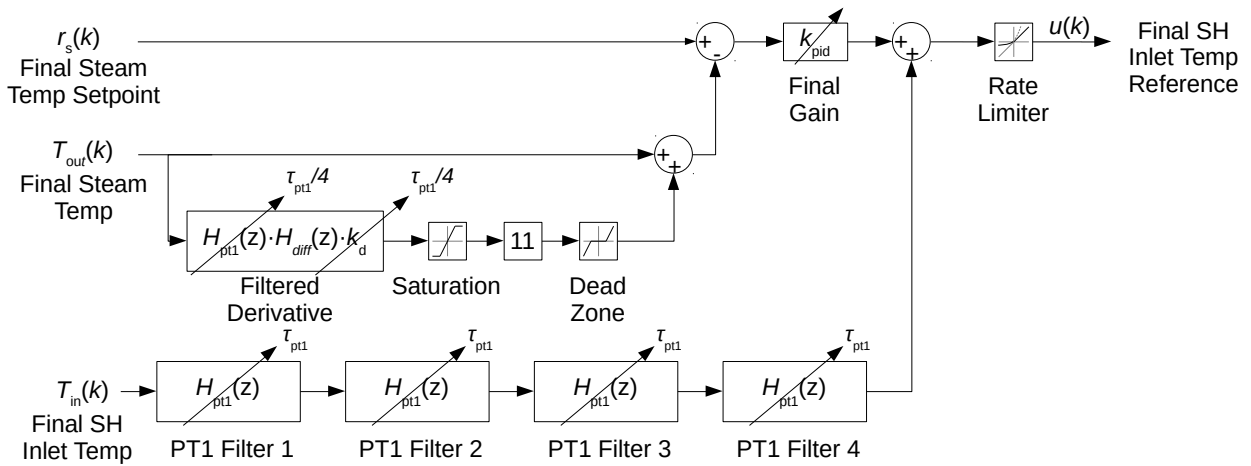


Figure 4: Current PID Control Strategy (Variable parameter indicated by arrows)

Table 1: Nomenclature for PID Controller

| Symbol | SI Unit | Description |
|---------------|---------|--|
| $r_s(k)$ | [°C] | Final steam temperature setpoint |
| $T_{out}(k)$ | [°C] | Final steam temperature |
| $T_{in}(k)$ | [°C] | Final superheater inlet temperature |
| k_{pid} | | Final PID Controller Gain |
| τ_{pt1} | [s] | Variable response time constant |
| $u(k)$ | [°C] | Final superheater inlet temperature setpoint |
| $H_{pt1}(z)$ | | PT1 filter transfer function |
| $H_{diff}(z)$ | | Finite difference derivative transfer function |

Variable Filters and Gains

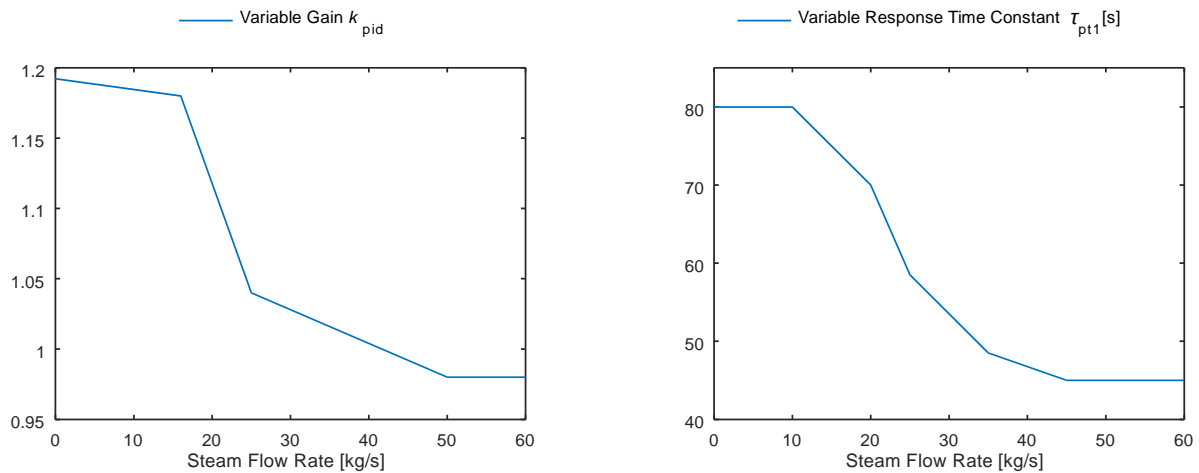


Figure 5: Variable Gain and Filter Time Constant

From *Figure 5* above it can be seen that the overall system gain is tuned down as the unit load and steam flow rate increases. The filter time constant has an inverse relationship with steam flow rate as is expected, but it is capped at 10 kg/s and 45 kg/s steam flow rate. Details of the tuning of these parameters are not available. They will be discussed in more detail below in the following sections.

PLC Programming and Programme Execution

Programming the PLC in question uses a sequential function block language. It compiles and executes each block sequentially, within the 200ms unless there are signals that loop back into already compiled blocks. Outputs of signals that loop back would be subject to a zero-order hold. There is no looping back of signals for any of the diagrams presented here so it will not be discussed further.

Final Steam Temperature Control Algorithm

The controller calculates a setpoint for the inner control loop that controls the final superheater inlet temperature. The final steam temperature error from setpoint and derivative are added to a filtered final superheater steam inlet temperature. This filtered signal is a feedforward signal that encompasses the large thermal inertia of the system through the use of four first order low pass filters in series.

Chapter 2 System Analysis

To explain the feedforward signal more intuitively: It estimates the system response to a change in inlet steam temperature. The low pass filters attempt to capture the dynamic response in terms of a similar time constant of the superheater's thermal inertia, but with unity gain. This ensures that for a step disturbance the error and derivative component will be added to the controller output setpoint, producing a step change to correct the error. Once the actual plant output starts responding to the change in control, it will reduce the error to zero. If matched correctly with the plant time constant, the feedforward signal should also then respond to the step change, and will replace the reduced error component to maintain the step change in the controller output signal.

The PT1 filter is a standard implementation used extensively throughout the distributed control system (DCS) interface. The name PT1 only refers to the fact that it is first order filter with no explanation given for the acronym itself [28]. References to PT1 will still be made in future sections, due to its widespread use, and should be noted here. The time constant for each of the blocks used, is in excess of 40 seconds at full load, compared to the PLC cycle time of 200 ms. It should be noted that the PLC cycle time is fixed due to the fact that it also performs several other automation tasks that occur much faster than this process. The controller response can be chosen on any multiple of the base cycle time. This large difference in cycle time (t_{s-plc}) and system response time constant (τ_{pt1}) therefore explains the pole placement of the PT1 blocks so close to the unit circle. The transfer function for the PT1 block is given in (1) adapted from source [28].

$$H_{pt1}(z) = \frac{\frac{t_{s-plc}}{t_{s-plc}/2 + \tau_{pt1}}}{1 + \left(\frac{t_{s-plc}}{t_{s-plc}/2 + \tau_{pt1}} - 1\right)z^{-1}} \quad (1)$$

It is clear that this function is somehow derived from a first order low pass filter. The closest relationship to standard discretisation functions are to the backward Euler transformation and the zero-order hold (ZOH) equivalents.

$$H_{lowpass}(z) = \frac{1 - e^{-\frac{t_{s-plc}}{\tau_{pt1}}}}{z - e^{-\frac{t_{s-plc}}{\tau_{pt1}}}} \quad (2)$$

ZOH equivalent low pass filter is expressed as in (2). The first two terms of the Maclaurin series,

$e^{-\frac{t_{s-plc}}{\tau_{pt1}}} \approx 1 - \frac{t_{s-plc}}{\tau_{pt1}}$, comes close to the representation used for the PT1 function. It is also clear

that these two approximations converge if τ_{pt1} is significantly larger than t_{s-plc} . A quick analysis

Chapter 2 System Analysis

shows that the approximation used, $e^{-\frac{t_{s-plc}}{\tau_{pt1}}} \approx 1 - \frac{t_{s-plc}}{t_{s-plc}/2 + \tau_{pt1}}$, provides a good approximation at smaller τ_{pt1} values. At the internal limit of $\tau_{pt1} = \frac{t_{s-plc}}{2}$ the error of this approximations for $e^{-\frac{t_{s-plc}}{\tau_{pt1}}}$ is just 12% of the Maclaurin series two term approximation. This approximation is not as accurate for the positive x half of e^x , which is not used in this case.

Backward Euler transformation also shows some similarities. $s \leftarrow \frac{z-1}{zt_{s-plc}}$ is the standard substitution for Backward Euler transformation, while the same function in (1) can be achieved with the following substitution:

$$s \leftarrow \frac{z-1}{z} \left(\frac{1 - \frac{t_{s-plc}}{2\tau_{pt1}}}{t_{s-plc}} \right) \quad (3)$$

The filtered derivative block can also be seen in *Figure 4*. It is a single control block with two tuneable parameters. It consists internally of a PT1 filter block, a basic finite difference derivative as shown in (4) and a gain factor k_d also adapted from source [28]. The gain, k_d , is set equal to $\tau_{pt1}/4$ and the PT1 filter time constant is also scaled down from (1) by a factor of 4. The time constant τ_{pt1} is defined in *Figure 5* displayed after this subsection.

$$H_{diff}(z) = \frac{1-z^{-1}}{t_{s-plc}} \quad (4)$$

The error between the current final steam outlet temperature, including a small derivative component, and the setpoint is then simply added to this delayed or “past” CV to become the setpoint output going to the inner control loop. The controller would therefore be able to achieve zero error following. Although what has essentially been created is a “state space model” with at least 4 system states for the purpose of forward feeding. None of these states are used for control purposes other than the final state.

There are also slight changes to the near unity final gain value seen in *Figure 5*. The compensation it provides is small and the impact questionable. The highest gain value of 1.2 decreases gradually and from 16 kg/s drastically to 1.04 at 25 kg/s. In these ranges the final steam temperature control through spray water is applied infrequently. Tight control is usually only required as the steam flow rate increases to above 20 kg/s. This is generally also the area where

the worst response is seen from the existing controller. The system has a high reliance on the variable time constant's accuracy used in the PT1 filter blocks.

The model clearly shows the challenges that are faced with this system. All responses are subject to this large settling time to some extent. The better the response can be estimated, the earlier the controller can attempt to correct for known dynamics. This leaves only unknown disturbances and the model error subjected to the larger response time.

Heat is picked up across the entire length of superheater and not just supplied at the start, as with spray water. This means changes in the firing rate show a quicker response in the final steam temperature than a change in the superheater inlet steam temperature. The start of these disturbances or inputs might not coincide, but the peak of each's impulse response, seen the final steam temperature, might align and constructively interfere to create an even larger peak. A typical scenario showcasing this is analysed in section 2.3.1 *Failed Mill Start*. Responding to a disturbance, through feedforward, and not only to its transient response in the final steam temperature, reduces the compounding effect of disturbances that constructively interfere.

2.2. Operating Envelope

Deviations of the boiler outlet temperature, which is more or less equivalent to turbine inlet temperature, but delayed, have a variety of effects. The turbines at Komati are rated to run at 510 °C where they are at their most efficient. The steam pipework's long-term health is greatly reduced as the temperature increases. This is a metallurgical limitation in steam generating plants that can be generally applied with some variation based on the materials used. One source indicates a general limit of < 900 K [30]. To this end a high temperature trip will be initiated immediately at 530 °C, or if operated for longer than 3 minutes at above 525 °C. This trip will close the steam supply to the turbine and decouple the generator from the electrical grid.

The turbine is also protected against water carryover. Should the steam temperature drop at a rate faster than 5 °C/min, a trip would be initiated (details in section 5.2.3). For this reason, the spray water control system, is limited on how close to the steam saturation temperature it is allowed to operate. When the steam-water mixture becomes saturated, water droplets could remain in the steam without a change in temperature being measured.

Chapter 2 System Analysis

Tight final steam temperature control would also mean less wear on the low pressure (LP) turbine's final stage blades. Wear is caused by saturated ("wet") steam forming due to the lower than nominal inlet steam temperature. A tighter control margin will allow closer operation to the material limits which can be considered when determining optimal turbine performance. This falls outside the scope of this study.

Normal operating parameters are considered to be: Steam temperature setpoint at 510 °C, total full load steam flow rate of around 60 kg/s per steam leg, and has a response comparable to a first order plant with a 3-minute time constant increasing as the load decreases. This does not assume that the system is first order at this point.

Problematic system characteristics, and the current control strategy, revolve around heat transfer, disturbance rejection, and control robustness. Heat transfer in such a large structure is very complex and non-linear. The current control system only does rudimentary compensation for process delays and response times. This plant has some dead time and a slow response mainly due to thermal inertia. This is caused by the shear length, thickness and therefore mass of steel tubes used in the superheater. Transportation delays are almost insignificant in relation to this thermal inertia; however, they are strongly coupled dynamically. Based on rough calculations the steam passes through the entire superheater section in only a few seconds depending on the machine loading. The degree of convective versus radiative heat transfer also plays a role in the overall heat transfer. This ratio will be influenced by the location of combustion in the furnace, which can be influenced by airflows and the mill firing configuration. As the combustion process moves upward in the furnace from its nominal operating point, convective heat transfer gives way to more radiative heat transfer. This cannot be measured directly, but can be seen through in-depth analysis of combustion measurements. This is a difficult task for both human and computer analysis with the currently available sensor data.

2.3. Disturbance Analysis

Most of the system influences and disturbances have been discussed at this point and it is clear that the most notable, i.e. the steam flow rate and fuel firing, are in actual fact only considered as disturbances, as a result of not being designed for use in controlling the final steam temperature. These parameters are controllable, but are used directly for the control of other processes that are

considered more critical. This is an inherent problem with large processes that use many separated SISO control algorithms that each control one system parameter with usually only one actuating device or input. A closer look is taken at two scenarios that showcase some of these process related disturbances and what drives them. Some less notable disturbances to the process are also discussed briefly.

2.3.1. Failed Mill Start

The following incident resulted in a unit trip due to the rapid decay of final steam temperature which activated a protection system to guard the steam turbine against damage due to water carryover. The incident is chosen for a discussion of the disturbances that occurred due it showcasing a known “failed” mill-start trip event that is capable of leading to a sequence of events culminating in an eventual unit trip. The mill start failed in the sense that the mill initially fired correctly, but tripped within a short period after being put in service. There has been some expansion done as part of the already finalised internal investigation report for this event [36].

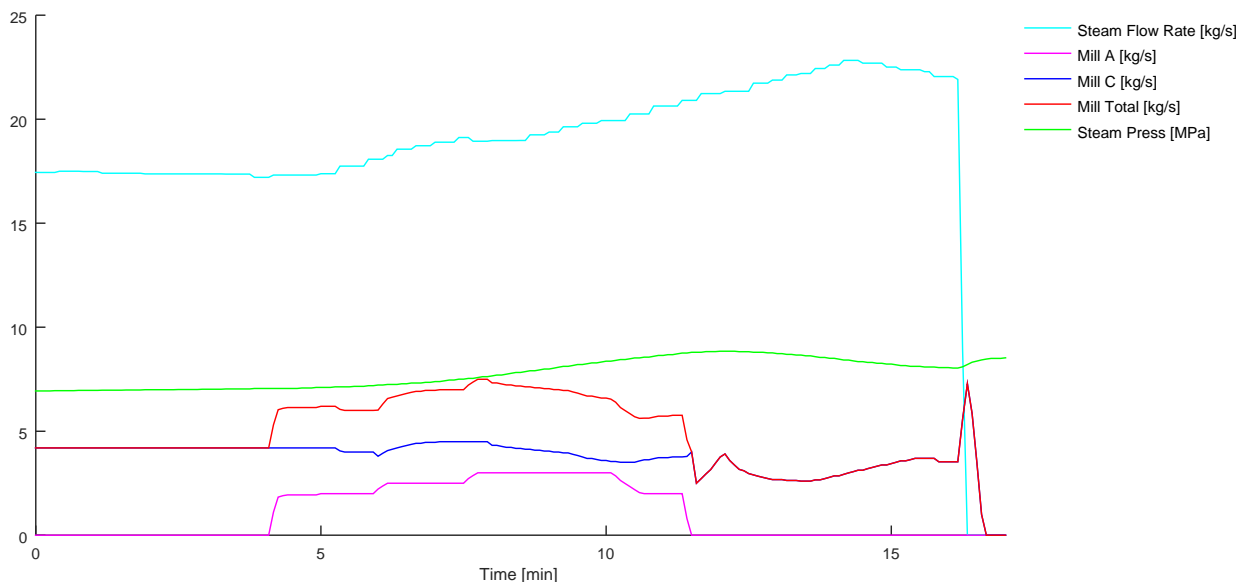


Figure 6: Failed Mill-Start and Trip at Low Steam Flow Rate

From *Figure 6* it can be seen that A mill (magenta) starts firing at minimum loading while C mill (blue) is already in service which increases the total firing rate (red). There is also a corresponding increase in steam flow rate (cyan) and pressure (green), as the machines load is increased with the increase in firing and pressure build-up.

Chapter 2 System Analysis

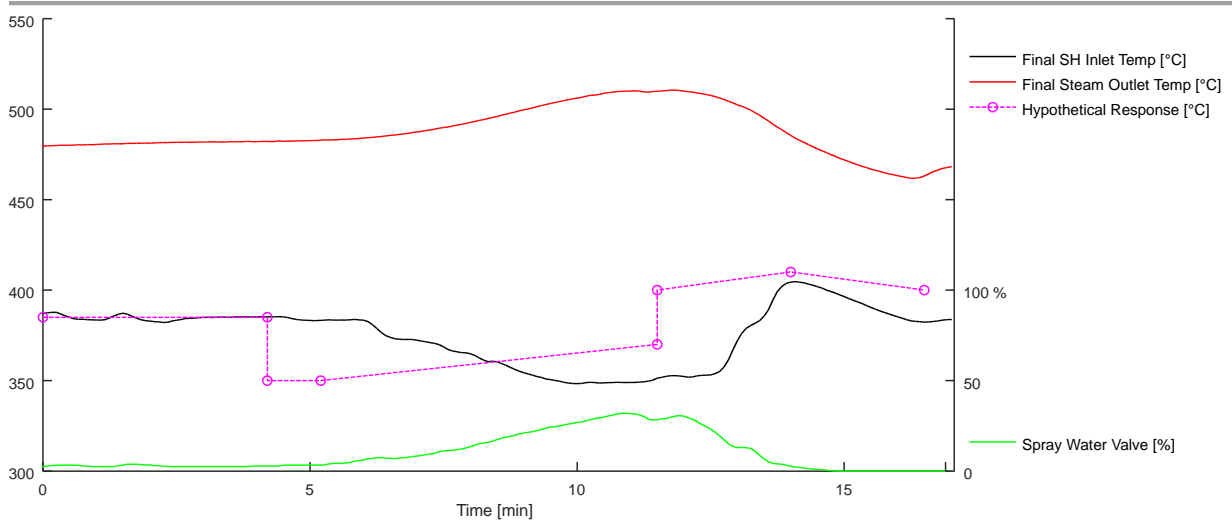


Figure 7: Process and Control Response to Failed Mill Start

From *Figure 7* it can be seen that the spray water valve (green) shows no initial response when mill firing is increased. After approximately a minute the controller responds due to the temperature increase in final steam (red). Then, due to an untimely mill trip, the mill loading is decreased again. This unfortunately coincides with the spray water valve position peaking. The heat energy transferred is then reduced once again to a similar rate as before the mill introduction. Now the superheater inlet temperature (black) is about 35 °C lower due to the control effort and the steam flow rate having increased. The final steam temperature will drop alarmingly due to these disturbance responses constructively interfering (constructive additive responses). The machine will trip on high rate of temperature decay protection.

The events occurred roughly 7 minutes apart and at 17-20 kg/s steam flow the first order time constant representing the system response is also about 7-9 minutes. Generally, the controller will have its peak reaction in terms of spray water response at this time. The quenching of the final steam temperature has just about started taking effect, evident by the arrested rate of increase. This response is still in its transient phase and will continue to drop towards the setpoint for at least another 7-9 minutes even if spray water valves were immediately closed fully. The general first order response of changes in firing would be as little as 3-5 minutes. This behaviour is explored more in 3.2. These transients will therefore align in dropping the final steam temperature drastically.

Chapter 2 System Analysis

A hypothetical response (magenta) is also shown on the trend that is based on the ratio change of fuel input (energy in) and steam flow rate (energy out). This hypothetical response does not take the closed loop negative feedback into account. Negative feedback still cannot react faster than the process delay permits. The hypothetical response only shows a feedforward element as it is expected to influence the process. It is also not meant to provide an analytical control solution to the event. A hypothetical response is constructed based on what a human operator would expect the control system to do, having perfect hindsight, more process variables at his disposal, and a estimated idea of how the system would respond. The controllers that will be designed and tested based on this knowledge will later be evaluated on this same event.

The hypothetical response proposes that the superheater inlet temperature setpoint should be decreased at the start of the mill firing increase and the response should increase again as soon as the mill trips. This should compensate for the heat energy imbalance that occurs. The transient should be much less severe and should not result in a unit trip. The ideal response also compensates for the reduction in the main steam flow rate that would have driven the temperature up even further. This drives the setpoint up as the steam flow increases. This provides a controller behaviour that is initially lowering the inlet temperature earlier, while the final steam temperature is rising. It then starts increasing the setpoint again as soon as steam flow rate increases, removing more energy. Again, when the mill trips it also increases the setpoint based on less energy being available. These transient conditions are all known and does not require waiting for a change in final steam temperature in order to respond.

A short discussion needs to be made here around concurrent controllers that maintain operation of other processes in the plant. An event, like the one analysed, does not easily occur without other process controllers also failing to control certain parameters. As one example; The unit coordinator is a controller that maintains an energy balance between the boiler and the turbine. If this balance is maintained, firing changes and steam flow rate are matched fairly quickly to avoid disturbances of many processes, including the final steam temperature. This controller can be seen from the response not to have been active at the time. This was due to operator error, but will not be discussed in more detail here. Incorrect or suboptimal operation of the steam temperature controller is therefore not at the root of this trip event. It is however analysed since it can be shown that despite this condition, the final steam temperature controller itself can react to

the same process parameters used by the unit coordinator. In this way a trip condition might be avoided, despite maloperation of other controllers or processes in the plant.

2.3.2. Over-Firing of a Furnace

The scenario depicted next resulted in a unit trip that was also related to a turbine protection device. It is designed to prevent major life reduction to main steam pipework and other metal components, when exposed to temperatures higher than the design specification. This investigation was completed internally [37], and additional information was gathered and analysed for research purposes.

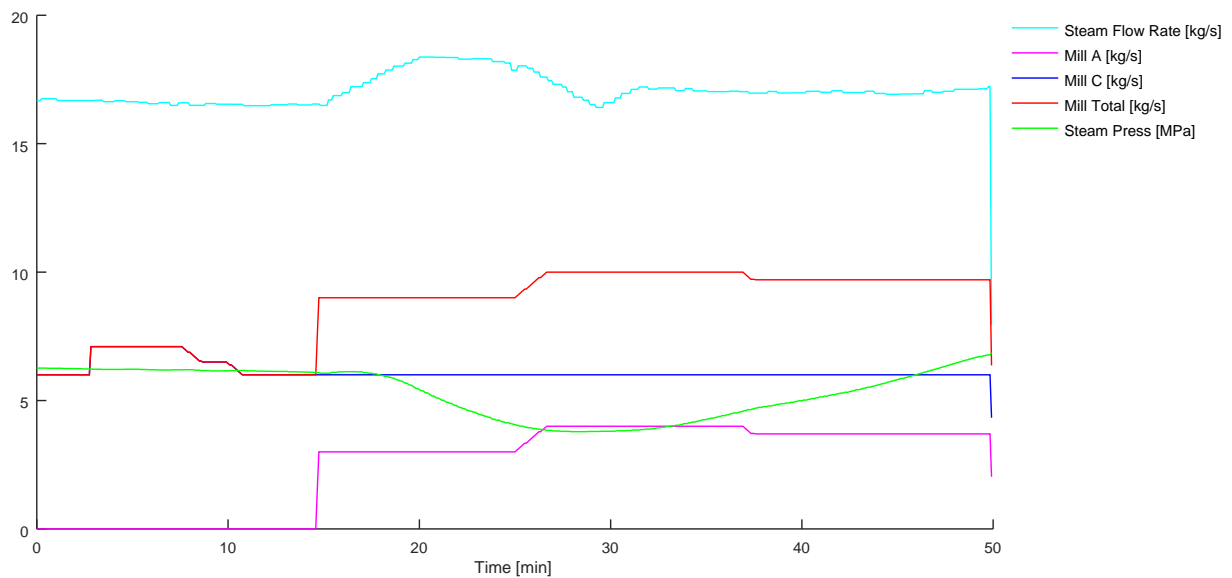


Figure 8: Over-Firing with No Corresponding Steam Flow Rate Increase

From *Figure 8* it can be seen that, again, mill A (magenta) starts firing at minimum loading while mill C (blue) is already in service which increases the total firing rate (red). In this scenario there is only a temporary increase in steam flow rate (cyan), as deloading follows in order to maintain pressure (green). This illustrates that changes in steam flow rate has a much quicker effect on final steam temperature compared to thermal heat transfer. It also illustrates the difficulty in controlling steam temperature, pressure and flow rate separately while being so closely related.

Chapter 2 System Analysis

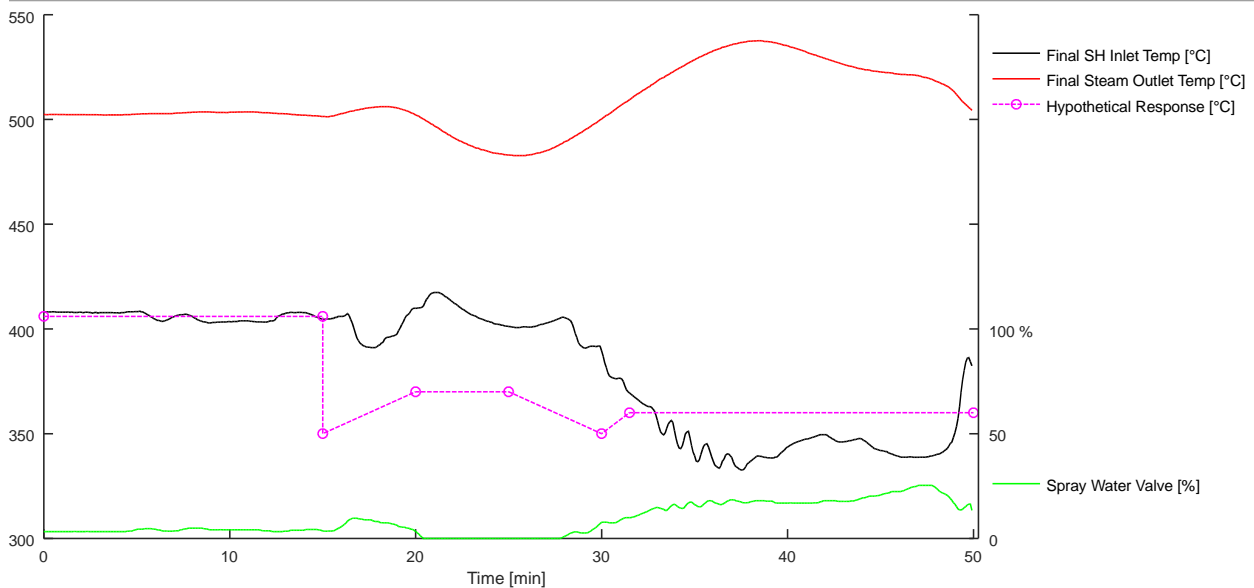


Figure 9: Process and Control Response to Over Firing

From *Figure 9* it can be seen again that the spray water valve (green) only respond to changes in final steam temperature (red). The final steam temperature initially drops due to the initial steam flow rate increase. After about 15 minutes the steam temperature starts to respond upwards to the increased firing rate. The temperature turned and was already back to 505 °C after peaking at 537 °C but tripped on the 530 °C turbine trip protection once propagated to the turbine protection measuring point. It should be noted that the turbine protection operates on the inlet to turbine steam temperature. A significant mass and length of pipework is required to transport the steam from the boiler to the turbine. The steam suffers negligible losses in temperature, but is subject to more thermal inertia between the two measuring points.

This is once again a scenario at a low steam flow rate. Many incidents happen under these conditions due to the non-linearity coupling the flow rate to the process delay time. Process activities such as pressure raising are also still taking place, which add to the disturbances experienced by the system.

A hypothetical response (magenta) once again shows an initial drop in the setpoint to be made and does so soon enough that the temperature excursion might have been prevented. It might be tempting to state that this hypothetical response could have also triggered a rate of change temperature decay trip. The final steam temperature initially drops as the superheater inlet

setpoint is reduced. The effect of spray water will, however, only manifest 63 % of its response after about 8 minutes after mill introduction estimated from an expected first order response. It therefore negates this notion, and also alludes to the difficulty of controlling plants with significant lag.

2.3.3. Less Notable Disturbances

Other system disturbances exist that are not directly measurable and include: Ash build-up, coal quality, mechanical plant defects, soot-blowing and operator error, just to name a few. Ash build-up and coal quality can only be inferred online through analysis of heat pickup. The rotating motion of soot-blowing lances while inserting makes it difficult to predict the dynamic response especially when taking the complexities of furnace behaviour into account. The control system response will still need to be evaluated against these unmeasured disturbances.

2.4. Methodology

From the literature study two options have been chosen as viable for this study to explore further. Model predictive as well Fuzzy control strategies will be explored to compensate for the process dynamics. For both cases, a state space representation will be used as a starting point for controller development.

2.4.1. Modelling

A state space model will be derived from a theoretical baseline. This model will comprise of a series of the divided superheater sections. System identification will be done online due to production constraints. Datasets of all the relevant variables will be gathered, with care taken to find as many independent and uncorrelated responses as possible. Least squares regression will be used to determine the plant parameters based on the theoretical model.

The proposed techniques both utilise a plant model to assist with output and process state prediction that can be used to compensate for process dead-time. The plant model will be based on system enthalpy states dependent on heat transfer principles with steady state error elimination through process feedback.

2.4.2. Control

The controllers will utilise observer states, dependent on the system model along with the actual process variables. The main capability is for a controller that will adequately respond to known and unknown disturbances and thereby maintain tighter control of final steam temperatures. This should address the main problems with the existing system. The MPC controller will utilise a varying sample time in order to compensate for the most significant non-linearity; Dependence of response time on the steam flow rate. The Fuzzy controller will inherently compensate for this non-linearity, as membership areas will be chosen based on steam flow rate and acceleration.

It is also noted that the inner control loop settling time is typically less than the maximum cycle time of 15 seconds and this is assumed throughout testing of the proposed control laws.

2.4.3. Simulation

Due to production constraints and boiler safety considerations, the proposed control system response will be simulated and compared as far as possible to actual events.

2.4.4. Evaluation

Based on the analysis of the system and past events, the following requirements have been captured for evaluation of the control solutions. The requirements are all baselined against the existing PID controller, which will not be altered for the purposes of this research.

- A reduction in the peak temperature excursion due to known disturbances. (excluding sootblowing)
 - The maximum steam temperature error from setpoint in the positive direction gives an indication of the controller's ability to prevent a grid separation occurring due to exceeding the 530 °C. The maximum temperature excursion should be reduced from the existing PID baseline by at least 50%.
 - The steam temperature error span and standard deviation are indication of the range in which control can be maintained. It is expected that the error span be reduced by 50% on average. The standard error deviation is required to be reduced by at least 30%. These metrics should ensure more grid separations relating to a rapid steam temperature decay can be avoided.

Chapter 2 System Analysis

- A reduction in peak control response time. This speaks directly to disturbance rejection of known disturbances. It is required that the large process lag be overcome and response time reduced to approximately 30% of the systems first order time constant.
- The avoidance of preventable trips as discussed under 2.3 *Disturbance Analysis*, will be an arbitrary requirement. This encapsulates the essence of the proposed research. Two case studies will be used for evaluation purposes. It is required that the proposed controllers prevent these events from resulting in a grid separation at least in the simulated environment.

Chapter 3

System Identification and Modelling

The heat transfer in a boiler is a very complex process that depends on many parameters. With any control application, the engineer is left to obtain a plant model that is fit for purpose. The model order can be reduced to capture dominant dynamics only, but at a certain point, vital dynamics could be excluded.

3.1. Description of Plant Disturbances and Dynamics

The current PID controller takes only steam flow, inlet and outlet temperatures into account. There are measurements and calculated process parameters available that could be used to improve on some controller shortcomings. Before system modelling can be started, a quick analysis of the most notable disturbances should be made to ensure that parameters are identified that will help construct an accurate model.

Thermal inertia, associated with the shear mass of pipework, leads to a rise time across the final superheater of around 3 minutes at full load. It can be as long as 15 minutes at 15 % load. This delay also affects the system response due to pressure changes as well as changes in firing. A model-based approach should prevent over quenching of steam due to, for instance a badly timed mill loss, if it is ensured that heat input into the furnace forms part of the model.

If energy input changes go hand in hand with load changes, the final steam temperature will remain largely undisturbed. An example would be if the steam flow rate is reduced immediately when a mill is taken out of service. A small transient will be seen without major step changes required. If these conditions are not coupled, it could eventually place the system outside a controllable range, resulting in step changes in temperature. Steam flow rate directly influences the heat pickup per volume of steam since it affects the steam's residence time in the system, not to be confused with heat transfer efficiency.

Chapter 3 System Identification and Modelling

The thermal inertia mentioned before is also directly coupled to the steam flow rate. Thermal inertia become prominent due to tube metal mass and its specific heat capacity. Changes in steady state operation means stored heat energy, in the metal tubes themselves, can only leave the system by being transported out with the steam flowing through the system. It intuitively suggests that a transient would die out slowly if the steam flow rate and firing rate is low. The speed of propagation of steam temperature through the superheater is highly dependent on the steam flow rate. This will become clearer in the next section, when the model is constructed.

It is further noted that since water and steam are mixed in the process under varying pressure conditions, it is prudent that enthalpy is used in the control law rather than working with temperature directly. This would not add any complexity to the system in terms of implementation, but further reduces non-linearities. The controller is intended to work across the full range of temperatures, pressures and combustion heat rate associated with process activities from start up to full load operation.

3.2. State Space Model

Much of the modelling is taken from the work of Eitelberg, and Boje [27]. Their model was developed for once through type boiler evaporators for the purpose of simulation, but will be adapted were necessary for the purpose of this study. A lumped model will be constructed by applying the model to subsections of the superheater. The number of subsections will be established experimentally. It was initially expected that in the region of 1-5 subsections will allow for enough states to be usable for feedback purposes and preserve dynamic responses through the delay. In later sections the number of subsections will be chosen to be only 2.

Through the model construction and fitting process, it became clear a higher order plant model alone would not capture the plant response discrepancies seen in the data. The inputs and disturbances to the process that were identified and included in the model response, was found to adequately reflect the unit's behaviour with only 2 subsections being used. These two subsections are reevaluated for the entire operating range. The plant's non-linear response is captured in the characteristics of these subsections as the steam flow rate changes. A single subsection would not suffice as it would not be able to model the combustion rate disturbance adequately, or differentiate it sufficiently from the application of spray water. Changes in the combustion rate

are reflected in all subsections with an equal response due to all subsections receiving a cross flow of heated flue gas in parallel. The application of spray water has to overcome the system's large thermal inertia as the transient response passes on through each subsection, represented in series. Further details will follow later in the chapter.

3.2.1. Thermodynamic Principles of a Superheater

As mentioned before, this derivation is covered in the work of Eitelberg, and Boje [27]. It will be discussed here with an explanation of the derivation and the assumptions made will be stated and explained.

The assumption that [27] makes is that heat energy of the metal tubes can be expressed as a lumped equation based on metal mass, its specific heat capacity, and the metal temperature. It is then assumed that this time derivative of the heat energy equates to the radiative heat supplied from the combustion process and subtracting the heat flow into the steam. This also assumes that convective heat transfer is minimal in the combustion process. This might not strictly be the case for this application. Due to measurement restrictions the term q_{rad} is maintained throughout the derivation, while later the dynamics of the combustion process will be estimated by a prefilter assuming no dependence on the tube metal temperature itself.

Table 2: Nomenclature for Thermodynamic Heat Transfer Equations

| Symbol | SI Unit | Description |
|------------------------|----------------------|--|
| h_{out} | [J/kg] | Specific enthalpy of steam at outlet |
| \dot{m}_{in} | [kg/s] | Mass flow rate of steam at inlet |
| \dot{m}_{out} | [kg/s] | Mass flow rate of steam at outlet |
| h_{in} | [J/kg] | Specific enthalpy of steam at inlet |
| q_{rad} | [J/s] | Heat flux through radiation from furnace firing |
| c_m | [J/(kg · K)] | Specific heat capacity of tube metal |
| m_m | [kg] | Mass of tube section |
| q_s | [J/s] | Heat flux from tube metal inner surface to steam |
| T_m | [°C] | Temperature of tube wall |
| T_s | [°C] | Temperature of steam |
| p | [Pa] | Pressure of steam |
| ρ | [kg/m ³] | Density of steam |
| V | [m ³] | Volume of inner tube section and steam |

Chapter 3 System Identification and Modelling

Any change in the heat energy of the tube wall will equate to the difference in heat energy supplied to, and removed from, the tube wall as shown in (5).

$$\frac{d}{dt}(m_m \cdot c_m \cdot T_m) = q_{\text{rad}} - q_s(T_m, T_s) \quad (5)$$

It is also assumed that m_m and c_m are constant due to it being physical properties of the steel. This will reduce (5), which can be reordered to give (6).

$$q_s(T_m, T_s) = q_{\text{rad}} - m_m \cdot c_m \frac{dT_m}{dt} \quad (6)$$

The time derivative of (6) can be taken on both sides to produce (7).

$$\frac{\partial q_s}{\partial T_m} \frac{dT_m}{dt} + \frac{\partial q_s}{\partial T_s} \frac{dT_s}{dt} = \frac{dq_{\text{rad}}}{dt} - m_m \cdot c_m \frac{d^2 T_m}{dt^2} \quad (7)$$

At this point, the equation for the enthalpy of the steam will be simplified to assume a stiff coupling between the tube wall and the steam. Instead of assuming $q_{\text{rad}} = q_s(T_m, T_s)$, [27] found that assuming $\frac{\partial q_s}{\partial T_s} = -\frac{\partial q_s}{\partial T_m}$ results in a much more accurate final representation for the same model order. It is also assumed that the $\frac{d^2 T_m}{dt^2}$ is negligible and can be ignored. Doing the substitution for stiff coupling and ignoring the $\frac{d^2 T_m}{dt^2}$ term therefore results in (8).

$$\frac{dT_m}{dt} = \left(\frac{\partial q_s}{\partial T_m}\right)^{-1} \left(\frac{dq_{\text{rad}}}{dt}\right) + \frac{dT_s}{dt} \quad (8)$$

From the thermodynamic relationship between temperature, enthalpy and pressure, the following equation is obtained (9).

$$\frac{dT_s}{dt} = \frac{\partial T_s}{\partial h_{\text{out}}} \frac{dh_{\text{out}}}{dt} + \frac{\partial T_s}{\partial p} \frac{dp}{dt} \quad (9)$$

Equation (9) is substituted into (8), and the result into (5), to produce (10).

$$q_s(T_m, T_s) = q_{\text{rad}} - m_m \cdot c_m \left[\left(\frac{\partial q_s}{\partial T_m}\right)^{-1} \left(\frac{dq_{\text{rad}}}{dt}\right) + \frac{\partial T_s}{\partial h_{\text{out}}} \frac{dh_{\text{out}}}{dt} + \frac{\partial T_s}{\partial p} \frac{dp}{dt} \right] \quad (10)$$

The same heat balance equation is also constructed for the steam side. The steam heat energy can be defined in terms of the steam density, volume, and enthalpy. The steam heat in an isolated section of tube is not just defined by the energy transferred from the tube wall, but also from steam transportation in and out of the tube section as shown in (11).

$$\frac{d}{dt}(\rho \cdot V \cdot h_{\text{out}}) = \dot{m}_{\text{in}} \cdot h_{\text{in}} - \dot{m}_{\text{out}} \cdot h_{\text{out}} + q_s(T_m, T_s) \quad (11)$$

Chapter 3 System Identification and Modelling

Starting from the conservation of mass, (12) can be assumed to hold for the superheater section. It is further assumed that the volume is constant due to it being a very rigid body.

$$\frac{d\rho}{dt} \cdot V = \dot{m}_{in} - \dot{m}_{out} \quad (12)$$

$$\rho \cdot V \cdot \frac{dh_{out}}{dt} + \frac{d\rho}{dt} \cdot V \cdot h_{out} = \dot{m}_{in} \cdot h_{in} - \dot{m}_{out} \cdot h_{out} + q_s(T_m, T_s) \quad (13)$$

Expanding (11) gives the result shown in (13), into which (12) can be substituted to get (14).

$$\rho \cdot V \cdot \frac{dh_{out}}{dt} + \dot{m}_{in} \cdot h_{out} - \dot{m}_{out} \cdot h_{out} = \dot{m}_{in} \cdot h_{in} - \dot{m}_{out} \cdot h_{out} + q_s(T_m, T_s) \quad (14)$$

Note the term $-\dot{m}_{out} \cdot h_{out}$ on both sides, which will be subtracted from the equation. After reordering this delivers (15).

$$\rho \cdot V \cdot \frac{dh_{out}}{dt} = \dot{m}_{in}(h_{in} - h_{out}) + q_s(T_m, T_s) \quad (15)$$

The final equation can now be assembled from the steam enthalpy equation (15) and reordered and reworked tube heat energy equation (10). This gives (16), and is reordered in the next section (17).

$$\rho \cdot V \cdot \frac{dh_{out}}{dt} = \dot{m}_{in}(h_{in} - h_{out}) + q_{rad} - m_m \cdot c_m \left[\left(\frac{\partial q_s}{\partial T_m} \right)^{-1} \left(\frac{dq_{rad}}{dt} \right) + \frac{\partial T_s}{\partial h_{out}} \frac{dh_{out}}{dt} + \frac{\partial T_s}{\partial p} \frac{dp}{dt} \right] \quad (16)$$

3.2.2. Model Development

The state estimation heat transfer equation below will be used in the lumped model of the superheater. Equation (17) describes the enthalpy state h_{out} of a generic superheater that will be divided into a specific number of subsections, as obtained from [27]. In this section N will be kept in symbolic form as it was derived. The terms under the line will be linearized to a constant that can be factored into each term above the line which represents our inputs. A discussion of the terms will follow. Subscripts will be added for each subsection as the general formula is being processed into the final form it will be used in.

Chapter 3 System Identification and Modelling

$$\frac{dh_{out}}{dt} = \frac{\dot{m}_{in}(h_{in}-h_{out})+q_{rad}-m_m \cdot c_m \left[\left(\frac{\partial q_s}{\partial T_m} \right)^{-1} \cdot \frac{dq_{rad}}{dt} + \frac{\partial T_s}{\partial p} \frac{dp}{dt} \right]}{\rho \cdot V + m_m \cdot c_m \frac{\partial T_s}{\partial h_{out}}} \quad (17)$$

Table 3: Nomenclature for System State Differential Equation

| Symbol | SI Unit | Description |
|----------------|----------------------|--|
| h_{out} | [J/kg] | Specific enthalpy of steam at outlet |
| \dot{m}_{in} | [kg/s] | Mass flow rate of steam from inlet to outlet |
| h_{in} | [J/kg] | Specific enthalpy of steam at inlet |
| q_{rad} | [J/s] | Heat flux through radiation from furnace firing |
| c_m | [J/(kg · K)] | Specific heat capacity of tube metal |
| m_m | [kg] | Mass of tube section |
| q_s | [J/s] | Heat flux from tube metal inner surface to steam |
| T_m | [°C] | Temperature of tube wall |
| T_s | [°C] | Temperature of steam |
| p | [Pa] | Pressure of steam |
| ρ | [kg/m ³] | Density of steam |
| V | [m ³] | Volume of inner tube section and steam |

The time derivative of this state, $\frac{dh_{out}}{dt}$, is firstly proportional to the steam flow rate, \dot{m}_{in} , multiplied by the state enthalpy, h_{out} , subtracted from the incoming steam enthalpy h_{in} . Each superheater subsection will connect to the previous through this h_{in} term. This first term is non-linear, since the steam flow rate is time variable and part of the state representation. A Fuzzy controller could handle this type of non-linearity. Another way of compensating for it through model manipulation will be investigated in a later section.

The q_{rad} term is in actual fact a function that depends on the nature of heat transfer, i.e. radiant, convective or a combination of these. This can become difficult to model. It has not been quantified, for the Komati Power Station boilers, how much of each type of heat transfer is taking place at the superheater stage. Additionally, firing rate changes could result in a shift in the general combustion location and therefore affect this ratio.

The main difference in the two types, without going into too much detail, is that radiant heat emanating from combustion is not strongly dependent on the tube surface metal temperature, rather on the emissivity and the temperature, to the power of 4, of the flue gasses and associated particles as seen [33, p. 94] referring to blackbody radiation. Convective heat transfer would be a product of a heat transfer coefficient, surface area, and the temperature difference between

Chapter 3 System Identification and Modelling

particles in the flue gasses and ash deposit on the tube surface. Convective heat transfer also exists between the flue gasses and the ash. This however also implies further dynamics between the ash layer, tube surface and the actual outer to inner tube conductive heat transfer.

There is also radiative heat emission from the ash layer to the flue gasses and surrounding tubes, in turn only dependent on its own surface temperature. The inner layers can be simplified to pure conductive heat transfer due to poor ash transparency on the top layer as discussed in [38]. A complicating factor is that large portions of radiative heat will be reabsorbed by neighbouring tubes directly or indirectly through the flue gasses and would not be considered real losses.

Important parameters like ash thickness, composition, tube coverage, corrosion, removal rate and efficiency are all essentially unmeasured and unknown. This is an entire field of research on its own as discussed thoroughly in [38] and [39]. From these fields we can gather the following information to aid understanding of the system dynamics, whether modelled or not:

- Superheater sections are especially susceptible to ash build-up, due to being the components with the highest metal temperatures.
- The ash-build-up itself will significantly affect the surface metal temperature and heat transferred to the steam.
- Komati Power Station is designed to burn coal with a high ash content, which will increase the rate of fouling.
- Heat transfer can be as much as halved after a few hours of operation and fouling.

This topic is too broad to cover in this research effort. Future work may wish to focus on adjusting the influence of heat transfer based on ash build-up and removal. There are research efforts that have defined heat transfer equations based on ash build-up [40]. There is also research material based on the removal of ash deposits and its effectiveness [41]. For this research project it is noted that these articles reinforce the need for robust control, since the model will not be able to reflect changes in the overall heat transfer accurately. The actual activity of sootblowing is generally done in sections, so that it is not too disruptive to the steam cycle and instantaneous changes in heat transfer.

Chapter 3 System Identification and Modelling

Modelling this entire process would result in many additional process states. It is not believed that these additional states would accurately model higher order dynamics in detail with the currently available measurements. Linearization is therefore favoured as part of a pre-filter to produce a best approximation of the final energy transfer q_{rad} into the system. For this reason, and the fact that linearization constants would be determined by using regression rather than theoretical approximation, no distinction between the types of heat transfer is made. This furnace input energy would also be a calculation from other measurable parameters like mill and fuel oil firing and are also subject to error and bias. Modelling the exact dynamics of heat transfer would bear no fruit, without equally accurate process measurements.

The last two inputs are $\frac{dq_{\text{rad}}}{dt}$ and $\frac{dp}{dt}$ where p is the steam pressure, assumed to be time varying but equal from inlet to outlet. These terms affect the system enthalpy based on steam table properties and heat conduction through the tube metal and will be linearized around the operating point.

The terms under the line, $\left(\rho \cdot V + m_m \cdot c_m \frac{\partial T_s}{\partial h}\right)$, have been assumed to be constant for now. It is known that the steam density ρ will change if steam is superheated, and that $\frac{\partial T_s}{\partial h}$ is a function of the steam table and our current operating point. These will be linearized as well, to reduce the model order and complexity. It is rather a large assumption to make, but the rationale behind this decision is that the current system functions without modelling these terms, therefore the model should at least be good enough for control purposes at the same level as the current controller. Only practical evaluation will be able to tell if this assumption is fair. Furthermore, the researcher believes that through feedback control and compensation for the major non-linearities, e.g. steam flow rate dependence in the system, these assumptions may not affect control system accuracy significantly.

The equation can now be broken down to a form that will be used for the system's state-space representation.

$$\dot{h}_i = -\frac{k_{\dot{m}_{\text{in}}}}{k_{1_i}} h_i + \frac{k_{\dot{m}_{\text{in}}}}{k_{1_i}} h_{i-1} + \frac{k_{\dot{m}_{\text{in}}}}{k_{1_i}} \left(\frac{q_{\text{rad}}}{k_{\dot{m}_{\text{in}}}}\right) + \frac{k_{3_i} \cdot k_{\dot{m}_{\text{in}}}}{k_{1_i}} \left(\frac{\dot{q}_{\text{rad}}}{k_{\dot{m}_{\text{in}}}}\right) + \frac{k_{4_i} \cdot k_{\dot{m}_{\text{in}}}}{k_{1_i}} \left(\frac{\dot{p}}{k_{\dot{m}_{\text{in}}}}\right) \quad (18)$$

$$\text{with } k_{1_i} = \rho \cdot V + m_m \cdot c_m \frac{\partial T_s}{\partial h}; \quad k_{\dot{m}_{\text{in}}} = \dot{m}_{\text{in}}; \quad k_{3_i} = -m_m \cdot c_m \left(\frac{\partial q_s}{\partial T_m}\right)^{-1}; \quad k_{4_i} = -m_m \cdot c_m \frac{\partial T_s}{\partial p} \quad (19)$$

Chapter 3 System Identification and Modelling

The constants in (19) will be linearized at the operating point for each superheater. The main steam flow rate is assumed to be slowly varying in reference to other process dynamics for most operating conditions. For the purpose of developing the model it is considered to be constant. The steam flow rate will be the same for all subsections. Further it can be noted that the q_{rad} , \dot{q}_{rad} and \dot{p} terms were normalised against the steam flow rate by multiplying in $\frac{k_{\dot{m}_{\text{in}}}}{k_{\dot{m}_{\text{in}}}}$. After refactoring, all the constants to the input terms now have a common factor $k_{\dot{m}_{\text{in}}}$. This will be used as an advantage to compensate for the non-linearity associated with changes in main steam flow rate, \dot{m}_{in} . In section 4.1 it is shown that the model, once taken into the digital time domain, may be constructed independently of the various main steam flow rates. This however requires that the inputs, except for h_{in} , are normalised with respect to the steam flow rate. For this reason, the \mathbf{B}_m matrix is also scaled to achieve this result.

The state space model of the lumped sections can be represented by state space matrixes (20), (21) and (22). The first subsections will start from state equation \dot{h}_1 with $h_0 = h_{\text{in}}$ the actual input enthalpy to the entire superheater. Subsequent subsection state equations, e.g. \dot{h}_i reference the state variable of the previous subsection, h_{i-1} , as its input. The last state will be the superheater final output state. Together these are shown for a generic number of subsections, N.

$$\mathbf{A}_{m \ N \times N} = \begin{bmatrix} -\frac{1}{k_{1N}} & \frac{1}{k_{1N}} & 0 & & 0 & 0 & 0 \\ 0 & -\frac{1}{k_{1N-1}} & \frac{1}{k_{1N-1}} & \dots & 0 & 0 & 0 \\ 0 & 0 & -\frac{1}{k_{1N-2}} & & 0 & 0 & 0 \\ & \vdots & & \ddots & & \vdots & \\ 0 & 0 & 0 & & -\frac{1}{k_{13}} & \frac{1}{k_{13}} & 0 \\ 0 & 0 & 0 & \dots & 0 & -\frac{1}{k_{12}} & \frac{1}{k_{12}} \\ 0 & 0 & 0 & & 0 & 0 & -\frac{1}{k_{11}} \end{bmatrix} \cdot k_{\dot{m}_{\text{in}}} \quad (20)$$

Chapter 3 System Identification and Modelling

$$\mathbf{B}_{m \ N \times 4} = \begin{bmatrix} 0 & \frac{1}{k_{1N}} & \frac{k_{3N}}{k_{1N}} & \frac{k_{4N}}{k_{1N}} \\ & \vdots & & \\ 0 & \frac{1}{k_{12}} & \frac{k_{32}}{k_{12}} & \frac{k_{42}}{k_{12}} \\ \frac{1}{k_{11}} & \frac{1}{k_{11}} & \frac{k_{31}}{k_{11}} & \frac{k_{41}}{k_{11}} \end{bmatrix} \cdot k_{\dot{m}_{in}} \quad (21)$$

$$\mathbf{c}_m = [1 \ 0 \ \cdots \ 0]; \quad \mathbf{d}_m = [0 \ \cdots \ 0] \quad (22)$$

$$\mathbf{h} = \begin{bmatrix} h_N(t) \\ \vdots \\ h_2(t) \\ h_1(t) \end{bmatrix} \text{ and } \mathbf{u}_m = \left[h_{in}(t) \quad \frac{q_{rad}(t)}{k_{\dot{m}_{in}}} \quad \frac{\dot{q}_{rad}(t)}{k_{\dot{m}_{in}}} \quad \frac{\dot{p}(t)}{k_{\dot{m}_{in}}} \right]^T \quad (23)$$

These parameters are used to define the final model equations shown in (24) and (25) for a model of a generic order. The input matrixes are shown in (23).

$$\dot{\mathbf{h}} = \mathbf{A}_m \cdot \mathbf{h} + \mathbf{B}_m \cdot \mathbf{u}_m \quad (24)$$

$$h_{c_{out}}(t) = \mathbf{c}_m \cdot \mathbf{h} + \mathbf{d}_m \cdot \mathbf{u}_m \quad (25)$$

Table 4: Nomenclature continuous state space model

| Symbol | SI Unit | Description |
|--|---------|--|
| $\mathbf{A}_m, \mathbf{B}_m, \mathbf{c}_m, \mathbf{d}_m$ | | Continuous time state space matrix variables |
| \mathbf{h} | [J/kg] | Generic continuous time model enthalpy states |
| $h_{in}(t)$ | [J/kg] | Specific enthalpy of final superheater steam inlet |
| $h_{c_{out}}(t)$ | [J/kg] | Continuous time model specific steam enthalpy |
| $k_{\dot{m}_{in}}$ | | Linearization factor based on \dot{m}_{in} |
| N | | Specific number of superheater subsections |
| $p(t)$ | [Pa] | Pressure of final superheater steam |
| $q_{rad}(t)$ | [J/s] | Heat flux through radiation from furnace firing |
| \mathbf{u}_m | | Continuous state space model inputs |

As mentioned before, to simplify the model, it will still be assumed that energy transfer between the tube wall and furnace is independent of the tube wall temperature. A first order approximation of energy transferred to the system is used rather than a model based on flue gas and metal temperatures. During final system identification, all three levels where fuel is admitted into the furnace, will be linearized separately. The top mill is closer to the final superheater and is commonly spoken of as a temperature mill, due to its energy contribution to superheat steam. The bottom mill conversely is commonly spoken of as a pressure mill, due to its energy contribution to the furnace wall tubes that circulate the boiler drum water. The middle mill is a combination of both. System identification will be done by means of iterative least squares regression to datasets

of live plant data to fit the chosen model. This is due to the fact that responses cannot be tested in isolation and step responses can cause furnace instability, which will not be allowed.

The number of final superheater divisions is arbitrary and will be established during system identification. The model order and training will determine if sufficient dominant system dynamics are captured.

3.3. Model Parameter Determination

From this base model the final model, was fine-tuned based on 38 datasets (19 scenarios each for the left-hand side and right-hand side of the system) of plant data for around a 2-hour period containing various types of system disturbances. Initially an arbitrary starting point of $N = 4$ superheater subsections were chosen as this was expected to be sufficient to capture the highest order dynamics. System disturbances included: Mill trips and reintroduction on each of the three firing levels, pressure cycling and spiking behaviour, two full light-ups, open loop responses with no applied spray water, a shutdown sequence, and rapid steam flow rate changes. All these scenarios were chosen to include as many types of disturbances as possible. This ensure that between the scenarios enough statistically independent responses could be gathered. This is largely due to system complexity and the inability to perform significant step responses on the live plant for purposes of model identification.

Tuning was done by iteratively stepping plant modelling parameters and reducing the square of the error between all scenarios simultaneously, to ensure statistical independence. This includes pre-filter parameters for the firing input to compensate for the response of the tube mills and fuel oil burners. Only a second order response was necessary to capture the plant dynamics accurately when including measured process parameters of steam flow rate, pressure firing and their derivatives. Higher order disturbances exist, but are considered to be noise for the purposes of modelling as it could not be explained by known and measured disturbances. A state observer was also introduced in the model to ensure that dynamics are captured while preventing offsets from skewing the sum of squared errors. The state observer was chosen to have a response sufficiently slower than the plant model to ensure it does not adversely interfere in model tuning and dynamic response. The observer used is discussed in more detail in section 3.5.

Chapter 3 System Identification and Modelling

The continuous time state space model used at full load condition is shown below. This model was taken to the digital time domain after initial parameter estimation based on a few scenarios. This assisted in determining appropriate choices for the number of subsections to be used, which determines the model order. With the final value of 2 subsections chosen, the model was converted to the digital domain using a zero-order hold approximation, and further optimised across all 38 datasets in the digital domain. This included finding appropriate parameters for the firing prefilter. The final discrete state space model representation is discussed in section 3.6. These state space model equations are repeated here for completeness along with the state space matrixes:

$$\mathbf{A}_{m\ 2 \times 2} = \begin{bmatrix} -0.01728 & 0.01728 \\ 0 & -0.02017 \end{bmatrix} \quad (26)$$

$$\mathbf{B}_{m\ 2 \times 4} = \begin{bmatrix} 0 & 0.00864 & 2.453 & 1.025 \\ 0.02017 & 0.01008 & 2.862 & 1.653 \end{bmatrix} \quad (27)$$

$$\mathbf{c}_m = [1 \ 0] \quad (28)$$

$$\mathbf{d}_m = [0 \ 0 \ 0 \ 0] \quad (29)$$

For reference from section 3.2.2.

$$\mathbf{h}_m = \begin{bmatrix} h_2(t) \\ h_1(t) \end{bmatrix} \text{ and } \mathbf{u}_m = \begin{bmatrix} h_{in}(t) & \frac{q_{rad}(t)}{k_{\dot{m}_{in}}} & \frac{\dot{q}_{rad}(t)}{k_{\dot{m}_{in}}} & \frac{\dot{p}(t)}{k_{\dot{m}_{in}}} \end{bmatrix}^T \quad (23)$$

$$\dot{\mathbf{h}} = \mathbf{A}_m \cdot \mathbf{h}_m + \mathbf{B}_m \cdot \mathbf{u}_m \quad (24)$$

$$h_{c_{out}}(t) = \mathbf{c}_m \cdot \mathbf{h}_m + \mathbf{d}_m \cdot \mathbf{u}_m \quad (25)$$

Continuous-time Superheater Model

Table 5: Nomenclature for Continuous Time State Space Model

| Symbol | SI Unit | Description |
|--|---------|---|
| $h_{c_{out}}$ | [J/kg] | Continuous time model specific steam enthalpy |
| \dot{m}_{in} | [kg/s] | Mass flow rate of steam from inlet to outlet |
| $k_{\dot{m}_{in}}$ | | Linearization factor based on \dot{m}_{in} |
| h_{in} | [J/kg] | Specific enthalpy of steam at inlet |
| q_{rad} | [J/s] | Heat flux through radiation from furnace firing |
| \dot{p} | [Pa/s] | Pressure of steam rate of change |
| $\mathbf{A}_m, \mathbf{B}_m, \mathbf{c}_m, \mathbf{d}_m$ | | Continuous time state space matrix variables |
| \mathbf{h}_m | [J/kg] | Continuous time model enthalpy states |

3.4. Firing Prefilter

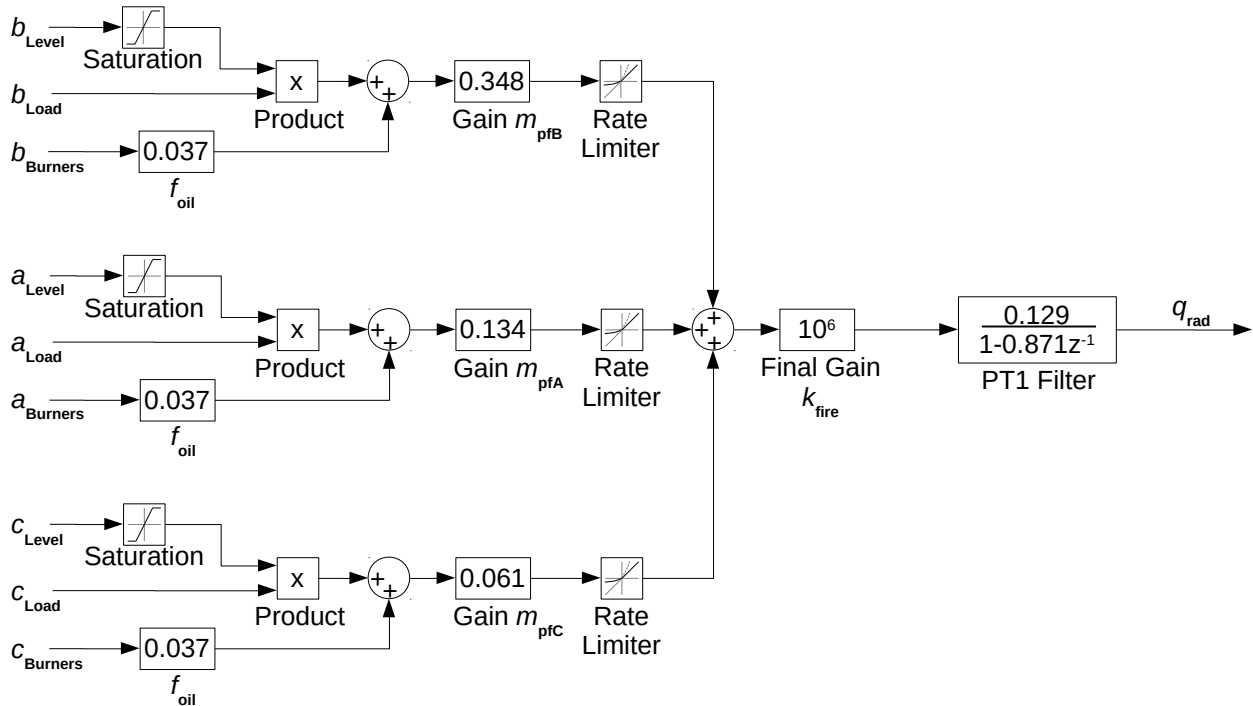


Figure 10: Prefiltered Firing Input Calculation (15 second sample time)

Up to this point not much has been said of the firing input and the prefilter that has been used to calculate the q_{rad} input. There are so many dynamics, that affects especially tube type mills, that it would be an entirely separate project to model them accurately. For this reason, the researcher has used his own experience in the behaviour of these mills to construct a prefilter and has left it to the model identification process to determine what factors best fit the solution. Similar to model fitting, the actual heat energy transferred to the steam was fitted to the prefilter response based on the 38 datasets used for training. Due to the variability in the combustion process and milling plant, fitting over all datasets simultaneously would produce an average representation of the combustion process with significant damping by the final low pass filter. With more reliable and accurate combustion process measurements, the heat energy transferred to the steam can surely be modelled with a much higher accuracy in future. An explanation of the prefilter follows.

Chapter 3 System Identification and Modelling

Table 6: Nomenclature for Firing Prefilter

| Symbol | Value | SI Unit | Description |
|---------------|-----------|--------------------|---|
| f_{oil} | 0.036949 | | Fuel oil burners firing gain |
| l_{sat1} | 56.957 | [%] | Saturation limiter upper limit for a unity output |
| l_{sat0} | 21.547 | [%] | Saturation limiter lower limit for a zero output |
| r_{limit} | 0.0027856 | $[J \cdot s^{-2}]$ | Rate limiter allowed value change per second |
| τ_{fire} | 108.6440 | [s] | Time constant for firing rate PT1 low pass filter |
| k_{fire} | 10^6 | | Final firing gain |
| m_{pfA} | 0.13394 | | Row A pulverised fuel burner relative firing gain |
| m_{pfB} | 0.34832 | | Row B pulverised fuel burner relative firing gain |
| m_{pfC} | 0.060567 | | Row C pulverised fuel burner relative firing gain |
| q_{rad} | | [J/s] | Heat flux through radiation from furnace firing |
| a_{Level} | | [%] | Mill A fuel level measurement |
| b_{Level} | | [%] | Mill B fuel level measurement |
| c_{Level} | | [%] | Mill C fuel level measurement |
| a_{Load} | | [kg/s] | Mill A coal loading rate |
| b_{Load} | | [kg/s] | Mill B coal loading rate |
| c_{Load} | | [kg/s] | Mill C coal loading rate |
| $a_{Burners}$ | | | Mill A fuel oil support burners in service |
| $b_{Burners}$ | | | Mill B fuel oil support burners in service |
| $c_{Burners}$ | | | Mill C fuel oil support burners in service |

The overall heat energy transferred to the steam is calculated by the prefilter at a sample rate of 15s. Mill firing is modulated by a factor, dependent on the level in the coal mill. At a certain level, the mill is seen as at capacity and the response is not modulated. There is also a cut-off level, where the mill is considered not to produce any significant energy into the boiler and still needs to be filled to normal working level. In between these points the modulation ramps up linearly. This is a simplification of what is seen on the real plant. It is based on the fact that the coal has a residence time before being fine enough to be classified and transported out of the mill. It is therefore usual that the mill level has some relationship as to what the load output can be, within some variation. Coal enters the mill as various sized chunks, some as large as a few centimetres, and is pulverised to a few microns to form a powder. Classification is a mechanical process where only sufficiently pulverised coal, by virtue of its size, will be able to be picked up by the primary air through the mill and is passed through a classifier that can further distinguish and be adjusted for a certain Pulverised Fuel (PF) size. The classifier essentially uses an adjustable cyclone effect to reject particles that are too large, back to the mill.

Each level of firing is limited by a ramp rate. This, similar to the level modulation, ensures that the effect of the mill reaching the new desired working level is captured. It captures this response associated with the mill reaching the new rate as well as some heat transfer transients in the furnace. This is represented as a ramp rate rather than a first order filter due to coal needing to dry out and have the required residence time in the mill before being able to be transported into the furnace. This process does not scale linearly by just adding more coal and air. The gain of each physically separated level of firing differs as firing rows are arranged from top, middle, to bottom for codified mills B, A, & C. Higher mills contribute more to temperature pickup higher up in the furnace, having less exposure to risers and more toward superheaters. This mill therefore has a higher gain. Lower mills contribute more to raise and maintain pressure, due to more exposure to risers and less toward superheaters. This mill therefore has a lower gain.

The sum of each level of firing is then also passed through a first order filter. This compensates for the combustion process and energy transfer to stabilise. The parameters obtained through optimisation is given in *Table 6*.

3.5. Iterative Least Squares Regression

Raw data gathered for all scenarios were sampled from the system at a 5 sec sample interval. Due to model dependence in steam flow rate, modelling was initially performed by computing the model matrixes at each sample step as the steam flow rate changed. This was time consuming as optimised library functions could not be utilised to find the system response. It also means more computations to be done, since sample time is not increased when system dynamics slow down.

An initial estimated model was obtained that could be trained once the base assumptions about its required order and input variables could be established. This is done due to the fact that over training the model on a single scenario would not result in a generally applicable model. Simultaneous training on all scenarios is required, since a correlation between input parameters in one scenario will not be present in all scenarios. In different modes of operation, different correlations can arise. A few examples are listed below to illustrate:

- The main steam flow rate and pressure become correlated if the unit is set to control pressure through limited load regulation.

Chapter 3 System Identification and Modelling

-
- The main steam pressure and the total mill firing rate can correlate during normal operation if the unit is set to control pressure through the regulation of mill firing.
 - All mill firing signals correlate with each other once placed on automatic control due to following identical setpoints.

Training the initial estimate model was mostly done through iterative tuning interventions to remove the largest model deviations. Code for the iterative tuning of the single case and eventual least squares tuning can be found in *Appendix B.1* and *Appendix B.2*. This was first done per scenario for a few key scenarios. This resulted in an estimate model representation that was manually inspected to remove correlated tuning factors. A very prominent factor that required manual intervention was the heat energy contribution from each mill m_{pfA} , m_{pfB} , and m_{pfC} . These factors are naturally very closely related and mills are also mostly operated with identical command signals. Although dynamically very related, they have a very different heat energy contribution to the superheater due to their physical location in the boiler.

Since all scenarios were not used for training simultaneously the average was still only an initial estimation. It supplied sufficient information to justify selection of the number of subsections and allow for further tuning through iterative least square regression. A cost function is used to determine the sum of square model errors from the training data. The sum is also normalised by dividing by the number of samples. This is essentially the standard deviation of the modelled final steam temperature ($h_{m_{out}}$ converted to temperature in °C, y_{model}) from the training data final steam temperature ($y_{measured}$). Initial samples of stable operation and model settling are also ignored in the sum. This is to ensure that slight errors in capturing initial conditions for each dataset has time to settle. All scenario data included a sufficient period of stable starting data, before the start of any disturbances. This cost function J provides the standard model deviation from the training data.

$$J = \frac{\sqrt{\sum_{i=1}^n (y_{measured}(i) - y_{model}(i))^2}}{n}$$

with n = sample count

(30)

The model that will be developed will be of the state space model shown in section 3.2.2 taken to the digital domain.

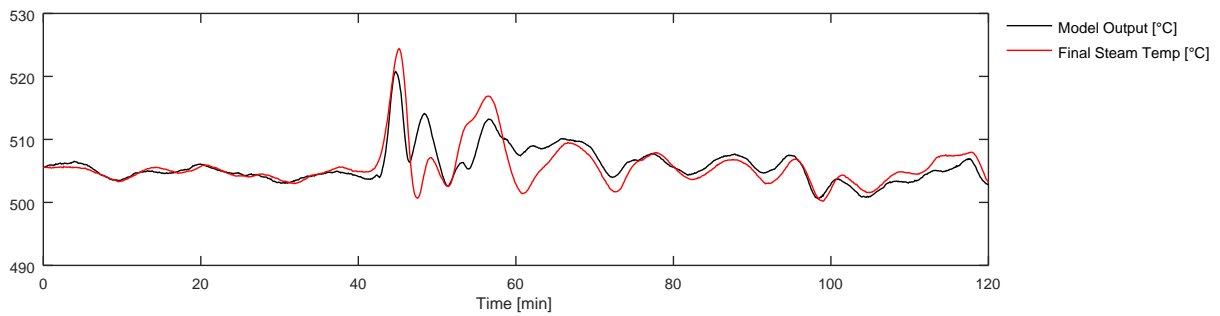
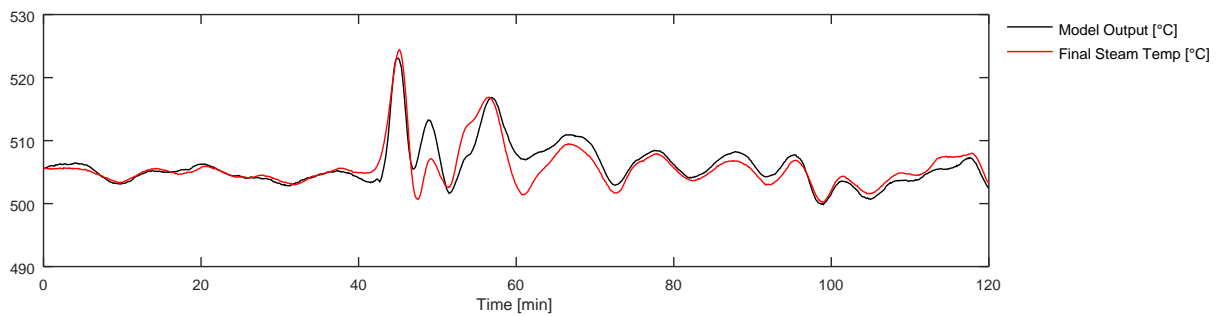
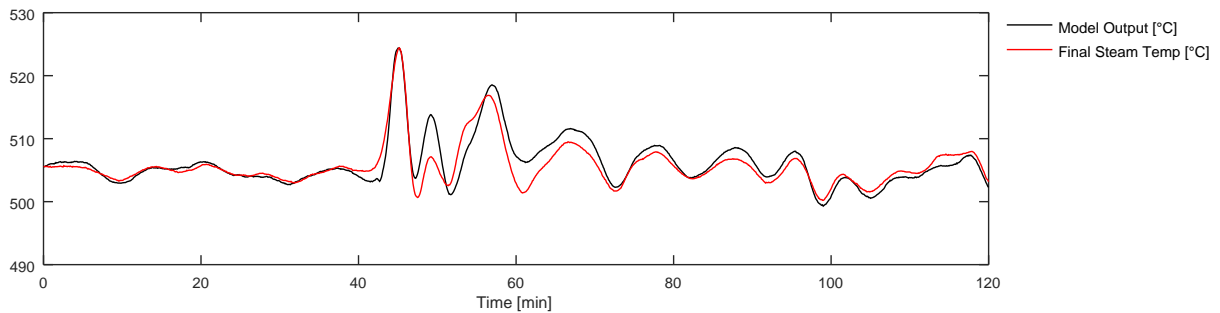
Chapter 3 System Identification and Modelling

The final model form developed is shown at the end of this chapter in section 3.6 for reference. The model lumps the inner control loop in with the model representation. The model inputs are the enthalpy of the steam entering the final superheater, along with the normalised firing prefilter inputs, and normalised pressure derivative input. The model outputs the final superheater steam enthalpy which is converted to temperature for display and plotting purposes. In the next few paragraphs some model assumptions are discussed including the number of subsections chosen to represent the final superheater. From section 3.5.1 onward the model is evaluated after being fitted. The results are all of a single model designed to be an aggregate best fit for all scenarios.

Figure 11 and *Figure 12* show that the model error is not significantly affected until $N=1$ which can be seen from the model response and a cost function increase of 26 %. The number of stages, N , was chosen as 2. The benefit gained by choosing a higher order is minimal w.r.t the cost function, this choice will also provide a reduction in the model order. It should be stated that the cost is not the only measure used for evaluation purposes. A first order model simply does not capture the necessary dynamics and does not accurately represent the thermal inertia in the system, even when fine tuning the first order model. With a 2nd order model the disturbance peaks aligned much better. This can be intuitively justified as well as described in section 3.2. With $N=1$ this distinction cannot be made while tuning the model, since both the disturbance and the input will affect the first and only subsection equally. Having at least 2 subsections allows firing to be used as a disturbance input to both subsections while spraywater inlet will only be an input to the first subsection. This will then allow distinguishing their response during tuning.

The figures below show the three cases with $N = 1, 2$ and 3, as well as the process measurements for the scenario tested. The black trend is the model output while the red is the actual measured output, i.e. the final steam temperature.

Chapter 3 System Identification and Modelling

Figure 11: Model Response $N=1$, $J=2.37$ °CFigure 12: Model Response $N=2$, $J=1.88$ °CFigure 13: Model Response $N=3$, $J=1.81$ °C

In the sections to come the following colour scheme will be maintained unless otherwise stated: The steam flow rate (cyan), final superheater inlet temperature (black), final steam outlet (red), steam pressure (green), and fuel firing (levels: B=red, A=magenta and C=blue) for a specific test scenario will be shown by solid trends. In this scenario the mill firing on all levels are identical (solid blue). Dotted lines indicate fuel oil support on the corresponding level indicated by the colour (red dotted graph for mill B in this case). In *Figure 14* below only oil burners on level B

Chapter 3 System Identification and Modelling

were used while all mills fired in coordinated mode and are shown by a single trend. Other event sequences that were used for optimisation will be discussed in more detail later in this section.

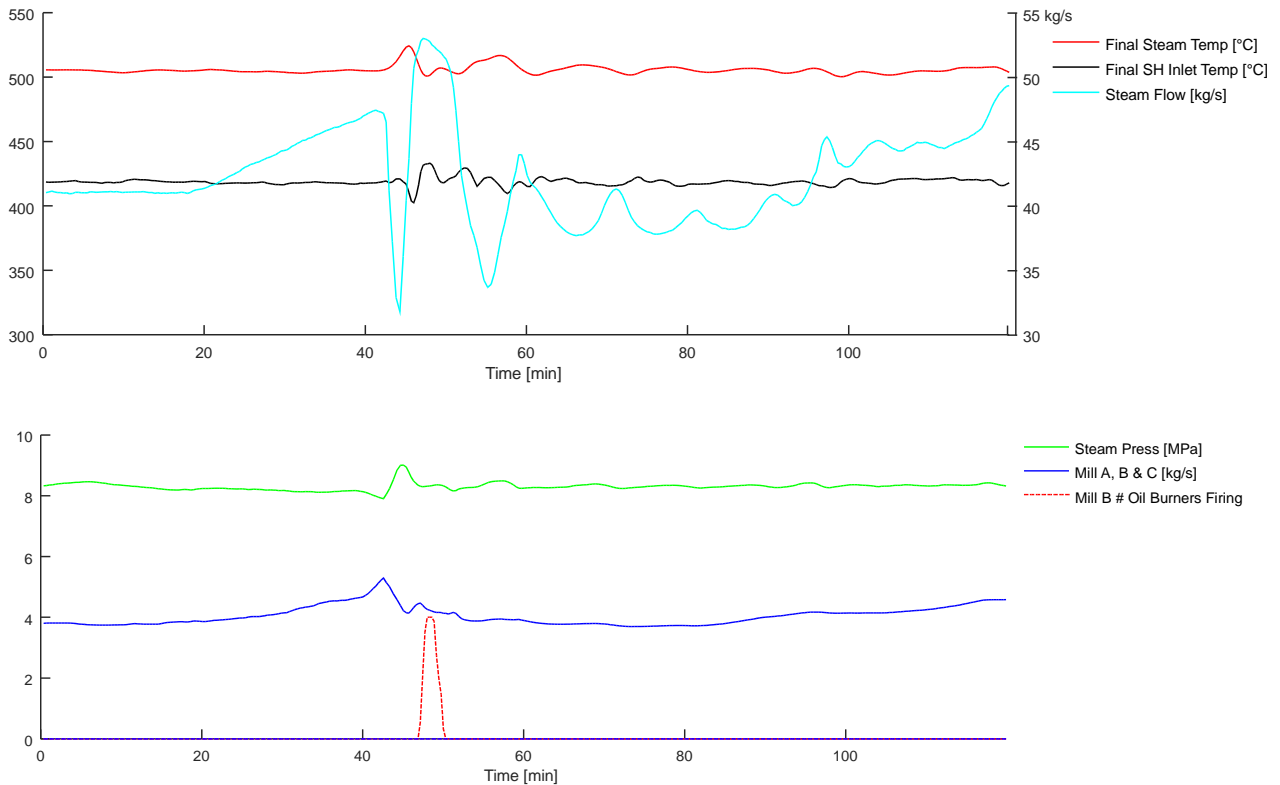


Figure 14: First Model Estimation Process Measurements

The iterative least squares regression modelling process would require utilisation of control libraries that would significantly speed up minimisation standard model deviation. To do this, the raw data was resampled at the variable sample rate, dictated by the steam flow rate, by taking the average between sample points and the timestamps recorded. The identified discrete model is constant, but with a variable sample time. The final model can be seen in 3.6.

The sum of squared errors is affected by steady state error offsets that would skew tuning in favour of reducing steady state components for every sample, as opposed to areas of quicker dynamics that only affect the sum for a few samples. To remove this effect an observer was added to the system that would reduce estimation error when comparing the model response to measured data over the steady state.

Chapter 3 System Identification and Modelling

In the process of model identification through iteration, changes will occur to the state space representation. The observer can only be calculated based on the state space model at that specific iteration, and recalculated for every iteration of regression. The initial model before the first iteration was based on construction from estimate physical properties for equation (17). The observer gains were calculated based on [26] with an $\alpha=0.1$ as the predefined radius in the unit circle.

In [26] the observer gains are calculated recursively using a Kalman filter. Although this can be precalculated, for the purpose of least squares regression, the model will change with each regression step. To this end the observer gains are recalculated with every regression step to within a specified radius from the unit circle. This radius is chosen to allow a sufficiently slow settling of the error term. This assist the model to correct for steady estimation error that skews the cost function, while not completely damping the higher frequency dynamic responses.

To pre-calculate the observer gains before each regression step, the following iterative equation (31) was performed and (32) to calculate \mathbf{k}_{ob} . To ensure the closed loop observer poles are assigned inside the unit circle, at radius α , it is substituted into the equation.

$$\mathbf{P}(i+1) = \mathbf{F}\alpha \left\{ \mathbf{P}(i) - \mathbf{P}(i)\mathbf{G}^T\alpha(\Gamma + \mathbf{G}\alpha\mathbf{P}(i)\mathbf{G}^T\alpha)^{-1}\mathbf{G}\alpha\mathbf{P}(i) \right\} \mathbf{F}^T\alpha + \Theta \quad (31)$$

$$\mathbf{k}_{ob}(i) = \mathbf{F}\alpha\mathbf{P}(i)\mathbf{G}^T\alpha(\Gamma + \mathbf{G}\alpha\mathbf{P}(i)\mathbf{G}^T\alpha)^{-1} \quad (32)$$

This came with a choice for Γ and Θ covariance matrix shown below:

$$\Gamma = 4338.4 \quad \text{and} \quad \Theta = \begin{bmatrix} 4338.4 & 0 & 0 \\ 0 & 4338.4 & 0 \\ 0 & 0 & 4338.4 \end{bmatrix} \quad (33)$$

The augmented representation of the model, discussed in section 4.2.1, was used during iteration. The augmentation does not change model behaviour, but does increase the model order by one. The resultant three observer gains varied with each iteration, as one example, the final model obtained resulted in the following observer gains:

$$\mathbf{k}_{ob} = [8.5025 \cdot 10^{-5}, 4.9131 \cdot 10^{-6}, 1.0175 \cdot 10^{-2}] \quad (34)$$

The observer gains are implemented in the augmented model (4.2.1), in the following form.

$$\hat{\mathbf{x}}(k+1) = \mathbf{F} \cdot \hat{\mathbf{x}}(k) + \mathbf{G} \cdot \Delta \mathbf{u}(k) + \mathbf{k}_{ob}(y(k) - \mathbf{C} \cdot \hat{\mathbf{x}}(k)) \quad (35)$$

Chapter 3 System Identification and Modelling

To explain this further a few things were taken into consideration. The model will be prone to developing a steady state offset compared to the training data. This is because the events themselves are not short controlled step changes. In most cases the scenarios represent several disturbances across different operating ranges. This is due to the inability to do step change measurements on a live unit. Large and varying disturbances may also settle over a large period of time. This observer should not be confused with the actual observer that will be designed for control purposes. The steady state offset should also not be confused with controller steady state offset. The control system will be designed to control with zero steady state offset regardless. The observer is purely used during tuning and all future scenario analysis will show the results without the state observer.

Below, the same result as from *Figure 12* for a second order model, is repeated, but the observer is removed to show the effect in *Figure 15*. It is clear that the model is still quite accurate even in the final stages of the graph. Visually it is definitely confirmed as being a steady state error that accumulates from some modelling error around minute 60, which remains for the remainder of the response. Should the steady state error have been included in the cost function, the tuning process would have favoured reducing the steady state offset at the cost of the, generally very good, dynamic response. Any steady state offsets that remain after tuning would be expected to be removed through the control feedback loop. In the following section, 5 scenarios will be discussed in more detail. The first scenario is a continuation of the events depicted in *Figure 14*. In those discussions it will be clear that modelling error has significantly reduced from what is seen in *Figure 15* through the iterative tuning process described next.

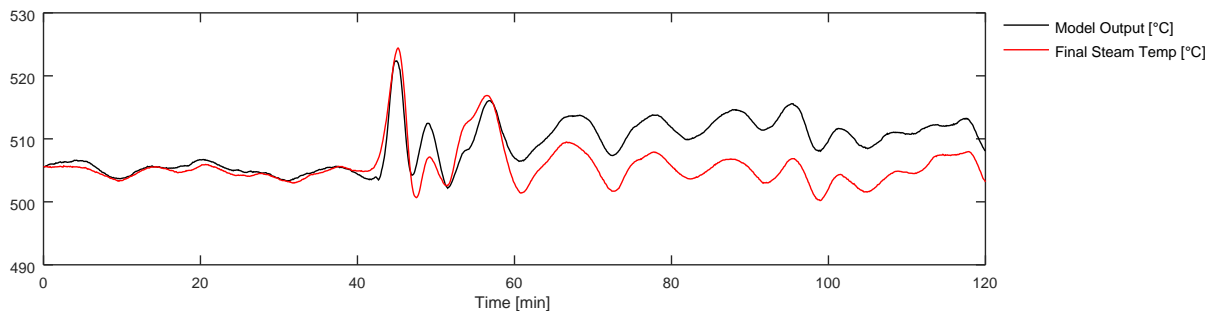


Figure 15: Steady State Modelling Error

Chapter 3 System Identification and Modelling

The iteration process consisted of tuning the model parameter constants with multiplication factors. This was initially done by tuning only a single parameter at a time, but sequentially and maintaining the direction of the change until the sum of squares worsened again. Once the reduction in the sum was becoming insignificant and slow, a random element was added that would make slight manipulations to more than one parameter at a time and by a random amount. This approach achieved another reduction in the sum of square errors and helped to get the model out of local minima, due to the complex interaction of parameters in the model.

For each iteration of regression, all 38 datasets will be run through the same model shown in 3.6. The model is however trained in its augmented form, but this does not change its behaviour. The result of the cost function (30) for each of the training scenarios are summed. With each iteration, the model parameters are tuned, and the iteration is only saved if the total cost function over all scenarios has decreased.

The modelling error of a few of the models are discussed below. The majority of the remaining model errors are very likely as a result of a lack of sufficient process measurements to estimate a complex process like combustion. A disturbance signal was then calculated, in the form of a disturbance to the firing signal, that would reduce the remaining model error to zero and will be applied to the model when testing the controllers.

3.5.1. Sudden Steam Flow Rate Swing

This scenario is quite interesting, since it showcases events that occurred when the coordinated pressure controller on the unit had initiated rapid adjustments to the steam flow rate. This occurred in order to recover from a significant pressure drop that went unnoticed by the operator while adjusting the machine's loading. This is the same scenario used in the first part of section 3.5 explaining the iterative regression process. This scenario is analysed in more detail in this section, followed by 4 other scenarios.

The switch in the boiler's operating mode caused quite a few transients that the final steam temperature controller had to compensate for. There are two controllers that could potentially control for main steam pressure: The boiler pressure controller and the coordinated pressure controller. The first adjusts the firing rate to maintain main steam pressure. It is the primary means of control since it will settle to match the energy in with the energy taken out through

Chapter 3 System Identification and Modelling

steam generation. The coordinated pressure controller, when active, works in parallel with boiler pressure controller. It throttles the steam flow rate to preserve main steam pressure, while the boiler pressure controller is still increasing the firing rate. During start-up, this mode of operation is preferred until stable combustion can be achieved. In this event the coordinated controller was switched on as part of a protection function. Should the pressure not be maintained by the boiler pressure controller, the coordinated pressure controller is forced into operation. Switching over with an active main steam pressure error from setpoint is much more disruptive compared to running in this mode before operating activities are started. Such a switch can be due to plant defects, perturbations or operating errors, leading to the boiler pressure controller's inability to respond correctly to arrest significant pressure drops.

From the 20-minute mark in *Figure 16*, the steam flow rate increases. This is an operation by the desk operator to increase the load of the machine. The final steam pressure starts dropping as early as 5 minutes into *Figure 17*, and mill firing gradually increasing starting from about 15 minutes. The pressure drops off quite sharply at 40 minutes accompanied by a sharp increase in the mill firing rate. The boiler pressure controller fails in this instance to maintain the main steam pressure within 0.3 MPa of its setpoint. This is a trigger for the load controller to relinquish control over to a coordinated pressure controller.

The steam flow rate is controlled in cascade. The desired machine loading is first determined by the load or pressure coordinated controllers, depending on the mode of operation. This desired load is then sent through as the setpoint for the governor valve control of the steam throughput. In coordinated pressure control mode, the load will be decreased to recover the final steam pressure to setpoint. The controller's (PID) integral component state, through direct setting of its initial condition, is set to the current load while not in operation. This implies that, under steady state plant conditions, this mode of control can be selected by an operator and, with close to zero error, there will be a seamless transfer of control. In the scenario the coordinated pressure controller will immediately reduce load upon transfer due to the 0.3 MPa steam pressure error from setpoint.

Chapter 3 System Identification and Modelling

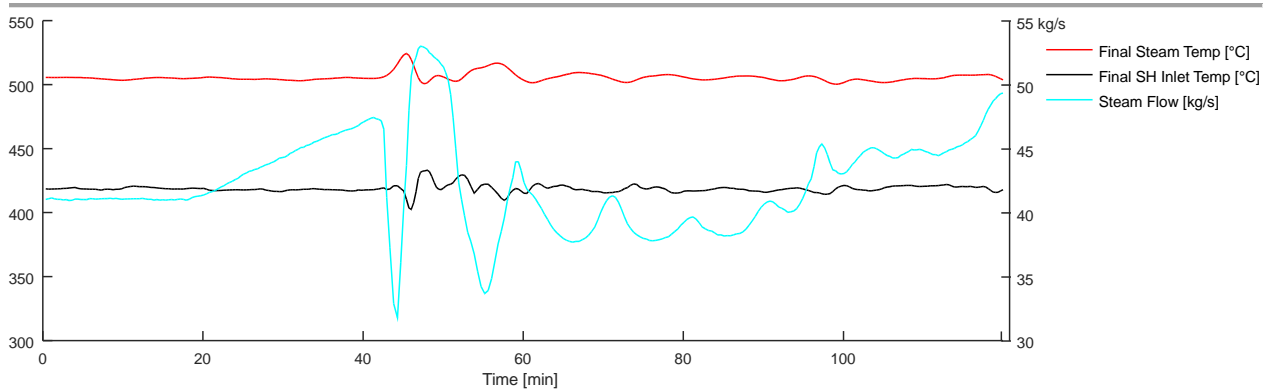


Figure 16: Sudden Steam Flow Rate Swing – Flow Rate and Superheater Inlet Temperature

Figure 16 above is repeated here from *Figure 14* for ease of reference. It is noticed that the superheater Inlet Temperature (black) responds quite late to the initial and largest steam flow transient response. This is partly due to its proportional nature that does not pre-empt the system response to the steam flow rate (cyan) and firing rate changes. During the periods of low steam flow rate, the system response time is also reduced. The response time improves once the steam flow rate increases again.

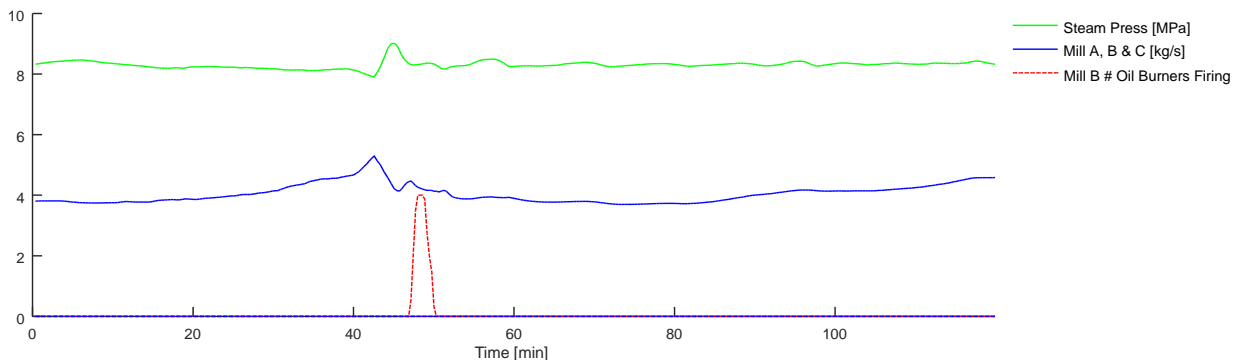


Figure 17: Sudden Steam Flow Rate Swing – Mill, Fuel Oil Firing and Steam Pressure

Figure 17 above is also repeated here from *Figure 14* for ease of reference. It shows the steam pressure's reaction (green) and changes in mill firing rates. Note that for each mill level a dotted line indicates fuel oil burners in service while the solid line indicates coal firing. In this scenario the unit was running in a coordinated mill mode. All mills are running at the same load and overlap in *Figure 17* as indicated by the legend. Unless stated otherwise by the legend, the following general colour arrangement is used: Magenta for mill level A, Red for mill level B, Blue for mill level C, solid lines for mill firing, and dotted lines indicating fuel oil burner firing.

Chapter 3 System Identification and Modelling

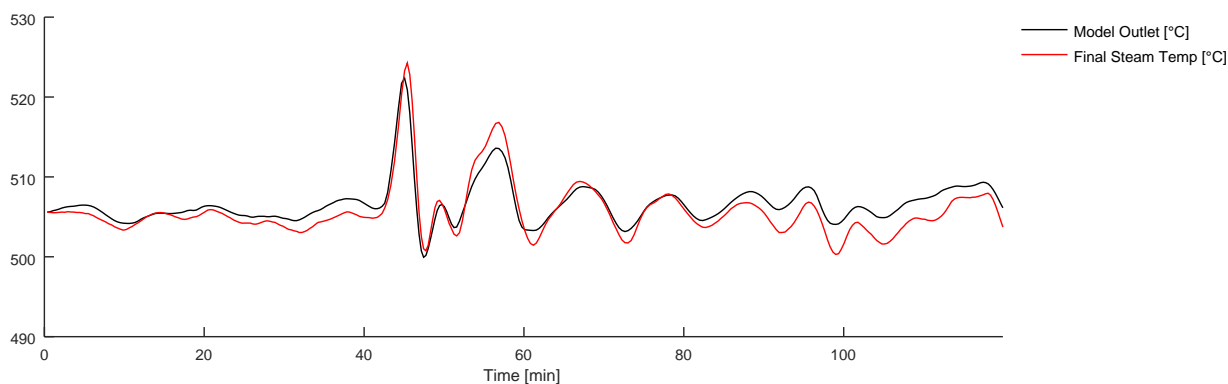


Figure 18: Sudden Steam Flow Rate Swing – Modelled Output

From *Figure 18* above it can be seen that there is a quite good dynamic relationship between the model output (black) and the actual final steam temperature (red). It must be noted that the response shown is without an active state observer. The observer is used during tuning, as described previously, and removed once tuning is completed so that the response can be analysed. This is the case for all following discussions.

Model optimisation was done with all scenarios simultaneously contributing to the cost function. This produces a good overall representation as opposed to fitting individual scenarios more accurately. There will be room for improvement based on any individual response being discussed. The model generally undershoots the actual response in amplitude with the first few peaks in this scenario. Despite this, the model has a standard deviation per sample of only 1.95 °C and a maximum absolute error of 5.6 °C. These measures might be less meaningful in later scenarios where steady state error accumulates. The highest and average absolute rate of model departure from measurement should give a more comparable measure between scenarios. For this scenario they are 6.6 °C/min at its maximum and averages at 0.53 °C/min.

Figure 19 below shows the inputs to the model. The firing rate (red) and its time derivative (magenta) is the output after the prefilter. It is also normalised with the steam flow rate as is all other inputs except for the superheater inlet enthalpy (black). The pressure derivative is shown in blue. The last signal, model disturbance (green), is the remaining disturbance in the form of a firing rate error that would reduce model error to zero when applied. This will be used to disturb

Chapter 3 System Identification and Modelling

the plant while testing close loop control responses and thereby enable a fair comparison between the two control systems based on this model.

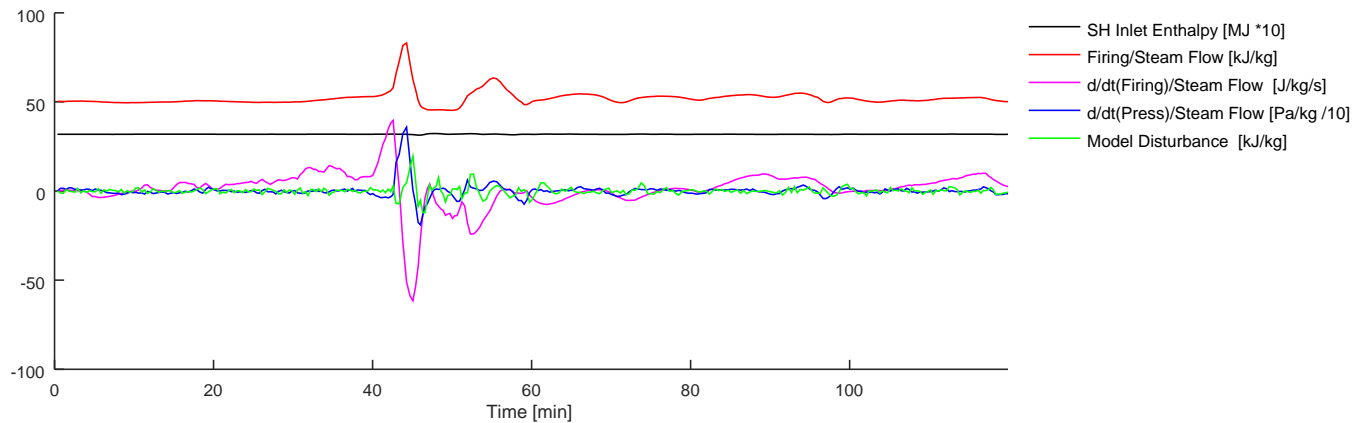


Figure 19: Sudden Steam Flow Rate Swing – Model Inputs

It should be noted that because the model inputs are normalised w.r.t steam flow rate, the normalised firing signal derivative is not a time derivative of the normalised firing signal. Normalisation occurs after the time derivative is taken as per the derivation in equation (37).

Both firing signal time derivative, before and after normalisation, remain mostly positive after the 80-minute mark. These are seen as magenta in *Figure 20* and *Figure 19* respectively. From *Figure 17* and *Figure 20* it can be seen that the firing signal (before normalisation) is increasing in this same period and has a positive time derivative. Both the firing signal and its time derivative are then scaled by the inverse of the steam flow rate, not before taking the derivative. The steam flow rate inverse will always be positive and will not change the sign of the inputs once normalised, only their magnitudes. It is represented in *Figure 20* in a scaled form.

Chapter 3 System Identification and Modelling

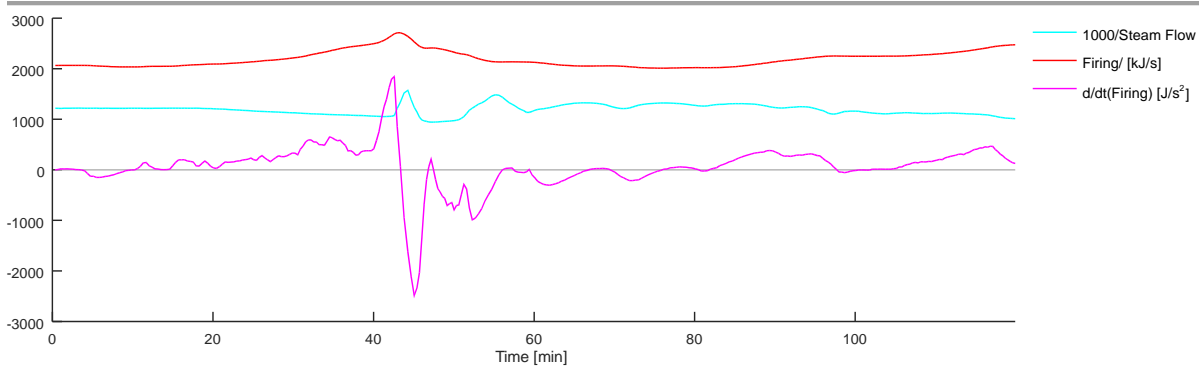


Figure 20: Sudden Steam Flow Rate Swing – Non-Normalised Firing Parameters

A negative gradient in the normalised firing signal can therefore be due to the steam flow rate increasing and will not always correspond with a negative gradient in the actual firing signal. A negative firing rate time derivative, normalised or not, will always correspond to a negative gradient in the non-normalised firing signal. As per equation (37) this will not necessarily be reflected in the gradient because the normalisation factor is also time dependent. The steam flow rate as seen in *Figure 16* is increasing and changing the normalisation of the input parameters to the model as well as the model state space representation. The larger normalisation factor now actually causes the still positive and increasing firing signal to trend downwards after normalisation. This then distracts from the fact that the actual normalised firing signal time derivative should remain positive as it does.

3.5.2. Machine Deloading and Mill Outage

The following scenario was chosen to show the transient response of deloading the machine. In order to reduce the steam flow rate, and deload the machine, a mill firing rate reduction is necessary to maintain the energy balance. In this case, firing is reduced through a controlled mill shutdown, requiring it to be run empty of coal. The coal feeder is stopped or reduced significantly while the overall air throughput is only reduced slightly.

There is a long residence time of coal in the mill to allow it to sufficiently pulverise through grinding. The mill stores a significant amount of coal in this way, even after a coal feeder is stopped. After the coal level in the mill has dropped sufficiently for shutdown, mill loading and airflow is steadily reduced to minimum. Only then is the mill stopped and cause less of a transient response. It is still a significant event as it exposes the model to various process ranges.

Chapter 3 System Identification and Modelling

In particular we look at the response as steam flow rate drops, as this is one of the major non-linearities in the system. This scenario will help to ensure that the model preserves accuracy as we move through a non-linear state change. Note that colour and legend allocation in the following figures for all scenarios are general, with deviations indicated in the legend.

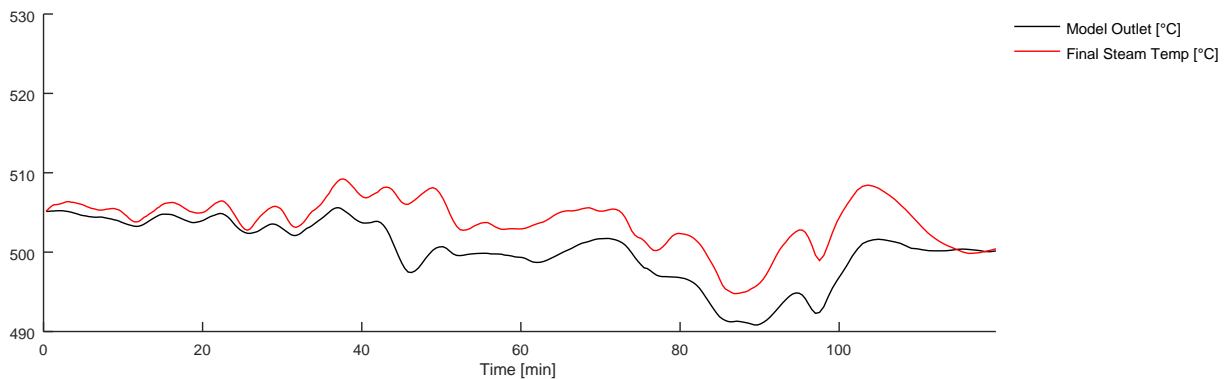


Figure 21: Machine Deloading and Mill Outage – Modelled Output

In *Figure 21* above we see that steady state error accumulates with a few unmodeled disturbances making it more difficult to compare to the first scenario. It is clear that there is a much larger steady state error that accumulates in this scenario. This model response has an average absolute error per sample of $4.96\text{ }^{\circ}\text{C}$ and a maximum absolute error of $9\text{ }^{\circ}\text{C}$. The model response is skewed by the steady state error.

Looking at the highest, $1.84\text{ }^{\circ}\text{C}/\text{min}$, and average, $0.46\text{ }^{\circ}\text{C}/\text{min}$, absolute rate of model departure from the measurement, this model actually diverges significantly slower than the previous scenario. Since the dynamic response accuracy is of higher importance, this is still a valid result for a scenario that spans a 28 kg/s change in steam flow rate (*Figure 22*). This is just short of half the total nominal range, from its maximum of 49 kg/s at 24 minutes and minimum of 21 kg/s at 111 minutes.

Chapter 3 System Identification and Modelling

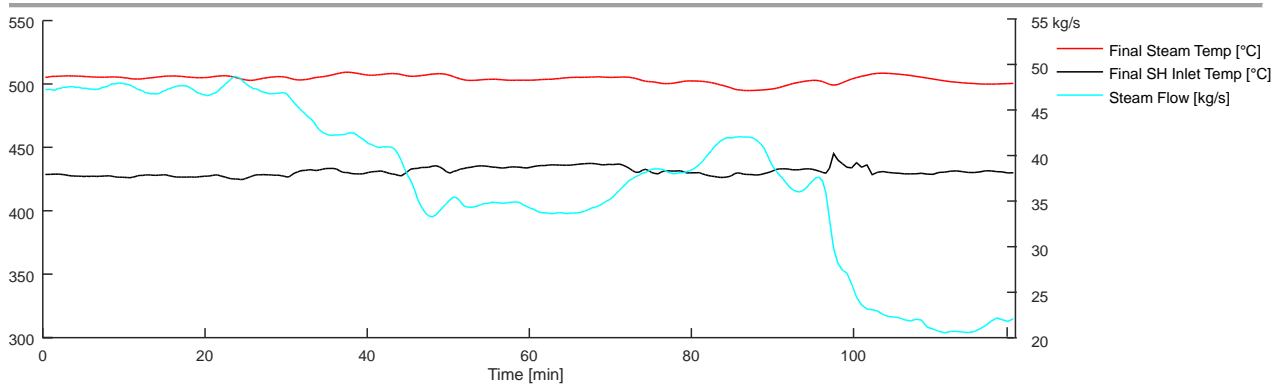


Figure 22: Machine Deloading and Mill Outage – Flow Rate and Superheater Inlet Temperature

On *Figure 23* and *Figure 24* there are plenty of mill and fuel oil firing activities taking place which are matched with a decrease in steam flow rate. Mill A and C have been separated into a separate graph for clarity. As mill B is ramped down to minimum load, it is supported with fuel oil burners. Before mill B is shut down, mill C is also supported with fuel oil firing to compensate for the loss of energy. This is standard operation to ensure flame stability during the transition. After mill B is shut down, mill A is also supported with fuel oil firing. The two remaining mills are taken off coordinated firing mode and mill C is ramped down further.

Any single scenario's modelled behaviour can become too complex for visual and intuitive validation. This is especially true for the coupled nature of steam flow rate and the other input parameters. Intuitive and visual analysis are done with a low degree of accuracy. Applying all scenario datasets to the model simultaneously provides confidence in the model and its response. Many independent process parameter changes and sequences are evaluated on the same model concurrently. This ensures that the modelled response of one parameter is not confused for another, due to the interaction of these variables.

Chapter 3 System Identification and Modelling

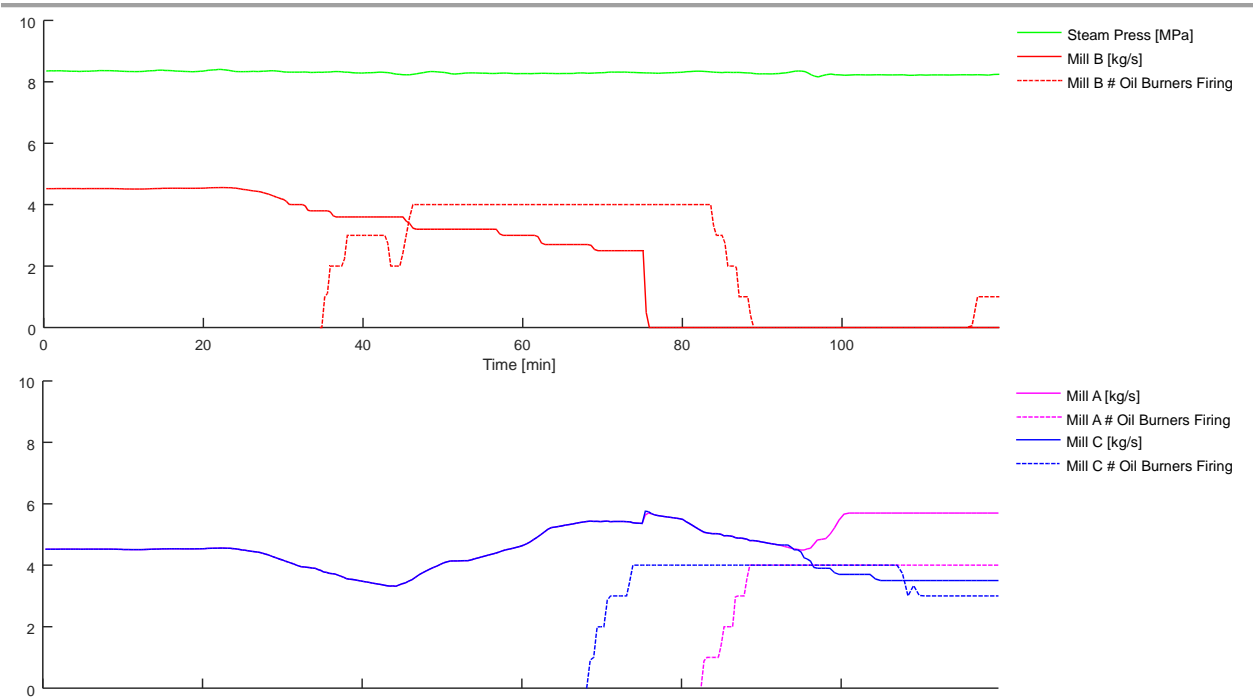


Figure 23: Machine Deloading and Mill Outage – Mill, Fuel Oil Firing and Steam Pressure

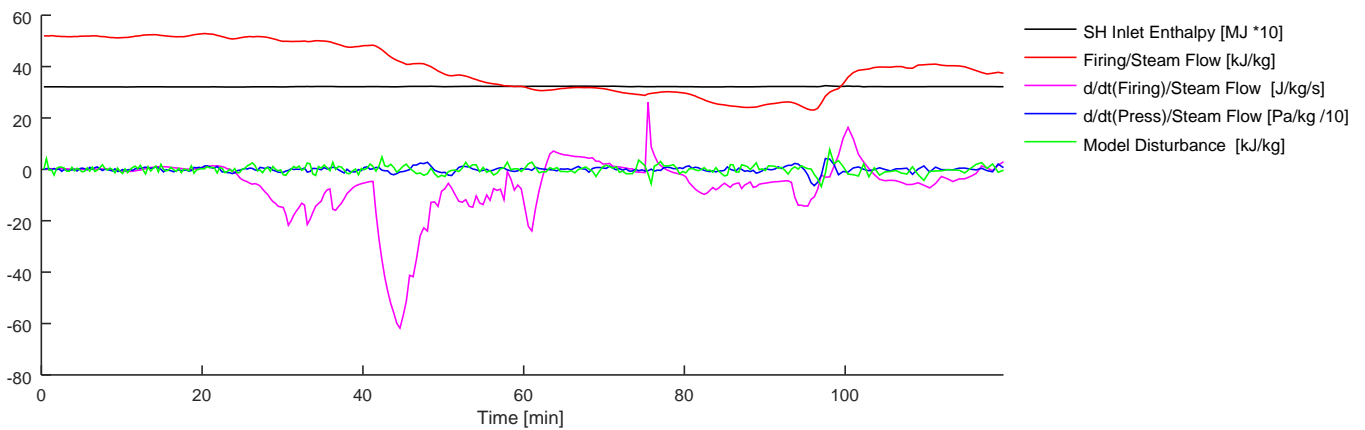


Figure 24: Machine Deloading and Mill Outage – Model Inputs

3.5.3. Steam Flow Rate Cycling while Deloading

This scenario showcases an initial steam flow rate reduction which is followed by some steam pressure cycling, induced by combustion instability. This cycling is induced in part by another controller responding to the combustion process, but this will not be discussed in very much detail here. Some of the interactions between various controllers in the system have been discussed in section 3.5.1. In short, cycling behaviour in the combustion process reflects in the

Chapter 3 System Identification and Modelling

steam pressure and is being fed back to the main steam flow rate controller, which then also cycles. Important in this scenario is that the mill firing rate does not change significantly. Remembering that steam flow rate is not a model input on its own, it is expected to see cycling in the final steam temperature, due to normalisation of the model inputs. This is a good scenario to see how this normalisation and variable sample rate performs in the absence of significant changes to the firing rate.

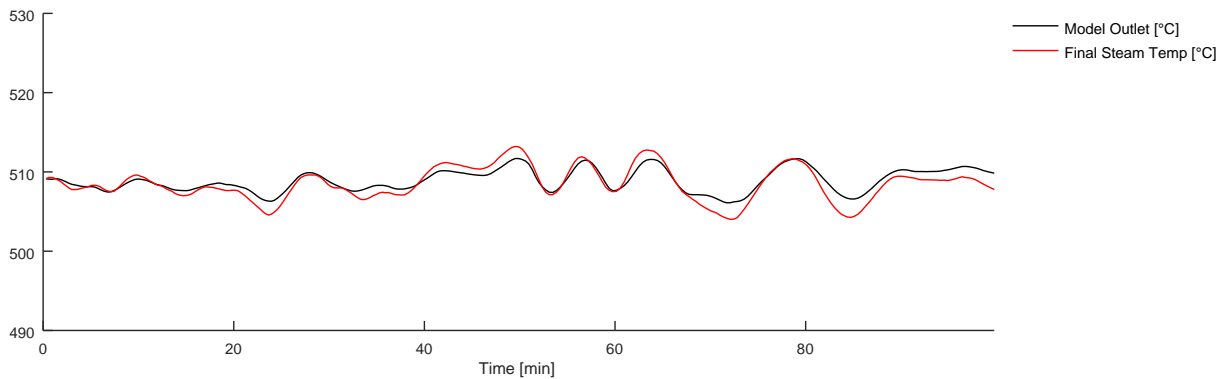


Figure 25: Steam Flow Cycling while Deloading – Modelled Output

Figure 25 definitely shows quite an accurate model response which is verified by looking at its comparison to the other scenarios presented. The response has a standard deviation of $1.10\text{ }^{\circ}\text{C}$, a maximum absolute error of $2.4\text{ }^{\circ}\text{C}$, a highest absolute rate of model departure from measurement of $1.31\text{ }^{\circ}\text{C}/\text{min}$, and on average $0.33\text{ }^{\circ}\text{C}/\text{min}$.

Although this is considered a good result, it must also be noted that this scenario has less severe transient behaviours than the scenarios previously discussed, as can be seen in *Figure 27* and *Figure 28*. Again, in this scenario the unit was running in a coordinated mill mode. All mills are running at the same load and overlap in *Figure 27*. It also shows, in *Figure 26*, that the steam flow rate related responses manifest themselves quite accurately through the model in the form of normalising other inputs and though the use of a variable sample rate.

Chapter 3 System Identification and Modelling

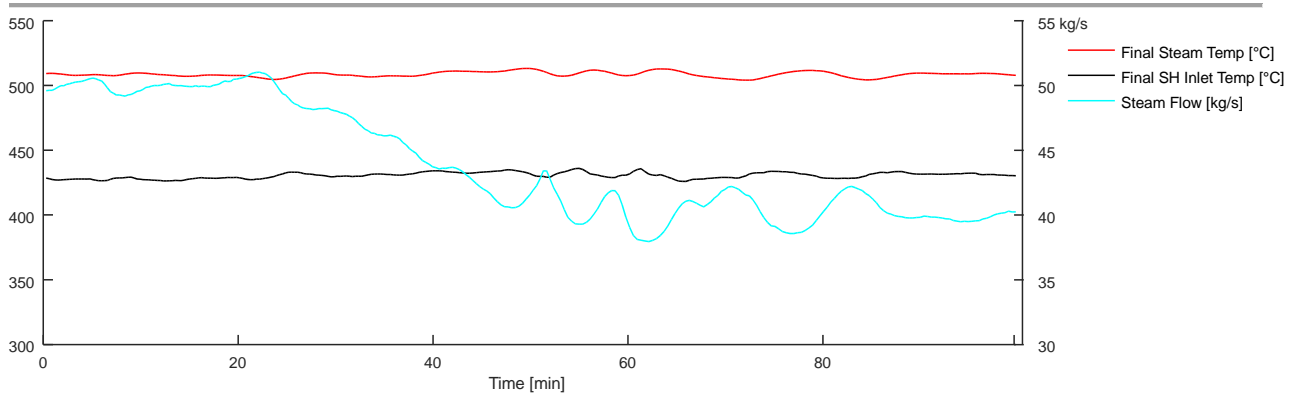


Figure 26: Steam Flow Cycling while Deloading – Flow Rate and Superheater Inlet Temperature

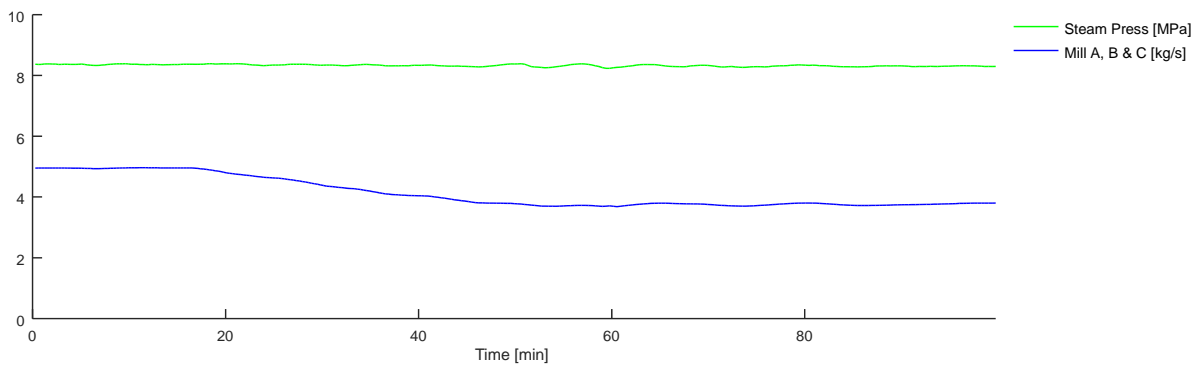


Figure 27: Steam Flow Cycling while Deloading – Mill, Fuel Oil Firing and Steam Pressure

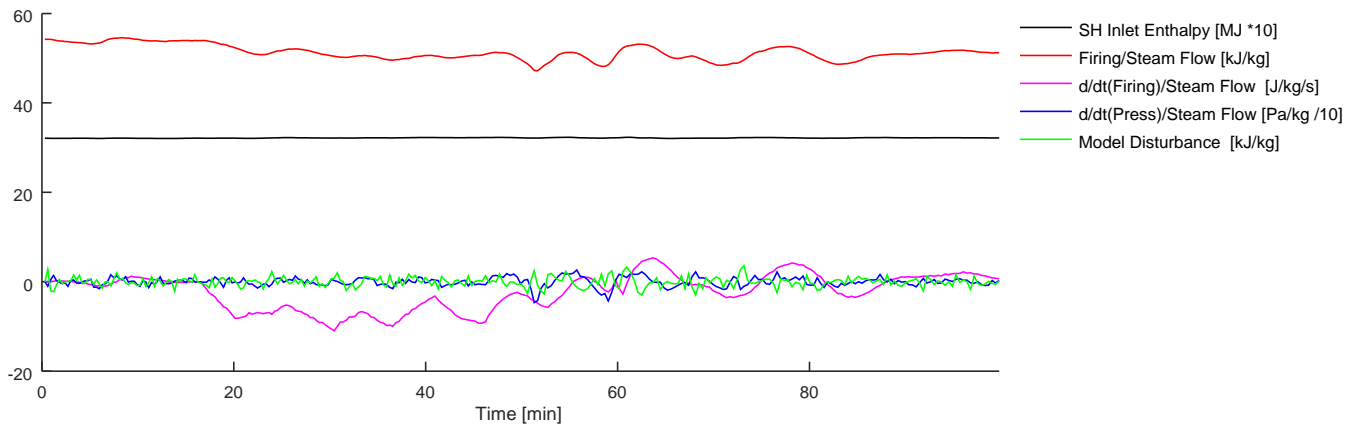


Figure 28: Steam Flow Cycling while Deloading – Model Inputs

3.5.4. Various Load Changes

The next scenario has less significance than the ones before, but it still has some unique attributes worth looking at. It displays a steam flow rate closer to the full-load rate. Up to this scenario,

Chapter 3 System Identification and Modelling

most transients occurred as the load was decreasing or already low. It contains two incidents, one where the steam flow rate spikes up along with a change in mill firing, as well as one later on where the steam flow rate that spikes down, while close to full load. This will therefore also show that the model is accurate for the more trivial, but common full-load condition, where transients and system responses are faster.

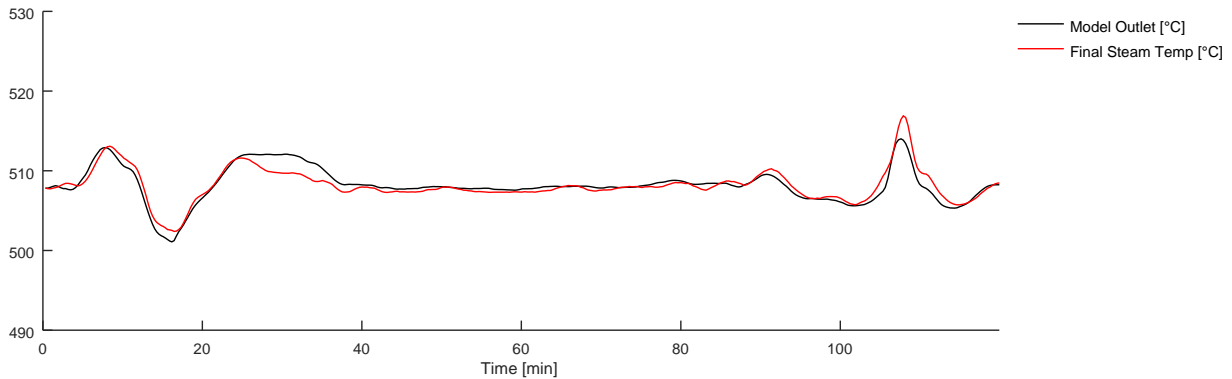


Figure 29: Various Load Changes – Modelled Output

Figure 29 again shows quite an accurate model response. It has an average absolute error per sample of $0.84\text{ }^{\circ}\text{C}$, a maximum absolute error of $3.3\text{ }^{\circ}\text{C}$, a highest absolute rate of model departure from measurement of $3.08\text{ }^{\circ}\text{C}/\text{min}$, and on average $0.33\text{ }^{\circ}\text{C}/\text{min}$. There is not much to scrutinise in this scenario. It serves only to cover the full load condition and transients during full load. The model seems to have no major deviations during higher loads. In *Figure 31* note again the overlapping mill loads as they are firing in coordinated mode.

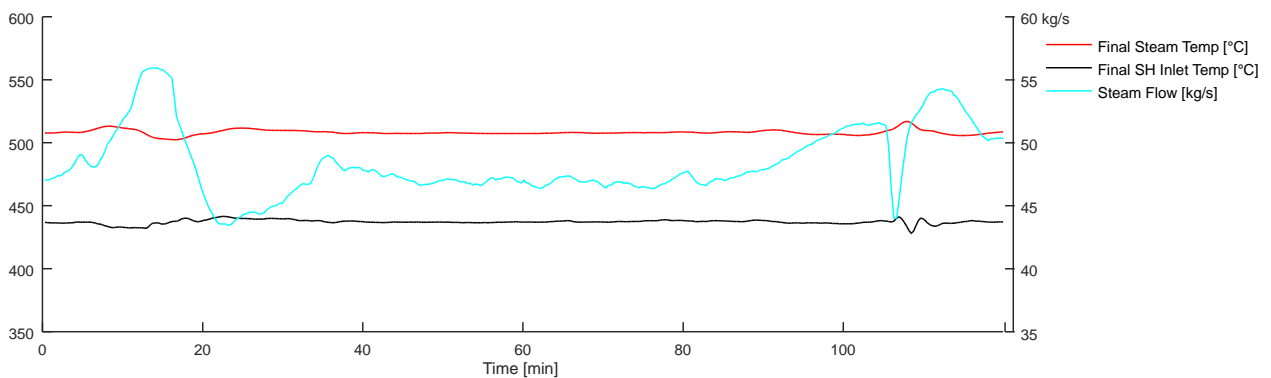


Figure 30: Various Load Changes – Flow Rate and Superheater Inlet Temperature

Chapter 3 System Identification and Modelling

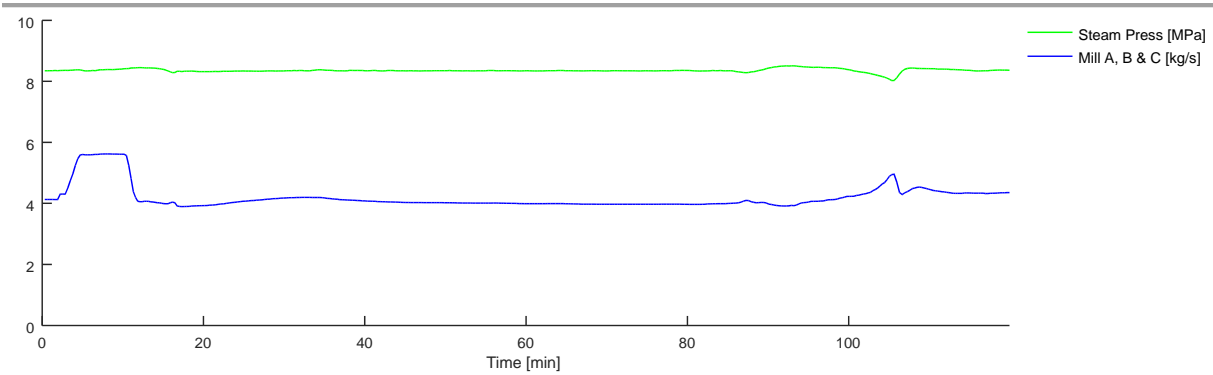


Figure 31: Various Load Changes – Mill, Fuel Oil Firing and Steam Pressure

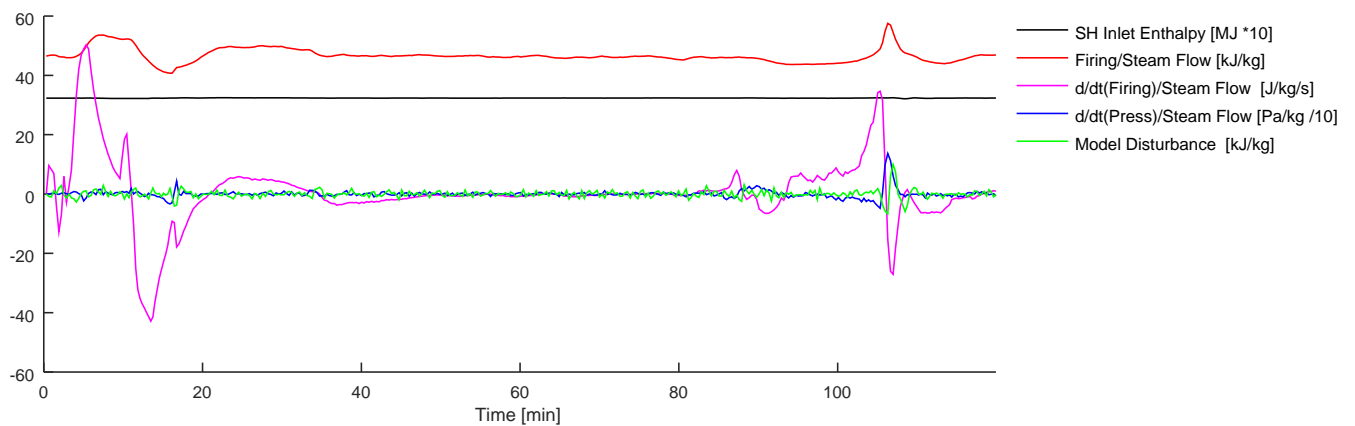


Figure 32: Various Load Changes – Model Inputs

3.5.5. Introduction of Mill and Load Increase

This scenario was chosen since it shows some of the shortcomings in the model that will need to be evaluated on a closed loop system to ensure that the system remains accurate. The reason is that this scenario displays quite a lot of unmodeled higher order dynamics or other unknown plant perturbations. This model inaccuracy could compromise the controller's ability to adequately reject known and unknown disturbances. This is also an opportunity for further development of the solution in future.

Chapter 3 System Identification and Modelling

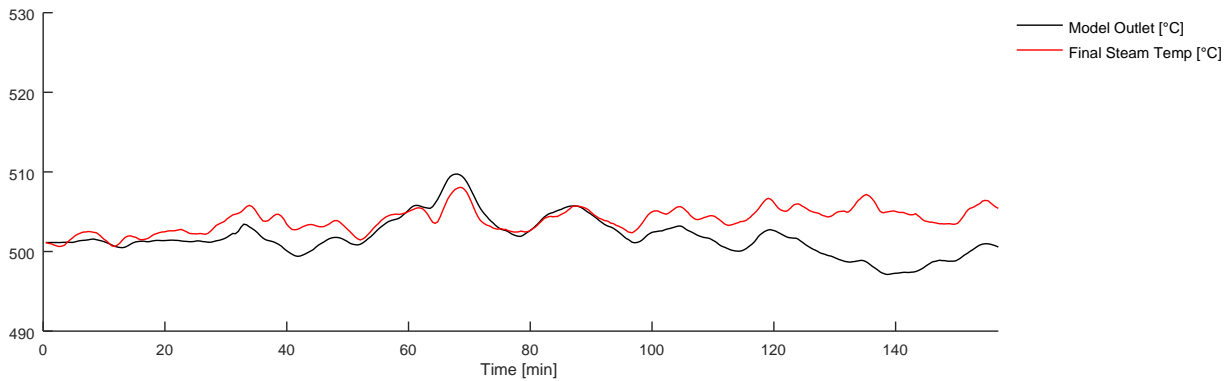


Figure 33: Introduction of Mill and Load Increase – Modelled Output

Figure 33 shows that, in general, the model approximates the actual plant output when it comes to lower order dynamics. There is also clearly residual higher order dynamics at work which is not being accurately represented by the model. The response has an average absolute error per sample of $3.81\text{ }^{\circ}\text{C}$, a maximum absolute error of $8.5\text{ }^{\circ}\text{C}$, a highest absolute rate of model departure from measurement of $1.65\text{ }^{\circ}\text{C}/\text{min}$, and on average $0.32\text{ }^{\circ}\text{C}/\text{min}$. This does not seem too bad at first, however, this type of disturbance could cause instability in a controller if not robust enough and will have to be considered when it is evaluated.

The response is not entirely uncorrelated to the inputs already used in the model, but is more pronounced in this scenario. This is due to a defective spray water valve that fails to atomise the spray water sufficiently. This causes a perturbation of the response to the measured superheater inlet steam temperature. Other factors include ash build-up being very small on the tubes, which can be just as bad. This can be due to excessive washing during a boiler outage. Lastly the mills could be out of calibration resulting in furnace over-firing, or incorrect classification, causing secondary combustion. All of which can cause a more pronounced response to firing changes.

All things considered, the model seems to approximate most scenarios, even this one, sufficiently for control purposes. There might be an excessive control effort in a scenario like this. As long as the controller is designed to be robust enough to remain stable under such perturbations, there should be no reason for concern. A maximum deviation in the model of $8.5\text{ }^{\circ}\text{C}$ would not be enough to trigger any of the protections associated with a unit trip, even if the effect is doubled.

Chapter 3 System Identification and Modelling

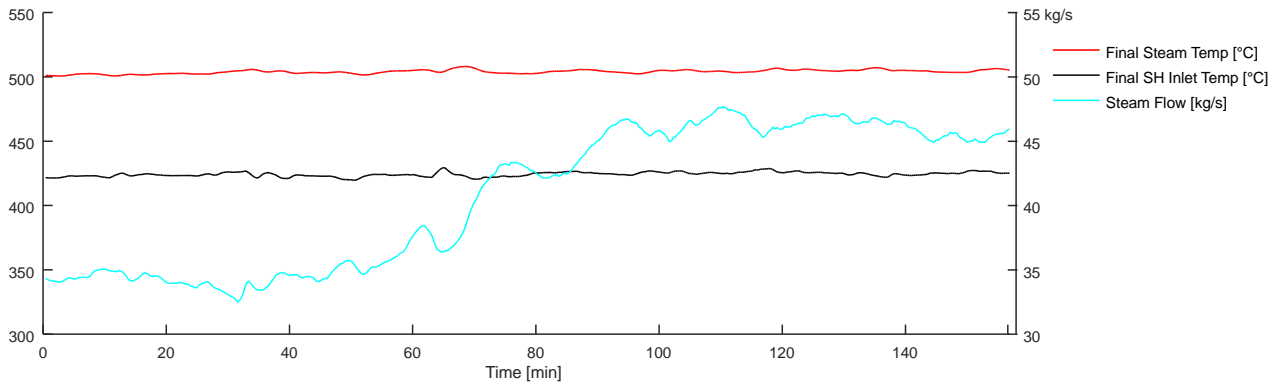


Figure 34: Introduction of Mill and Load Increase – Flow Rate and Superheater Inlet Temperature

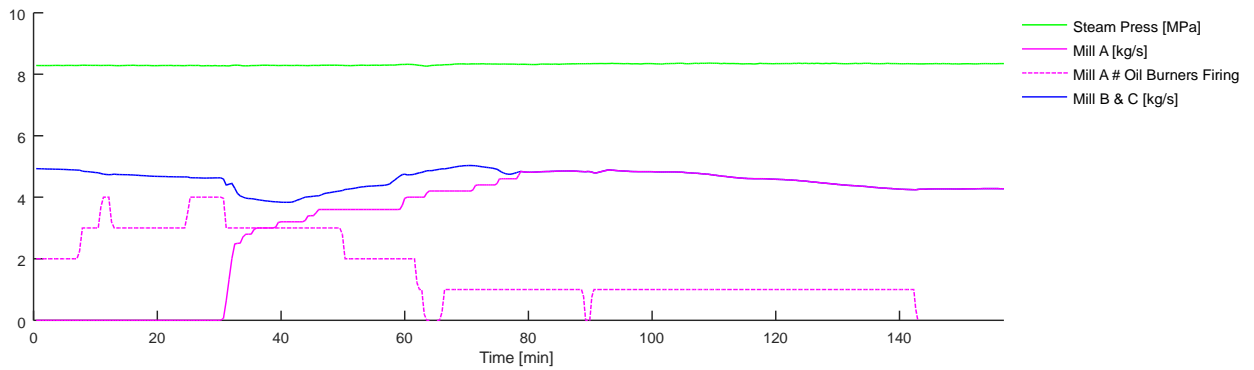


Figure 35: Introduction of Mill and Load Increase – Mill, Fuel Oil Firing and Steam Pressure

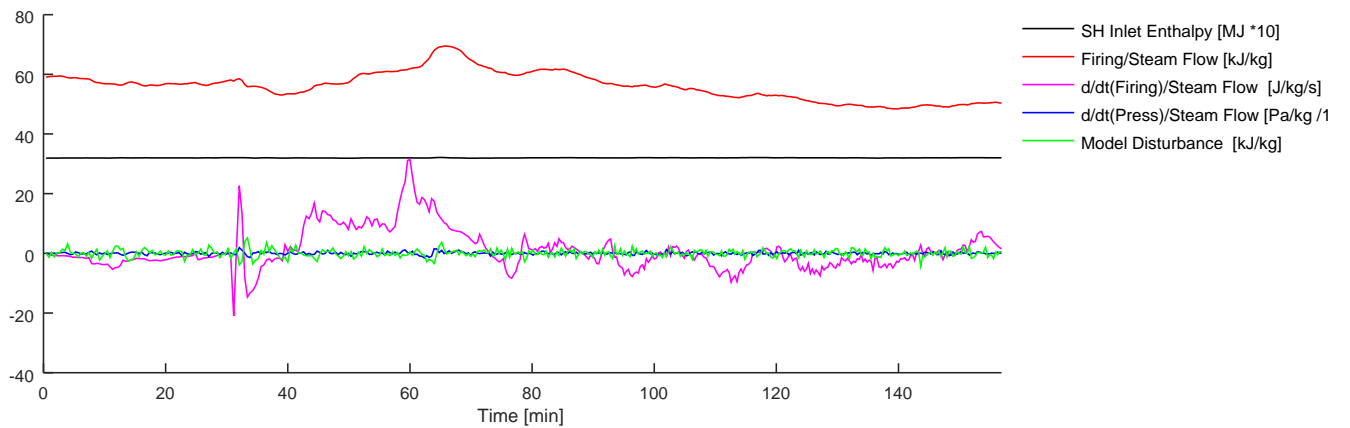


Figure 36: Introduction of Mill and Load Increase – Model Inputs

3.5.6. Scenario Sample Summary

The following table sums up the comparison between the scenarios as well as giving an average for the remaining models in the training set. The table headers are as follows:

- J_{avg} = Standard error deviation [$^{\circ}\text{C}$]
- J_{max} = Maximum absolute error [$^{\circ}\text{C}$]
- err_{max} = Highest rate of model departure from measurement [$^{\circ}\text{C}/\text{min}$]
- err_{avg} = Average rate of model departure from measurement [$^{\circ}\text{C}/\text{min}$]

Table 7: Model Performance Summary

| Scenario | ID | J_{avg} | J_{max} | err_{max} | err_{avg} |
|---|--------------------|-----------|-----------|-------------|-------------|
| Sudden Steam Flow Rate Swing | 1 | 1.95 | 5.6 | 6.59 | 0.53 |
| Machine Deloading and Mill Outage | 3 | 4.96 | 9.0 | 1.84 | 0.46 |
| Steam Flow Rate Cycling while Deloading | 9 | 1.10 | 2.4 | 1.31 | 0.33 |
| Various Load Changes | 16 | 0.84 | 3.3 | 3.08 | 0.33 |
| Introduction of Mill and Load Increase | 37 | 3.81 | 8.5 | 1.65 | 0.32 |
| Average across all scenarios *(3 outliers removed) | 0-38 17, 18, 22 | *4.01 | 9.3 | 2.73 | 0.44 |

The performance parameter averages of all scenarios are close to that of the sampled scenarios for the err parameters. However, there are a few other scenarios that do show steady state errors similar to that of scenario 3, which increase the cost function average, J , performance parameters. These are often due to scenario data starting from a low load condition and ramping up. This usually cause some steady state error due to many slow dynamics relating to start-up sequences before heat transfer has stabilised. This would not affect model optimisation as much and would be eliminated by a closed loop controller through negative feedback.

3.6. Final Discrete State Space Model

Below is the final discrete time state space model that is used for the design of the MPC and Fuzzy control systems as well as modelling of the results. It implements a 15 sec sample time for the purpose of construction, but the sample time will actually be variable in the discrete implementation and will be discussed further in *4.1 State Space Model with a variable sample time*. Input signals have been averaged between variable sample times and outputs timestamped with variable sample time to achieve this goal during modelling. For convenience of future

Chapter 3 System Identification and Modelling

reference, the input signals have been given new names for the already normalised signals against the steam flow rate. The final model was selected to consist of $N = 2$ subsections and therefore makes the overall model 2nd order. The augmented model is discussed in more detail, and given in full in section 4.2.1. It is however merely refactoring the model shown below and does not change the dynamic system represented by it.

$$fire_{in} = \frac{q_{rad}}{k\dot{m}_{in}} \quad (36)$$

$$\dot{fire}_{in} = \frac{\dot{q}_{rad}}{k\dot{m}_{in}} \quad (37)$$

$$\dot{p}_{in} = \frac{\dot{p}}{k\dot{m}_{in}} \quad (38)$$

$$\begin{matrix} \mathbf{F}_m & & \mathbf{G}_m \\ \begin{bmatrix} h_2(k+1) \\ h_1(k+1) \end{bmatrix} = \begin{bmatrix} 0.8108 & 0.24 \\ 0 & 0.738 \end{bmatrix} \begin{bmatrix} h_2(k) \\ h_1(k) \end{bmatrix} + \begin{bmatrix} 0 & 0.1935 & 23.15 & 9.165 \\ 0.1433 & 0.03657 & 19.23 & 13.63 \end{bmatrix} \begin{bmatrix} h_{in}(k) \\ fire_{in}(k) \\ fire_{in}(k) \\ \dot{p}_{in}(k) \end{bmatrix} \end{matrix} \quad (39)$$

$$\begin{matrix} \mathbf{c}_m & \mathbf{d}_m \\ h_{m_{out}}(k) = [1 \ 0] \begin{bmatrix} h_2(k) \\ h_1(k) \end{bmatrix} + [0 \ 0 \ 0 \ 0] \begin{bmatrix} h_{in}(k) \\ fire_{in}(k) \\ fire_{in}(k) \\ \dot{p}_{in}(k) \end{bmatrix} \end{matrix} \quad (40)$$

Sampling time: 15 s(Variable)
Discrete-time Superheater Model

Table 8: Nomenclature for Non-Augmented Discrete Time Model

| Symbol | SI Unit | Description |
|--|---------------------|---|
| $h_{m_{out}}$ | [J/kg] | Discrete time model specific steam enthalpy |
| \dot{m}_{in} | [kg/s] | Mass flow rate of steam from inlet to outlet |
| $k\dot{m}_{in}$ | | Linearization factor based on \dot{m}_{in} |
| h_{in} | [J/kg] | Specific enthalpy of steam at inlet |
| q_{rad} | [J/s] | Heat flux through radiation from furnace firing |
| \dot{p} | [Pa/s] | Pressure of steam rate of change |
| $\mathbf{F}_m, \mathbf{G}_m, \mathbf{c}_m, \mathbf{d}_m$ | | Digital domain state space matrix variables |
| $h_i(k)$ | [J/kg] | Discrete time model subsection states |
| $fire_{in}$ | [J/s] | Normalised firing rate input |
| \dot{fire}_{in} | [J/s ²] | Normalised firing rate derivative input |
| \dot{p}_{in} | [Pa/s] | Normalised pressure rate of change input |

Chapter 4

Controller Design

Two control strategies will be investigated and developed in this chapter: MPC and Fuzzy Control. These techniques are chosen to provide a stable and robust solution to the control problem, in the light of non-linearities present in the system.

The control system design will be conducted in the digital domain and therefore first requires some adaptation of the system model developed in the previous section. For the case of Fuzzy control design the discrete time model can be transformed for various membership areas based on steam flow rate and acceleration. It will also be shown that by substituting a variable sample time to the digital state representation, the discrete state space model used for the MPC controller will remain constant across the range of the variable steam flow rate. This will be discussed first before the MPC and Fuzzy controller designs are presented.

4.1. State Space Model with a variable sample time

With a theoretical system identification done, it was seen from the model that the parameter \dot{m}_{in} is present in every term of state space matrix A . \dot{m}_{in} represents the steam flow rate, the most notable non-linearity as it is present in the state space representation. The linearized common factor $k_{\dot{m}_{in}}$ can be seen as directly influencing the system response time. Future research might be able to look at a less restrictive linearisation to the main steam flow rate, to improve model accuracy. This section assumes a constant or at least very slowly changing steam flow rate, to allow for this transformation. By manipulating the inputs into this model, it was shown that $k_{\dot{m}_{in}}$ can also be included into input matrix B .

$$\mathbf{F}_m = e^{\mathbf{A}_m \cdot t_{s-mpc}} \quad (41)$$

$$\mathbf{G}_m = \int_0^{t_{s-mpc}} e^{\mathbf{A}_m \cdot \theta} \cdot \mathbf{B}_m d\theta \quad (42)$$

Equation (41) and (42) enables the transformation from the continuous to digital domain for state variable represented system models as seen in [42] and [43]. Only transformation of the \mathbf{A}_m and \mathbf{B}_m matrixes are required, while the \mathbf{c}_m and \mathbf{d}_m matrixes are conserved. The equivalent matrixes

Chapter 4 Controller Design

of \mathbf{A}_m and \mathbf{B}_m are given to be \mathbf{F}_m and \mathbf{G}_m respectively in the digital domain. The subscript is added for later distinction between models in the discrete domain.

When the system is converted to the digital domain, one can show that the resultant system in the digital domain is independent of $k_{\dot{m}_{in}}$, if the sample time is chosen inversely proportional to $k_{\dot{m}_{in}}$. For any slow change in \dot{m}_{in} , the linearization factor will not change the model in the digital domain, only the system sample time will need to change. This independence is first shown for equation (41) by substituting in (43) resulting in equation (44). This substitution and calculation assume a zero-order hold function at the input and a sampler after the continuous system.

$$t_{s\text{-mpc}} \cdot k_{\dot{m}_{in}} = k_t; \quad \mathbf{A}_m = \mathbf{A}_m' \cdot k_{\dot{m}_{in}}; \quad (43)$$

$$\mathbf{F}_m = e^{\mathbf{A}_m' \cdot k_t} \quad (44)$$

The proposed sample time substitution is given in (43). The sample time, $t_{s\text{-mpc}}$, is chosen to be inversely proportional to $k_{\dot{m}_{in}}$. These equations also show substitutions for the \mathbf{A}_m and \mathbf{B}_m matrixes from equations (20) and (21). These substitutions merely separate the common $k_{\dot{m}_{in}}$ term from the rest of the matrix leaving \mathbf{A}_m' and \mathbf{B}_m' invariant to the steam flow rate linearization factor. A variable system sample time now applies to the digital domain representation based on the main steam flow rate.

$$t_{s\text{-mpc}} \cdot k_{\dot{m}_{in}} = k_t; \quad \mathbf{B}_m = \mathbf{B}_m' \cdot k_{\dot{m}_{in}} \quad (45)$$

$$\text{integration substitutions:} \quad \beta = k_{\dot{m}_{in}} \cdot \theta; \quad d\beta = k_{\dot{m}_{in}} \cdot d\theta \quad (46)$$

$$\mathbf{G}_m = \int_0^{k_t} e^{\mathbf{A}_m' \cdot \beta} \cdot \mathbf{B}_m' d\beta \quad (47)$$

The same independence can now be shown for equation (42). Substituting \mathbf{B}_m and $t_{s\text{-mpc}}$ in (45) into the transformation for \mathbf{G}_m in (42) becomes slightly more involved since integration substitutions in (46) also need to be made. The result is shown in equation (47). This transformation also reduces the equation to terms invariant to the steam flow rate linearization factor, with an implied variable sample time in the system.

Table 9: Nomenclature for Digital Domain Model with Variable Sample Time

| Symbol | SI Unit | Description |
|--|---------|--|
| \dot{m}_{in} | [kg/s] | Mass flow rate of steam from inlet to outlet |
| $k_{\dot{m}_{in}}$ | | Linearization factor equal to \dot{m}_{in} |
| $\mathbf{A}_m, \mathbf{B}_m, \mathbf{c}_m, \mathbf{d}_m$ | | Continuous time state space matrix variables |
| $\mathbf{F}_m, \mathbf{G}_m, \mathbf{c}_m, \mathbf{d}_m$ | | Digital domain state space matrix variables |
| t_{s-mpc} | [s] | Variable digital domain system sample time |

The state space representation in the digital domain is now independent of \dot{m}_{in} . The sample time is variable and adjusted as per the substitution given in (43). This means that the MPC gain factors can be calculated for one system in the digital domain and the sample time can be adjusted as loading on the machine changes. It should be noted that the transition between loads does not change the physical state representations. They each represent the outlet enthalpy of one of the superheater nodes, which are unaffected by the immediate change in steam flow rate.

It should also now be clear that in doing this the steam flow rate has partially been captured as an input since it will be present in the augmented inputs $fire_{in}$, \dot{fire}_{in} and \dot{p}_{in} . These are the model inputs q_{rad} , \dot{q}_{rad} and \dot{p} each normalised with a factor based on the steam flow rate operating point. Although not exactly a direct input, the steam flow rate changes the model reaction to its inputs.

4.2. MPC Control Strategy

For the MPC controller design much of the theory will be taken from [26]. To start off in designing the MPC controller the system response needs to be calculated from the system's initial state. Each successive control law is applied based on the model identified for the system for a predefined event horizon. This response is then used to construct a cost function that will be minimised in order to come to a feedback gain calculation that can be applied to the control law. The system model is also augmented at this stage with a free integrator to ensure zero steady state error.

4.2.1. Augmented System model

To introduce a free integrator into the state space representation of the system, [26] proposes that the state space equation be transformed to the delta of each state as seen in equations (48). Each state is changed so that it represents the value change in the old state per sample. The additional

Chapter 4 Controller Design

state, that is used as the output, can be seen to integrate this input and state increments based on the existing state matrixes. This assumption is that the model has no feedforward component, i.e. a zero \mathbf{d} matrix, as is the case for this model. The augmentation also results in the inputs being transformed into their respective deltas as per equation (49). Another state, essentially the system output, is then added to integrate the delta states and retrieve the output. The details can be found in [26, p. 4] and the augmented state can be seen in equation (49) and (50) by increasing the order of the matrix \mathbf{F}_m . Vector $\mathbf{0}_m$ represents a zero filled row vector of length N .

$$\Delta \mathbf{x}_m(k+1) = \mathbf{x}_m(k+1) - \mathbf{x}_m(k)$$

$$\text{and } \Delta \mathbf{u}(k) = \mathbf{u}(k) - \mathbf{u}(k-1) \quad (48)$$

$$\begin{array}{c} \mathbf{x}(k+1) \\ \left[\begin{array}{c} \Delta \mathbf{x}_m(k+1) \\ y_m(k+1) \end{array} \right] \end{array} = \begin{array}{c} \mathbf{F} \\ \left[\begin{array}{cc} \mathbf{F}_m & \mathbf{0}_m^T \\ \mathbf{c}_m \cdot \mathbf{F}_m & 1 \end{array} \right] \end{array} \begin{array}{c} \mathbf{x}(k) \\ \left[\begin{array}{c} \Delta \mathbf{x}_m(k) \\ y_m(k) \end{array} \right] \end{array} + \begin{array}{c} \mathbf{G} \\ \left[\begin{array}{c} \mathbf{G}_m \\ \mathbf{c}_m \cdot \mathbf{G}_m \end{array} \right] \end{array} \begin{array}{c} \Delta \mathbf{u}(k) \\ \left[\begin{array}{c} \Delta h_{in}(k) \\ \Delta fire_{in}(k) \\ \Delta fire_{in}(k) \\ \Delta \dot{p}_{in}(k) \end{array} \right] \end{array} \quad (49)$$

$$\begin{array}{c} y(k) \end{array} = \begin{array}{c} \mathbf{c} \\ \left[\begin{array}{cc} \mathbf{0}_m & 1 \end{array} \right] \end{array} \begin{array}{c} \Delta \mathbf{x}_m(k) \\ y(k) \end{array} \quad (50)$$

Sampling time: 15 s
Discrete – time model

The following equations show the values for the matrixes in (49) and (50) based on the discrete time model in section 3.6.

$$\mathbf{F} = \begin{array}{c} \Delta h_2(k+1) \\ \Delta h_1(k+1) \\ y_m(k+1) \end{array} \begin{array}{c} \Delta h_2(k) \quad \Delta h_1(k) \quad y_m(k) \\ \left[\begin{array}{ccc} 0.8108 & 0.24 & 0 \\ 0 & 0.738 & 0 \\ 0.8108 & 0.24 & 1 \end{array} \right] \end{array} \quad (51)$$

$$\mathbf{G} = \begin{array}{c} \Delta h_2(k+1) \\ \Delta h_1(k+1) \\ y_m(k+1) \end{array} \begin{array}{c} \Delta h_{in}(k) \quad \Delta fire_{in}(k) \quad \Delta fire_{in}(k) \quad \Delta \dot{p}_{in}(k) \\ \left[\begin{array}{cccc} 0 & 0.1935 & 23.15 & 9.165 \\ 0.1433 & 0.03657 & 19.23 & 13.63 \\ 0 & 0.1935 & 23.15 & 9.165 \end{array} \right] \end{array} \quad (52)$$

$$\mathbf{c} = y(k) \begin{bmatrix} \Delta h_2(k) & \Delta h_1(k) & y_m(k) \\ 0 & 0 & 1 \end{bmatrix} \quad (53)$$

$$\mathbf{d} = y(k) \begin{bmatrix} \Delta h_{in}(k) & \Delta fire_{in}(k) & \Delta fire_{in}(k) & \Delta \dot{p}_{in}(k) \\ 0 & 0 & 0 & 0 \end{bmatrix} \quad (54)$$

Sampling time: 15 s
Discrete – time model

Table 10: Nomenclature for Augmented Discrete Time Model

| Symbol | SI Unit | Description |
|---|---------------------|--|
| F, G, c, d | | Augmented digital domain state space matrixes |
| F_m, G_m, c_m, d_m | | Digital domain state space matrixes |
| y_m | [J/kg] | System output state |
| $\Delta fire_{in}$ | [J/s] | Normalised delta firing rate input |
| $\Delta fire_{in}$ | [J/s ²] | Normalised delta firing rate derivative input |
| Δh_1 | [J/kg] | First superheater section enthalpy state |
| Δh_2 | [J/kg] | Second superheater section enthalpy state |
| Δh_{in} | [J/kg] | Specific delta enthalpy of final superheater steam inlet |
| $\Delta \dot{p}_{in}$ | [Pa/s] | Normalised pressure rate of change input |

4.2.2. Predicted Output Variables

The predicted system response, over a horizon of N_p samples, will be represented by a matrix set of discrete outputs as seen in equation (55). It includes samples from just after the initial state of the system to a defined prediction horizon number of samples, N_p . The control horizon number of samples is defined as N_c , with N_i initial samples to ignore in the prediction horizon. Some initial samples of the prediction horizon are ignored in the cost function and subsequent control law calculation. This is done based on the large lag associated with the process. The controller would produce a very aggressive control signal in an attempt to control for deviations essentially subject to significant process lag, with control interventions being largely ineffective for the initial prediction period. The motivation of these parameter choices is discussed in more detail in section 4.2.4. The augmented state space matrixes are used to construct two matrixes as seen in equations (56) and (57) that calculate this response based on the model, its inputs, and initial state.

Chapter 4 Controller Design

$$\mathbf{y}_p = \mathbf{E} \cdot \mathbf{x}(k_i) + \Phi_1 \cdot \Delta \mathbf{h}_{in} + \Phi_2 \cdot \Delta \mathbf{fire}_{in} + \Phi_3 \cdot \Delta \dot{\mathbf{fire}}_{in} + \Phi_4 \cdot \Delta \dot{\mathbf{p}}_{in} \quad (55)$$

$$\mathbf{E}_{(N_p - N_i) \times 3} = \begin{bmatrix} \boldsymbol{\epsilon} \cdot \mathbf{F} \\ \boldsymbol{\epsilon} \cdot \mathbf{F}^2 \\ \mathbf{c} \cdot \mathbf{F}^3 \\ \vdots \\ \mathbf{c} \cdot \mathbf{F}^{N_p} \end{bmatrix} \quad (56)$$

$$\Phi_g_{(N_p - N_i) \times N_c} = \begin{bmatrix} \boldsymbol{\epsilon} \cdot \mathbf{g}_{*,g} & \emptyset & \emptyset & \dots & \emptyset \\ \boldsymbol{\epsilon} \cdot \mathbf{F} \cdot \mathbf{g}_{*,g} & \boldsymbol{\epsilon} \cdot \mathbf{g}_{*,g} & \emptyset & \dots & \emptyset \\ \mathbf{c} \cdot \mathbf{F}^2 \cdot \mathbf{g}_{*,g} & \mathbf{c} \cdot \mathbf{F} \cdot \mathbf{g}_{*,g} & \mathbf{c} \cdot \mathbf{g}_{*,g} & \dots & 0 \\ \vdots & \vdots & \vdots & \dots & \vdots \\ \mathbf{c} \cdot \mathbf{F}^{N_p - 1} \cdot \mathbf{g}_{*,g} & \mathbf{c} \cdot \mathbf{F}^{N_p - 2} \cdot \mathbf{g}_{*,g} & \mathbf{c} \cdot \mathbf{F}^{N_p - 3} \cdot \mathbf{g}_{*,g} & \dots & \mathbf{c} \cdot \mathbf{F}^{N_p - N_c} \cdot \mathbf{g}_{*,g} \end{bmatrix} \quad (57)$$

Table 11 : Nomenclature for Predicted Output Variable Equations

| Symbol | SI Unit | Description |
|--|---------------------|--|
| $\Delta \mathbf{h}_{in}$ | [J/kg] | Vector of CV deltas across the control horizon |
| $\Delta \mathbf{fire}_{in}$ | [J/s] | Vector of DV deltas across the control horizon |
| $\Delta \dot{\mathbf{fire}}_{in}$ | [J/s ²] | Vector of DV deltas across the control horizon |
| $\Delta \dot{\mathbf{p}}_{in}$ | [Pa/s] | Vector of DV deltas across the control horizon |
| $\mathbf{F}, \mathbf{G}, \mathbf{c}, \mathbf{d}$ | | Augmented digital domain state space matrixes |
| N_p | | Prediction horizon number of samples |
| N_c | | Control horizon number of samples |
| N_i | | Number of ignored initial samples |
| \mathbf{y}_p | [J/kg] | Predicted output state response vector |
| \mathbf{E} | | Predictive free impulse response matrix from the initial state |
| $\mathbf{x}(k_i)$ | [J/kg] | System states at time of prediction k_i |
| k_i | | Sample index at time of prediction |
| Φ_g | | Predictive impulse response matrix for control and disturbance input changes |
| $\mathbf{g}_{*,g}$ | | Column reference to the \mathbf{G} matrix |

The \mathbf{E} matrix captures the model's response to its initial conditions, settling out in the form of an impulse response. Similarly, Φ_g captures the impulse response to each of the input changes for each sample time in the control horizon. The indexed column vector $\mathbf{g}_{*,g}$ represents the columns of the \mathbf{G} matrix indexed by the variable g as they correspond to each input to the system. Vectors $\Delta \mathbf{fire}_{in}$, $\Delta \dot{\mathbf{fire}}_{in}$ and $\Delta \dot{\mathbf{p}}_{in}$ are shown, although only the first term at k_i of each will be known and the future terms will be zero. The equation will be kept in this generic form until simplified later. The measured disturbances are uncorrelated and only the immediately measured value is known. No future values of the disturbances are known for the rest of the control horizon. The

Chapter 4 Controller Design

matrixes in equation (56) and (57) also have the first two rows deleted. This is not only for the benefit of observing the pattern, but brings us to the cost function construction that ignores a certain number of initial samples. The representation shows N_i as 2 based on the number of rows deleted; This is merely an illustration, while a proper value for N_i will still be chosen and discussed later.

4.2.3. Cost Function

To determine the control law, a cost function (58) is used, comprising of the square of the error from the reference setpoint vector, \mathbf{r}_s , with an additional term measuring the control effort. The control effort is measured using the square of the delta input multiplied by a tuning constant r_u .

$$J_{\text{mpc}} = (\mathbf{r}_s - \mathbf{y}_p)^T (\mathbf{r}_s - \mathbf{y}_p) + \Delta \mathbf{h}_{\text{in}}^T \cdot r_u \cdot \mathbf{I}_{N_c \times N_c} \cdot \Delta \mathbf{h}_{\text{in}} \quad (58)$$

$\Delta \mathbf{h}_{\text{in}}$ is considered to be the only controllable variable, while the other disturbances can only be measured. The predicted system response, \mathbf{y}_p , still includes these measurable disturbances. Equation (55) will be substituted into (58) to obtain the full cost function. The next step is then to minimise J_{mpc} by setting $\frac{\partial J_{\text{mpc}}}{\partial \Delta \mathbf{h}_{\text{in}}} = 0$ which leads to equation (59). The derivation is covered in detail in [26, p. 9] and has been adapted for the purpose of this system.

$$\Delta \mathbf{h}_{\text{in}} = (\Phi_1^T \cdot \Phi_1 + r_u \cdot \mathbf{I}_{N_c \times N_c})^{-1} \Phi_1^T (\mathbf{r}_s - \mathbf{E} \cdot \mathbf{x}(k_i) - \Phi_2 \cdot \Delta \mathbf{fire}_{\text{in}} - \Phi_3 \cdot \Delta \mathbf{fire}_{\text{in}} - \Phi_4 \cdot \Delta \mathbf{p}_{\text{in}}) \quad (59)$$

Table 12: Nomenclature for MPC cost function

| Symbol | SI Unit | Description |
|------------------------------------|---------------------|---|
| $\Delta \mathbf{h}_{\text{in}}$ | [J/kg] | Vector of CV deltas across the control horizon |
| $\Delta \mathbf{fire}_{\text{in}}$ | [J/s] | Vector of DV deltas across the control horizon |
| $\Delta \mathbf{fire}_{\text{in}}$ | [J/s ²] | Vector of DV deltas across the control horizon |
| $\Delta \mathbf{p}_{\text{in}}$ | [Pa/s] | Vector of DV deltas across the control horizon |
| \mathbf{y}_p | [J/kg] | Predicted output states |
| \mathbf{E} | | Predictive free impulse response from initial state |
| $\mathbf{x}(k_i)$ | [J/kg] | System states at time of prediction k_i |
| k_i | | Sample index at time of prediction |
| Φ_g | | Predictive impulse responses to input changes |
| \mathbf{r}_s | [J/kg] | Setpoint reference vector over control horizon |
| r_u | | Control effort cost tuning constant |

The resultant equation (59) gives a control law with respect to the setpoint reference, the current system states, and the measured disturbances. Only the gains are of interest at this point as there

Chapter 4 Controller Design

is no need to compute for the entire control horizon of $\Delta \mathbf{h}_{in}$ in (59). For this reason, a vector to isolate the first index is defined in equation (60) and defined as the common term \mathbf{k}_{phi} . With the substitution of \mathbf{k}_{phi} into (59) and after rearranging equation (61) is derived.

$$\mathbf{k}_{phi} = [1 \ 0 \ 0 \ \dots] \cdot (\Phi_1^T \cdot \Phi_1 + r_u \cdot \mathbf{I}_{Nc \times Nc})^{-1} \Phi_1^T \quad (60)$$

$$\Delta h_{in}(k_i) = \mathbf{k}_{phi} \mathbf{r}_s - \mathbf{k}_{phi} \cdot \mathbf{E} \cdot \mathbf{x}(k_i) - \mathbf{k}_{phi} (\Phi_2 \cdot \Delta \mathbf{fire}_{in} + \Phi_3 \cdot \Delta \mathbf{fire}_{in} + \Phi_4 \cdot \Delta \mathbf{p}_{in}) \quad (61)$$

The reference setpoint is considered constant across the control horizon although it is allowed to vary. The vector \mathbf{r}_s is described as the unity vector multiplied with the setpoint variable $r_s(k_i)$ in (62). This unity vector is incorporated into the gain k_{ref} in (63) which then operates on the setpoint variable $r_s(k_i)$ directly as will be seen in the final control law later in equation (69).

$$\mathbf{r}_s_{(N_p - N_i) \times 1} = [1 \ 1 \ 1 \ 1 \ \dots]^T \cdot r_s(k_i) \quad (62)$$

$$k_{ref} = \mathbf{k}_{phi} \cdot [1 \ 1 \ 1 \ 1 \ \dots]^T \quad (63)$$

In the case of a ramped setpoint change, the k_{ref} gain can be variable in terms of the \mathbf{r}_s matrix of future setpoint values. This should facilitate close to error free following of a ramped setpoint change. It is not explored further in this section as step changes are significantly limited by the control system. Zero error following of a ramped setpoint is also not a requirement for the control system.

The state feedback gains \mathbf{k}_{state} are calculated in a similar fashion in equation (64). This gain will operate on the state variables $\mathbf{x}(k_i)$ directly in the control law (69). It will also be noticed later that the setpoint feedback gain, k_{ref} , will be the same but negative compared to the system output state feedback gain for state, $y_m(k)$ in the augmented model (49). This difference in the output and setpoint multiplied by this gain essentially gives the traditional error feedback term.

$$\mathbf{k}_{state \ 1 \times 3} = -\mathbf{k}_{phi} \cdot \mathbf{E} \quad (64)$$

\mathbf{k}_{ff} is seen as a feed forward control gain from the measured model disturbances. Since the disturbance can only be measured at k_i only the initial value is known for the vectors in equations (66), (67) and (68). The vectors used to construct these equations from their respective measurements at k_i is incorporated into the gain calculation of \mathbf{k}_{ff} in (65). The gain then operates on the disturbance measurements at k_i directly in the control law (69).

Chapter 4 Controller Design

$$\mathbf{k}_{ff} \ 1 \times 3 = -\mathbf{k}_{phi} \cdot [\ \Phi_2 \cdot [1 \ 0 \ 0 \ \dots]^T \ \Phi_3 \cdot [1 \ 0 \ 0 \ \dots]^T \ \Phi_4 \cdot [1 \ 0 \ 0 \ \dots]^T \] \quad (65)$$

$$\Delta \mathbf{fire}_{in} \ N_c \times 1 = [1 \ 0 \ 0 \ \dots]^T \cdot \Delta fire_{in}(k_i) \quad (66)$$

$$\Delta \dot{\mathbf{fire}}_{in} \ N_c \times 1 = [1 \ 0 \ 0 \ \dots]^T \cdot \Delta \dot{fire}_{in}(k_i) \quad (67)$$

$$\Delta \dot{\mathbf{p}}_{in} \ N_c \times 1 = [1 \ 0 \ 0 \ \dots]^T \cdot \Delta \dot{p}_{in}(k_i) \quad (68)$$

Equation (69) represents the control law in its final form with the various feedback terms and gain factors separated out.

$$\Delta h_{in}(k_i) = k_{ref} \cdot r_s(k_i) - \mathbf{k}_{state} \cdot \mathbf{x}(k_i) - \mathbf{k}_{ff} \cdot [\Delta fire_{in}(k_i) \ \Delta \dot{fire}_{in}(k_i) \ \Delta \dot{p}_{in}(k_i)]^T \quad (69)$$

4.2.4. MPC Control Parameter Calculation

These feedback gains are precalculated since the plant model has been adapted to stay constant over the operating range. From the derivation of these feedback gains it can be seen that the controller output is calculated for the entire control horizon, although the calculation is re-evaluated every cycle. The theoretical model was augmented which increased the order of the \mathbf{F} matrix by one from the original \mathbf{F}_m . The states are rewritten in terms of their deltas, and the control law output is then also expressed in a delta form. This was covered in section 4.2.1.

The MPC gains can be precalculated and fixed for the case where no constraints are added. The calculations were covered in section 4.2.2 for the derivation of the predicted output variables which are then used in the cost function calculation in section 4.2.3. The results of following through with these equations can be seen in *Table 13*. To compensate for the deadtime and thermal inertia in the plant response, the MPC gains calculation is modified to ignore a certain number of samples directly succeeding the control law application. This prevents skewing the sum of square errors in the initial system response where the controller has no significant influence. A number of ignored samples of 5 has been chosen which relates to 1.25 minutes. The process has a time constant, at full load conditions, of an estimated 3 minutes or about 12 samples. When analysing the controller performance later in section 5.2.1 the lag associated with this process will become very clear. The ignored samples amount is therefore chosen at just short of half that of the system time constant.

The prediction horizon is chosen at 20 samples relating to 5 minutes. These time figures relate to the full load operation at 60kg/s, and will increase as the loading decreases. The settling time of

Chapter 4 Controller Design

the process is considered to be just slightly more than 5 minutes at full load. Choosing the prediction horizon too long will again result in skewing of the cost function due to the system having already settled for a larger portion of the prediction horizon.

The control horizon is chosen to be 1 sample as it has shown to result in the best response. This can also be motivated by the fact that due to deadtime a single step change is preferential since the system filters any high frequency actuation limiting the benefit you would get from a larger control horizon. It also provides the best guess final state for the spray water thereby reducing steam over quenching and overshoot in the control response.

Table 13: Precalculated MPC Controller Parameters

| Symbol | Value | Description |
|-----------------------------|---------------------------|-----------------------------|
| N_i | 5 | Ignored states responses |
| N_p | 20 | Prediction horizon |
| N_c | 1 | Control horizon |
| r_u | 1 | Control effort cost factor |
| m | 1 | Reduced order observer gain |
| $\mathbf{k}_{\text{state}}$ | [5.803, 5.912, 1.469] | State feedback gains |
| k_{ref} | 1.469 | Reference feedback gain |
| \mathbf{k}_{ff} | [1.593, 274.945, 143.071] | Input feedforward gains |

A reduced order observer was designed for the $\Delta h_1(k)$ state that cannot be measured, and observer gain, m , experimentally determined. The details of the reduced order observer will be discussed in the next section.

Implied at the moment is that there is a much faster cascade controller that would control the inlet temperature based on the control law of this controller. Due to the fast nature its transfer function is ignored and lumped with the modelled plant response.

4.2.5. Reduced Order Observer – MPC Controller

From the state representation in equation (51) to (54) we can measure the $y_m(k)$ state directly and calculate $\Delta h_2(k)$ as the difference in $y_m(k)$ between samples. A reduced order state observer will be designed to estimate $\Delta h_1(k)$ only. The reduced order filter equations from [42, p. 523] have been used to produce the following equations for calculation of $\Delta \hat{h}_1(k + 1)$.

$$\Delta \hat{h}_1(k+1) = \left(\begin{array}{c} [0 \quad \mathbf{f}_2 \quad 0] \begin{bmatrix} \Delta h_2(k) \\ \Delta \hat{h}_1(k) \\ y_m(k) \end{bmatrix} + \\ [0.1433 \quad 0.03657 \quad 19.23 \quad 13.63] \begin{bmatrix} \Delta h_{in}(k) \\ \Delta fire_{in}(k) \\ \Delta fire_{in}(k) \\ \Delta \dot{p}_{in}(k) \end{bmatrix} + error(k) \end{array} \right) \quad (70)$$

The above terms can be derived directly from multiplying the state equations from (51) to (54) for state Δh_1 only. The error term will be introduced in the next equation and will include the observer gain m . The error terms can also be derived directly from multiplying the state equations from (51) to (54) for Δh_2 only and moving all the terms to one side of the equation.

$$error(k) = m \times \left(\begin{array}{c} \Delta h_2(k+1) - [0.8108 \quad \mathbf{f}_1 \quad 0.24 \quad 0] \begin{bmatrix} \Delta h_2(k) \\ \Delta \hat{h}_1(k) \\ y_m(k) \end{bmatrix} - \\ [0 \quad 0.1935 \quad 23.15 \quad 9.165] \begin{bmatrix} \Delta h_{in}(k) \\ \Delta fire_{in}(k) \\ \Delta fire_{in}(k) \\ \Delta \dot{p}_{in}(k) \end{bmatrix} \end{array} \right) \quad (71)$$

In practice a predicted $\Delta h_1(k+1)$ will be calculated as with any current observer and then updated at the start of the next sample time. $\Delta \hat{h}_1(k+1)$ is the updated state prediction taking the Δh_2 measurement at $(k+1)$ into account.

4.2.6. MPC Controller

In the figure below the full controller can be seen. The controller will be subject to a variable sample time. The inputs will be averaged between samples, while the controller output will be passed to a zero-order hold function.

4.3. Fuzzy Control Strategy

A TSK Fuzzy control system will be designed and simulated as an alternative to the proposed MPC controller. The TSK Fuzzy controller differs from Mamdani Fuzzy controllers in the way that the output is defined as seen in references [18], [44] and [25]. The output for each rule is crisply defined, usually linearly or sometimes just constant. Weighted averaging is then used to provide the inferred output. Much of the work discussed so far as part of the MPC controller will feed into the TSK Fuzzy controller as well. Due to the nature of the model that was developed it is easy to adapt it to obtain a basic model-based control law for each operating region used with the TSK Fuzzy controller. From that starting point the Fuzzy controller will be developed and optimised further for each operating region. This is also in line with [35, pp. 284-289] where it is described how this type of model-based control can be integrated into the Fuzzy controller. Further methods of model-based Fuzzy control are also described in [45, p. 33]. The Fuzzy controller can be said to define the linear operating regions while each region at its peak utilises a linear model-based approach for crisp control in that region.

The same augmented model will be used and indeed the controller feedback gains will be initially calculated similar to the MPC controller design. The controller will have a fixed sample time and therefore cannot use the exact MPC control strategy. The MPC controller's linear representation relied upon a variable sample time implementation. Using a fixed sample time, the fuzzy control rules, and the regions they define, would need to specifically control for regions with a high steam flow acceleration. This implies that although at least one region could be very easily defined from the MPC control law, adaptations would be required for the other control regions as defined by the fuzzy controller rules. The control laws for each rule will also include feedback based on the steam flow acceleration which was not part of the models derived so far or the MPC controller.

The fuzzy controller will consist of a 2 by 3 grid of overlapping triangular membership functions of steam flow rate and acceleration. This will be discussed in more detail in this section. There will be an inference rule and control law for each position of the inference grid. The consequent of a TSK Fuzzy controller is the weighted average defuzzification of rule-based state space proportional control laws based on the inputs to the Fuzzy controller. The state observer will only

Chapter 4 Controller Design

differentiate based on the steam flow rate alone, It will have only two rules for each membership function of steam flow rate. This will be seen from the inference rules in the following sections. Adaptations made to the cost function will be discussed in more detail in order to derive model-based control laws for each inference rule.

4.3.1. Membership Functions

The Fuzzy controller will use a sample time of 15 seconds. This is equivalent to the fastest sample time associated with full load operation at a 60 kg/s steam flow rate as used for the MPC controller. The Fuzzy controller, at 15 seconds, will always be at least as fast as the MPC controller at its faster sampling time. This should be sufficient to allow comparable results across the entire operating range. Before the control parameters for each membership function are calculated, some basic decisions need to be made about the nature of the membership functions.

Two triangular membership functions have been chosen for the steam flow rate inference; One peaking at full load, 60 kg/s, and one at 10 kg/s each tapering off to zero while summing to unity over the operating range. The system is usually only in full and consistent operation at about 15 kg/s. Triangular membership functions to the steam flow rate have been chosen for this application and fully overlap across the steam flow range. As there are only two membership functions for the steam flow rate, the end points are capped at 10 kg/s and 60 kg/s.

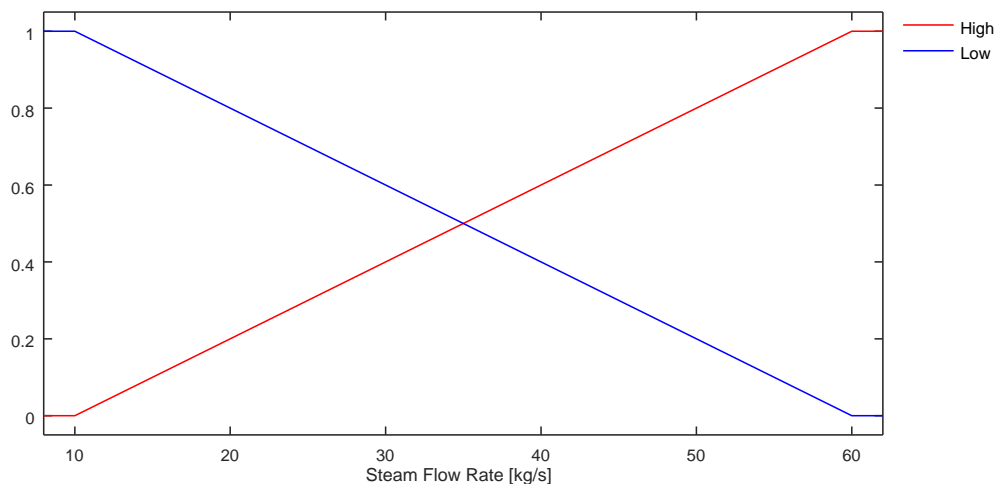


Figure 38: TSK Fuzzy Steam Flow Rate Membership Functions

Chapter 4 Controller Design

Initially, the Fuzzy controller was tested with only steam flow rate related inference rules to see if 2 membership functions would suffice over the full operating range. The testing revealed that at a certain steam flow acceleration the MPC controller error was still high. Since the dynamic interactions that caused this could not be identified in the model it could not be compensated for in the MPC controller. It was therefore identified that steam flow acceleration could be incorporated successfully into the fuzzy controller membership functions to gain an additional performance increase over the MPC controller. After analysing all the scenarios used for training a maximum and minimum rate of change was identified along with the steady state condition.

Three triangular membership functions have been chosen for the steam flow acceleration inference; The 'Positive' and 'Negative' triangular membership functions peak at $\pm 0.193 \text{ kg/s}^2$, and both taper off completely at 0 kg/s^2 . The 'Small' triangular membership function starts at zero and tapers off completely to each side by $\pm 0.193 \text{ kg/s}^2$. The three membership functions have been chosen to overlap across the range and sum to unity. The two triangular membership functions at the end points are capped at $\pm 0.193 \text{ kg/s}^2$ as this is considered the end of the range of operation. The training that informed these specific parameters will be discussed in the next section.

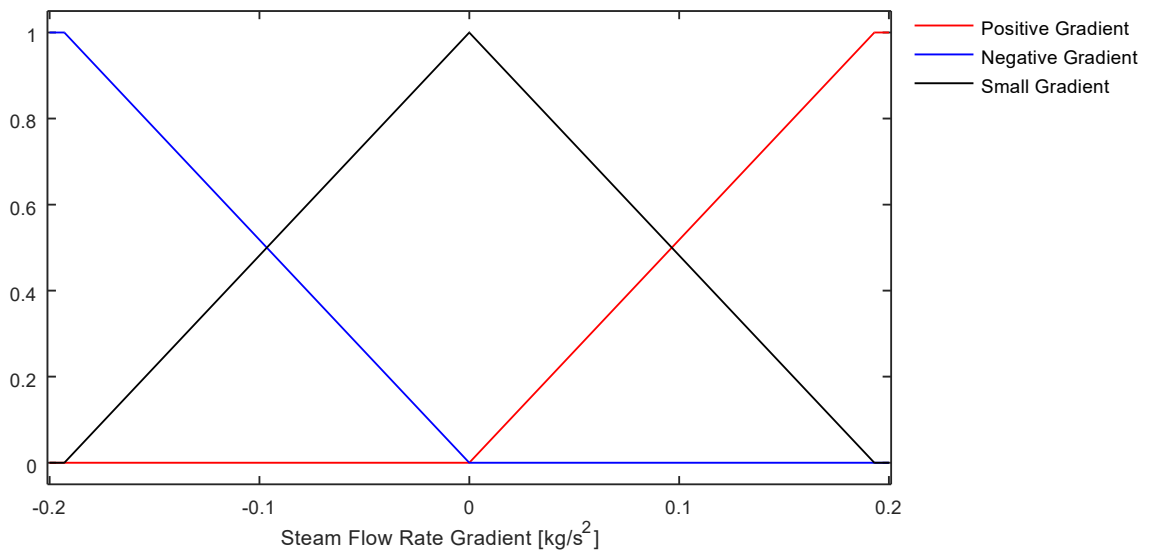


Figure 39: TSK Fuzzy Steam Flow Rate Derivative Membership Functions

Chapter 4 Controller Design

The other parameters used for control are also inputs to the Fuzzy controller. No membership functions have been defined for them as they are not used for rule definition. They are only used for the control laws for each rule. As already mentioned, with this type of Fuzzy control technique, the only inference required to define the control law is the weighted average of the linear or constant control laws. The control law is still crisply defined based on the state feedback and input signals of the system. Defuzzification of the control law of each rule is based on weighted average.

4.3.2. Rules

As seen from the previous section, 3 membership functions exist for the steam flow acceleration, and 2 membership functions exist for the steam flow rate. These membership functions can easily be visualised on a 2 by 3 grid or membership area. The rules can then be defined on the various membership function peaks of each of the two parameters. This then results in 6 rules emerging, using the product rule for the AND function. The Fuzzy controller rules are shown below:

1. If (\dot{m}_{in} is High) and (\ddot{m}_{in} is Negative) then $\Delta h_{in}(k) = \Delta h_{in_rule_1}(k)$
2. If (\dot{m}_{in} is High) and (\ddot{m}_{in} is Small) then $\Delta h_{in}(k) = \Delta h_{in_rule_2}(k)$
3. If (\dot{m}_{in} is High) and (\ddot{m}_{in} is Positive) then $\Delta h_{in}(k) = \Delta h_{in_rule_3}(k)$
4. If (\dot{m}_{in} is Low) and (\ddot{m}_{in} is Negative) then $\Delta h_{in}(k) = \Delta h_{in_rule_4}(k)$
5. If (\dot{m}_{in} is Low) and (\ddot{m}_{in} is Small) then $\Delta h_{in}(k) = \Delta h_{in_rule_5}(k)$
6. If (\dot{m}_{in} is Low) and (\ddot{m}_{in} is Positive) then $\Delta h_{in}(k) = \Delta h_{in_rule_6}(k)$

Table 15: TSK If-Then Rules Grid

| | | Steam Flow Acceleration | | |
|-----------------|------|---|---|---|
| | | Negative | Small | Positive |
| Steam Flow Rate | High | 1 $\Delta h_{in_rule_1}(k)$ | 2 $\Delta h_{in_rule_2}(k)$ | 3 $\Delta h_{in_rule_3}(k)$ |
| | Low | 4 $\Delta h_{in_rule_4}(k)$ | 5 $\Delta h_{in_rule_5}(k)$ | 6 $\Delta h_{in_rule_6}(k)$ |

With the state observer it was not found necessary to specify rules based on the steam flow acceleration. A state observer is however still required since state space feedback controllers are utilised in each region identified by the controller rules. It is unsure how the plant model really

Chapter 4 Controller Design

changes with a high rate of acceleration. The state observer is seen to perform adequately without this added complexity. Further justification stems from the fact that only one system state is unmeasured. Enough information can be obtained from the measured states to assume that any remaining error would be insignificant. Each state observation rule is represented by a reduced order state space observer as discussed previously. The rules are defined on the basis of the steam flow rate. The Fuzzy observer rules are shown below with parameter calculation presented in section 4.3.4:

7. If (\dot{m}_{in} is High) then $\Delta'h_1(k) = \Delta'h_{1_rule_1}(k)$

8. If (\dot{m}_{in} is Low) then $\Delta'h_1(k) = \Delta'h_{1_rule_2}(k)$

With the TSK Fuzzy controller a weighted average defuzzification method is implied. The specifics of the control laws for each rule will be discussed next.

4.3.3. TSK Fuzzy Control Law Calculation

Before work is started on the fuzzy controller some clarification is needed. Up to this point the membership functions and control laws have been defined, but the actual consequent has not. The TSK-Fuzzy controller uses a crisp control law for each rule that goes through the inference process to produce the consequent. It is necessary to construct a crisp control law for each rule that has been defined at this point.

The Fuzzy controller does not rely on the MPC controller implementation. During development of the fuzzy controller, it was believed useful to reuse some of the work done to construct the MPC controller in defining at least a starting point for the crisp control laws that will be used for the Fuzzy controller. The Fuzzy controller will not have a variable sample time and only the static gain values are sought after for each operating region. The MPC controller performed admirably after all. This also helps reduce the number of degrees of freedom when optimising the fuzzy controller. Thereafter the fuzzy controller is optimised and includes the steam flow acceleration as part of its control laws and will no longer resemble the MPC controller.

Base Model for Fuzzy Rules Derived from MPC Cost Function

As per the previous design technique used for the MPC controller, initial control laws for rules 2 and 5 have been calculated similarly to the MPC controller without having a variable sample

Chapter 4 Controller Design

time. The state space model for the low steam flow rate case, rule 5, was converted from a digital state with a 90 second sample time (variable sample time at low steam flow rate) to a digital state with a 15 second sample time. This was done with a using a zero-order hold approximation. This will now be a fixed model with a fixed sample time. The model and control law derived will only serve as a starting point. The Fuzzy controller will include direct feedback from the steam flow acceleration. The final gains were determined during optimisation and will be discussed more, later in this section.

For rules 1, 3, 4 and 6 feedback gains were calculated by modifying the cost function parameters from equations (55) (56) and (57) repeated here for ease of reference. Matrixes \mathbf{E} and Φ_g can be seen to only take the \mathbf{F} and \mathbf{g} into account when calculating the term \mathbf{y}_p across the prediction horizon. Rules 1, 3, 4 and 6 however are based on the premise of \ddot{m}_{in} not being ‘Small’.

$$\mathbf{y}_p = \mathbf{E} \cdot \mathbf{x}(k_i) + \Phi_1 \cdot \Delta h_{in} + \Phi_2 \cdot \Delta \text{fire}_{in} + \Phi_3 \cdot \Delta \dot{\text{fire}}_{in} + \Phi_4 \cdot \Delta \dot{p}_{in} \quad (55)$$

$$\mathbf{E}_{(N_p - N_i) \times 3} = \begin{bmatrix} \mathbf{e} \cdot \mathbf{F} \\ \mathbf{e} \cdot \mathbf{F}^2 \\ \mathbf{c} \cdot \mathbf{F}^3 \\ \vdots \\ \mathbf{c} \cdot \mathbf{F}^{N_p} \end{bmatrix} \quad (56)$$

$$\Phi_g_{(N_p - N_i) \times N_c} = \begin{bmatrix} \mathbf{e} \cdot \mathbf{g}_{*,g} & \emptyset & \emptyset & \dots & \emptyset \\ \mathbf{e} \cdot \mathbf{F} \cdot \mathbf{g}_{*,g} & \mathbf{e} \cdot \mathbf{g}_{*,g} & \emptyset & \dots & \emptyset \\ \mathbf{c} \cdot \mathbf{F}^2 \cdot \mathbf{g}_{*,g} & \mathbf{c} \cdot \mathbf{F} \cdot \mathbf{g}_{*,g} & \mathbf{c} \cdot \mathbf{g}_{*,g} & \dots & 0 \\ \vdots & \vdots & \vdots & \dots & \vdots \\ \mathbf{c} \cdot \mathbf{F}^{N_p - 1} \cdot \mathbf{g}_{*,g} & \mathbf{c} \cdot \mathbf{F}^{N_p - 2} \cdot \mathbf{g}_{*,g} & \mathbf{c} \cdot \mathbf{F}^{N_p - 3} \cdot \mathbf{g}_{*,g} & \dots & \mathbf{c} \cdot \mathbf{F}^{N_p - N_c} \cdot \mathbf{g}_{*,g} \end{bmatrix} \quad (57)$$

The system state space representation will change for each step in the prediction horizon based on steam flow rate changes. The end goal is to modify matrixes \mathbf{E} and Φ_g per sample of prediction (or row) to incorporate the change in the system response. This is still done by resampling the variable sample rate model to a fixed sample time for the corresponding steam flow rate for each subsequent sample.

This represents a slight problem as there is no knowledge of future values of the steam flow rate having only the instantaneous steam flow acceleration. It is therefore necessary to estimate the steam flow rate for future samples based on the premise that the steam flow acceleration would decay at an estimated exponential rate.

Chapter 4 Controller Design

$$H(z) = \frac{15 z^2}{z^2 - 1.85 z + 0.85} \quad (76)$$

The steam flow rate over the prediction horizon is then estimated by a simple digital filter (76). It takes the steam flow acceleration as an impulse input and the current steam flow rate as the initial condition. The steam flow rate dynamics impulse response has a time constant of around 85 seconds and will settle to a maximum value of 100 times the impulse, or current acceleration. That equates to about ± 20 kg/s at the maximum gradient from the initial value. To ensure that for rule 4 the steam flow rate does not go negative the transfer function output has been capped at 4 kg/s.

The choices for the maximum and minimum steam flow acceleration was based on analysing the worst cases of the scenarios that were captured. Looking at *Figure 16*, it represents one of the two cases with the most severe swings in steam flow rate. Looking at the time derivative of the steam flow rate the maximum flow acceleration was above 0.2 kg/s^2 . Since the steam flow rate decay was maintained for around a minute, it was decided to average the values over that minute which delivered a 0.193 kg/s^2 decay rate. This was done to avoid setting the limit on an outlier in the data. From the data in *Figure 16*, it is also seen that such a disturbance caused a steam flow rate swing of 20 kg/s in just under 2 minutes. How long a disturbance would last is however not scalable between scenarios. It is noted again that a few samples are ignored in the calculation of the gains for the controller. This is done due to the lag in the system that limits the effectiveness of control interventions on the first few samples of the final steam temperature. This then leads to the assumption that the predicted steam flow rate is important for these initial samples. Any inaccuracy in the predicted value of the steam flow rate, after these initial ignored samples, has the potential to still be corrected for. The prediction is updated at each sample with measured new steam flow rate data. It therefore mostly relies on the relative accuracy of the prediction in the first few samples of the prediction horizon. The time constant of the steam flow acceleration prediction is then chosen, with these assumptions, to be just more of 5 sample times long.

The future values of steam flow rate need to be estimated from the starting values for peak membership to steam flow rate and acceleration for each rule. The digital filter (76) takes \dot{m}_{in} as its initial value and \ddot{m}_{in} as an impulse to the filter to estimate steam flow rate progression. The particular values for each rule are defined in *Table 16*, with the results plotted in *Figure 40*.

Chapter 4 Controller Design

Table 16: TSK Peak Rule Membership

| | | Steam Flow Acceleration | |
|-----------------|------|---|---|
| | | Negative | Positive |
| Steam Flow Rate | High | 1 $\dot{m}_{in} = 60 \text{ kg/s}$ $\ddot{m}_{in} = -0.193 \text{ kg/s}^2$ | 3 $\dot{m}_{in} = 60 \text{ kg/s}$ $\ddot{m}_{in} = +0.193 \text{ kg/s}^2$ |
| | Low | 4 $\dot{m}_{in} = 10 \text{ kg/s}$ $\ddot{m}_{in} = -0.193 \text{ kg/s}^2$ | 6 $\dot{m}_{in} = 10 \text{ kg/s}$ $\ddot{m}_{in} = +0.193 \text{ kg/s}^2$ |

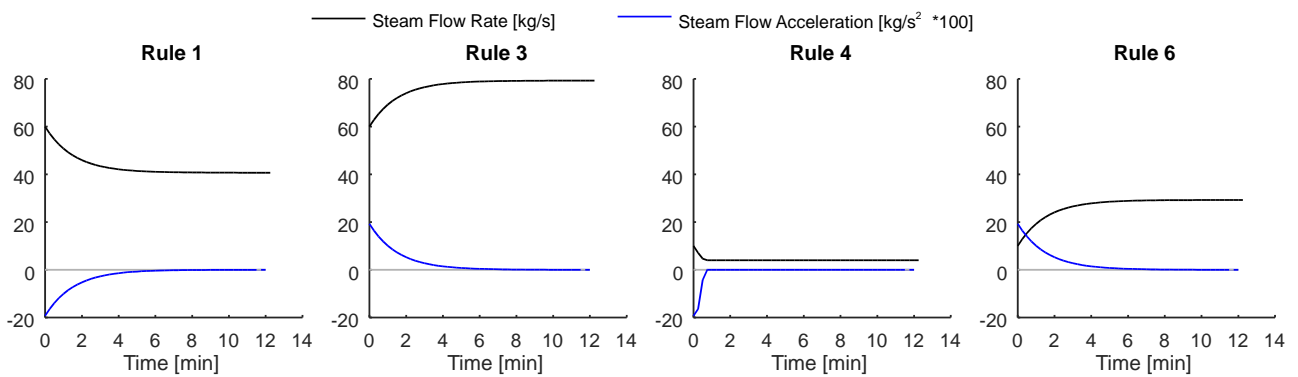


Figure 40: Estimated Flow Rate Per Rule

Getting back to the purpose of this activity, it is now necessary to recalculate equations (56) and (57) based on the changing system representation over the prediction horizon. With the steam flow rate estimated at an interval of 15 seconds the state representation is resampled at each sample, i starting at 1, to obtain a set of \mathbf{F}_i and \mathbf{g}_i matrixes. This was done through the use of a basic, zero-order hold, discrete-time dynamic system resampling function. A d2d function exists for this purpose in control system toolboxes for both Octave and MATLAB. Sampling the variable sample time system as estimated steam flow down to a 15 second fixed sample time system. The modified generic representation is then given in equation (77) and (78).

Chapter 4 Controller Design

$$\mathbf{E}_{N_p \times 3} = \begin{bmatrix} \mathbf{c} \cdot \mathbf{F}_1 \\ \mathbf{c} \cdot \mathbf{F}_2 \cdot \mathbf{F}_1 \\ \mathbf{c} \cdot \mathbf{F}_3 \cdot \mathbf{F}_2 \cdot \mathbf{F}_1 \\ \vdots \\ \mathbf{c} \cdot \mathbf{F}_{N_p} \cdots \mathbf{F}_1 \end{bmatrix} \quad (77)$$

$$\Phi_g \mathbf{N}_p \times \mathbf{N}_c = \begin{bmatrix} \mathbf{c} \cdot \mathbf{g}_{1*,g} & 0 & 0 & \dots & 0 \\ \mathbf{c} \cdot \mathbf{F}_2 \cdot \mathbf{g}_{1*,g} & \mathbf{c} \cdot \mathbf{g}_{2*,g} & 0 & \dots & 0 \\ \mathbf{c} \cdot \mathbf{F}_3 \cdot \mathbf{F}_2 \cdot \mathbf{g}_{1*,g} & \mathbf{c} \cdot \mathbf{F}_3 \cdot \mathbf{g}_{2*,g} & \mathbf{c} \cdot \mathbf{g}_{3*,g} & \dots & 0 \\ \vdots & \vdots & \vdots & \dots & \vdots \\ \mathbf{c} \cdot \mathbf{F}_{N_p} \cdots \mathbf{F}_2 \cdot \mathbf{g}_{1*,g} & \dots & \dots & \dots & \mathbf{c} \cdot \mathbf{F}_{N_p} \cdots \mathbf{F}_{N_c+1} \cdot \mathbf{g}_{N_c*,g} \end{bmatrix} \quad (78)$$

Table 17: Nomenclature for Predicted Output Variable Equations for Fuzzy Controller

| Symbol | Description |
|------------------------------|---|
| \mathbf{E} | Predictive free impulse response matrix from the initial state |
| Φ_g | Predictive impulse response matrix to control and disturbance input changes |
| $\mathbf{F}_p, \mathbf{G}_p$ | Resampled augmented digital domain state space matrixes at future index p |
| \mathbf{c}, \mathbf{d} | Original augmented digital domain state space matrixes |
| $\mathbf{g}_{p*,g}$ | Column reference to the \mathbf{G}_p matrix |

Table 18: Parameters for Initial Fuzzy Controller Gain Calculation

| | | Rules 1-3 High Steam Flow Rate | Rules 4-6 Low Steam Flow Rate |
|--------------------------|-------|-----------------------------------|----------------------------------|
| Ignored States Responses | N_i | 5 | 30 |
| Prediction Horizon | N_p | 20 | 120 |
| Control Horizon | N_c | 1 | 1 |
| Control Effort Cost | r_u | 1 | 100 |

It can be noted that, for rules 4-6, N_i and N_p are chosen as 6 times that of what was designed for the MPC controller of section 4.2.4. This is done due to the steam flow rate being a factor 6 smaller in this section and the process time constant a factor 6 longer.

There is no strikethrough to indicate the samples that are ignored as in the original equations (56) and (57). This is done not to obscure the matrix representation while the concept has already been discussed previously. The same principle is still applied when calculating the feedback gains. The same fundamental procedure, used in section 4.2.3 *Cost Function*, is applied again to arrive at a similar control law representation as in equation (69) repeated below.

$$\Delta h_{\text{in}}(k_i) = k_{\text{ref}} \cdot r_s(k_i) - \mathbf{k}_{\text{state}} \cdot \mathbf{x}(k_i) - \mathbf{k}_{\text{ff}} \cdot [\Delta \text{fire}_{\text{in}}(k_i) \quad \Delta \dot{\text{fire}}_{\text{in}}(k_i) \quad \Delta \dot{p}_{\text{in}}(k_i)]^T \quad (69)$$

This control law will be further altered to incorporate steam flow rate directly into the control law feedback. It will also be local to a specific rule defined region of operation. This is discussed next.

Steam Flow Acceleration as Direct Feedback for Control

The model shows that the steam flow rate does not directly serve as an input to the system, neither its acceleration. Upon further analysis of the scenarios used for training, it remained clear that those scenarios with large steam flow rate swings still suffer from significantly higher peak transient responses. The steam flow acceleration was therefore added as a feedback gain to the control laws for each rule. A significant improvement was achieved when this feedback is added for scenarios with a high rate of change in steam flow rate. It was identified during controller training that with smaller changes in steam flow rate, performance is worsened by adding the same proportional steam flow acceleration feedback, indicating this is not a linear relationship. Using a smaller proportional feedback during lower acceleration rates proved to add to the overall performance of the controller.

The feedback gains as well as the membership functions for the steam flow acceleration were determined through training on all datasets simultaneously. This is done in Appendix B.3. The cost function chosen here is slightly different than before. The difference between the peak positive and negative temperature excursions, or span, was still high during testing of the MPC controller for many scenarios. In an attempt to reduce the peak excursions, the decision was made to construct a cost function that would minimise this span at a possible cost to the standard deviation. The mean temperature error from setpoint was included to ensure that an offset was not induced during the training process since the standard deviation would not be included in the cost function. Since more than one parameter was used for the cost function they were also scaled. The scaling factors were approximately the mean and span values before they were optimised.

$$J_{TSK}^{-1} = \frac{0.84}{\text{Mean}} + \frac{6}{\text{Max-Min}} \quad (79)$$

All the parameters used in the control law have been summarized in the *Table 19* and

Chapter 4 Controller Design

Table 20 for the 6 rules. As mentioned before defuzzification will be done with a weighted average. The control law is shown below.

$$\Delta h_{\text{in,rule}_x}(k_i) = k_{\text{ref}_x} \cdot r_s(k_i) - \mathbf{k}_{\text{state}_x} \cdot \mathbf{x}(k_i) - \mathbf{k}_{\text{ff}_x} \cdot [\Delta \text{fire}_{\text{in}}(k_i) \ \Delta \dot{\text{fire}}_{\text{in}}(k_i) \ \Delta \dot{p}_{\text{in}}(k_i)]^T - k_{\text{dm}_x} \cdot \dot{m}_{\text{in}}(k_i) \quad (80)$$

Table 19: TSK Fuzzy Controller Parameters, Rule 1 – 3

| High Steam Flow Rate | | Steam Flow Acceleration | | |
|-------------------------|-------------------------------|-------------------------|----------------------|----------------------|
| | | Rule 1 | Rule 2 | Rule 3 |
| Control Parameters | | Negative | Small | Positive |
| Feedback State Gains | $\mathbf{k}_{\text{state}_x}$ | [6.32, 6.37, 1.38] | [5.80, 5.91, 1.47] | [5.41, 5.51, 1.54] |
| Reference Feedback Gain | k_{ref_x} | 1.38 | 1.47 | 1.54 |
| Input Feedforward Gains | \mathbf{k}_{ff_x} | [1.64, 283, 147] | [1.59, 275, 143] | [1.56, 269, 140] |
| Steam Flow Rate Deriv. | k_{dm_x} | $-2.5259 \cdot 10^5$ | $-6.5012 \cdot 10^4$ | $-2.5259 \cdot 10^5$ |

Table 20: TSK Fuzzy Controller Parameters, Rule 4 – 6

| Low Steam Flow Rate | | Steam Flow Acceleration | | |
|-------------------------|-------------------------------|-------------------------|----------------------|----------------------|
| | | Rule 4 | Rule 5 | Rule 6 |
| Control Parameters | | Negative | Small | Positive |
| Feedback State Gains | $\mathbf{k}_{\text{state}_x}$ | [14.4, 9.40, 0.297] | [9.54, 8.75, 0.370] | [3.11, 2.80, 0.262] |
| Reference Feedback Gain | k_{ref_x} | 0.297 | 0.370 | 0.262 |
| Input Feedforward Gains | \mathbf{k}_{ff_x} | [0.407, 63.4, 31.0] | [0.399, 68.7, 35.7] | [0.168, 28.7, 14.9] |
| Steam Flow Rate Deriv. | k_{dm_x} | $-5.8647 \cdot 10^5$ | $-1.5339 \cdot 10^5$ | $-5.8647 \cdot 10^5$ |

The following meshes have been constructed for each feedback gain to visualise how they change as the steam flow rate changes. Note k_{ref_x} is equal to the third element in $\mathbf{k}_{\text{state}_x}$ and is only shown once.

Chapter 4 Controller Design

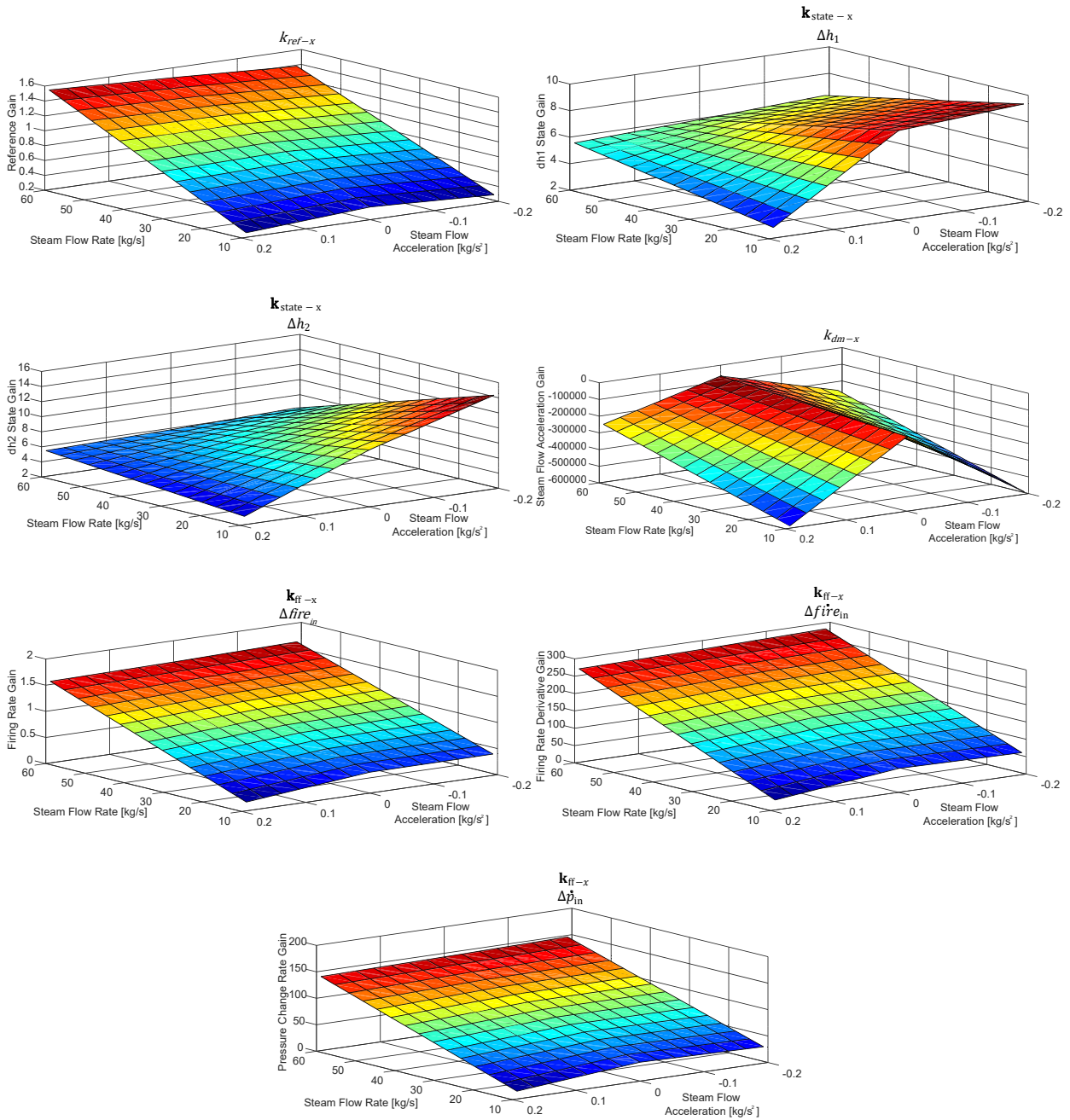


Figure 41: Fuzzy Controller Gain Mesh Representation

4.3.4. Reduced Order Observer – Fuzzy Controller

The reduced order observer for the Fuzzy controller rules depend only on the membership functions of the steam flow rate. The same reduced order state observer is used as defined in (70)

Chapter 4 Controller Design

(71). The gains used per rule are summarised in the table below. They are based on the model parameters used in the regions defined by rules 2 & 5 respectively.

Table 21: Reduced Order Observer – Fuzzy Controller Parameters

| Rule | Steam Flow Rate | m | f_{11} | f_{12} | f_{22} |
|------|-----------------|-----------------------------------|----------|-----------------------------------|----------|
| 7 | High | 1 | 0.8108 | 0.24 | 0.738 |
| 8 | Low | 1 | 0.9656 | 0.04952 | 0.9506 |
| | | \mathbf{g}^1 | | \mathbf{g}^2 | |
| 7 | High | [0, 0.1935, 23.15, 9.165] | | [0.1433, 0.03657, 19.23, 13.63] | |
| 8 | Low | [-0.003256, 0.0343, 3.766, 1.354] | | [0.02701, 0.006892, 3.624, 2.569] | |

4.3.5. TSK Fuzzy Controller

The Fuzzy controller is shown in the figure below. The basic composition is the same as for the MPC controller although the Fuzzy controller encapsulates two membership functions for this application. The controller has a fixed sample time of 15 seconds.

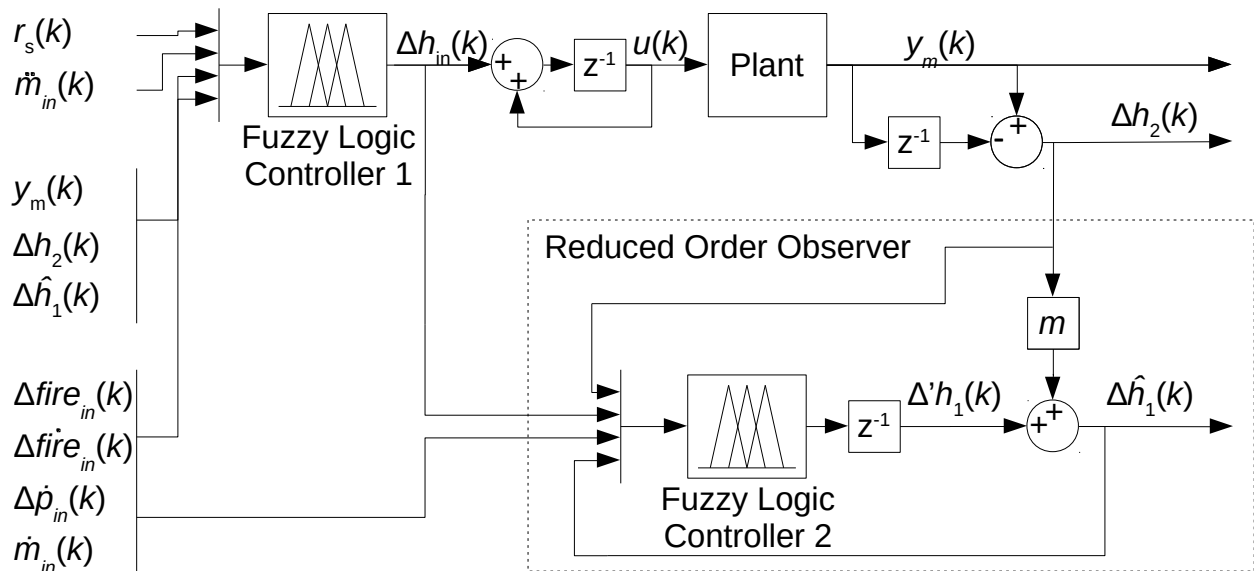


Figure 42: Fuzzy Logic Controller

Table 22: Nomenclature for Final Fuzzy Controller

| Symbol | SI Unit | Description |
|--------------------------|---------------------|--|
| \dot{m}_{in} | [kg/s] | Mass flow rate of steam from inlet to outlet |
| $r_s(k)$ | [J/kg] | Final steam enthalpy setpoint |
| y_m | [J/kg] | System output state |
| $u(k)$ | [J/kg] | Final superheater inlet enthalpy setpoint |
| $\Delta fire_{in}$ | [J/s] | Normalised delta firing rate input |
| $\Delta \dot{fire}_{in}$ | [J/s ²] | Normalised delta firing rate derivative input |
| $\Delta \hat{h}_1$ | [J/kg] | First superheater section observed enthalpy state |
| Δh_1 | [J/kg] | First superheater section intermediate observer state |
| Δh_2 | [J/kg] | Second superheater section enthalpy state |
| Δh_{in} | [J/kg] | Specific delta enthalpy of final superheater steam inlet |
| $\Delta \dot{p}_{in}$ | [Pa/s] | Normalised pressure rate of change input |

Fuzzy Logic Controller 1

The Fuzzy Logic Controller 1 can be described by the following rules:

1. **IF** (\dot{m}_{in} is High) **AND** (\ddot{m}_{in} is Negative)

$$\text{THEN } \Delta h_{in}(k) = 1.38 \cdot r_s(k) - [6.32, 6.37, 1.38] \cdot \mathbf{x}(k) - [1.64, 283, 147] \cdot \mathbf{u}_{Dist}(k) + 2.5259 \cdot 10^5 \cdot \dot{m}_{in}(k)$$

2. **IF** (\dot{m}_{in} is High) **AND** (\ddot{m}_{in} is Small)

$$\text{THEN } \Delta h_{in}(k) = 1.47 \cdot r_s(k) - [5.80, 5.91, 1.47] \cdot \mathbf{x}(k) - [1.59, 275, 143] \cdot \mathbf{u}_{Dist}(k) + 6.5012 \cdot 10^4 \cdot \dot{m}_{in}(k)$$

3. **IF** (\dot{m}_{in} is High) **AND** (\ddot{m}_{in} is Positive)

$$\text{THEN } \Delta h_{in}(k) = 1.54 \cdot r_s(k) - [5.41, 5.51, 1.54] \cdot \mathbf{x}(k) - [1.56, 269, 140] \cdot \mathbf{u}_{Dist}(k) + 2.5259 \cdot 10^5 \cdot \dot{m}_{in}(k)$$

4. **IF** (\dot{m}_{in} is Low) **AND** (\ddot{m}_{in} is Negative)

$$\text{THEN } \Delta h_{in}(k) = 0.297 \cdot r_s(k) - [14.4, 9.40, 0.297] \cdot \mathbf{x}(k) - [0.407, 63.4, 31.0] \cdot \mathbf{u}_{Dist}(k) + 5.8647 \cdot 10^5 \cdot \dot{m}_{in}(k)$$

5. **IF** (\dot{m}_{in} is Low) **AND** (\ddot{m}_{in} is Small)

$$\text{THEN } \Delta h_{in}(k) = 0.370 \cdot r_s(k) - [9.54, 8.75, 0.370] \cdot \mathbf{x}(k) - [0.399, 68.7, 35.7] \cdot \mathbf{u}_{Dist}(k) + 1.5339 \cdot 10^5 \cdot \dot{m}_{in}(k)$$

6. **IF** (\dot{m}_{in} is Low) **AND** (\ddot{m}_{in} is Positive)

$$\begin{aligned} \text{THEN } \Delta h_{in}(k) &= 0.262 \cdot r_s(k) - [3.11, 2.80, 0.262] \cdot \mathbf{x}(k) - [0.168, 28.7, 14.9] \cdot \\ \mathbf{u}_{Dist}(k) &+ 5.8647 \cdot 10^5 \cdot \ddot{m}_{in}(k) \end{aligned} \quad (81)$$

$$\text{With } \mathbf{u}_{Dist}(k) = \begin{bmatrix} \Delta fire_{in}(k) \\ \Delta fire_{in}(k) \\ \Delta \dot{p}_{in}(k) \end{bmatrix} \text{ and } \mathbf{x}(k) = \begin{bmatrix} \Delta h_2(k) \\ \Delta \hat{h}_1(k) \\ y_m(k) \end{bmatrix} \quad (75)$$

Membership function definitions can be seen in *Figure 38* and *Figure 39*. The output of the fuzzy controller is defuzzied using a weighted average of the fuzzy rule's degree of membership.

Fuzzy Logic Controller 2

The Fuzzy Logic Controller 2 is responsible for linear scheduling of the reduced order observer and can be described by the following rules:

$$9. \text{ IF } (\dot{m}_{in} \text{ is High}) \text{ THEN } \Delta' h_1(k+1) = [0.1433, -0.1569, -3.920, 4.465] \cdot \begin{bmatrix} \Delta h_{in}(k) \\ \mathbf{u}_{Dist}(k) \end{bmatrix} + [-0.8108, 0.4980, 0] \cdot \mathbf{x}(k)$$

$$10. \text{ IF } (\dot{m}_{in} \text{ is Low}) \text{ THEN } \Delta' h_1(k+1) = [0.03027, -0.02741, -0.1420, 1.215] \cdot \begin{bmatrix} \Delta h_{in}(k) \\ \mathbf{u}_{Dist}(k) \end{bmatrix} + [-0.9656, 0.9011, 0] \cdot \mathbf{x}(k) \quad (82)$$

$$\text{With } \mathbf{u}_{Dist}(k) = \begin{bmatrix} \Delta fire_{in}(k) \\ \Delta fire_{in}(k) \\ \Delta \dot{p}_{in}(k) \end{bmatrix} \text{ and } \mathbf{x}(k) = \begin{bmatrix} \Delta h_2(k) \\ \Delta \hat{h}_1(k) \\ y_m(k) \end{bmatrix} \quad (75)$$

Membership function definitions for the steam flow rate can be seen in *Figure 38*. The output of the fuzzy controller is again defuzzied using a weighted average of the fuzzy rule's degree of membership.

Chapter 5

Simulation and Evaluation

5.1. Simulation Strategy and Evaluation Criteria

The simulated results of both control strategies will be discussed in this section. The evaluation will look at several aspects:

- The controller response is evaluated qualitatively against the typical disturbances as were discussed in in section 3.5 during process modelling.
- Each controller will be evaluated based on the evaluation criteria set out in section 2.4.4:
 - The response time of the controller.
 - System peak temperature excursion: Mean, standard deviation, minimum and maximum values.
 - Avoidance of preventable trips: Two case studies, as discussed in section 2.3.

Simulation was done in the Octave [46] environment with the aid of the Xsteam [47] library for steam table conversions. The code used for simulation and plotting functions can be found in the *Appendix B.4* and *Appendix B.5*.

Simulation of all 38 Scenarios were conducted, and results summarised for each controller. Only the 5 case studies are looked at in more detail to provide insight into the results. There are a further 2 case studies that resulted in unit trips. These will be evaluated both on survivability as well as being a small exercise in robustness. These two trip conditions did not occur on the same unit used for training and evaluation. The result gives some insight into how generally applicable the model and the control laws are to other units. Model error is used as an unmeasured disturbance to the system to further test controller robustness. In the absence of controller on-line testing, it was decided to test scenarios for both controllers on an operations simulator to evaluate their performance on an independent platform.

5.2. MPC Control Strategy

For the following case studies the same scenarios are used that were discussed in detail in section 3.5. In each case only the controller's response is simulated, while the PID controller response is taken from the actual recorded response for the event with no tuning or alteration made to it.

5.2.1. Case Study Analysis for MPC Controller

Sudden Steam Flow Rate Swing

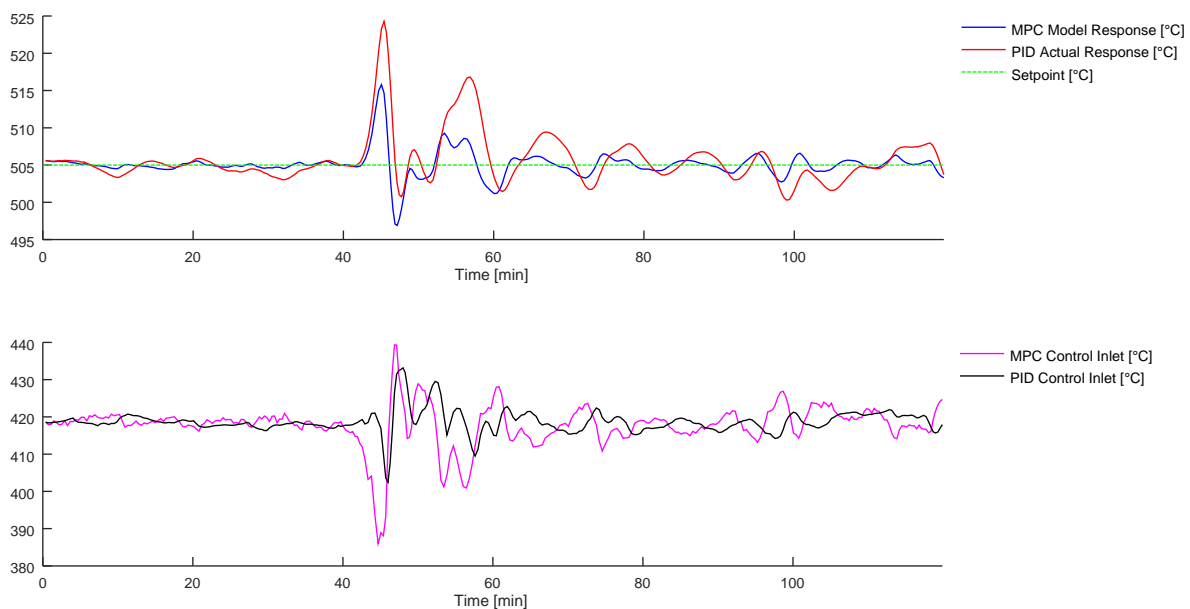


Figure 43: Sudden Steam Flow Rate Swing – MPC Control Response

From the controller response in *Figure 43* it can be seen that the MPC controller has significantly reduced the final steam temperature excursions. Reducing the maximum peak from 524 °C to 516 °C. The minimum peak response worsened for this test case, but the peak-to-peak amplitude is still reduced by 5 °C and is centred around the setpoint. This response has significantly increased the margin to the protection function limits. It can be seen that the control law is more aggressive in this case, but more importantly responds significantly earlier than the PID response.

From *Figure 43* it seems as if the MPC controller responds before the disturbance in the output. The system inputs were shown and discussed in section 3.5.1, *Figure 16* and *Figure 17*. From there it can be seen that the MPC responds to the feedforward of measurable disturbances. Due to

the large lag and thermal inertia of the system, the output is seen to only start changing as much as a minute or more after the MPC controller has started responding. It can also be seen that the PID controller differential gain is subtle and has almost no early effect. Again, it is important to point out that the existing PID controller is presented as is, without tuning or alteration.

A statistical analysis of all scenarios will be done in section 5.2.2. It is shown there that the standard final steam temperature deviation from setpoint reduces to 1.78 °C. This, and the peak steam temperature excursion reduction, constitutes a significant control effort improvement, and fulfil the evaluation criteria set out in in section 3.5.

Machine Deloading and Mill Outage

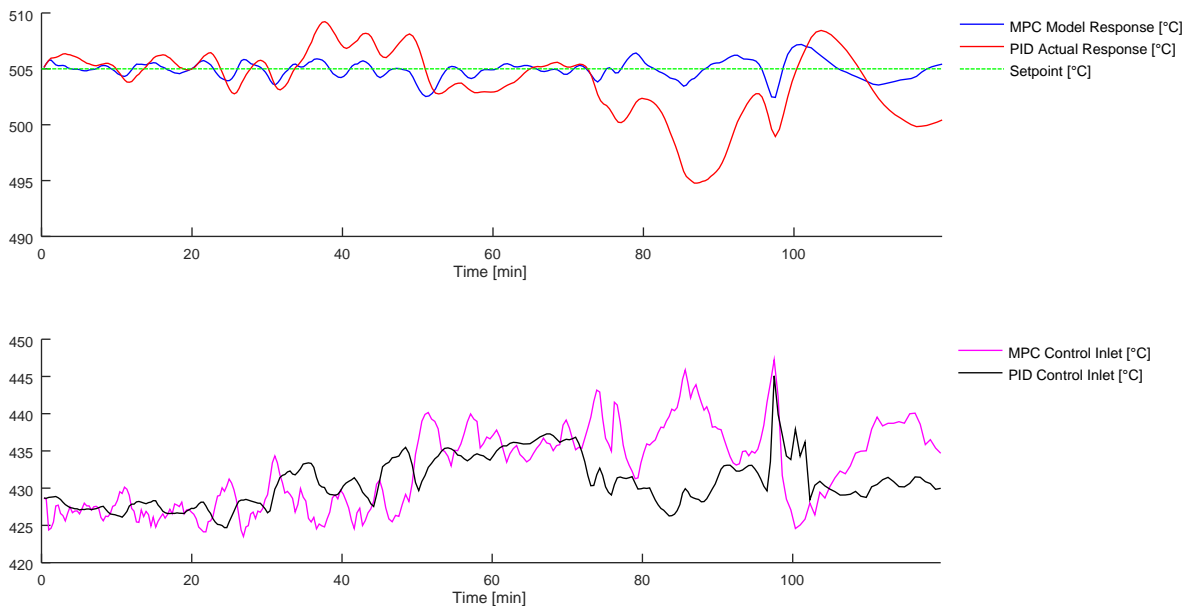


Figure 44: Machine Deloading and Mill Outage – MPC Control Response

The system response during deloading of a unit, as shown in *Figure 44*, is highly dynamic due to many interconnected controllers and process parameters that are changing together. It becomes difficult to analyse any specific section of the controller response visually. We see that the standard deviation from setpoint is significantly reduced to almost 24 % of the PID controller, resulting in a low 0.76 °C standard deviation. This tighter control means that the controller

Chapter 5 Simulation and Evaluation

setpoint can be operated closer to the setpoint under a variety of conditions. This reduces the need to lower the setpoint during process changes.

It can be seen that the feedforward gains are really assisting in mitigating known process disturbances. Soon after Mill B is taken out of service around the 75-minute mark the MPC controller responds almost opposite that of the PID controller. The system inputs can be referred to, back in section 3.5.2, *Figure 22* and *Figure 23*. It achieves a much better result due to this knowledge. Just before the 100-minute mark the load also drops significantly and again the MPC controller has a faster insight into what will happen next, and responds appropriately.

Steam Flow Cycling while Deloading

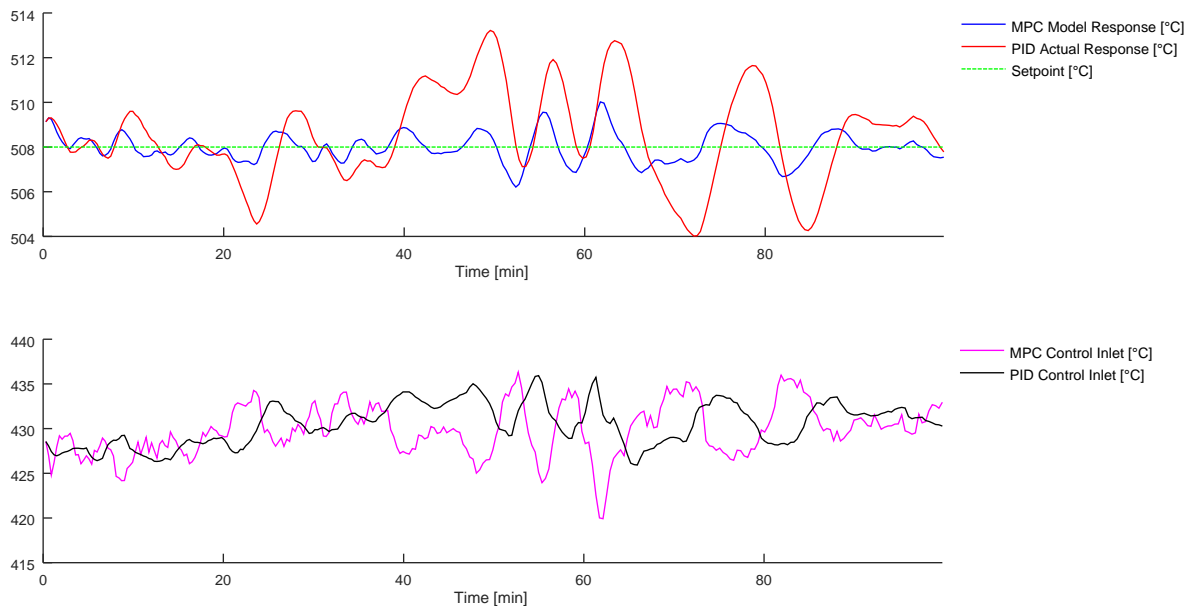


Figure 45: Steam Flow Rate Cycling while Deloading – MPC Control Response

For this scenario even the MPC controller is struggling to control the final steam temperature under the perturbed plant conditions and cycling steam flow, as seen in *Figure 45*. The cycling output amplitudes are still significantly reduced and from the control law it can be seen that there is no significant change in absolute control effort, but the responses are seen to be 180° out of phase due to the earlier, and therefore more effective response. The result is admirable as the standard deviation is only 31% compared to the PID controller and a 3.2°C reduction is achieved

Chapter 5 Simulation and Evaluation

in the steam temperature peak value. Looking back at section 3.5.3, *Figure 26* and *Figure 27* the system disturbances are not severe in amplitude, but a constant cycling steam flow and pressure is present.

Various Load Changes

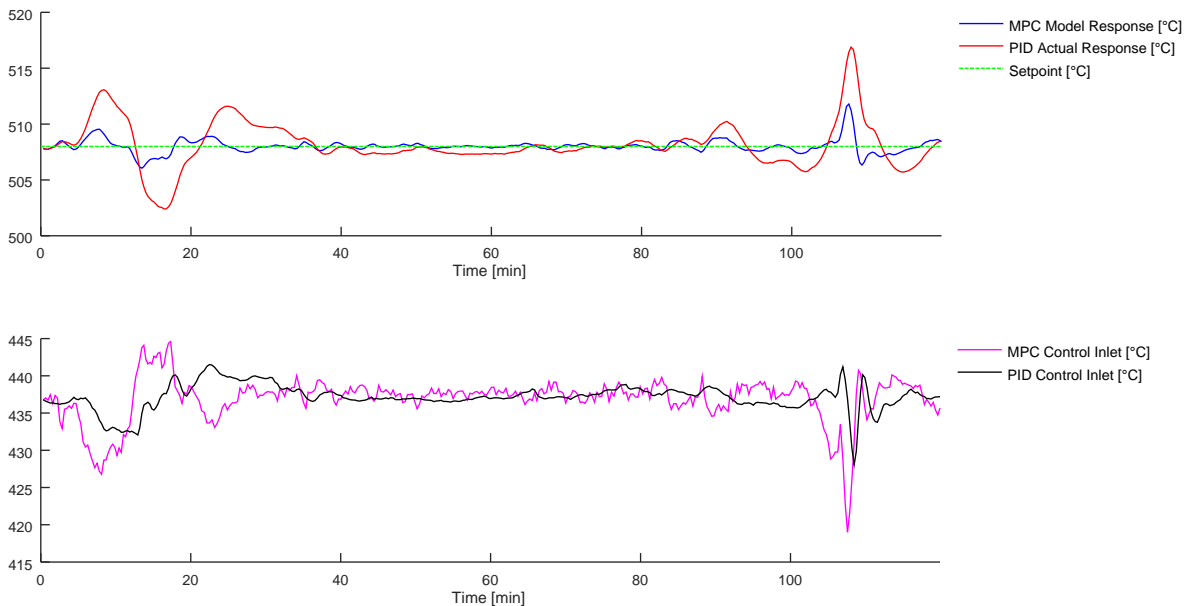


Figure 46: Various Load Changes – MPC Control Response

The sharp loading changes present in this scenario still pose a challenge to the MPC controller; however, it shows a significant improvement in peak temperature excursions. The maximum is only 43 % compared to the PID controller and the minimum 35 %. It also showcases a very low 0.61 °C standard deviation.

Standing out at both the beginning and end of the graphs in *Figure 46*, are the two larger disturbances. In this instance a clear control attempt is seen long before the PID controller responds sufficiently. In this scenario the controller adequately responds to the rapid loading and unloading of the machine that coincides with a change in the firing rate in the first 20 minutes. This and other disturbance inputs can be referred to, back in section 3.5.4, *Figure 30* and *Figure 31*. Later, after the 100-minute mark, a load spike without corresponding changes in the firing rate occurs. This can be seen as a bigger shock to the system. The controller response, at least for

the second disturbance after the 100-minute mark, is almost entirely dictated by the change in steam flow rate, which is not a direct input into the control law calculation. Because the plant and inputs are normalised with the steam flow it detects an imbalance in energy in the boiler.

Introduction of Mill and Load Increase

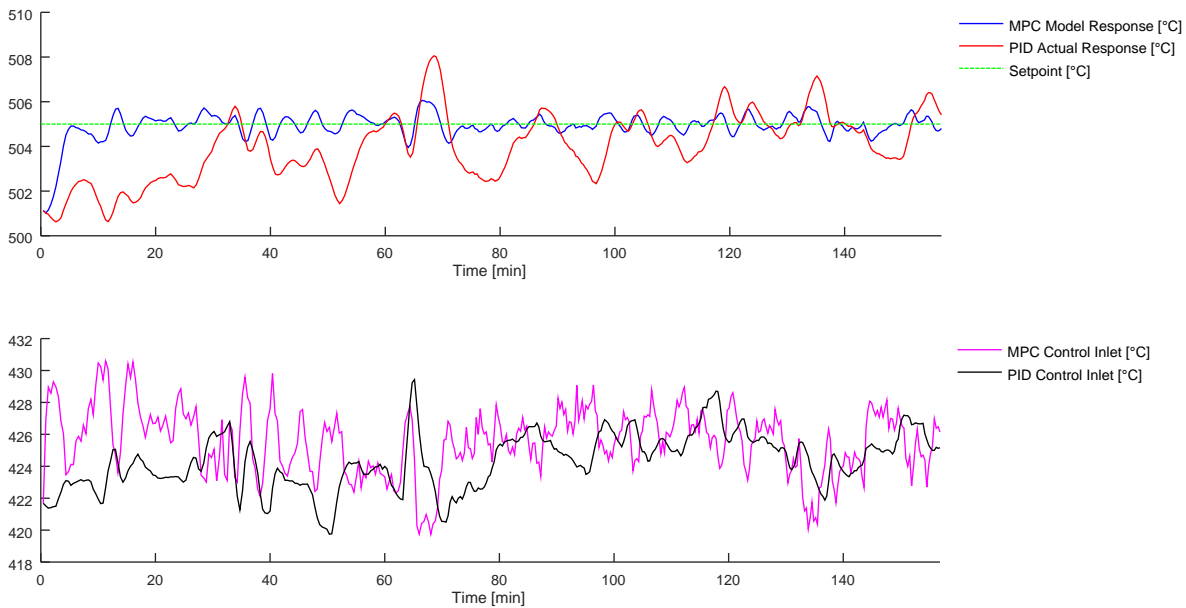


Figure 47: Introduction of Mill and Load Increase – MPC Control Response

The PID control in this scenario was already quite stable and responsive so the improvement due to the MPC controller is marginal. *Figure 47* shows that the controller operates appropriately when increasing machine loading, and when introducing a new mill when the machine is well coordinated. The steam flow rate and mill loading can be seen to increase proportionately in section 3.5.5, *Figure 34* and *Figure 35*, and thereby reduces the transient response in the system.

5.2.2. MPC Performance Evaluation

Simulated MPC results can be summarised across all scenarios in the following tables. In *Table 23* the first set of statistics calculated for the scenarios are the standard deviation and arithmetic mean of the steam temperature error from setpoint. The standard deviation is compared as the percentage reduction of the MPC controller achieved over the PID controller. The mean value is compared based on the reduction in absolute mean error i.e. the difference between the absolute

Chapter 5 Simulation and Evaluation

values of the two means. This is done to ensure that negative and positive deviations from the mean are treated equally. The value represents how much closer the MPC mean error is to zero compared to the PID controller response.

In *Table 23*, it can be seen that on average, the standard deviation in the system response from the setpoint is reduced to 46 % of the PID controlled response. The mean temperature error from setpoint does reduce, but this can likely be attributed to the ideal environment of simulation. It is also not a parameter that is too concerning.

Table 23: MPC Standard Temperature Error Deviation and Mean Temperature Error Performance Evaluation

| Scenario | Temperature Setpoint | Standard Temperature Error Deviation σ | | | Mean Temperature Error Value | | |
|--|----------------------|---|---------|---|------------------------------|-----------|-------------------------|
| | | PID | MPC | Percent $\frac{\sigma_{MPC}}{\sigma_{PID}}$ | PID | MPC | MPC Change in mean °C |
| Sudden Steam Flow Rate Swing | 505 °C | 3.33 °C | 1.78 °C | 53 % | 0.627 °C | 0.009 °C | -0.618 °C |
| Machine Deloading and Mill Outage | 505 °C | 3.12 °C | 0.76 °C | 24 % | -1.072 °C | -0.071 °C | -1.002 °C |
| Steam Flow Rate Cycling while Deloading | 508 °C | 2.03 °C | 0.64 °C | 31 % | 0.450 °C | -0.006 °C | -0.443 °C |
| Various Load Changes | 508 °C | 2.07 °C | 0.61 °C | 30 % | 0.146 °C | 0.000 °C | -0.146 °C |
| Introduction of Mill and Load Increase | 505 °C | 1.26 °C | 0.37 °C | 30 % | -0.554 °C | 0.002 °C | -0.552 °C |
| Remainder of the 38 total scenarios included in average calculation below. | | | | | | | |
| Average | | 2.67 °C | 1.24 °C | 46% | -0.446 °C | -0.249 °C | -0.707 °C |

Table 24 below summarises the improvement in the final steam temperature maximum and minimum values. This is important as it applies directly to the limits associated with the protection functions. The comparison is computed as the peak temperature error (minimum and maximum respectively) from the setpoint as a percentage. Equation (83) below shows the calculation:

Chapter 5 Simulation and Evaluation

$$\text{Percent peak error max} = \frac{T_{max\ mpc\text{-setpoint}}}{T_{max\ pid\text{-setpoint}}} \cdot 100$$

$$\text{and Percent peak error min} = \frac{T_{min\ mpc\text{-setpoint}}}{T_{min\ pid\text{-setpoint}}}. 100 \quad (83)$$

Here it can be seen, for the MPC controller response, that the maximum peak temperature error is only 51 % of the PID controlled response on average. This applies to the triggering of the high temperature protection. Similarly, the minimum peak error is 71 % of the PID controlled response on average. This applies more indirectly to the rate of change trip condition, and is a positive result.

Table 24: MPC Minimum and Maximum Temperature Bounds Performance Evaluation

| Scenario | Temperature Setpoint | Maximum Temperature | | | Minimum Temperature | | |
|--|----------------------|---------------------|----------|------------------------|---------------------|----------|------------------------|
| | | PID | MPC | Percent Peak Error Max | PID | MPC | Percent Peak Error Min |
| Sudden Steam Flow Rate Swing | 505 °C | 524.3 °C | 515.8 °C | 56 % | 500.3 °C | 496.9 °C | 172 % |
| Machine Deloading and Mill Outage | 505 °C | 509.2 °C | 507.2 °C | 52 % | 494.8 °C | 502.4 °C | 25 % |
| Steam Flow Rate Cycling while Deloading | 508 °C | 513.2 °C | 510.0 °C | 39 % | 504.0 °C | 506.2 °C | 45 % |
| Various Load Changes | 508 °C | 516.9 °C | 511.8 °C | 43 % | 502.4 °C | 506.1 °C | 35 % |
| Introduction of Mill and Load Increase | 505 °C | 508.1 °C | 506.1 °C | 35 % | 501.4 °C | 504.0 °C | 29 % |
| Remainder of the 38 total scenarios included in average calculation below. | | | | | | | |
| Average | | 511.4 °C | 508.2 °C | 51 % | 498.3 °C | 500.5 °C | 71 % |

Table 25 is a qualitative analysis, since it is difficult to quantify what an “earlier” response is in a dynamic system. In general, what was done to compute these figures was to look at the control signal peaks to deduce a reduction in the peak response time. In some scenarios signal peaks were not pronounced enough to determine a relationship, especially in slower more stable responses. In these instances, the time difference in well-defined ramps or step changes in the control output

Chapter 5 Simulation and Evaluation

signals were used to measure the time offset. This was measured where both ramps or steps crossed a horizontal line drawn across their rising edges.

This time difference also needs to be normalised to the overall system time constant to make sense of it. This is done to avoid the average being skewed in favour of a low load condition scenario. An estimated normalising time constant of 180 s was used at full load. This time constant was chosen as inversely proportional to load. The peak response time percentage reduction to the system time constant was used to compare the MPC controlled response performance, to the PID controlled response. Although this is a qualitative measure, it is clear to see that a significantly earlier response is achieved with the MPC controller and the feed forward gains.

Table 25: MPC Response Time Performance Evaluation

| Scenario | Peak Response Time Reduction | Average Steam Flow | System Time Constant | Percentage of Time Constant |
|--|------------------------------|--------------------|----------------------|-----------------------------|
| Sudden Steam Flow Rate Swing | -74 s | 43 kg/s | 253 s | -29 % |
| Machine Deloading and Mill Outage | -60 s | 39 kg/s | 275 s | -22 % |
| Steam Flow Rate Cycling while Deloading | -137 s | 44 kg/s | 244 s | -56 % |
| Various Load Changes | -53 s | 49 kg/s | 222 s | -24 % |
| Introduction of Mill and Load Increase | -65 s | 41 kg/s | 261 s | -25 % |
| Remainder of the 38 total scenarios included in average calculation below. | | | | |
| Average | -88 s | 41 | 278 s | -33 % |

5.2.3. MPC Avoidance of Failed Mill Start Trip

Figure 48 below shows the MPC controlled response to the trip event discussed in section 2.3.1. To be noted here is that the steady state offset makes no difference to the trip condition. The protection circuit monitors for two conditions to occur sequentially before a trip signal is issued. This can also be visually interpreted with the coloured areas drawn on in *Figure 48*, for the respective instances represented by the colour in the legend. Firstly, the protection system monitors for the first instance of the final steam temperature exceeding $-5\text{ }^{\circ}\text{C}/\text{min}$. For this reason, the coloured areas start at different points for the two responses. The protection function will then monitor if the final steam temperature deviates further from this allowed gradient (top edge of coloured area) by more than $-25\text{ }^{\circ}\text{C}$ (bottom edge of coloured area). The protection function will trigger if the steam temperature exits the marked area through the bottom. It

Chapter 5 Simulation and Evaluation

indicates that the final steam temperature has decayed by 25 °C more in a given period than what is still expected to be a safe decay rate of -5 °C/min.

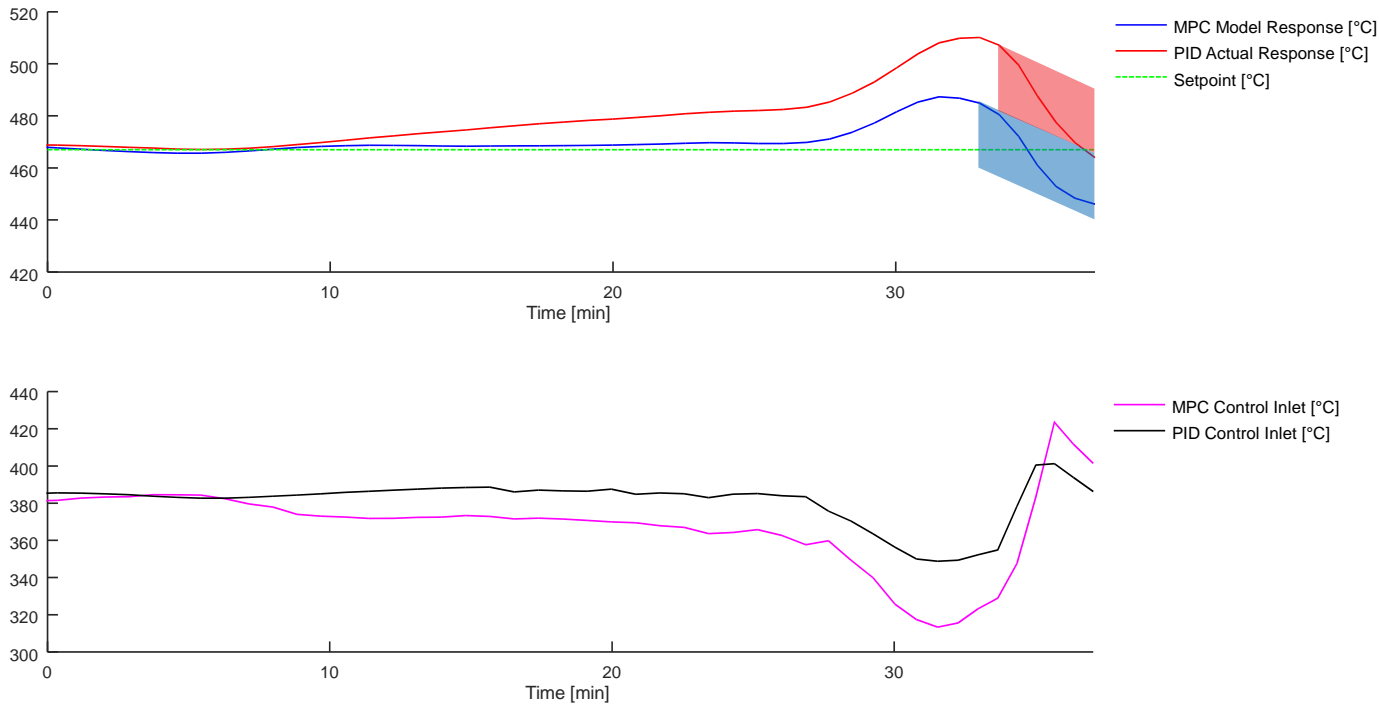


Figure 48: Failed Mill Start Trip – MPC Control Response

It can be seen that the MPC controller successfully reduced the ramp down rate's duration to avoid the trip condition. Both responses show an almost similar peak decay rate, but the MPC manages to arrest this gradient faster to avoid exceeding 25 °C below the gradient line. The protection function will only stop monitoring when the steam temperature crosses the marked area top edge, which has not happened yet by the end of *Figure 48*. Raw data recording ends after the actual unit has tripped. The future response cannot be simulated with any accuracy after this point, due to it still being in transient condition. Looking only at the steam temperature gradient, and the response of the spraywater system, the transient behaviour has been dampened in time and will stabilise. It can be safely assumed that this protection would have cleared the marked area in the future response, with no further disturbances being applied to the system.

Noting from *Figure 48*, the MPC control final superheater inlet temperature reaches 320 °C. Referring back to 2.3.1 *Failed Mill Start*, *Figure 6* the steam pressure can be seen to be around 8.9 MPa at its maximum. This is still above the saturation temperature of steam at 300 °C.

5.2.4. MPC Avoidance of Over-Firing Trip

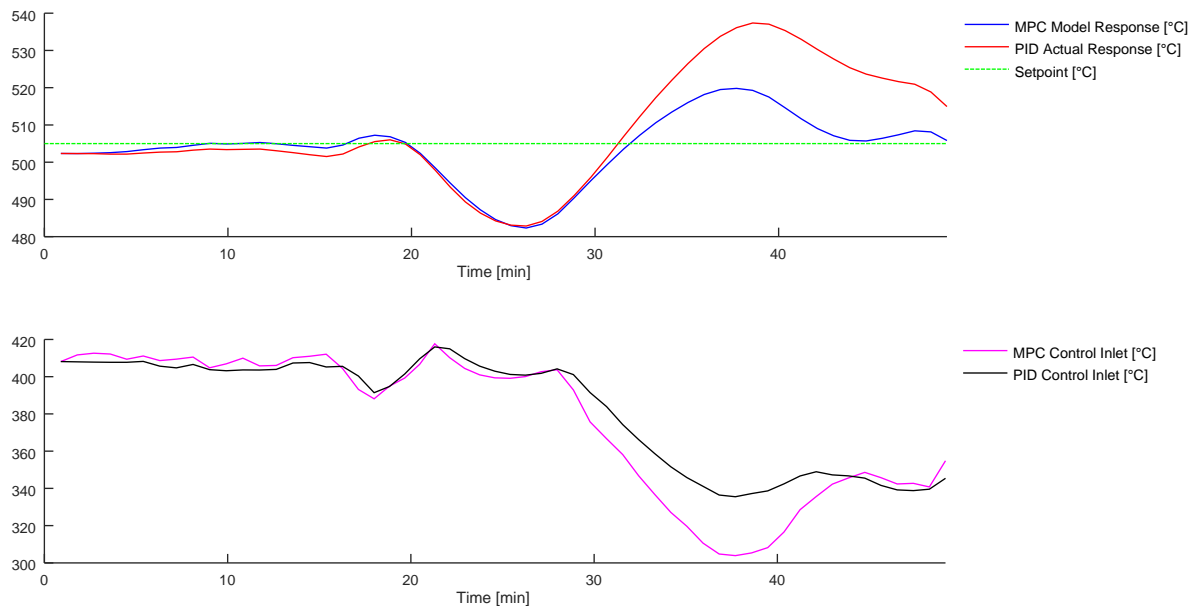


Figure 49: Over-Firing Trip – MPC Control Response

The over-firing condition above is clearly a much easier case to analyse. The MPC controller has significantly improved the overshoot in the steam temperature response. The peak response just barely reaches 520 °C which is still at least 5 °C from the delayed trip level, and almost 20 °C below the PID controlled peak response. It can be seen that this trip would have been avoided with the MPC controller as proposed. The inputs and disturbances to this system can be seen in section 2.3.2, *Figure 8*.

5.3. Fuzzy Control Strategy

5.3.1. Case Study Analysis for Fuzzy Controller

Sudden Steam Flow Rate Swing

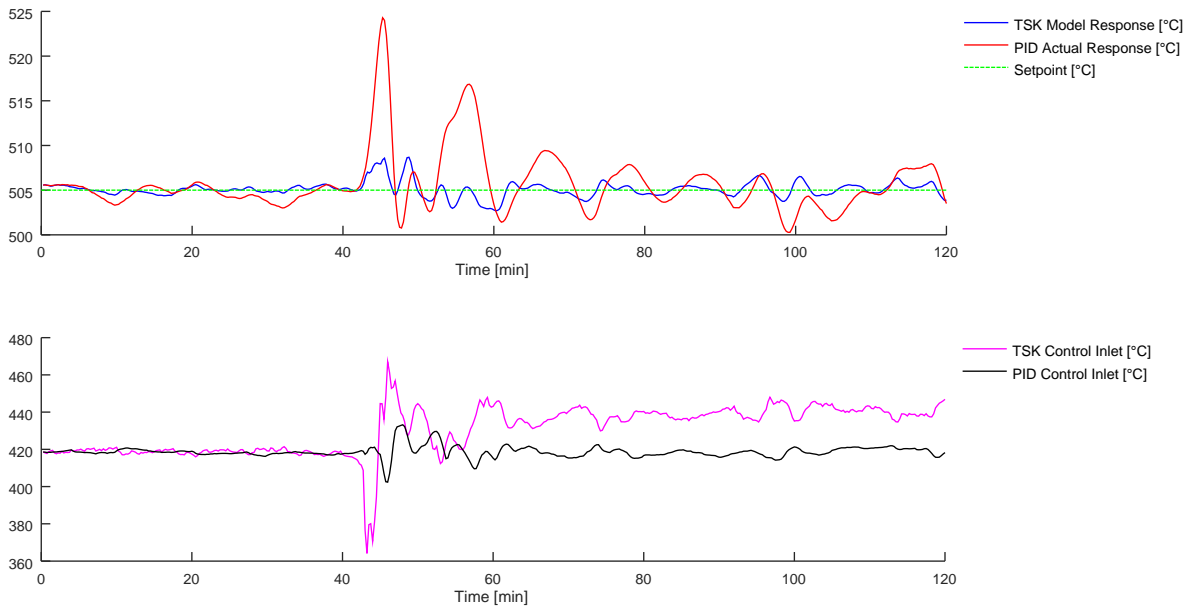


Figure 50: Sudden Steam Flow Rate Swing – Fuzzy Control Response

Visually there is a clear improvement with the Fuzzy controller in *Figure 50* over the MPC controller in *Figure 43*. This is mostly attributed to the presence of rather large steam flow rate change in this scenario. The Fuzzy Controller completely reduced the first, and highest, peak response to a similar amplitude of the next highest peak. The entire response is smaller in amplitude than even the 3rd highest peak excursion of the PID controlled response. The maximum temperature excursion is even less than the MPC's second largest excursion. This comes as a result of a very quick response to a rapid change in steam flow rate. The Fuzzy control law is much more aggressive compared to both the PI controller and MPC controller. Section 3.5.1, *Figure 16* and *Figure 17* shows the inputs to the system on which the feedforward gains are based

It should be noted that for this specific event the final control law has a steady state offset compared to the PI controller. This is due to modelling error and the fact that the final control law

is reconstructed from an inlet temperature delta. This effect is not present in the other scenarios presented, likely due to the severity of change in the steam flow rate.

Machine Deloading and Mill Outage

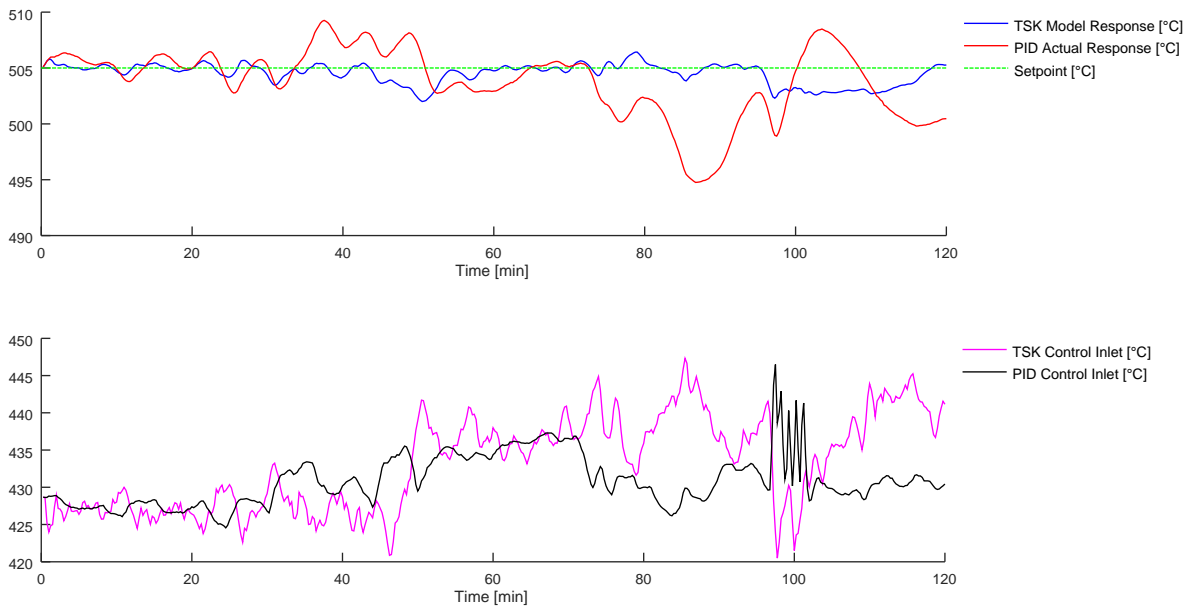


Figure 51: Machine Deloading and Mill Outage – Fuzzy Control Response

The Fuzzy controller response in *Figure 51* for this scenario deteriorates slightly compared to the MPC controller in *Figure 44*, both in peak response and standard deviation. This is one of the few events, in which the Fuzzy controller's response, was worse than the MPC controller's response. The response is still comparable to the MPC controller. Section 3.5.2, *Figure 22* and *Figure 23* highlight the system inputs and disturbances for this event.

The reduction in performance of a few events are considered acceptable, if the overall controller performance is improved. This will also increase robustness. In fact, although not the case in this scenario, it would have been acceptable to have a higher standard deviation if it came with a significantly reduced peak steam temperature excursion. This is due to the fact that the protections operate on peak excursion limits, while tight control results in efficiency increases. Tripping a unit is costlier to long term plant health as long as standard deviation from setpoint is at least maintained to within the current performance.

Steam Flow Cycling while Deloading

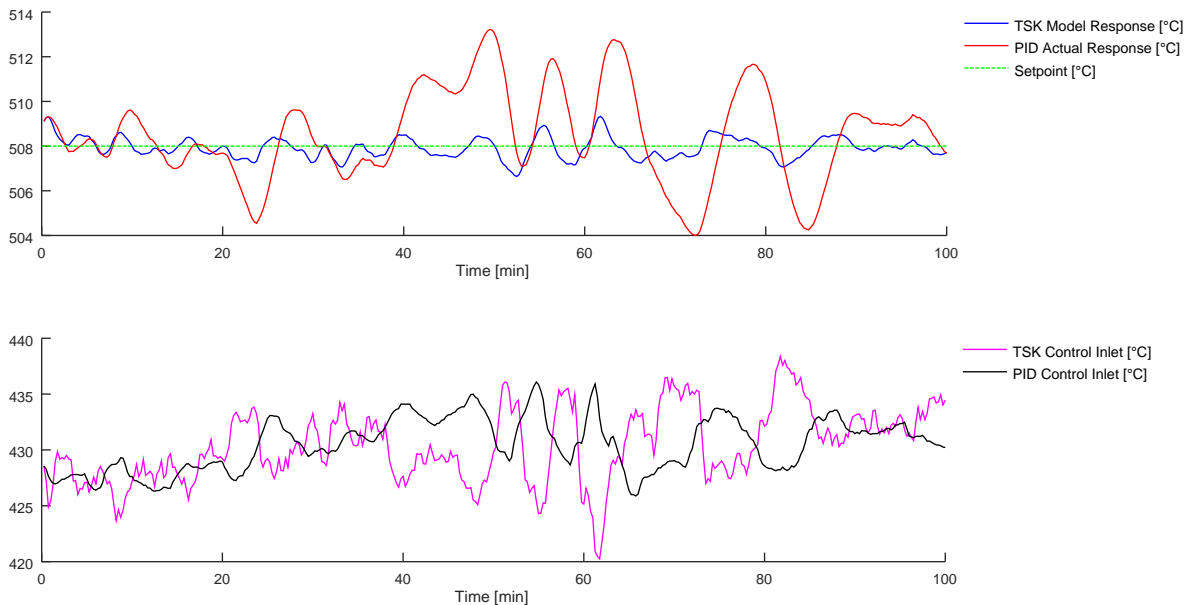


Figure 52: Steam Flow Rate Cycling while Deloading – Fuzzy Control Response

The scenario shown in *Figure 52*, once again reflects the out of phase response by the Fuzzy controller when compared to the PID controller. It has a very good performance and reduces the maximum temperature excursion as well as the standard deviation from the temperature setpoint to a quarter of the PID controlled response. It also outperforms the MPC controller, as seen in *Figure 45*. The MPC controller only achieved 31 % and 39 % for the respective comparison to the PID controller seen in *Table 23* and *Table 24*.

The performance gain is undoubtedly due to main steam flow rate cycling, seen in section 3.5.3, *Figure 26* and *Figure 27*. This non-linear behaviour was specifically identified and controlled for by the Fuzzy controller. The controller output is not significantly harsher in terms of amplitude; however, it is quicker to respond once the steam flow is seen to change. The edges seen on the control inlet steam temperature is sharper, almost to the point of step changes when compared to *Figure 45* of the MPC controller.

Various Load Changes

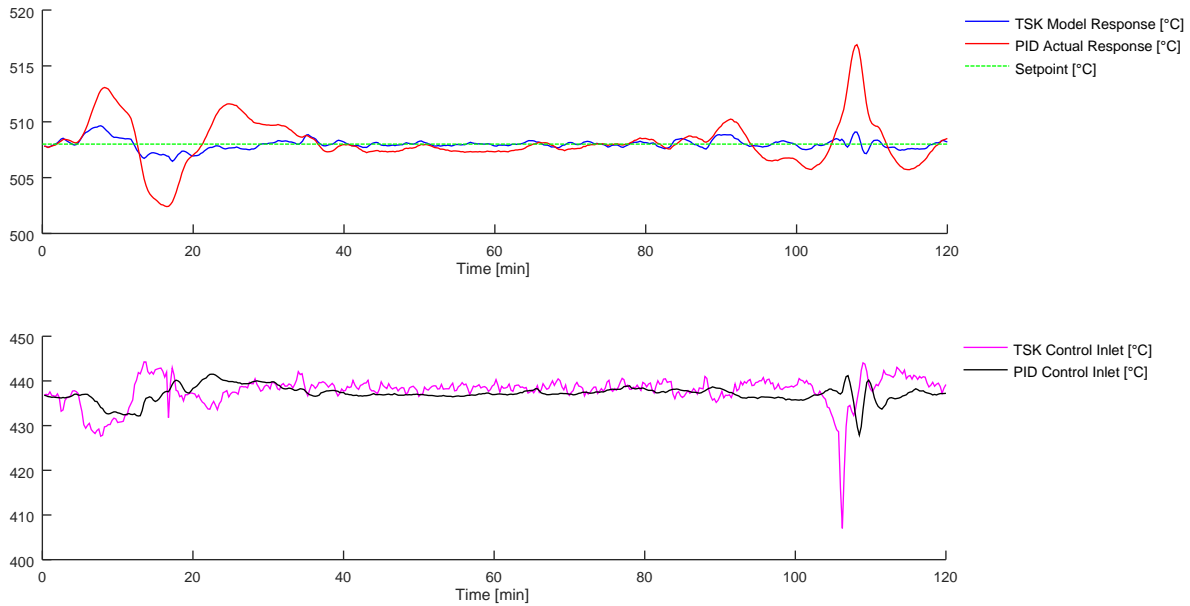


Figure 53: Various Load Changes – Fuzzy Control Response

Figure 53 also shows a rather large response in order to reduce the temperature excursion that was still present in the MPC controller in *Figure 46*. The remaining transient response is now only slightly distinguishable from small plant perturbations and unmeasured disturbances. Again, it seems that this particular non-linearity, the specific focus of the fuzzy controller, has brought significant improvements in reducing peak excursions. The system inputs can be seen in section 3.5.4, *Figure 30* and *Figure 31*.

Introduction of Mill and Load Increase

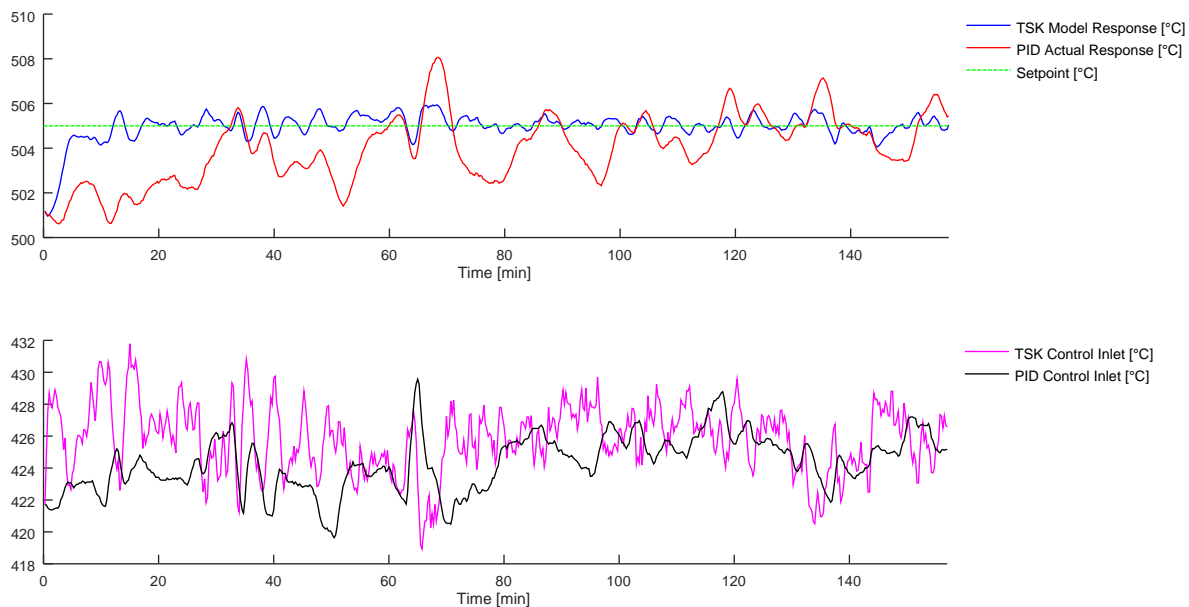


Figure 54: Introduction of Mill and Load Increase – Fuzzy Control Response

This event has essentially an identical response when compared to the MPC controller in *Figure 47*. This is due to only small changes in steam flow rate being present in this scenario as seen in section 3.5.5, *Figure 34* and *Figure 35*. From the scale of both graphs in *Figure 54* it can be seen that the event does not have large disturbances, only frequent smaller changes.

5.3.2. TSK Fuzzy Performance Evaluation

Simulated Fuzzy results can be summarised across all scenarios in the following tables. Overall the Fuzzy controller has responded slightly better compared to the MPC controller when looking at standard deviation in *Table 26*. The Fuzzy controller does have a significantly improved response for a certain set of scenarios, namely, scenarios with a high rate of steam flow acceleration. This has improved the standard deviation overall, but more importantly, also reduced high peak temperature excursions.

Chapter 5 Simulation and Evaluation

Table 26: Fuzzy Standard Temperature Error Deviation and Mean Temperature Error Performance Evaluation

| Scenario | Temperature Setpoint | Standard Temperature Error Deviation σ | | | Mean Temperature Error Value | | |
|--|----------------------|---|---------|---|------------------------------|-----------|---|
| | | PID | Fuzzy | Percent $\frac{\sigma_{\text{Fuzzy}}}{\sigma_{\text{PID}}}$ | PID | Fuzzy | Fuzzy Change in $ \text{mean} ^{\circ}\text{C}$ |
| Sudden Steam Flow Rate Swing | 505 °C | 3.33 °C | 0.85 °C | 26 % | 0.627 °C | 0.095 °C | -0.532 °C |
| Machine Deloading and Mill Outage | 505 °C | 3.12 °C | 0.93 °C | 30 % | -1.072 °C | -0.506 °C | -0.566 °C |
| Steam Flow Rate Cycling while Deloading | 508 °C | 2.03 °C | 0.47 °C | 23 % | 0.450 °C | -0.077 °C | -0.373 °C |
| Various Load Changes | 508 °C | 2.07 °C | 0.46 °C | 22 % | 0.146 °C | -0.015 °C | -0.131 °C |
| Introduction of Mill and Load Increase | 505 °C | 1.26 °C | 0.36 °C | 29 % | -0.554 °C | 0.080 °C | -0.474 °C |
| Remainder of the 38 total scenarios included in average calculation below. | | | | | | | |
| Average | | 2.67 °C | 1.15 °C | 43 % | -0.446 °C | -0.203 °C | 0.609 °C |

The final steam temperature maximum and minimum value in many scenarios have been improved significantly with the added Fuzzy controller's response to rapid changes in steam flow acceleration, as seen in Table 27. Overall the maximum excursion reduction is still close to the 51 % achieved by the MPC controller. The fuzzy controller has managed to reduce the minimum excursion value significantly over the MPC and PID controllers.

Chapter 5 Simulation and Evaluation

Table 27: Fuzzy Minimum and Maximum Temperature Bounds Performance Evaluation

| Scenario | Temperature Setpoint | Maximum Temperature | | | Minimum Temperature | | |
|--|----------------------|---------------------|----------|------------------------|---------------------|----------|------------------------|
| | | PID | Fuzzy | Percent Peak Error Max | PID | Fuzzy | Percent Peak Error Min |
| Sudden Steam Flow Rate Swing | 505 °C | 524.3 °C | 508.7 °C | 19 % | 500.3 °C | 502.7 °C | 49 % |
| Machine Deloading and Mill Outage | 505 °C | 509.2 °C | 506.4 °C | 34 % | 494.8 °C | 502.0 °C | 29 % |
| Steam Flow Rate Cycling while Deloading | 508 °C | 513.2 °C | 509.3 °C | 25 % | 504.0 °C | 506.6 °C | 34 % |
| Various Load Changes | 508 °C | 516.9 °C | 509.6 °C | 19 % | 502.4 °C | 506.5 °C | 28 % |
| Introduction of Mill and Load Increase | 505 °C | 508.1 °C | 505.9 °C | 31 % | 501.4 °C | 504.1 °C | 26 % |
| Remainder of the 38 total scenarios included in average calculation below. | | | | | | | |
| Average | | 511.4 °C | 507.9 °C | 50 % | 498.3 °C | 501.7 °C | 45 % |

The system response time measurement is mostly a qualitative measure, with spot checks being done on certain characteristic response curves, there are some disparities in the data. The average value shows a 24 second further improvement over the MPC controller in *Table 28*. This is small and points out that the Fuzzy controller, with its fixed sample time, has the opportunity to respond slightly earlier in most cases. This will mostly lead to an improvement in the system response to unmeasured disturbances. It is also skewed by events with a high rate of change in the steam flow rate. These show a significantly earlier response in the peak of the control law response for that specific rapid change. On average the Fuzzy controller performs similarly to the MPC controller against other measurable disturbances. Both controllers' main objective is to respond earlier to known disturbances, in which both succeed. This can be attributed to the use of feedforward control.

Chapter 5 Simulation and Evaluation

Table 28: Fuzzy Response Time Performance Evaluation

| Scenario | Peak Response Time Reduction | Average Steam Flow | System Time Constant | Percentage of Time Constant |
|--|------------------------------|--------------------|----------------------|-----------------------------|
| Sudden Steam Flow Rate Swing | -150 s | 43 kg/s | 253 s | -59 % |
| Machine Deloading and Mill Outage | -178 s | 39 kg/s | 275 s | -65 % |
| Steam Flow Rate Cycling while Deloading | -199 s | 44 kg/s | 244 s | -82 % |
| Various Load Changes | -83 s | 49 kg/s | 222 s | -37 % |
| Introduction of Mill and Load Increase | -93 s | 41 kg/s | 261 s | -36 % |
| Remainder of the 38 total scenarios included in average calculation below. | | | | |
| Average | -112 s | 41 | 278 s | -43 % |

5.3.3. TSK Fuzzy Avoidance of Failed Mill Start Trip

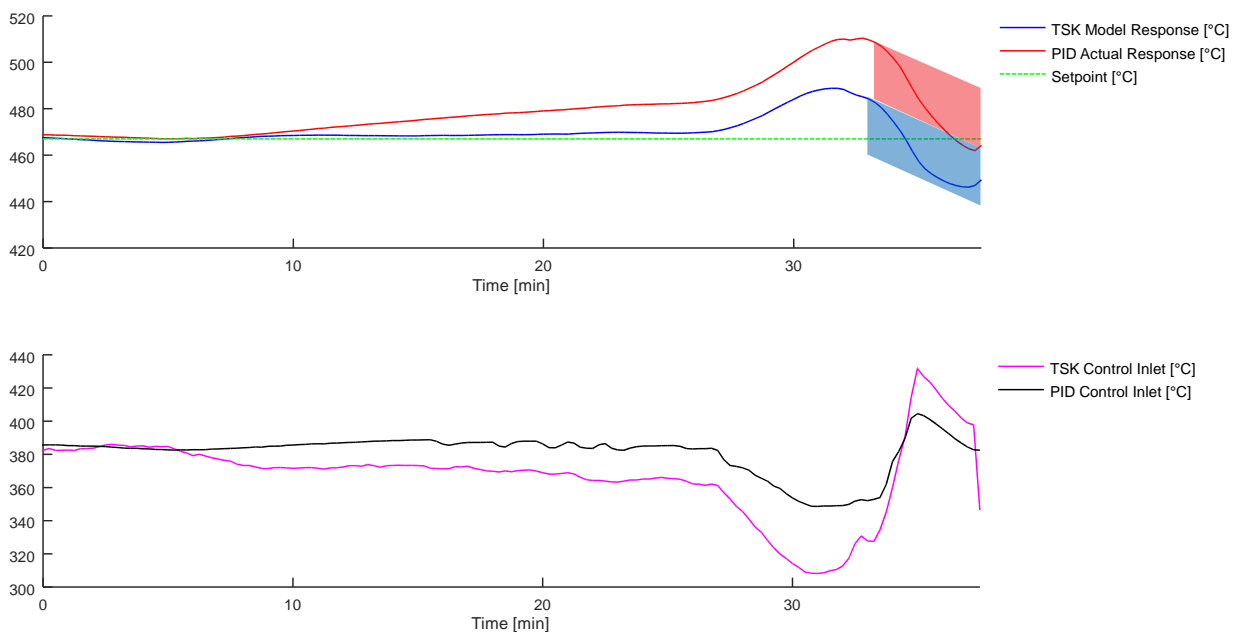


Figure 55: Failed Mill Start Trip – Fuzzy Control Response

In *Figure 55* above it can be seen that the Fuzzy controller also successfully avoids triggering the trip condition. To summarise the explanation in section 5.2.3 the steam temperature must not exit the bottom of the marked area that ramps down by $-5\text{ }^{\circ}\text{C}/\text{min}$. It has an allowable deviation range of $-25\text{ }^{\circ}\text{C}$ from the ramp line. Due to the Fuzzy controller's fixed sample time, there is a slightly more dynamic response to the events, compared to the MPC controlled response in section 5.2.3. It can however be seen that this does not result in a significant improvement. The Fuzzy controller can react slightly earlier to any measured and unmeasured disturbances, but the large

filter behaviour of the plant make this mostly ineffective. We do not see the benefit of the Fuzzy controller in this and the next instant. There, only steady changes occur in the steam flow rate. This leaves both controllers to perform similarly, but satisfactorily. Again it is noted that the protection function will only stop monitoring when the temperature exits the marked area through the top. In the absence of further disturbances, the gradient shown at the end of *Figure 55* indicates that this would occur and clear the protection function completely. Lastly it is noted that the peak decay rate is similar for both responses, however the Fuzzy controller arrests the decay rate faster and in this way prevents the trip. Referring back to *2.3.1 Failed Mill Start, Figure 6* with a steam pressure of 8.9 MPa at its maximum, the more aggressive fuzzy controller response is still above the saturation temperature of steam at 300 °C.

5.3.4. TSK Fuzzy Avoidance of Over-Firing Trip

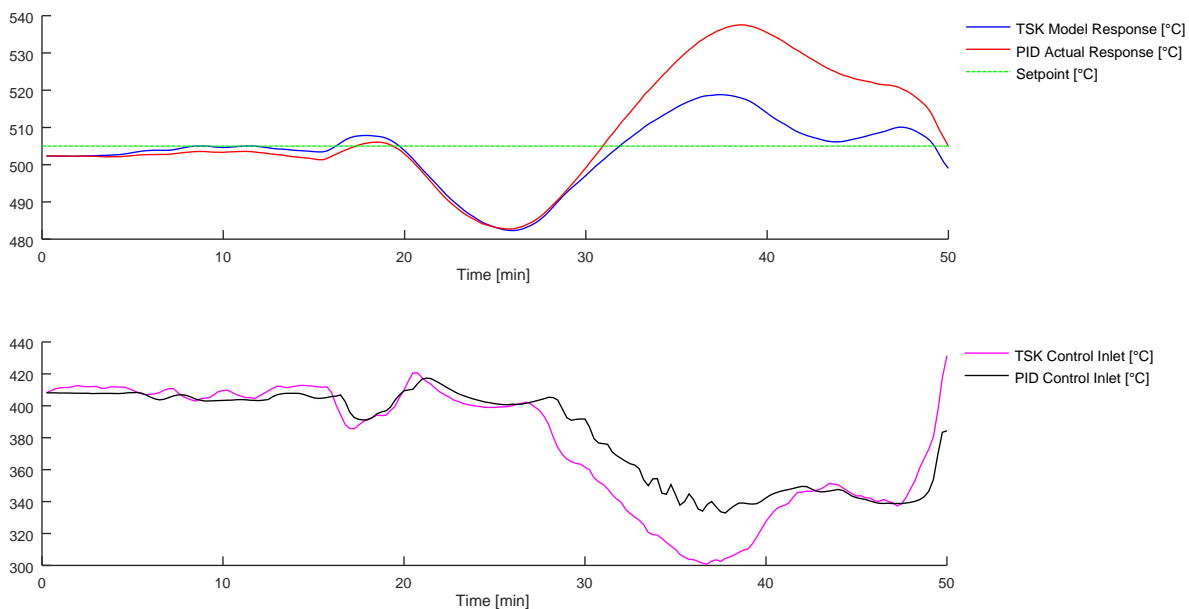


Figure 56: Over-Firing Trip – Fuzzy Control Response

The over-firing condition is successfully avoided by the Fuzzy controller in *Figure 56*. There is a marginal improvement in the peak response of about - 1 °C over the MPC controller in *Figure 49*. The control law is more dynamic with the Fuzzy control law, but there is no significant improvement due to this. Both controllers show an almost immediate response to disturbances

and both are able to compensate for the response adequately. The inputs and disturbances to this system can be seen in section 2.3.2, *Figure 8*.

5.4. High Fidelity Operations Simulator Results

Up to this point the two controllers under investigation were analysed through simulation, based on the model determined in *Chapter 3 System Identification and Modelling*. Komati Power Station has an operations training simulator on site for simulating the entire unit's dynamics, while the simulated unit is operated from a control panel similar to the actual units. This simulator is often referred to as a high-fidelity simulator due to the following properties:

- It emulates process dynamics through plant configuration computer emulation from first principles.
- It simulates the control interface all the way down to PLC level and maintains the same user interface that would be expected in the real environment.
- The system response is optimised to match real unit response as close as possible including emulation of physical plant failures and interventions.

The primary use of the simulator is for the training of operating personnel. Fundamentally it is not a simulator for testing new engineering designs, like controllers and control sequences, however changes can be facilitated on the simulator if required. It was possible to test the two control strategies on the operations training simulator for two scenarios to compare the results between the controllers. It also provides an independent means of verifying the controller responses, not bound to system identification and simulation done as part of this study.

5.4.1. Mill C Trip Simulation

The first test that was conducted on the simulator was a mill trip event. The system parameters are displayed in *Figure 57* and *Figure 58*. The same test was conducted for both controllers.

Chapter 5 Simulation and Evaluation

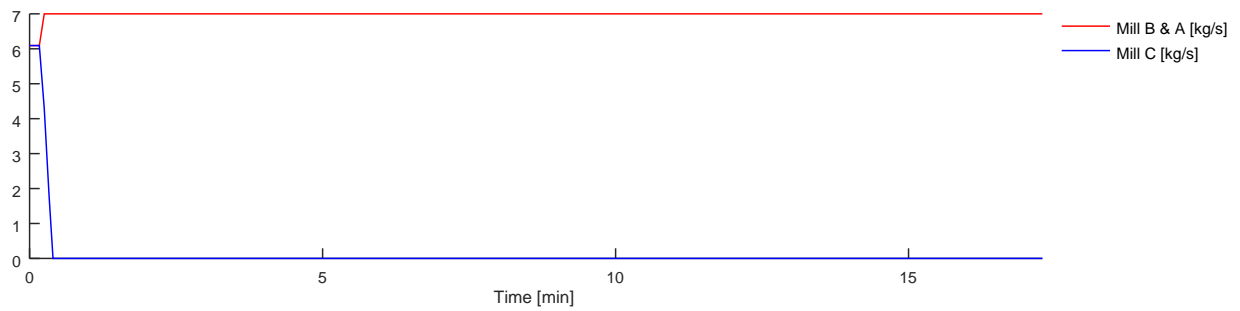


Figure 57: Simulator Mill C Trip – Firing Parameters

In this test the mill on C row was tripped immediately taking out fires on that row (blue). This then results in the other mills on B and A rows to increase in firing rate (red) with the unit coordinator seeking to maintain the total energy input into the boiler. The unit coordinator is a high-level controller that manages the furnace firing rate, but its function is not important here only its response as indicated. The remaining mills in question were already at 6 kg/s, close to maximum capacity. After the mill trip, both remaining mills increase to a maximum loading of 7 kg/s.

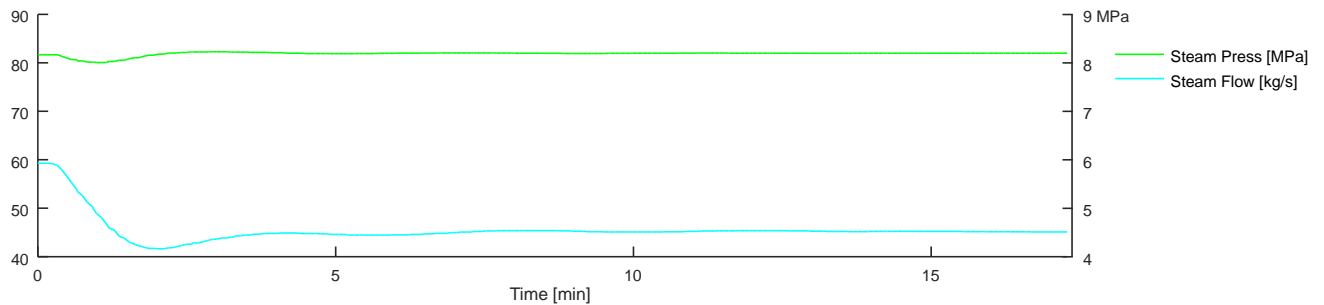


Figure 58: Simulator Mill C Trip – Steam Parameters

In *Figure 58* it can then be seen that the machine deloads the steam flow rate (cyan). This is done proactively by the unit coordinator due to the maximum limits reached by the other two firing mills. During deloading the pressure initially decreases, and as the steam flow settles to a new steady state, it recovers to its normal working level (green).

MPC Control Performance

The MPC controller response is shown in *Figure 59*. In line with previous plots the MPC control law response and the steam temperature response are shown in purple and blue respectively. The

Chapter 5 Simulation and Evaluation

control setpoint is shown in green with the PID control law response and the steam temperature response are shown in black and red respectively

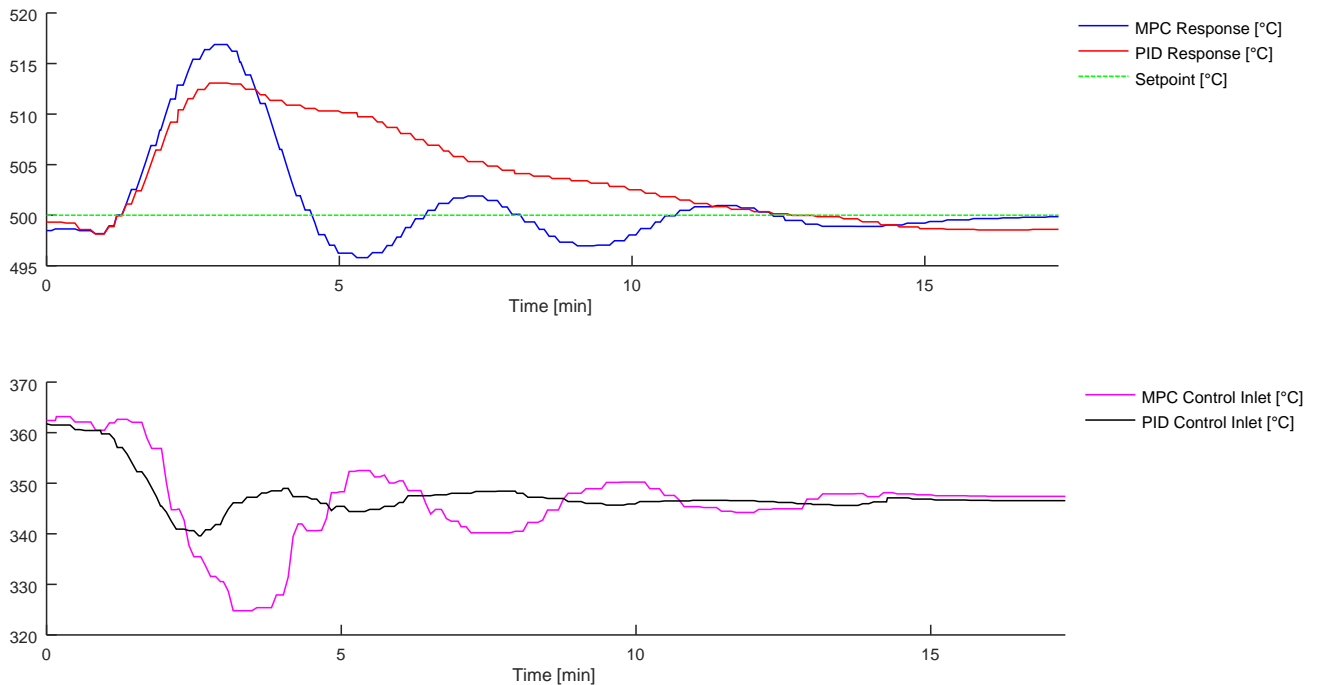


Figure 59: Simulator Mill C Trip – MPC Control Response

From *Figure 59* it can be seen that the MPC controller causes an overshoot compared to the PID controller. This has not been the case in previously simulated scenarios. In almost all cases both control techniques resulted in less overshoot. This will be discussed more in the next sub-section, but will be noted here as a negative result. The main steam temperature peak is seen to be 517 °C with the MPC controller and only 513 °C with the PID controller.

Both controllers achieve settling below 1 °C at about the same time of 11.3 minutes after the disturbance. The MPC controller achieves settling below 5 °C error within 3.9 minutes, while the PID controller takes 7.3 minutes to reach that point.

It is in some borderline cases favourable to have the temperature settling below its setpoint value faster even at the cost of limited overshoot. This is due to the delayed trip condition mentioned in section *2.2 Operating Envelope*. Should the temperature exceed 525 °C it needs to drop below that limit before the 3-minute timer runs out. It would be best to avoid dropping too far below the

setpoint to avoid triggering the rate of change protection, but this is still within the limit. This would be case dependent as the added overshoot could end up triggering the higher 530 °C immediate trip limit.

Overall the results are not clearly positive or negative when compared to the PID response. It is worse compared to the previously simulated responses. This prompted the researcher to also review the simulator response compared to the model determined as part of this study in the next sub-section.

Simulator and Model Comparison

Due to the results obtained from the MPC controller on the simulator it became evident that the simulator response is not equal to that of the model used. This is also a good test for controller stability as it can be seen to perform at least reasonably well compared to the PID controller, against a perturbed model.

It should also be noted that it cannot be said that either the model or the simulator is more accurate at this point. The simulator has grouped representations of the Komati units. At Komati there is less standardisation than with a new build station, due to the fact that each unit was returned from a mothball state with varying degrees of ageing on components. This has resulted in a large mixture of capability ratings and technologies used in the combustion process. The simulator does not precisely represent every unit's dynamic process. It accurately represents them from a fundamental principal of operation with some degree of freedom given to the proportions of dynamic behaviour as dictated by physical plant properties.

In *Figure 60* the results comparing the simulator's response to the model's response for the previous scenario is shown. It should be noted that the responses are smoother as the model uses average values between samples as inputs.

Chapter 5 Simulation and Evaluation

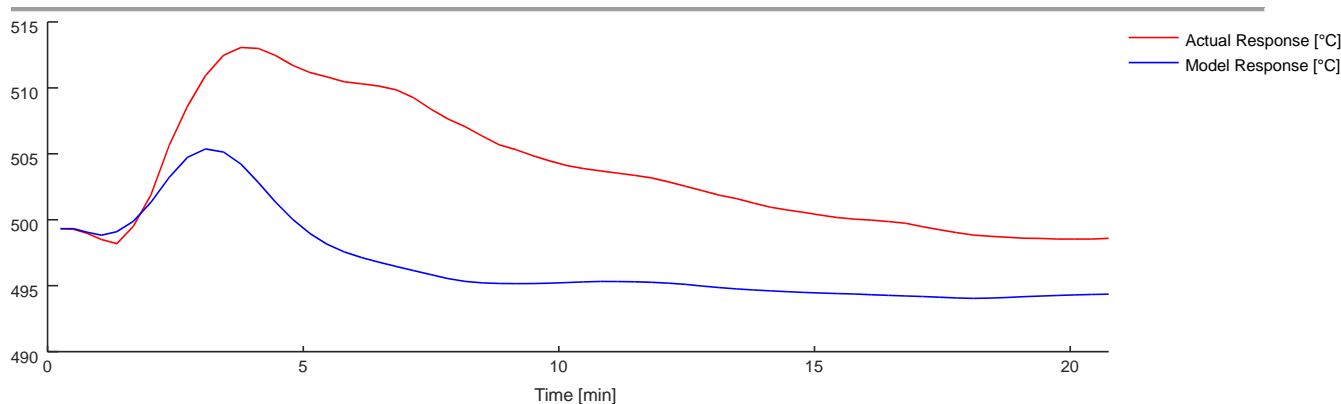


Figure 60: Simulator Mill C Trip – Model versus Simulator Response

This is a system in closed loop operation with many other controllers running in parallel making a standard step response near impossible. Taking this into consideration it is still immediately clear that the simulator plant response to a steam flow rate and firing rate downward combined step has a much higher gain. The simulator response is at least double that of the model and arguably of the actual generating unit under investigation. It can also be seen that the overall time constant for the simulator's plant response is 24 % larger if the peak responses are used as reference.

These perturbations combined make for a rather different plant than what was designed for. The response seems to remain semi-stable despite the larger plant gain and extra phase lag. Considering that the controllers were not optimised for this specific 'unit', that is the emulated plant model on the simulator, it has performed surprisingly robustly. It should also be evident that a better response should be achievable with some model adjustments. This would be required for each unit of operation and also the simulator. This is not explored further as both controllers are compared essentially against the same plants and give us further insight into controller robustness.

Fuzzy Control Performance

The Fuzzy controller response is shown in *Figure 61*. Again, in line with previous plots, the Fuzzy control law and the steam temperature responses are shown in purple and blue

Chapter 5 Simulation and Evaluation

respectively. The control setpoint is shown in green with the PID control law response and the steam temperature response are shown in black and red respectively.

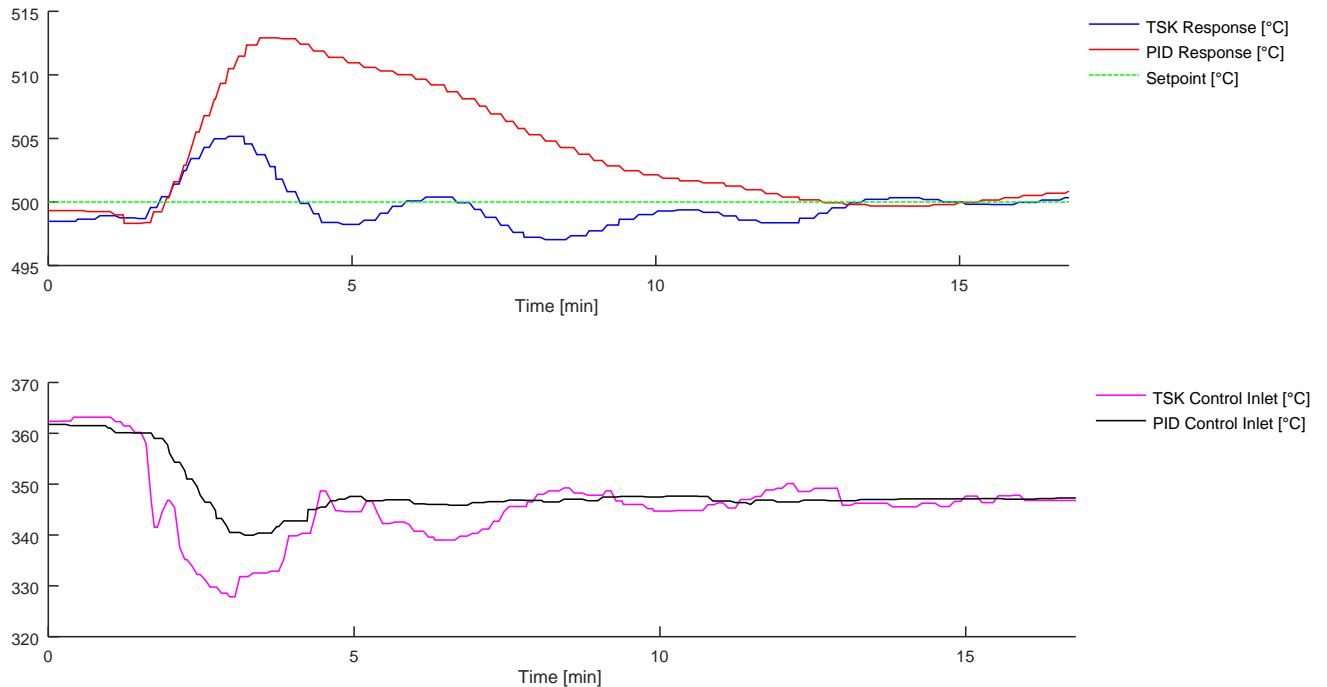


Figure 61: Simulator Mill C Trip – Fuzzy Control Response

From first glance the Fuzzy controller has a much better response compared to the PID and MPC controllers. The response occurs significantly faster and the peak response in steam temperature just reaches the 505 °C mark. This peak response is at least half that of both the MPC and the PID controllers. It is clear that there is still some instability during the transient condition. This again can also likely be attributed to the response of the perturbed plant. Realising here that model error will present itself as an unmeasured disturbance and will settle out at a much slower rate than known disturbances.

Looking at the control law we see that it indeed achieves a much faster response to the changing process parameters. This is likely a combination of the faster cycling time as well as being optimised for a control region with a high steam flow acceleration. The Fuzzy controller has achieved a 62 % reduction in the peak temperature response as well as an estimated 26 %

reduction in response time to the initial disturbance. This is considered a very good result, especially considering that the control law has been applied unoptimized to a perturbed plant.

5.4.2. Rapid Pressure Raising Simulation

The second test that was conducted, depict an event of rapid steam pressure raising. The input parameters can be seen in *Figure 62* & *Figure 63*. The same test was conducted with both controllers.

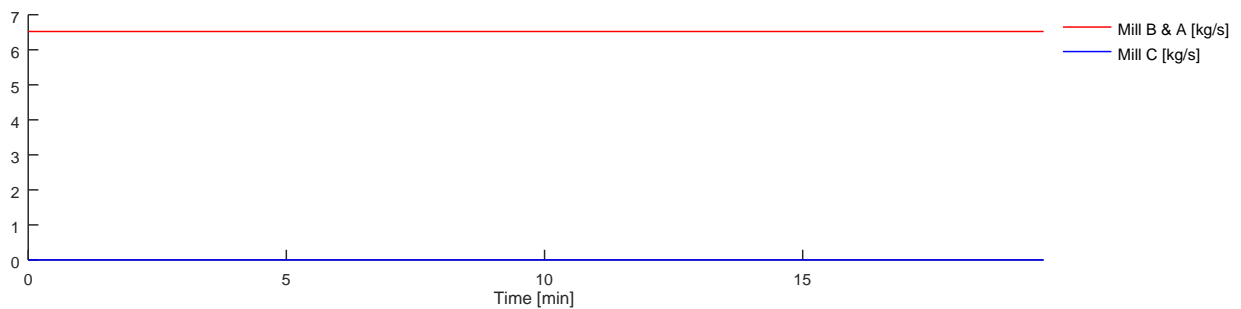


Figure 62: Simulator Rapid Pressure Raising – Firing Parameters

This test was not conducted at full load. The unit was stable and producing steam at a rate of 47 kg/s. This was achieved by having mills A & B at full load before mill C is put in service. Mill C is not introduced during this test and there are no changes in firing.

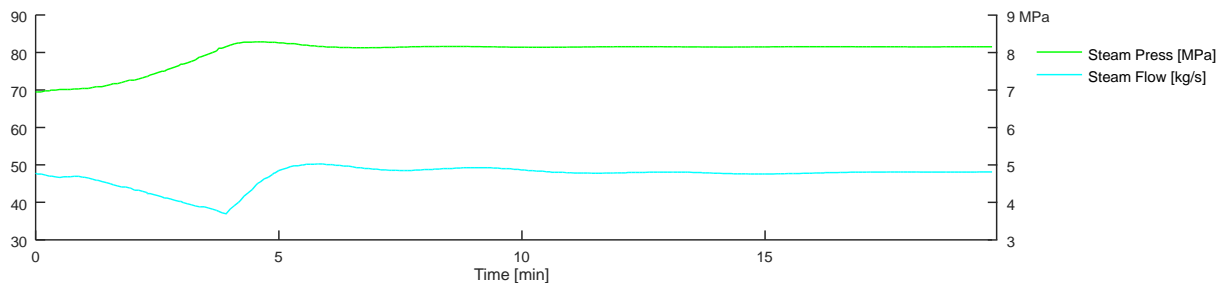


Figure 63: Simulator Rapid Pressure Raising – Steam Parameters

The machine is then deloaded in favour of raising the steam pressure to normal working level. The rate at which this is done is excessive, and the main source of disturbance to the system. The pressure is then maintained at normal working level, after which the machine loads up very fast to its previous operating level, to ensure the pressure is maintained. After this, both controllers need some time to settle completely.

MPC Control Performance

The MPC controller response is shown in *Figure 64*. The MPC control law response and the steam temperature response are shown in purple and blue respectively. The control setpoint is shown in green with the PID control law response and the steam temperature response shown in black and red respectively.

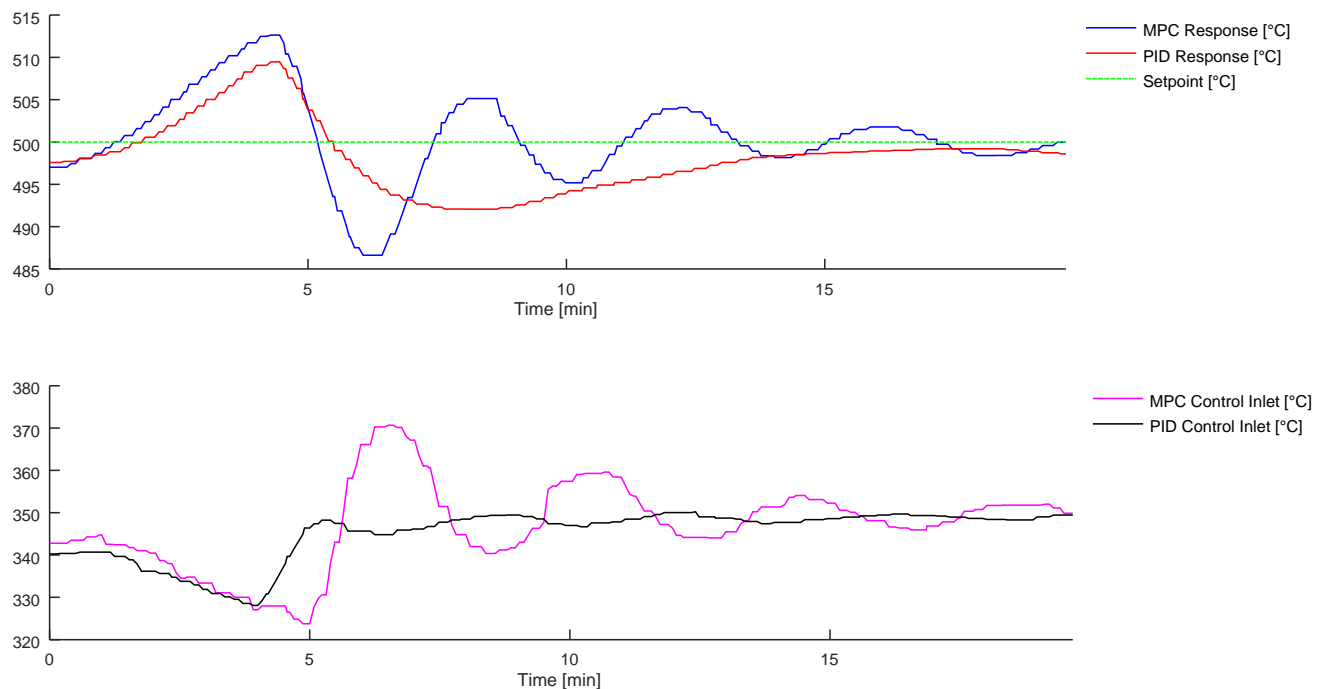


Figure 64: Simulator Rapid Pressure Raising – MPC Control Response

As with the previous test the MPC controller does not perform as expected at least partly due to the differences in plant dynamics that the model is based on. It can be seen that the MPC overshoots, this time both in the upward and downward directions due to the two rapid load changes.

The controller is only semi-stable, but remains largely within the envelope of the PID controller system response after the initial overshoot. In this scenario it can be said that the PID has outperformed the MPC controller on the perturbed plant. The overshoot has increased by 24 % and an undershoot 69 % larger than that of the PID minimum response. There also seems to be no

Chapter 5 Simulation and Evaluation

significant early response by the MPC controller. In fact, its response is quite late on the second disturbance.

This finding by no means illustrates failure of the controller. It shows clearly that the accuracy of the model is a paramount requirement for this controller's success. It therefore brings its robustness in question, although the perturbation of this plant is quite significant.

Fuzzy Control Performance

The Fuzzy controller response is shown in *Figure 65*. The control law response and steam temperature responses are shown in purple and blue respectively. The control setpoint is shown in green with the PID control law and steam temperature responses shown in black and red respectively.

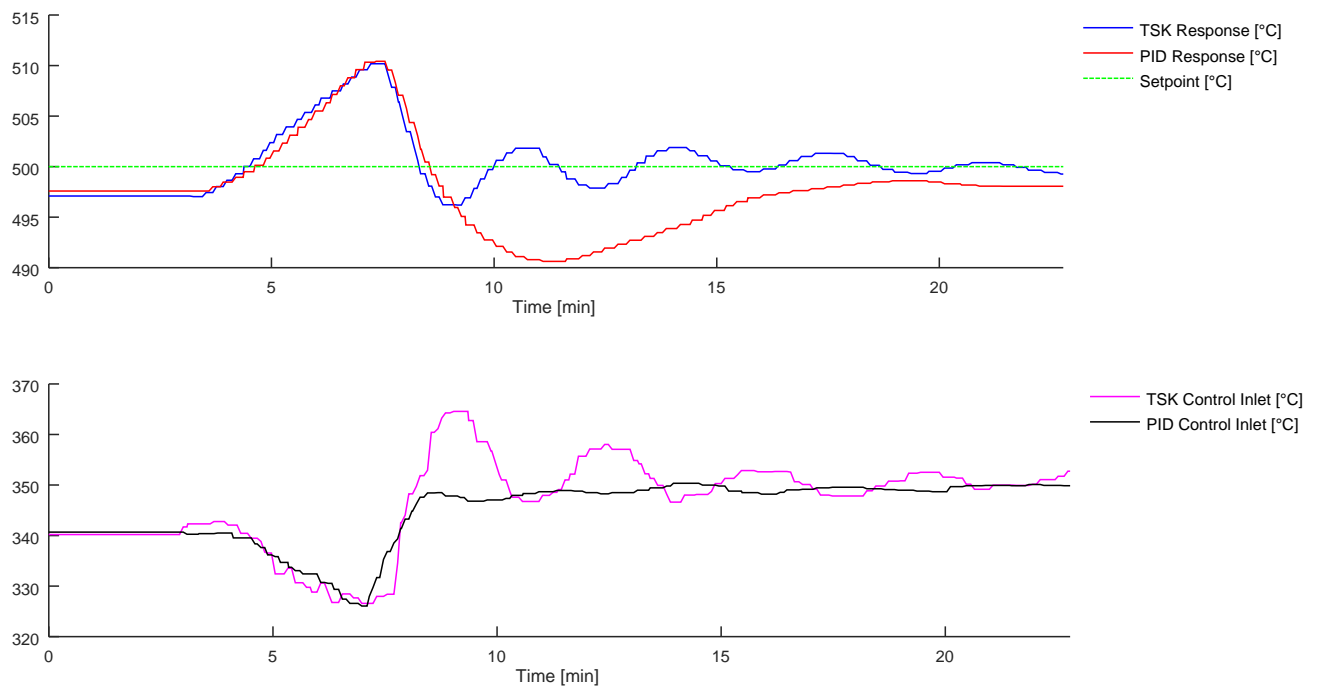


Figure 65: Simulator Rapid Pressure Raising –Fuzzy Control Response

Once again Fuzzy control achieves a significantly better result compared to the MPC and PID controllers on the simulator. Initially it responds almost identically to the PID controller. The

Fuzzy controller effectively controls for the second disturbance and settles significantly quicker than the PID controller.

It can be seen that there are still some oscillations in the response as it settles. The controller settles below 5 °C within 5 minutes after the disturbance and below 1 °C within 15 minutes. Controlling through two sequential disturbances is often required due to the nature of the higher-level controller that manage the firing conditions in the furnace. The Fuzzy controller seems to handle such an event with ease, even for a perturbed plant.

5.5. Holistic Evaluation of Various Results

The following tables summarise the PID, MPC and Fuzzy controllers' evaluation results. *Table 29* gives an index of the scenarios that were discussed as they appear in the tables that follow. For the full set of results comparing all three controllers over all 38 datasets, *Appendix A: Performance Evaluation Extended Tables* can be consulted.

5.5.1. Direct MPC and Fuzzy Performance Comparison

Table 29: Scenario Description index

| Scenario | ID |
|---|----|
| Sudden Steam Flow Rate Swing | 1 |
| Machine Deloading and Mill Outage | 3 |
| Steam Flow Rate Cycling while Deloading | 9 |
| Various Load Changes | 16 |
| Introduction of Mill and Load Increase | 37 |

The first set of parameters that will be discussed is the standard temperature error deviation shown in *Table 30*. Some of the results have been discussed individually. It can now be seen that the Fuzzy Controller outperforms the MPC controller in some cases, like the first case. There are also many other results that either show a performance similar to, or in some cases worse than, the MPC controller. We see that Both MPC and Fuzzy controllers consistently performs better than the PID controller with average reductions in the standard deviation 46% and 43%, respectively. On average the Fuzzy controller only has 93% the standard deviation of the MPC controller.

Chapter 5 Simulation and Evaluation

Table 30: Standard Temperature Error Deviation

| Scenario | Temperature Setpoint | Standard Temperature Error Deviation σ | | | $\sigma_{MPC}/\sigma_{PID}$ | $\sigma_{Fuzzy}/\sigma_{PID}$ | $\sigma_{Fuzzy}/\sigma_{MPC}$ |
|----------|----------------------|---|---------|---------|-----------------------------|-------------------------------|-------------------------------|
| | | PID | MPC | Fuzzy | | | |
| 1 | 505 °C | 3.33 °C | 1.78 °C | 0.85 °C | 53 % | 26 % | 48 % |
| 3 | 505 °C | 3.12 °C | 0.76 °C | 0.93 °C | 24 % | 30 % | 123 % |
| 9 | 508 °C | 2.03 °C | 0.64 °C | 0.47 °C | 31 % | 23 % | 74 % |
| 16 | 508 °C | 2.07 °C | 0.61 °C | 0.46 °C | 30 % | 22 % | 75 % |
| 37 | 505 °C | 1.26 °C | 0.37 °C | 0.36 °C | 30 % | 29 % | 96 % |
| Average | | 2.67 °C | 1.24 °C | 1.15 °C | 46 % | 43 % | 93 % |

The mean temperature error has not been discussed in much detail previously. The tabulated results are shown in full in *Appendix A.2* while *Table 31* shows an abridged version of only the cases that were analysed in detail.

Table 31: Mean Temperature Error

| Scenario | Temperature Setpoint | Mean Temperature Error | | | Change in mean °C | | |
|----------|----------------------|------------------------|----------|----------|--------------------|--------------|--------------|
| | | PID | MPC | Fuzzy | MPC vs PID | Fuzzy vs PID | Fuzzy vs MPC |
| 1 | 505 °C | 0.63 °C | 0.01 °C | 0.09 °C | -0.62 °C | -0.53 °C | 0.09 °C |
| 3 | 505 °C | -1.07 °C | -0.07 °C | -0.51 °C | -1.00 °C | -0.57 °C | 0.44 °C |
| 9 | 508 °C | 0.45 °C | -0.01 °C | -0.08 °C | -0.44 °C | -0.37 °C | 0.07 °C |
| 16 | 508 °C | 0.15 °C | 0.00 °C | -0.02 °C | -0.15 °C | -0.13 °C | 0.02 °C |
| 37 | 505 °C | -0.55 °C | 0.00 °C | 0.08 °C | -0.55 °C | -0.47 °C | 0.08 °C |
| Average | | -0.45 °C | -0.25 °C | -0.20 °C | -0.71 °C | -0.61 °C | 0.10 °C |

The results are generally not discussed in detail as the mean error is expected to be close to zero in an ideal simulated environment. However, there is merit in discussing the MPC control in comparison to the Fuzzy controller, since they are subjected to the same ideal simulated environment. From *Table 31* it can be seen that on average the mean for each controller is only 0.05 °C apart while the absolute change in mean averaged over all samples is 0.1 °C. This would indicate that on a case by case bases the Fuzzy controller deviates from the mean by more than

Chapter 5 Simulation and Evaluation

the MPC controller. However overall the mean errors are distributed around $-0.20\text{ }^{\circ}\text{C}$ almost the same average as the MPC controller.

Table 32 summarises the case specific results for the maximum temperature error. The full list of results can be consulted in *Appendix A.3*. The results shown below have been expressed as maximum error rather than the absolute maximum temperature.

Table 32: Maximum Temperature Error

| Scenario | Temperature Setpoint | Maximum Temperature Error | | | MPC/ PID | Fuzzy/ PID | Fuzzy/ MPC |
|----------|----------------------|---------------------------|----------|---------|-------------|---------------|---------------|
| | | PID | MPC | Fuzzy | | | |
| 1 | 505 °C | 19.26 °C | 10.79 °C | 3.68 °C | 56 % | 19 % | 34 % |
| 3 | 505 °C | 4.22 °C | 2.18 °C | 1.42 °C | 52 % | 34 % | 65 % |
| 9 | 508 °C | 5.22 °C | 2.02 °C | 1.33 °C | 39 % | 25 % | 66 % |
| 16 | 508 °C | 8.89 °C | 3.79 °C | 1.65 °C | 43 % | 19 % | 43 % |
| 37 | 505 °C | 3.06 °C | 1.06 °C | 0.94 °C | 35 % | 31 % | 88 % |
| Average | | 6.32 °C | 3.12 °C | 2.80 °C | 49 % | 44 % | 90 % |

The average of maximum errors for all cases were $3.12\text{ }^{\circ}\text{C}$ and $2,80\text{ }^{\circ}\text{C}$ for the MPC and Fuzzy controllers respectively. There were a few specific cases for both controllers where these errors were around $10\text{ }^{\circ}\text{C}$ but from the average it can be seen that they were isolated. Comparing this to the PID controller it is clear that both controllers reduce the maximum error by more than 50%. The Fuzzy only manages to reduce the average maximum error by 10% compared to the MPC controller. In 34% of cases the Fuzzy controller reduced the maximum error compared to the MPC controller. This is a very consistent reduction. The reason the maximum error is focused on more readily is due to the protection philosophy that will trip a machine on a high temperature. Reducing the peak error is therefore important to keep units on load.

To prevent unit trips caused by a rapid decay rate the total span of the error over the data range is analysed. *Table 33* summarises these results while *Appendix A.4* contains the unabridged version.

Chapter 5 Simulation and Evaluation

Table 33: Temperature Error Total Span

| Scenario | Temperature Setpoint | Temperature Error Total Span | | | MPC/ PID | Fuzzy/ PID | Fuzzy/ MPC |
|----------|----------------------|------------------------------|----------|---------|-------------|---------------|---------------|
| | | PID | MPC | Fuzzy | | | |
| 1 | 505 °C | 23.98 °C | 18.89 °C | 5.99 °C | 79 % | 25 % | 32 % |
| 3 | 505 °C | 14.45 °C | 4.74 °C | 4.42 °C | 33 % | 31 % | 93 % |
| 9 | 508 °C | 9.20 °C | 3.81 °C | 2.69 °C | 41 % | 29 % | 71 % |
| 16 | 508 °C | 14.50 °C | 5.74 °C | 3.19 °C | 40 % | 22 % | 56 % |
| 37 | 505 °C | 6.65 °C | 2.11 °C | 1.88 °C | 32 % | 28 % | 89 % |
| Average | | 13.13 °C | 7.68 °C | 6.21 °C | 58 % | 47 % | 81 % |

This does not provide a definitive indication that a trip would be avoided with a larger disturbance. The reductions in the total span of the error at least provides an idea of the decay rates that might currently be present and how far they can be reduced. We see the Fuzzy controller achieves less than half the error span on average of the PID controller. The MPC controller reduces the error span to 58% of the PID controller. The Fuzzy controller does really well here and reduces the error span to 81% of the MPC controller.

Table 34 summarises the peak response time reduction with *Appendix A.5* showing all the results. Again, it will be emphasised that the results are slightly more subjective due to it measuring early response based on known disturbances. This again should not be confused with being able to respond earlier to unknown disturbances. Unknown disturbances can only be responded to as fast as they present in the system output or other measurable state. It can be seen that the Fuzzy controller has an additional 10% improvement over the MPC controller. This may be due to the specific tuning to allow it to respond earlier to rapid changes in the steam flow rate. Some of the earlier response seen may also be due to the aggressive response it presents, when compared to the MPC controller.

Table 34: Peak Response Time Reduction

| Scenario | Average Steam Flow Rate | System Time Constant | Peak Response Time Reduction | | Percentage of Time Constant | |
|----------|-------------------------|----------------------|------------------------------|-------|-----------------------------|-------|
| | | | MPC | Fuzzy | MPC | Fuzzy |
| 1 | 43 kg/s | 253.47 s | 74 s | 150 s | 29 % | 59 % |
| 3 | 39 kg/s | 274.53 s | 60 s | 178 s | 22 % | 65 % |
| 9 | 44 kg/s | 243.67 s | 137 s | 199 s | 56 % | 82 % |
| 16 | 49 kg/s | 222.43 s | 53 s | 83 s | 24 % | 37 % |
| 37 | 41 kg/s | 260.55 s | 65 s | 93 s | 25 % | 36 % |
| Average | | | 88 s | 112 s | 33 % | 43 % |

5.5.2. Practical Implications and Considerations

During the evaluation phase it could be seen that the MPC and Fuzzy controllers succeed in improving on all the metrics used to evaluate them. This seems to be largely due to two consequences of the design: The early response to known disturbances as well as more aggressive responses. It would be hoped that by responding earlier the control error could be reduced enough to not warrant a more aggressive response. Unfortunately, as seen through analysis, some very severe disturbances and energy imbalances can result in a very aggressive controller response. These responses, can be argued, are warranted, but perhaps only due to maloperation of the machine in a condition it should have never been placed in.

Accepting that, in certain situations, an aggressive control response might be required, the impact should also be discussed or possible limitations. One impact of an aggressive response is excessive wearing of the valve and actuator in operation. This must be carefully analysed based on the potential gain from a more aggressive controller response. If a trip conditions can be avoided while valve operation is not compromised it could be worth the extra wear. Unit trips cause significant revenue loss and have a cost associated with recovery. The valve design and preventative maintenance frequency would need to be increased in order to compensate for the possibility of a higher wear rate. If a unit can safely be run between overhaul schedules, without risking a valve or actuator failure, this can be considered. If additional valve wear cannot be accommodated, limits need to be placed on the valve operation.

Chapter 5 Simulation and Evaluation

Realistically looking at the events analysed requiring a severe controller response it is noted that they were chosen specifically since they present a large disturbance. The majority of daily operation do not comprise of complex control objectives, which further highlights that: Although a more aggressive control response might be required in certain situations, this is not the norm. In terms of the MPC controller the design in some ways also attempt to reduce wear on the valve and actuator components. The variable sample times reduces the frequency of operation during low loads, and only increases when the load is increased again.

The saturation limit of steam has been discussed a few times at this point. In the scenarios used, no operation exceeded the saturation limit. This operation would be limited in practice to avoid the possibility of water carryover. Another aspect to quenching steam is thermal shock on the piping in the superheater. Rapidly cooling the steam with water will rapidly cool the steam pipework where it comes into contact. This will compromise the integrity of the steel, and may result in failure. To prevent this, to some extent, the valve is designed with a protective sleeve, as well as ensuring feedwater that is admitted to the steam flow path is atomised to allow it to quickly vaporise. The design of the sleeve and boiler tubes should also be consulted to ensure that allowable temperature decay rates are not exceeded.

Water carry over to the turbine is essentially avoided through several precautions. The design of the spraywater system is such that water is applied before the final superheater and atomised in the process. This allows quick vaporisation as well as providing sufficient pipe length for this to fully complete. By preventing operation at the saturation temperature of steam, formation of liquid in the vapour mixture can be avoided. As a last resort the turbine will be automatically separated from the grid in the event of measuring a rapid decay in steam temperature.

These simulated results provide an ideal analysis that is limited to model accuracy and not subject to implementation restrictions. Results are therefore not overstated, but provide an indication that further research and testing could provide positive results and are worth further exploration. It is also noted that the current PID controller could likely also be improved based on the results obtained. It is used as a baseline for this study, but should not be reflected on as a negative result for PID controllers in general.

Chapter 6

Conclusions and Recommendations

6.1. Summary

This thesis has investigated the use of advanced control systems and the specific application on superheated steam temperature control through spray water quenching. This was done with the specific purpose of gaining a performance increase compared to the widely used PID control technique that is currently also in use on this system.

Through the study of literature surrounding superheater temperature control, specifically in boilers, two techniques were singled out for further research. The MPC and Fuzzy control techniques are supported by other researchers, for the control of superheater temperature with spray water quenching. Fuzzy and MPC control solutions was investigated further as a solution for better performing temperature control. Literature review also highlighted several techniques available to attempt to control for plant non-linearity. This included controlling with a variable sample time depending on the system parameters. Alternatively, Fuzzy control also has the built-in ability to facilitate control over a range of variable plant dynamics.

Process analysis was presented in as much as the superheater system fits into the entire power generation process. The particulars of boiler operations at Komati Power Station were investigated with specific emphasis on known non-linearity, process dynamics, disturbances as well as the interface between various other control systems in the process.

The control strategy for the superheater itself is in fact also a cascade controller consisting of an outer control loop feeding into an inner loop to control the inlet temperature to the final superheater. This is done to achieve the desired outlet steam temperature exiting the final superheater. The inner loop is a trivial control loop that applies the spray water necessary to reach the desired inlet steam temperature. It is trivial in the sense that it is a much faster control loop

Chapter 6 Conclusions and Recommendations

compared to the outer loop. It does not suffer from any significant non-linearity that hamper its operation. The study focuses on optimisation of the outer control loop.

Practically, many disturbances are in-fact due to the parallel operation of process controllers that control the system as a whole. The reason behind the segregation of these processes and controllers were discussed, while the need was established to still include the outputs of these controllers into the superheater steam temperature control.

The controller's operating range is also investigated, as part of the operating envelope for the process, and non-linearities were identified. The system dependence on the steam flow rate was a major non-linearity that needed to be addressed to ensure adequate operation across the entire allowable range. Secondly, the fact that this is a thermodynamic process that operates across various temperatures and pressures, also results in non-linearity in the process model. The combustion process itself is highly variable with too few measurements to accurately model. This contributes to uncertainty in the process model.

System identification was then performed using a large variety of on-load operation data of a particular generating unit at Komati Power Station. The basic model, fit for purpose, was identified through literature review, and adapted for this application. The model was fitted for the particulars of this project with the data gathered from the unit. A state space model was constructed taking firing rates, superheater-inlet steam temperature and -outlet steam temperature and pressure as inputs. The state space model was linearized at full load. Through the application of a variable sample time, it was shown that the model dependency on the steam flow rate could be mitigated.

The combustion process was not modelled directly, rather a pre-filter was constructed to be applied to the firing rate measurements that feed the combustion process. An iterative least squares regression method was used to fit the model to the available data. The model response was compared to the actual plant response. Model deviations from the actual plant would also later be used to construct an unmeasured disturbance signal to be used during simulation.

A cost function for the MPC controller was constructed using the single system input and was combined with the measurable disturbances. An optimised control law was then constructed from

Chapter 6 Conclusions and Recommendations

the cost function at its minimum. A reduced order observer was also constructed to estimate the unmeasured system state. The MPC control law is intended to be applied at a variable sample rate based on the operating load condition, as measured by steam throughput.

The fuzzy controller was based on Takagi-Sugeno-Kang Fuzzy control architecture where optimised controllers are designed for each rule-based region. Each rule was based on the steam flow rate (high and low) and acceleration of steam (positive, small and negative) creating a two-dimensional region map with overlapping triangular membership functions.

The controller for each region was optimised with a fixed sample time based on the original model. An adapted cost function was used to determine feedback gains for the states and measured disturbances. The system response takes advantage of the fact that steam flow acceleration, is generally limited, and compensates for the change in plant dynamics, as the flow rate is expected change. This compensation is encapsulated in the cost function.

The two control techniques were evaluated through simulation. The model used for simulation was also disturbed with an unmeasured disturbance to mimic the model error that was remaining after system identification. 5 case studies were taken from the 38 datasets for detailed discussion, as well as average performance indicators for all the results.

The MPC controller proved during simulation to reduce the standard deviation from setpoint by 54 % compared to the current PID controller response. It also reduced the maximum and minimum deviations from setpoint by 49 % and 29 % respectively. Qualitatively it can also be said that the incorporation of measured disturbances in the controller feedback significantly reduce the reaction time of the controller specifically to those disturbances.

The MPC controller was also shown to avoid two tripping scenarios, in which the PID controller had failed to maintain operating parameters within safe limits. The same positive result was also achieved when simulating the Fuzzy controller.

The fuzzy controller achieved results similar to that of the MPC controller, when compared to the PID controller. It reduced the standard deviation from setpoint by 57 %, and the maximum and minimum deviations from setpoint by 50 % and 55 % respectively. In general, the Fuzzy

Chapter 6 Conclusions and Recommendations

controller out-performed the MPC controller, but especially in areas of high non-linearity, with a high absolute acceleration in steam flow.

Both controllers were then tested on the operations simulator's perturbed representation of the plant in question. The results showed that although the emulated plant had significantly higher gain and larger time constant, the MPC controller performed at least comparably well against the PID controller.

The MPC controller suffered from overshoot, but generally returned back to setpoint much faster. Some oscillations were still present in the response. In both test cases the controller settled at least as fast as the PID controller. Under these conditions there were positive and negative aspects of the responses. The test also pointed out that the controller responded within the operating envelope for a perturbed plant and shows some degree of robustness.

The fuzzy controller outperformed the PID and MPC controllers again during testing on the operations simulator. It settled significantly faster and reduced the peak temperature responses to a large extent. Again, there is some oscillation before settling out due to the perturbation of the plant. Nonetheless, the controller performed significantly better than the MPC and PID controllers and is shown to be robust enough for general application between the varying units at Komati Power Station.

6.2. Recommendations

The Fuzzy controller presented has proved to be the most effective solution for the effective control of the superheater final steam temperature. It is recommended for field testing in this application and should significantly improve final steam temperature control, as well as avoid grid separations related to final steam temperature safe operating margins.

The MPC controller generally underperformed the Fuzzy controller, but has nonetheless outperformed the current PID controller. Should resource constraints allow for on-line testing of both proposed controllers before final implementation, the MPC controller has shown its ability to reduce the steam temperature's deviation from setpoint and peak excursion values.

Chapter 6 Conclusions and Recommendations

Testing and simulation the performance of these two control techniques was carried out only based on one unit at Komati Power Station. Future work will therefore also include applying the techniques developed in this research to other units at the Station. This work will identify which control technique transfer more easily to other units.

The foundation to develop the two control techniques for other units has been given in this thesis. The first requirement would be to gather raw data from the remaining units. In gathering data, the researcher should consider the factors pointed out in *Chapter 2*. Scenarios should include a variety of operating conditions to ensure that, within the complete set, it contains independent and uncorrelated process measurements. It should also be noted that future research might explore more possibilities of gathering process data on-line. It could advocate for, and design techniques for impulse and step response testing to be done online for system identification. This is no small task considering that the entire power generating process has many interdependent systems. This can be motivated for based on the positive results that can be achieved as highlighted in the research done in this thesis.

With suitably chosen training data the researcher can apply the same model identification techniques used in *Chapter 3*. Expansion of the model can also be suggested for future work. Assumptions are made and the model complexity determined by the researcher's findings during system analysis. This process continually evolves as well as new research and technology becoming available as time goes on. Modelling of the combustion processes is a large field of research on its own. It is an ideal area for focus to allow for more accurate modelled behaviour to be used for control purposes, not only for steam temperature control, but also many others.

Increasing model accuracy may include taking aspects like ash build up, coal quality and boiler efficiency into account on a real time basis. Other activities that affect the heat transfer rate could also be explored to better control these transient conditions. As mentioned before, in some cases the added complexity might not realise much of an improvement, and would have to be investigated case by case. Soot-blowing, as one example, causes significant combustion instability at Komati Power Station and could potentially add significant value to the control effort if it is adequately modelled and compensated for as a measured disturbance.

Chapter 6 Conclusions and Recommendations

During this research, installation of additional process measurements was not considered due to the hypothesis that a large performance increase could be obtained purely by applying more advanced control techniques. The research has clearly demonstrated this. This should not stop future researchers from identifying areas of improvement in process measurement that might be site specific. What comes to mind here specifically for Komati, is an additional measurement(s) of the final superheater stage at one or more points along the steam flow path. Currently the Measurement of CO gasses are also becoming mandatory. Installations are being carried out across all sites. This is a critical indication revealing much about combustion instability. The use of these and other measurements could drastically improve the performance of the final steam temperature controller and other combustion process controllers.

With model identification done the researcher can apply the same techniques provided in *Chapter 4* to develop the controller for each unit. Within the framework given, the MPC controller can easily be developed straight from the model. The Fuzzy controller requires further training to determine adequate response to steam flow acceleration. With the technique used during this research the degrees of freedom have been decreased and allow for training of the Fuzzy controller from base values derived from the model.

Within the two control techniques explored there remains room for expansion. It has to be acknowledged that the use of these and other more advanced control techniques, in the power industry in South Africa, is not widespread as also evident at Komati Power Station. It is paramount that these techniques are tested and adopted in the industry through proof of application before more complex versions are introduced into the industry. With future research, other features of the MPC controller, including more stringent constraint control and further compensation for non-linearities can be explored. The fuzzy controller itself can be expanded further to include typical human operator responses that are not limited to spraywater control, but may include the introduction of oil burner support or mill biasing.

There are also other topics related to the main steam temperature controller that fell outside the scope of this research topic, and can be considered for future focus. Optimization of the inner loop is currently not required. It can be explored further in future research topics especially in

Chapter 6 Conclusions and Recommendations

terms of robustness. This may include compensating the controller for changes in water temperature used to quench steam.

There also exist components of process automation and redundancy over just pure control when working with complex systems. Multiple measurements are available for this controller although not currently used. Measurements of water feed rate and temperature could be used to directly control the water flow rate along with the temperature at the superheater inlet. This could be used to provide more flexibility and robustness should one of these measurements fail while the system is in service, thereby avoiding shutdown, manual intervention or production delays.

On the other side of automation and control lies manual intervention. In an ideal research environment this is usually not of much importance as manual intervention defeats the whole purpose of the control system. The power generation industry faces the reality that components may fail and, in some instances, require manual intervention while issues are being corrected. With complex systems and processes, manually manipulating a system, like final steam temperature control, can be critical but outside the ability of a human operator. The human operator is in charge of the entire system and cannot divert all focus to this intervention. Future research could investigate aiding an operator who is required to manually intervene. One such instance is in the event that an actuator has to be manually operated by the human operator. Keeping track of the behaviour of non-linear systems with large time constants can be challenging for a human operator with focus on multiple processes. Providing more information relating to the process states and the system's predicted behaviour based on the models derived here could severely decrease the burden on the operators while they intervene.

6.3. Conclusion

In conclusion the researcher has presented evidence, through simulation, that both Fuzzy and MPC control techniques can significantly improve the superheater temperature control response at Komati Power Station. During this process the researcher has made contributions toward the development of advanced control techniques in the power station environment. This will allow higher levels of adoption for advanced control techniques and therefore more robust plant controls.

Chapter 6 Conclusions and Recommendations

This thesis has expanded on techniques and research from the industry to provide a systematic approach to the application of Fuzzy and MPC control techniques to particular the final steam temperature control system. This has included steps from disturbance analysis, model identification, and control system design and testing. Using a variable sample time on the MPC controller, it was shown how this could compensate for the model dependency on the steam flow rate. This can be seen as an alternative to gain scheduling, however the actual real-world implementation and performance would have to be tested for suitability first. Techniques were also developed to aid in the training of the TSK Fuzzy controller by decreasing the degrees of freedom and allowing the partial reuse of techniques used to develop the MPC controller.

Inclusion of important process disturbances for the use in control feedback have also made both controllers very robust to known system disturbances. The combustion firing rate, steam flow, pressure and temperature were all instrumental to realise an improved performance over the PID controller currently active on the plant. Here the researcher has contributed by expanding on research done by others, from a pure modelling point of view, leading to its application in the control of the plant.

The Fuzzy controller has displayed the best performance all round and can be seriously considered for future use in the field. On average the Fuzzy controller reduced the standard final steam temperature deviation from setpoint by an additional 4% over the already greatly reduced 41% standard deviation achieved by the MPC controller when compared to the PID controller. Both new controllers also reduced the peak positive temperature excursion, the main cause of grid separations, to almost 50% of the PID controlled plant.

Simulation has shown that the controller would have been capable of preventing related grid separations experienced in the past, were any one of the proposed controllers implemented. This means that the research conducted here has the potential to save hundreds of thousands of Rands in fuel costs and revenue loss for each avoided grid separation.

Both control techniques were found to be robust against plant perturbations to a large degree. Through testing of the control systems on an independent simulation platform, both controllers were evaluated to perform at least comparable to the PID controller optimised for the simulator. The MPC and Fuzzy controller was optimised for a live unit at Komati Power Station. Analysis

Chapter 6 Conclusions and Recommendations

revealed that the controllers achieved this remarkable performance on a plant with an estimated 24% increase in the first order response time constant, and a 100% increase in plant gain. This shows that, once implemented, these controllers would need very little maintenance, unless major plant design changes are carried out.

This research will also contribute to the long-term plant health of the turbine plant. With tighter control of main steam temperatures, the metal components in the turbine and associated piping, are subjected to far less stresses and are less prone to metal fatigue. The turbine blades will also be less subjected to damage caused by water vapour forming in inadequately temperature-controlled steam, especially on low pressure turbines.

The control techniques in the forms presented would also not require significant changes to the current hardware and software configuration on the plant and can be implemented directly without additional resources being required. It is also hoped that through the use of more advanced techniques in the industry higher adoption levels will be achieved and may lead to eventual widespread use, to the betterment of the industry. This will also lead to many new research opportunities due to the immensity of the industrial control field.

Symbols

Literature references

- [1] Eskom, "GENERATION PLANT MIX," 2017. [Online]. Available: <http://www.eskom.co.za/AboutElectricity/FactsFigures/Documents/GX0001GenPlantMixRev19.pdf>.
- [2] Department of Energy, "Integrated Resource Plan for Electricity," 2017. [Online]. Available: <http://www.ee.co.za/wp-content/uploads/2017/12/Eskom-IRP-2017-study-report-for-DoE-November-2017.pdf>.
- [3] Eskom, "Komati Power Station Historic Archived Operations Data [Internal Data Archive]".
- [4] K. Madisha, Interviewee, *Primary Energy Costs and Use at Komati Power Station [Internal - Komati Power Station Primary Energy Manager]*. [Interview]. 14 August 2017.
- [5] X. Li, "Dynamic behavior of superheated steam and ways of control," *Frontiers of Energy and Power Engineering in China*, vol. 2, no. 1, pp. 25-30, 1 March 2008.
- [6] H. Spliethoff, *Power Generation from Solid Fuels*, 1 ed., Springer-Verlag Berlin Heidelberg, 2010, p. 674.
- [7] X.-L. Song, C.-Y. Liu, Z.-Y. Song and X.-F. Song, "Robust PID control for steam superheater," in *Machine Learning and Cybernetics, 2004. Proceedings of 2004 International Conference on*, Shanghai, 2004.
- [8] Z. Machacek, M. Pies and S. Ozana, "Simulation of MIT Rule-Based Adaptive Controller of a Power Plant Superheater," in *Frontiers in Computer Education*, 1 ed., Springer-Verlag Berlin Heidelberg, 2012, pp. 473-479.
- [9] S. Matsumura, K. Ogata, S. Fujii, H. Shioya and H. Nakamura, "Adaptive Control for the Steam Temperature of Thermal Power Plants," *Control Engineering Practice*, vol. 2, no. 4, pp. 567-575, August 1994.
- [10] M. Liangyu, L. Yongjun and K. Lee, "Superheater steam temperature control for a 300MW boiler unit with Inverse Dynamic Process Models," in *Power and Energy Society General Meeting, 2010 IEEE*, Minneapolis, MN, 2010.
- [11] T. Moelbak, "Advanced control of superheater steam temperatures – an evaluation based on practical applications," *Control Engineering Practice*, vol. 7, no. 1, pp. 1-10, January 1999.
- [12] G.-L. Wang, W.-W. Yan, S.-H. Chen, X. Zhang and H.-H. Shao, "Multivariable constrained predictive control of main steam temperature in ultra-supercritical coal-fired power unit," *Journal of the Energy Institute*, vol. 88, no. 2, pp. 181-187, May 2015.

Symbols

- [13] J. Hlava, "Model predictive control of the superheater temperature based on a piecewise affine model," in *Control 2010, UKACC International Conference on*, Coventry, 2010.
- [14] J. Opalka and L. Hubka, "Nonlinear State and Unmeasured Disturbance Estimation for Use in Power Plant Superheaters Control," *Procedia Engineering*, vol. 100, pp. 1539-1546, 24 February 2015.
- [15] T. Nahlovsky, "Optimization of Fuzzy Controller Parameters for the Temperature Control of Superheated Steam," *Procedia Engineering*, vol. 100, pp. 1547-1555, 2015.
- [16] J. E. Normey-Rico and E. F. Camacho, *Control of Dead-time Processes*, 1 ed., Springer-Verlag London, 2007, p. 462.
- [17] Q.-C. Zhong, *Robust Control of Time-delay Systems*, 1 ed., Springer-Verlag London, 2006, p. 231.
- [18] H. Lam and F. Leung, "Sampled-Data Fuzzy Controller for Time-Delay Nonlinear Systems: Fuzzy-Model-Based LMI Approach," *Systems, Man, and Cybernetics, Part B: Cybernetics, IEEE Transactions on*, vol. 37, no. 3, pp. 617-629, June 2007.
- [19] S. Shi and L. Yu, "Adaptive Robust Control for Uncertain Nonlinear Systems with Time-Delay," in *Recent Advances in Computer Science and Information Engineering*, 1 ed., vol. 6, Springer-Verlag Berlin Heidelberg, 2012, pp. 135-140.
- [20] R. Sipahi, T. Vyhlídal, S.-I. Niculescu and P. Pepe, *Time Delay Systems: Methods, Applications and New Trends*, 1 ed., Springer-Verlag Berlin Heidelberg, 2012, p. 442.
- [21] M. Wu, Y. He and J.-H. She, *Stability Analysis and Robust Control of Time-Delay Systems*, 1 ed., Springer-Verlag Berlin Heidelberg, 2010, p. 335.
- [22] J. Xie, S. Wang, Y. Wang and J. He, "Research on Predictive Control of Evaporator Superheat System with Time-Delay Based on DMC Intelligent Optimization," in *Practical Applications of Intelligent Systems*, 1 ed., Z. Wen and T. Li, Eds., Springer-Verlag Berlin Heidelberg, 2014, pp. 785-793.
- [23] S. Yordanova, "Robust performance design of single-input fuzzy control system for plant with time delay," *Transactions of the Institute of Measurement and Control*, vol. 31, no. 5, pp. 381-399, October 2009.
- [24] S. Yordanova and T. Tashev, "Fuzzy Internal Model Control of Nonlinear Plants with Time Delay," *WSEAS TRANSACTIONS on CIRCUITS and SYSTEMS*, vol. 11, no. 2, February 2012.
- [25] R. S. Ranganathan, H. A. Malki and G. Chen, "Fuzzy Predictive PI Control for Processes with Large Time Delays," *Expert Systems*, vol. 19, no. 1, February 2002.
- [26] L. Wang, *Model Predictive Control System Design and Implementation Using MATLAB®*, 1 ed.,

Symbols

- Springer-Verlag London, 2009, p. 378.
- [27] E. Eitelberg and E. Boje, "Implicit Quasi-Steady-State Approximation and Application to a Power Plant Evaporator," *Transactions of the ASME*, vol. 129, no. 1, pp. 66-71, January 2007.
- [28] Siemens, "Siemens SPPA-T3000 Online Help [Distributed with Siemens SPPA-T3000 Software Solution]," Munich.
- [29] Steinmüller, *Komati Power Station Boiler 4 General Arrangements of Pressure Parts [Internal Drawing 05-014-04-01-99-999-001]*.
- [30] I. Martínez, "Lectures on Thermodynamics," Technical University of Madrid, 1995. [Online]. Available: <http://webserver.dmt.upm.es/~isidoro/bk3/>. [Accessed 18 July 2014].
- [31] NERSA, "The South African Grid Code - The Network Code," March 2008. [Online]. Available: [http://www.nersa.org.za/Admin/Document/Editor/file/Electricity/Compliance Monitoring/SAGC Network Version 7_March 2008.pdf](http://www.nersa.org.za/Admin/Document/Editor/file/Electricity/Compliance%20Monitoring/SAGC%20Network%20Version%207_March%202008.pdf). [Accessed 12 September 2017].
- [32] NERSA, "The South African Grid Code - The System Operation Code," March 2008. [Online]. Available: [http://www.nersa.org.za/Admin/Document/Editor/file/Electricity/TechnicalStandards/SAGC System Ops Version 7_March 2008.pdf](http://www.nersa.org.za/Admin/Document/Editor/file/Electricity/TechnicalStandards/SAGC%20System%20Ops%20Version%207_March%202008.pdf). [Accessed 12 September 2017].
- [33] Y. A. Çengel and M. A. Boles, *Thermodynamics: An engineering approach*, 5th ed., Boston: McGraw-Hill, 2006.
- [34] T. A. Badgwell and S. J. Qin, "Model-Predictive Control in Practice," in *Encyclopedia of Systems and Control*, J. Baillieul and T. Samad, Eds., Springer London, 2014, pp. 1-6.
- [35] Y. Bai, H. Zhuang and H. Zhuang, *Advanced Fuzzy Logic Technologies in Industrial Applications*, 1 ed., Springer-Verlag London, 2006, p. 334.
- [36] Eskom, "Unit 8 Tripped from 29MW on L/H Main-steam temperature decay protection [Internal Investigation Report - ON561]," 2015.
- [37] Eskom, "Unit 6 Tripped on Final Steam Temp High [Internal Investigation Report ON751]," 2014.
- [38] P. Furmański, "Thermal and Radiative Properties of Ash Deposits on Heat Transfer Surfaces of Boilers," *Journal of Power Technologies*, vol. 79, 1995.
- [39] L. Huang, J. Norman, M. Pourkashanian and A. Williams, "Prediction of ash deposition on superheater tubes from pulverized coal combustion," *Fuel*, vol. 75, no. 3, pp. 271-279, February 1996.

Symbols

- [40] M. Trojan and D. Taler, "Thermal simulation of superheaters taking into account the processes occurring on the side of the steam and flue gas," *Fuel*, vol. 150, pp. 75-87, 15 June 2015.
- [41] A. Zbogar, F. Frandsen, P. A. Jensen and P. Glarborg, "Shedding of ash deposits," *Progress in Energy and Combustion Science*, vol. 35, no. 1, p. 31–56, February 2009.
- [42] M. Gopal, *Digital Control and State Variable Methods*, McGraw-Hill, 2004.
- [43] G. F. Franklin, J. D. Powell and A. Emami-Naeini, *Feedback Control of Dynamic Systems*, 5th ed., New Jersey: Pearson Education, Inc., 2009.
- [44] The MathWorks Inc., "MATLAB 2017a," The MathWorks Inc., Natick, 2017.
- [45] P. Tatjewski, *Advanced Control of Industrial Processes*, 1 ed., Springer-Verlag London, 2007, p. 332.
- [46] J. W. Eaton, D. Bateman, S. Hauberg and R. Wehbring, "GNU Octave version 4.2.0 manual: a high-level interactive language for numerical computations."
- [47] M. Holmgren, "X Steam, Thermodynamic properties of water and steam."

Appendix A Performance Evaluation

Extended Tables

| Scenario | ID |
|---|-----|
| Sudden Steam Flow Rate Swing | 1* |
| Machine Deloading and Mill Outage | 3* |
| Steam Flow Rate Cycling while Deloading | 9* |
| Various Load Changes | 16* |
| Introduction of Mill and Load Increase | 37* |

Appendix A.1 Standard Temperature Error Deviation

| Scenario | Temperature Setpoint | Standard Temperature Error Deviation σ | | | $\sigma_{MPC}/\sigma_{PID}$ | $\sigma_{Fuzzy}/\sigma_{PID}$ | $\sigma_{Fuzzy}/\sigma_{MPC}$ |
|----------|----------------------|---|---------|---------|-----------------------------|-------------------------------|-------------------------------|
| | | PID | MPC | Fuzzy | | | |
| 1* | 505 °C | 3.33 °C | 1.78 °C | 0.85 °C | 53 % | 26 % | 48 % |
| 2 | 505 °C | 3.29 °C | 1.66 °C | 0.92 °C | 50 % | 28 % | 56 % |
| 3* | 505 °C | 3.12 °C | 0.76 °C | 0.93 °C | 24 % | 30 % | 123 % |
| 4 | 505 °C | 2.96 °C | 0.90 °C | 1.13 °C | 30 % | 38 % | 126 % |
| 5 | 500 °C | 3.71 °C | 2.69 °C | 1.97 °C | 72 % | 53 % | 73 % |
| 6 | 500 °C | 2.93 °C | 2.15 °C | 1.39 °C | 73 % | 47 % | 64 % |
| 7 | 508 °C | 2.98 °C | 0.69 °C | 0.59 °C | 23 % | 20 % | 85 % |
| 8 | 508 °C | 3.35 °C | 0.65 °C | 0.55 °C | 19 % | 17 % | 85 % |
| 9* | 508 °C | 2.03 °C | 0.64 °C | 0.47 °C | 31 % | 23 % | 74 % |
| 10 | 508 °C | 1.69 °C | 0.62 °C | 0.45 °C | 36 % | 27 % | 73 % |
| 11 | 508 °C | 4.82 °C | 5.88 °C | 5.68 °C | 122 % | 118 % | 97 % |
| 12 | 508 °C | 10.75 °C | 7.95 °C | 8.11 °C | 74 % | 75 % | 102 % |
| 13 | 510 °C | 1.70 °C | 0.59 °C | 0.59 °C | 35 % | 34 % | 100 % |
| 14 | 510 °C | 1.91 °C | 0.60 °C | 0.57 °C | 31 % | 30 % | 96 % |
| 15 | 508 °C | 2.72 °C | 0.63 °C | 0.43 °C | 23 % | 16 % | 68 % |
| 16* | 508 °C | 2.07 °C | 0.61 °C | 0.46 °C | 30 % | 22 % | 75 % |
| 17 | 500 °C | 2.63 °C | 1.46 °C | 1.70 °C | 55 % | 65 % | 116 % |
| 18 | 500 °C | 4.11 °C | 2.31 °C | 1.82 °C | 56 % | 44 % | 79 % |
| 19 | 505 °C | 2.97 °C | 0.82 °C | 0.71 °C | 27 % | 24 % | 87 % |

Appendix A Performance Evaluation Extended Tables

| Scenario | Temperature Setpoint | Standard Temperature Error Deviation σ | | | $\sigma_{MPC}/\sigma_{PID}$ | $\sigma_{Fuzzy}/\sigma_{PID}$ | $\sigma_{Fuzzy}/\sigma_{MPC}$ |
|----------|----------------------|---|---------|---------|-----------------------------|-------------------------------|-------------------------------|
| | | PID | MPC | Fuzzy | | | |
| 20 | 505 °C | 3.03 °C | 0.98 °C | 0.71 °C | 32 % | 23 % | 73 % |
| 21 | 500 °C | 3.87 °C | 1.71 °C | 2.86 °C | 44 % | 74 % | 167 % |
| 22 | 500 °C | 4.93 °C | 1.65 °C | 2.54 °C | 33 % | 51 % | 154 % |
| 23 | 505 °C | 1.22 °C | 0.48 °C | 0.57 °C | 40 % | 47 % | 119 % |
| 24 | 505 °C | 1.02 °C | 0.30 °C | 0.43 °C | 29 % | 42 % | 143 % |
| 25 | 505 °C | 1.73 °C | 0.82 °C | 0.66 °C | 47 % | 38 % | 81 % |
| 26 | 505 °C | 1.62 °C | 0.82 °C | 0.39 °C | 51 % | 24 % | 47 % |
| 27 | 505 °C | 0.79 °C | 0.27 °C | 0.26 °C | 35 % | 33 % | 94 % |
| 28 | 505 °C | 0.97 °C | 0.29 °C | 0.29 °C | 30 % | 30 % | 100 % |
| 29 | 505 °C | 2.38 °C | 0.69 °C | 0.60 °C | 29 % | 25 % | 87 % |
| 30 | 505 °C | 1.66 °C | 0.57 °C | 0.51 °C | 34 % | 31 % | 90 % |
| 31 | 505 °C | 2.42 °C | 0.65 °C | 0.58 °C | 27 % | 24 % | 90 % |
| 32 | 505 °C | 1.65 °C | 0.47 °C | 0.47 °C | 29 % | 28 % | 99 % |
| 33 | 505 °C | 2.10 °C | 0.65 °C | 0.70 °C | 31 % | 33 % | 108 % |
| 34 | 505 °C | 2.41 °C | 0.78 °C | 0.93 °C | 32 % | 39 % | 120 % |
| 35 | 505 °C | 1.74 °C | 0.49 °C | 0.59 °C | 28 % | 34 % | 121 % |
| 36 | 505 °C | 2.06 °C | 1.13 °C | 0.49 °C | 55 % | 24 % | 43 % |
| 37* | 505 °C | 1.26 °C | 0.37 °C | 0.36 °C | 30 % | 29 % | 96 % |
| 38 | 505 °C | 1.36 °C | 0.50 °C | 0.45 °C | 37 % | 34 % | 92 % |
| Average | | 2.67 °C | 1.24 °C | 1.15 °C | 46 % | 43 % | 93 % |

Appendix A.2 Mean Temperature Error

| Scenario | Temperature Setpoint | Mean Temperature Error | | | Change in mean °C | | |
|----------|----------------------|------------------------|----------|----------|--------------------|--------------|--------------|
| | | PID | MPC | Fuzzy | MPC vs PID | Fuzzy vs PID | Fuzzy vs MPC |
| 1* | 505 °C | 0.63 °C | 0.01 °C | 0.09 °C | -0.62 °C | -0.53 °C | 0.09 °C |
| 2 | 505 °C | 1.36 °C | 0.06 °C | 0.13 °C | -1.30 °C | -1.23 °C | 0.08 °C |
| 3* | 505 °C | -1.07 °C | -0.07 °C | -0.51 °C | -1.00 °C | -0.57 °C | 0.44 °C |
| 4 | 505 °C | -1.97 °C | -0.10 °C | -0.53 °C | -1.88 °C | -1.45 °C | 0.43 °C |
| 5 | 500 °C | 1.10 °C | 0.25 °C | -0.12 °C | -0.85 °C | -0.98 °C | -0.13 °C |
| 6 | 500 °C | 1.52 °C | 0.19 °C | 0.10 °C | -1.33 °C | -1.42 °C | -0.09 °C |
| 7 | 508 °C | -1.69 °C | -0.08 °C | -0.07 °C | -1.62 °C | -1.62 °C | 0.00 °C |

Appendix A Performance Evaluation Extended Tables

| Scenario | Temperature Setpoint | Mean Temperature Error | | | Change in mean °C | | |
|----------|----------------------|------------------------|----------|----------|--------------------|--------------|--------------|
| | | PID | MPC | Fuzzy | MPC vs PID | Fuzzy vs PID | Fuzzy vs MPC |
| 8 | 508 °C | -1.61 °C | -0.07 °C | -0.07 °C | -1.54 °C | -1.54 °C | 0.00 °C |
| 9* | 508 °C | 0.45 °C | -0.01 °C | -0.08 °C | -0.44 °C | -0.37 °C | 0.07 °C |
| 10 | 508 °C | 0.25 °C | 0.02 °C | -0.04 °C | -0.23 °C | -0.21 °C | 0.02 °C |
| 11 | 508 °C | -2.53 °C | -3.75 °C | -3.64 °C | 1.21 °C | 1.11 °C | -0.10 °C |
| 12 | 508 °C | -9.27 °C | -5.86 °C | -6.13 °C | -3.41 °C | -3.15 °C | 0.26 °C |
| 13 | 510 °C | -1.83 °C | -0.02 °C | 0.01 °C | -1.82 °C | -1.82 °C | -0.01 °C |
| 14 | 510 °C | -1.40 °C | -0.02 °C | 0.01 °C | -1.38 °C | -1.39 °C | -0.01 °C |
| 15 | 508 °C | -0.11 °C | -0.01 °C | -0.03 °C | -0.10 °C | -0.08 °C | 0.03 °C |
| 16* | 508 °C | 0.15 °C | 0.00 °C | -0.02 °C | -0.15 °C | -0.13 °C | 0.02 °C |
| 17 | 500 °C | 0.54 °C | 0.36 °C | 0.54 °C | -0.18 °C | 0.00 °C | 0.18 °C |
| 18 | 500 °C | 0.02 °C | -0.16 °C | 0.24 °C | 0.14 °C | 0.23 °C | 0.08 °C |
| 19 | 505 °C | -1.21 °C | 0.02 °C | 0.16 °C | -1.19 °C | -1.06 °C | 0.13 °C |
| 20 | 505 °C | -0.79 °C | -0.04 °C | 0.12 °C | -0.74 °C | -0.67 °C | 0.08 °C |
| 21 | 500 °C | -1.63 °C | -0.11 °C | 0.38 °C | -1.53 °C | -1.25 °C | 0.28 °C |
| 22 | 500 °C | -0.24 °C | -0.08 °C | 0.78 °C | -0.17 °C | 0.54 °C | 0.71 °C |
| 23 | 505 °C | -0.28 °C | 0.12 °C | 0.25 °C | -0.16 °C | -0.03 °C | 0.13 °C |
| 24 | 505 °C | 0.02 °C | 0.03 °C | 0.18 °C | 0.02 °C | 0.16 °C | 0.14 °C |
| 25 | 505 °C | 0.94 °C | 0.05 °C | 0.25 °C | -0.89 °C | -0.70 °C | 0.19 °C |
| 26 | 505 °C | 0.83 °C | 0.11 °C | 0.16 °C | -0.71 °C | -0.66 °C | 0.05 °C |
| 27 | 505 °C | 0.27 °C | 0.01 °C | 0.03 °C | -0.27 °C | -0.25 °C | 0.02 °C |
| 28 | 505 °C | 0.19 °C | 0.01 °C | 0.02 °C | -0.18 °C | -0.17 °C | 0.01 °C |
| 29 | 505 °C | 0.79 °C | 0.00 °C | -0.07 °C | -0.79 °C | -0.72 °C | 0.07 °C |
| 30 | 505 °C | 0.75 °C | 0.05 °C | -0.03 °C | -0.70 °C | -0.72 °C | -0.01 °C |
| 31 | 505 °C | -0.33 °C | -0.05 °C | 0.04 °C | -0.28 °C | -0.30 °C | -0.02 °C |
| 32 | 505 °C | 0.07 °C | -0.03 °C | 0.05 °C | -0.04 °C | -0.02 °C | 0.02 °C |
| 33 | 505 °C | 0.05 °C | -0.09 °C | -0.21 °C | 0.04 °C | 0.15 °C | 0.12 °C |
| 34 | 505 °C | -1.47 °C | -0.15 °C | -0.28 °C | -1.32 °C | -1.19 °C | 0.13 °C |
| 35 | 505 °C | 0.22 °C | 0.07 °C | 0.22 °C | -0.15 °C | 0.01 °C | 0.15 °C |
| 36 | 505 °C | 0.76 °C | -0.13 °C | 0.15 °C | -0.63 °C | -0.60 °C | 0.03 °C |
| 37* | 505 °C | -0.55 °C | 0.00 °C | 0.08 °C | -0.55 °C | -0.47 °C | 0.08 °C |
| 38 | 505 °C | 0.15 °C | 0.00 °C | 0.07 °C | -0.15 °C | -0.08 °C | 0.07 °C |
| Average | | -0.45 °C | -0.25 °C | -0.20 °C | -0.71 °C | -0.61 °C | 0.10 °C |

Appendix A Performance Evaluation Extended Tables

Appendix A.3 Maximum Temperature Error

| Scenario | Temperature Setpoint | Maximum Temperature Error | | | MPC/ PID | Fuzzy/ PID | Fuzzy/ MPC |
|----------|----------------------|---------------------------|----------|---------|-------------|---------------|---------------|
| | | PID | MPC | Fuzzy | | | |
| 1* | 505 °C | 19.26 °C | 10.79 °C | 3.68 °C | 56 % | 19 % | 34 % |
| 2 | 505 °C | 19.73 °C | 10.71 °C | 5.25 °C | 54 % | 27 % | 49 % |
| 3* | 505 °C | 4.22 °C | 2.18 °C | 1.42 °C | 52 % | 34 % | 65 % |
| 4 | 505 °C | 2.49 °C | 2.72 °C | 1.92 °C | 109 % | 77 % | 71 % |
| 5 | 500 °C | 10.92 °C | 7.21 °C | 4.56 °C | 66 % | 42 % | 63 % |
| 6 | 500 °C | 9.04 °C | 6.68 °C | 5.28 °C | 74 % | 58 % | 79 % |
| 7 | 508 °C | 2.64 °C | 1.61 °C | 1.47 °C | 61 % | 55 % | 91 % |
| 8 | 508 °C | 3.91 °C | 1.31 °C | 1.20 °C | 33 % | 31 % | 92 % |
| 9* | 508 °C | 5.22 °C | 2.02 °C | 1.33 °C | 39 % | 25 % | 66 % |
| 10 | 508 °C | 5.28 °C | 1.88 °C | 1.16 °C | 36 % | 22 % | 62 % |
| 11 | 508 °C | 7.73 °C | 3.74 °C | 3.65 °C | 48 % | 47 % | 98 % |
| 12 | 508 °C | 4.12 °C | 2.70 °C | 2.22 °C | 65 % | 54 % | 82 % |
| 13 | 510 °C | 1.08 °C | 1.18 °C | 1.26 °C | 110 % | 117 % | 107 % |
| 14 | 510 °C | 1.37 °C | 1.03 °C | 1.02 °C | 75 % | 75 % | 99 % |
| 15 | 508 °C | 8.44 °C | 4.14 °C | 1.62 °C | 49 % | 19 % | 39 % |
| 16* | 508 °C | 8.89 °C | 3.79 °C | 1.65 °C | 43 % | 19 % | 43 % |
| 17 | 500 °C | 13.76 °C | 9.37 °C | 8.59 °C | 68 % | 62 % | 92 % |
| 18 | 500 °C | 9.69 °C | 7.47 °C | 7.86 °C | 77 % | 81 % | 105 % |
| 19 | 505 °C | 5.53 °C | 2.51 °C | 2.52 °C | 45 % | 46 % | 100 % |
| 20 | 505 °C | 6.85 °C | 2.99 °C | 3.02 °C | 44 % | 44 % | 101 % |
| 21 | 500 °C | 6.26 °C | 3.37 °C | 9.49 °C | 54 % | 152 % | 282 % |
| 22 | 500 °C | 9.29 °C | 3.03 °C | 8.13 °C | 33 % | 88 % | 268 % |
| 23 | 505 °C | 2.46 °C | 2.32 °C | 2.76 °C | 94 % | 112 % | 119 % |
| 24 | 505 °C | 2.02 °C | 1.22 °C | 1.93 °C | 60 % | 95 % | 158 % |
| 25 | 505 °C | 4.35 °C | 2.47 °C | 3.37 °C | 57 % | 77 % | 136 % |
| 26 | 505 °C | 4.55 °C | 1.69 °C | 1.34 °C | 37 % | 29 % | 79 % |
| 27 | 505 °C | 2.01 °C | 0.74 °C | 0.74 °C | 37 % | 37 % | 100 % |
| 28 | 505 °C | 2.40 °C | 0.85 °C | 0.84 °C | 35 % | 35 % | 100 % |
| 29 | 505 °C | 9.45 °C | 2.37 °C | 1.94 °C | 25 % | 20 % | 82 % |
| 30 | 505 °C | 5.55 °C | 1.55 °C | 1.55 °C | 28 % | 28 % | 99 % |
| 31 | 505 °C | 6.83 °C | 2.75 °C | 2.54 °C | 40 % | 37 % | 93 % |
| 32 | 505 °C | 4.50 °C | 1.31 °C | 1.53 °C | 29 % | 34 % | 117 % |
| 33 | 505 °C | 5.71 °C | 1.60 °C | 1.34 °C | 28 % | 23 % | 84 % |
| 34 | 505 °C | 4.08 °C | 1.81 °C | 2.01 °C | 44 % | 49 % | 111 % |

Appendix A Performance Evaluation Extended Tables

| Scenario | Temperature Setpoint | Maximum Temperature Error | | | MPC/ PID | Fuzzy/ PID | Fuzzy/ MPC |
|----------|----------------------|---------------------------|---------|---------|-------------|---------------|---------------|
| | | PID | MPC | Fuzzy | | | |
| 35 | 505 °C | 4.61 °C | 2.08 °C | 2.03 °C | 45 % | 44 % | 98 % |
| 36 | 505 °C | 7.47 °C | 1.02 °C | 1.89 °C | 14 % | 25 % | 186 % |
| 37* | 505 °C | 3.06 °C | 1.06 °C | 0.94 °C | 35 % | 31 % | 88 % |
| 38 | 505 °C | 5.42 °C | 1.35 °C | 1.24 °C | 25 % | 23 % | 92 % |
| Average | | 6.32 °C | 3.12 °C | 2.80 °C | 49 % | 44 % | 90 % |

Appendix A.4 Temperature Error Total Span

| Scenario | Temperature Setpoint | Temperature Error Total Span | | | MPC/ PID | Fuzzy/ PID | Fuzzy/ MPC |
|----------|----------------------|------------------------------|----------|----------|-------------|---------------|---------------|
| | | PID | MPC | Fuzzy | | | |
| 1* | 505 °C | 23.98 °C | 18.89 °C | 5.99 °C | 79 % | 25 % | 32 % |
| 2 | 505 °C | 22.47 °C | 17.85 °C | 7.61 °C | 79 % | 34 % | 43 % |
| 3* | 505 °C | 14.45 °C | 4.74 °C | 4.42 °C | 33 % | 31 % | 93 % |
| 4 | 505 °C | 12.62 °C | 6.00 °C | 6.49 °C | 48 % | 51 % | 108 % |
| 5 | 500 °C | 17.97 °C | 11.92 °C | 9.09 °C | 66 % | 51 % | 76 % |
| 6 | 500 °C | 15.00 °C | 12.13 °C | 8.30 °C | 81 % | 55 % | 68 % |
| 7 | 508 °C | 14.11 °C | 3.68 °C | 3.47 °C | 26 % | 25 % | 94 % |
| 8 | 508 °C | 12.43 °C | 4.56 °C | 4.12 °C | 37 % | 33 % | 90 % |
| 9* | 508 °C | 9.20 °C | 3.81 °C | 2.69 °C | 41 % | 29 % | 71 % |
| 10 | 508 °C | 8.34 °C | 3.66 °C | 2.52 °C | 44 % | 30 % | 69 % |
| 11 | 508 °C | 23.42 °C | 23.79 °C | 23.10 °C | 102 % | 99 % | 97 % |
| 12 | 508 °C | 35.57 °C | 28.19 °C | 27.95 °C | 79 % | 79 % | 99 % |
| 13 | 510 °C | 8.16 °C | 3.26 °C | 3.28 °C | 40 % | 40 % | 101 % |
| 14 | 510 °C | 8.50 °C | 3.57 °C | 3.02 °C | 42 % | 36 % | 85 % |
| 15 | 508 °C | 16.72 °C | 6.22 °C | 2.81 °C | 37 % | 17 % | 45 % |
| 16* | 508 °C | 14.50 °C | 5.74 °C | 3.19 °C | 40 % | 22 % | 56 % |
| 17 | 500 °C | 17.66 °C | 14.52 °C | 14.43 °C | 82 % | 82 % | 99 % |
| 18 | 500 °C | 23.81 °C | 19.92 °C | 15.46 °C | 84 % | 65 % | 78 % |
| 19 | 505 °C | 13.13 °C | 7.64 °C | 4.65 °C | 58 % | 35 % | 61 % |
| 20 | 505 °C | 15.08 °C | 10.96 °C | 5.97 °C | 73 % | 40 % | 55 % |
| 21 | 500 °C | 14.01 °C | 7.70 °C | 14.21 °C | 55 % | 101 % | 184 % |
| 22 | 500 °C | 19.09 °C | 6.98 °C | 12.51 °C | 37 % | 66 % | 179 % |

Appendix A Performance Evaluation Extended Tables

| Scenario | Temperature Setpoint | Temperature Error Total Span | | | MPC/ PID | Fuzzy/ PID | Fuzzy/ MPC |
|----------|----------------------|------------------------------|----------|---------|-------------|---------------|---------------|
| | | PID | MPC | Fuzzy | | | |
| 23 | 505 °C | 6.27 °C | 2.86 °C | 3.22 °C | 46 % | 51 % | 112 % |
| 24 | 505 °C | 4.58 °C | 1.95 °C | 2.31 °C | 43 % | 50 % | 119 % |
| 25 | 505 °C | 8.81 °C | 6.10 °C | 4.16 °C | 69 % | 47 % | 68 % |
| 26 | 505 °C | 9.08 °C | 5.50 °C | 2.28 °C | 61 % | 25 % | 42 % |
| 27 | 505 °C | 3.47 °C | 1.63 °C | 1.30 °C | 47 % | 37 % | 80 % |
| 28 | 505 °C | 4.17 °C | 1.48 °C | 1.48 °C | 36 % | 35 % | 100 % |
| 29 | 505 °C | 15.28 °C | 4.36 °C | 3.28 °C | 29 % | 21 % | 75 % |
| 30 | 505 °C | 8.51 °C | 3.56 °C | 3.37 °C | 42 % | 40 % | 95 % |
| 31 | 505 °C | 14.39 °C | 4.92 °C | 4.20 °C | 34 % | 29 % | 85 % |
| 32 | 505 °C | 7.19 °C | 2.91 °C | 3.20 °C | 40 % | 44 % | 110 % |
| 33 | 505 °C | 9.54 °C | 4.62 °C | 4.28 °C | 48 % | 45 % | 93 % |
| 34 | 505 °C | 12.20 °C | 6.36 °C | 6.82 °C | 52 % | 56 % | 107 % |
| 35 | 505 °C | 9.25 °C | 3.31 °C | 2.86 °C | 36 % | 31 % | 86 % |
| 36 | 505 °C | 10.42 °C | 11.07 °C | 3.09 °C | 106 % | 30 % | 28 % |
| 37* | 505 °C | 6.65 °C | 2.11 °C | 1.88 °C | 32 % | 28 % | 89 % |
| 38 | 505 °C | 8.85 °C | 3.31 °C | 3.06 °C | 37 % | 35 % | 93 % |
| Average | | 13.13 °C | 7.68 °C | 6.21 °C | 58 % | 47 % | 81 % |

Appendix A.5 Peak Response Time Reduction

| Scenario | Average Steam Flow Rate | System Time Constant | Peak Response Time Reduction | | Percentage of Time Constant | |
|----------|-------------------------|----------------------|------------------------------|-------|-----------------------------|-------|
| | | | MPC | Fuzzy | MPC | Fuzzy |
| 1* | 43 kg/s | 253.47 s | 74 s | 150 s | 29 % | 59 % |
| 2 | 43 kg/s | 250.48 s | 27 s | 167 s | 11 % | 67 % |
| 3* | 39 kg/s | 274.53 s | 60 s | 178 s | 22 % | 65 % |
| 4 | 40 kg/s | 270.74 s | 60 s | 120 s | 22 % | 44 % |
| 5 | 33 kg/s | 322.78 s | 88 s | 171 s | 27 % | 53 % |
| 6 | 34 kg/s | 317.38 s | 59 s | 79 s | 19 % | 25 % |
| 7 | 49 kg/s | 218.35 s | 157 s | 180 s | 72 % | 82 % |
| 8 | 50 kg/s | 215.92 s | 88 s | 76 s | 41 % | 35 % |
| 9* | 44 kg/s | 243.67 s | 137 s | 199 s | 56 % | 82 % |
| 10 | 45 kg/s | 240.69 s | 116 s | 84 s | 48 % | 35 % |

Appendix A Performance Evaluation Extended Tables

| Scenario | Average Steam Flow Rate | System Time Constant | Peak Response Time Reduction | | Percentage of Time Constant | |
|----------|-------------------------|----------------------|------------------------------|-------|-----------------------------|-------|
| | | | MPC | Fuzzy | MPC | Fuzzy |
| 11 | 34 kg/s | 314.77 s | 57 s | 91 s | 18 % | 29 % |
| 12 | 35 kg/s | 306.48 s | 49 s | 88 s | 16 % | 29 % |
| 13 | 39 kg/s | 275.63 s | 117 s | 106 s | 42 % | 38 % |
| 14 | 40 kg/s | 271.97 s | 160 s | 106 s | 59 % | 39 % |
| 15 | 48 kg/s | 225.81 s | 71 s | 90 s | 31 % | 40 % |
| 16* | 49 kg/s | 222.43 s | 53 s | 83 s | 24 % | 37 % |
| 17 | 29 kg/s | 374.12 s | 57 s | 80 s | 15 % | 21 % |
| 18 | 29 kg/s | 366.70 s | 44 s | 101 s | 12 % | 28 % |
| 19 | 50 kg/s | 216.70 s | 66 s | 66 s | 30 % | 30 % |
| 20 | 50 kg/s | 214.52 s | 70 s | 57 s | 33 % | 27 % |
| 21 | 27 kg/s | 406.84 s | 110 s | 145 s | 27 % | 36 % |
| 22 | 27 kg/s | 397.10 s | 57 s | 142 s | 14 % | 36 % |
| 23 | 46 kg/s | 232.35 s | 69 s | 107 s | 30 % | 46 % |
| 24 | 47 kg/s | 229.41 s | 69 s | 109 s | 30 % | 48 % |
| 25 | 24 kg/s | 451.47 s | 142 s | 0 s | 31 % | 0 % |
| 26 | 25 kg/s | 438.51 s | 67 s | 0 s | 15 % | 0 % |
| 27 | 41 kg/s | 264.71 s | 26 s | 46 s | 10 % | 17 % |
| 28 | 41 kg/s | 260.88 s | 26 s | 78 s | 10 % | 30 % |
| 29 | 44 kg/s | 245.91 s | 197 s | 232 s | 80 % | 94 % |
| 30 | 44 kg/s | 242.70 s | 140 s | 154 s | 58 % | 63 % |
| 31 | 42 kg/s | 255.78 s | 187 s | 108 s | 73 % | 42 % |
| 32 | 43 kg/s | 252.25 s | 104 s | 117 s | 41 % | 46 % |
| 33 | 41 kg/s | 264.02 s | 74 s | 117 s | 28 % | 44 % |
| 34 | 42 kg/s | 260.04 s | 118 s | 110 s | 45 % | 42 % |
| 35 | 48 kg/s | 223.19 s | 65 s | 114 s | 29 % | 51 % |
| 36 | 49 kg/s | 220.60 s | 129 s | 149 s | 58 % | 68 % |
| 37* | 41 kg/s | 260.55 s | 65 s | 93 s | 25 % | 36 % |
| 38 | 42 kg/s | 256.37 s | 92 s | 147 s | 36 % | 57 % |
| Average | | | 88 s | 112 s | 33 % | 43 % |

Appendix B

Simulation Code

Appendix B.1 Initial Iterative Model Fitting

```

DataSmpl = 5; %Sample time of data in seconds
r = 0.0115; %Mill ramp time
rate = 0.006; %mill filter time constant
KK1 = 0.3994; %Delay scaling parameter
KK3 = -12.76; %Firing change transient scaling parameter
KK4 = -0.5196; %Pressure change transient scaling parameter
MM = 0.6; %Combined firing rate tuning factor
MB = 1.00*MM; %B row contribution factor
MA = 0.75*MM; %A row contribution factor
MC = 0.5*MM; %A row contribution factor
F = 0.05; %Fuel oil cv scaling factor
inc = 0.1; %starting increment changes on factors
k2st = 0; %unused tuning factor
k2st2 = 0; %unused tuning factor

function [H,J] = runner(r,rate,KK1,KK3,KK4,MB,MA,MC,F,k2st,k2st2)
    N = 2; % Number of superheater subsections
    clc

    load -binary data
    %Physical model based on physical properties
    l1 = (6.600*16 +2.900*4)*43; %Tube Lengths 1
    l2 = (4.700*16+2.900*4)*43; %Tube Lengths 2
    OD = 0.0508; %Outside Pipe Diameter
    OR = OD/2; %Outside Pipe Radius
    WT1 =0.0070; %Pipe Thickness 1
    WT2 =0.0084; %Pipe Thickness 2
    ID1 = OD-2*WT1; %Inside Pipe Diameter 1
    IR1 = ID1/2; %Inside Pipe Radius 1
    ID2 = OD-2*WT2; %Inside Pipe Diameter 2
    IR2 = ID2/2; %Inside Pipe Radius 2
    rhomst1 = 7850; %Steel Density kg/m3
    %Metal Mass
    mm = ((pi.*OR.^2 - pi.*IR1.^2)*l1 + (pi.*OR.^2 - pi.*IR2.^2)*l2).*rhomst1;
    %Pipe Inner Volume
    V = ( pi.*IR1.^2)*l1 + ( pi.*IR2.^2)*l2;
    %Steel Heat Capacity
    cm = 620;

    %full load steam flow rate for both legs combined
    K2full = 125;
    %Stead state normal operating range for superheater
    % steam pressures and temperatures for steam table linearization
    Pstdy = linspace (8.7,8.3,N*2+1);
    Tstdy = linspace (350,510,N*2+1);

    DataSmpl = 5; % Sample time of data in seconds

```

Appendix B Simulation Code

```

samplesN = length(TDRHSTMPR);    %Data Sample Count

%set up state space
clear states
states = {"H1"};
states_out = {"Hout1"};

for ii = 2:N
    states = {"H",num2str(ii)},states{:}};
    states_out = {"Hout",num2str(ii)},states_out{:}};
endfor

clear AA
clear BB
c = zeros(1,N);
c(1) = 1;
d = zeros(1,4);

Jbest = inf;
J = 0;

%Load initial state values from data

states = 1000*XSteam("h_pT",TDRHSTMPR(1,1).*10,TDRHBLROUT(1,1));
states = [zeros(N,1);states];
clear temps
fire =0;
clear U

for tt = 1:samplesN
    oldstates = states;
    %K2 = live steam flow data for step tt
    K2 = TDRHSTMFL(tt);
    % Compute state matrixes based on physical properties multiplied by tuning
factors
    for ii = 1:N
        rho = XSteam ("rho_pT",Pstdy(ii*2)*10,Tstdy(ii*2));
        dTdh = (Tstdy(ii*2+1)-Tstdy(ii*2-1))/1000/(XSteam
("h_pT",Pstdy(ii*2)*10,Tstdy(ii*2+1))-XSteam ("h_pT",Pstdy(ii*2)*10,Tstdy(ii*2-1)));
        K1 = rho*V/N + mm/N*cm*dTdh;
        K1=K1*K1;

        Uval = 2000; %overall heat transfer U value
        dqdTm = Uval*(l1+l2)/N*pi*ID1;    %heat transfer metal to steam per Metal
temp change.
        K3 = -mm/N*cm/dqdTm;
        K3=K3*K3;

        %K4 = -mm*cm*(dT/dp)
        hpoint = XSteam ("h_pT",Pstdy(ii*2)*10,Tstdy(ii*2));
        dTdp = (XSteam ("T_ph",Pstdy(ii*2+1)*10,hpoint)-XSteam ("T_ph",Pstdy(ii*2-
1)*10,hpoint))/(Pstdy(ii*2+1)-Pstdy(ii*2-1))/10^6;
        K4 = -mm/N*cm*dTdp;
        K4=K4*K4;

        %fuel input per section is actually the system input divided across the
elements
        if (ii ==1 )
            AA = zeros(N,N);
            AA(N,N) = [-K2/K1];

            BB = [K2/K1,K2/N/K1,K2*K3/N/K1,K2*K4/K1];

```

Appendix B Simulation Code

```

else
    AA(N-ii+1,N-ii+1) = [-K2/K1];
    AA(N-ii+1,N-ii+2) = [K2/K1];

    BB = [0,K2/N/K1,K2*K3/N/K1,K2*K4/K1;BB];
endif
endfor

CC = zeros(1,N);
CC(1) = 1;
DD = 0;
sysN = ss (AA, BB, CC, DD, 0);

%//observer
sysDSS = c2d(sysN,DataSmpl,'ZOH');
alpha = 0.1;%0.01
Cm = sysDSS.c;
Am = sysDSS.a;
Bm = sysDSS.b;
[m1,n1]=size(Cm);
A = [Am,linspace(0,0,n1)';Cm*Am,1];
B = [Bm;Cm*Bm];
C = [linspace(0,0,n1),1];
dhh = (XSteam("h_pT",8.7,512)-XSteam("h_pT",8.7,510))*10^3;
P=0.0;
Po = ones(N+1,N+1)*P;
temp = linspace(dhh,dhh,N+3);
thet = temp(2:N+2)*eye(3,3);
lamb = dhh;

%//observer
for II = 0:50
    Pp = A*alpha*(Po -
Po*C'*alpha*inv(lamb+C*alpha*Po*C'*alpha)*C*alpha*Po)*A'*alpha + thet;
    Po = Pp;
    P = [P,Pp(2,2)];
endfor
Kob = A*alpha*Pp*C'*alpha*inv(lamb+C*alpha*Pp*C'*alpha);

%Spraywater temperature as input and converted to enthalpy
U(1,tt) =XSteam("h_pT",TDRHSTMPR(tt).*10,TDRHSUPIN(tt))*1000;

%mill firing input and tuning factors for prefilter
oldfire = fire;
fullmill = 0.5;
cutoff = -0.5;
top = 1/(fullmill-cutoff);

mlAFact = min(1.0,max(0.0,(TDMLALVL(tt)/100.0-cutoff)*top));
mlBFact = min(1.0,max(0.0,(TDMLBLVL(tt)/100.0-cutoff)*top));
mlCFact = min(1.0,max(0.0,(TDMLCLVL(tt)/100.0-cutoff)*top));

if(tt==1)
    fireA =MA*(max(0,TDMLALOAD(tt)*mlAFact)+ F*TDBRNSONA(tt));
    fireB = MB*(max(0,TDMLBLOAD(tt)*mlBFact)+ F*TDBRNSONB(tt));
    fireC = MC*(max(0,TDMLCLOAD(tt)*mlCFact)+ F*TDBRNSONC(tt));
endif

fireA = fireA + max(-r,min(r,(MA*(max(0,TDMLALOAD(tt)*mlAFact)+
F*TDBRNSONA(tt))-fireA)));
fireB = fireB + max(-r,min(r,(MB*(max(0,TDMLBLOAD(tt)*mlBFact)+
F*TDBRNSONB(tt))-fireB)));

```

Appendix B Simulation Code

```

    fireC = fireC + max(-r,min(r,(MC*(max(0,TDMLCLOAD(tt)*mlCFact)+
F*TDBRNSONC(tt))-fireC)));
    fireNow = (fireA+fireB+fireC)*1000000;

    if(tt==1)
        fire = fireNow;
    endif

    if(tt==1)
        firein1 = fireNow./K2;
    endif

    firein1 = firein1.*(1-rate) +fireNow./K2.*(rate);
    fire = fire*(1-rate) +fireNow*(rate);
    %fire/mdot
    U(2,tt) =firein1;

    %firedot/mdot
    %Pdot/mdot
    if(tt==1)
        U(3,tt) =0;
        U(4,tt) =0;
    else
        U(3,tt) =(fire-oldfire)/DataSmpl/K2;
        U(4,tt) =(TDRHSTMPR(tt)-TDRHSTMPR(tt-1))*10^6/DataSmpl/K2;
    endif

    if(tt==1)
        states = A*oldstates;
    elseif
        err = XSteam ("H_pT",TDRHSTMPR(tt-1).*10,TDRHBLROUT(tt-1))*1000 -
oldstates(N+1);
        states = A*oldstates + B*(U(:,tt)-U(:,tt-1)) + Kob*err;
    endif

    if(tt == 1)
        temps = XSteam ("T_ph", TDRHSTMPR(tt).*10, states(N+1).*0.001);
    else
        temps = [temps; XSteam("T_ph", TDRHSTMPR(tt).*10, states(N+1).*0.001)];
    endif
endfor

Jall = (temps(2:length(temps))-temps(1:length(temps)-1) -
TDRHBLROUT(2:length(TDRHBLROUT))-TDRHBLROUT(1:length(TDRHBLROUT)-1)).^2;
skipstart = 100;
J = sum(Jall(skipstart:length(Jall)));

H = figure('Position',[50,50,1800,900]);
subplot(2,1,1)
hold on
plot(temps,"k ;Model;")
plot(TDRHBLROUT,"r ;RH Blr Out Temp;")
plot(TDRHSUPIN,"r ;RH Sup In Temp;")
plot((TDMLALOAD+TDMLBLOAD+TDMLCLOAD)./TDRHSTMFL.*200 + 420,"b ;Mill Total/Flow;")
plot(TDRHSTMFL.*10,"c ;RH Stm Flow;")
legend boxoff

plot((temps - TDRHBLROUT).*5+400,"b ;err;")
subplot(2,1,2)
hold on
plot(TDRHSTMPR,"g ;RH Stm Press;")
plot(TDMLBLOAD,"r ;Mill B;")

```

Appendix B Simulation Code

```

plot(TDMLALOAD,"m ;Mill A;")
plot(TDMLCLOAD,"b ;Mill C;")

plot(TDBRNSONB,"--r")
plot(TDBRNSONA,"--m")
plot(TDBRNSONC,"--b")
legend boxoff

%print params
text(0,-2,["J=",num2str(J,4),"", r=", num2str(r,4),"", rate=", num2str(rate,4),"",
KK1=", num2str(KK1,4),"", KK3=", num2str(KK3,4),"", KK4=", num2str(KK4,4),"", MB=",
num2str(MB,4),"", MA=", num2str(MA,4),"", MC=", num2str(MC,4),"", F=", num2str(F,4),"",
k2st=", num2str(k2st,4),"", k2st2=", num2str(k2st2,4)]]

J = J/(samplesN-skipstart);

endfunction

load -binary fl
outname = "OUT-";

[H,J] = runner(r,rate,KK1,KK3,KK4,MB,MA,MC,F,k2st,k2st2);
print(H, [outname, int2str(fl++)], "-dpdf", "-landscape", "-S1800,900")
save -binary fl fl;
close (H)

Jbase = J;

kkml = -0.03; %Tuning amounts and direction
kkm3 = -0.03;
kkm4 = 0.03;
kk2st = -0.03;
kk2st2 = -0.03;
kkmm = 0.03;

%adjusts each tuning factor iteratively and in sequence
%Save if cost function reduces otherwise change the gradient direction of tuning.
runs = 100;
if (runs>=1)

for temp = 1:runs

[H,J] = runner(r,rate,KK1*(1+kkml),KK3,KK4,MB,MA,MC,F,k2st,k2st2);
if(J<Jbase)
Jbase = J
KK1 = KK1*(1+kkml);
print(H, [outname , int2str(fl++)], "-dpdf", "-landscape", "-S1800,900")
save -binary fl fl;
["J=",num2str(J,4),"", r=", num2str(r,4),"", rate=", num2str(rate,4),"", KK1=",
num2str(KK1,4),"", KK3=", num2str(KK3,4),"", KK4=", num2str(KK4,4),"", MB=",
num2str(MB,4),"", MA=", num2str(MA,4),"", MC=", num2str(MC,4),"", F=", num2str(F,4),"",
k2st=", num2str(k2st,4),"", k2st2=", num2str(k2st2,4)]]
save -binary params r rate KK1 KK3 KK4 MB MA MC F k2st k2st2;
elseif
kkml= kkm1*-1;
endif
close (H)

[H,J] = runner(r,rate,KK1,KK3*(1+kkm3),KK4,MB,MA,MC,F,k2st,k2st2);
if(J<Jbase)
Jbase = J
KK3 = KK3*(1+kkm3)
print(H, [outname , int2str(fl++)], "-dpdf", "-landscape", "-S1800,900")

```

Appendix B Simulation Code

```

save -binary fl fl;
["J=",num2str(J,4),"",r=",num2str(r,4),"",rate=",num2str(rate,4),"",KK1=",
num2str(KK1,4),"",KK3=",num2str(KK3,4),"",KK4=",num2str(KK4,4),"",MB=",
num2str(MB,4),"",MA=",num2str(MA,4),"",MC=",num2str(MC,4),"",F=",num2str(F,4),"",
k2st=",num2str(k2st,4),"",k2st2=",num2str(k2st2,4)]
save -binary params r rate KK1 KK3 KK4 MB MA MC F k2st k2st2;
elseif
kkm3= kkm3*-1;
endif
close (H)

[H,J] = runner(r,rate, KK1, KK3, KK4*(1+kkm4), MB, MA, MC, F, k2st, k2st2);
if(J<Jbase)
Jbase = J
KK4 = KK4*(1+kkm4);
print(H, [outname , int2str(fl++)], "-dpdf", "-landscape", "-S1800,900")
save -binary fl fl;
["J=",num2str(J,4),"",r=",num2str(r,4),"",rate=",num2str(rate,4),"",KK1=",
num2str(KK1,4),"",KK3=",num2str(KK3,4),"",KK4=",num2str(KK4,4),"",MB=",
num2str(MB,4),"",MA=",num2str(MA,4),"",MC=",num2str(MC,4),"",F=",num2str(F,4),"",
k2st=",num2str(k2st,4),"",k2st2=",num2str(k2st2,4)]
save -binary params r rate KK1 KK3 KK4 MB MA MC F k2st k2st2;
elseif
kkm4= kkm4*-1;
endif
close (H)

[H,J] = runner(r,rate, KK1, KK3, KK4, MB, MA, MC, F, k2st*(1+kk2st), k2st2);
if(J<Jbase)
Jbase = J
k2st = k2st*(1+kk2st);
print(H, [outname , int2str(fl++)], "-dpdf", "-landscape", "-S1800,900")
save -binary fl fl;
["J=",num2str(J,4),"",r=",num2str(r,4),"",rate=",num2str(rate,4),"",KK1=",
num2str(KK1,4),"",KK3=",num2str(KK3,4),"",KK4=",num2str(KK4,4),"",MB=",
num2str(MB,4),"",MA=",num2str(MA,4),"",MC=",num2str(MC,4),"",F=",num2str(F,4),"",
k2st=",num2str(k2st,4),"",k2st2=",num2str(k2st2,4)]
save -binary params r rate KK1 KK3 KK4 MB MA MC F k2st k2st2;
elseif
kk2st= kk2st*-1;
endif
close (H)

[H,J] = runner(r,rate, KK1, KK3, KK4, MB, MA, MC, F, k2st, k2st2*(1+kk2st2));
if(J<Jbase)
Jbase = J
k2st2 = k2st2*(1+kk2st2);
print(H, [outname , int2str(fl++)], "-dpdf", "-landscape", "-S1800,900")
save -binary fl fl;
["J=",num2str(J,4),"",r=",num2str(r,4),"",rate=",num2str(rate,4),"",KK1=",
num2str(KK1,4),"",KK3=",num2str(KK3,4),"",KK4=",num2str(KK4,4),"",MB=",
num2str(MB,4),"",MA=",num2str(MA,4),"",MC=",num2str(MC,4),"",F=",num2str(F,4),"",
k2st=",num2str(k2st,4),"",k2st2=",num2str(k2st2,4)]
save -binary params r rate KK1 KK3 KK4 MB MA MC F k2st k2st2;
elseif
kk2st2 = kk2st2*-1;
endif
close (H)

[H,J] =
runner(r,rate, KK1, KK3, KK4, MB*(1+kkm), MA*(1+kkm), MC*(1+kkm), F, k2st, k2st2);
if(J<Jbase)
Jbase = J

```

Appendix B Simulation Code

```

k2st2 = k2st2*(1+kk2st2);

MM = MM*(1+kkmm);
MB = 1.00*MM; %B row contribution factor
MA = 0.75*MM; %A row contribution factor
MC = 0.5*MM; %A row contribution factor

print(H, [outname , int2str(fl++)], "-dpdf", "-landscape", "-S1800,900")
save -binary fl fl;
["J=", num2str(J, 4), ", r=", num2str(r, 4), ", rate=", num2str(rate, 4), ", KK1=",
num2str(KK1, 4), ", KK3=", num2str(KK3, 4), ", KK4=", num2str(KK4, 4), ", MB=",
num2str(MB, 4), ", MA=", num2str(MA, 4), ", MC=", num2str(MC, 4), ", F=", num2str(F, 4), ",
k2st=", num2str(k2st, 4), ", k2st2=", num2str(k2st2, 4)]
save -binary params r rate KK1 KK3 KK4 MB MA MC F k2st k2st2;
elseif
    kkmm = kkmm*-1;
endif
close (H)
endfor
endif

```

Appendix B.2 Simultaneous Iteration of Scenarios

```

%Load Filtered and Sample time adjustments
DataSmpl = 5; % Sample time of data in seconds
FastestSample = 15;
fullLoad = 60;

%Tuning Factors Updated on each iteration
dddd =
[1.0849;0.71824;0.68359;1.9931;0.82746;1.0168;0.79935;0.62561;1.0557;1.0507;0.95049;1.2
259;0.44796;1.4832;0.62499;0.56514;1.1275;-0.042447;0.83051;0.18892];

dirdir = ones(20,1);
errsqsuold = 100000000000;
errsqsu = errsqsuold+1;
deltait = 0.1;
rowedit = 1;
for iter = 1:500

    %Save on decrease in cost function
    if errsqsuold > errsqsu
        dddd = rr;
        errsqsuold = errsqsu;
        disp("saved")
        outcopy = ["dddd = [", num2str(dddd(1))];

        for qw = 2:length(dddd)
            outcopy = [outcopy, ";", num2str(dddd(qw))];
        endfor
        outcopy = [outcopy, "];"]
        save -binary saved outcopy dddd fullmill cutoff r rate MB MA MC F sysDSS
    errsqsuold
    else
        dirdir(rowedit) = dirdir(rowedit)*-1;
    endif

    iter
    fflush(stdout);

```

Appendix B Simulation Code

```

rowedit = floor(rand()*20)+1
dirdir'
if iter == 1
    rr = dddd
else
    temp = "-----"
    zr = zeros(20,1);
    zr(rowedit) = rand()*deltait*dirdir(rowedit);
    rr = dddd + zr;
    rr'
endif

fullmill = 0.5*1.05*rr(1);
cutoff = (0.1+0.2)*rr(2);
top = 1/(fullmill-cutoff);

r = 0.0815*0.75*rr(3);    %Mill ramp time new 0.1115
rate = 0.006*12*0.9*rr(4); %mill filter time
MM = 0.6*0.6*rr(5);
MB = 1.00*MM*1.15*rr(6); %B row contribution factor
MA = 0.75*MM*0.75*rr(7); %A row contribution factor
MC = 0.5*MM*0.65*rr(8); %A row contribution factor
F = 0.05*0.7*rr(9);    %Fuel oil cv scaling factor

load -binary sysDSS
%Model Tuning factors
sysDSS.a(1,1) = sysDSS.a(1,1)*rr(10);
sysDSS.a(2,2) = sysDSS.a(2,2)*rr(10)*rr(11);
sysDSS.a(1,2) = sysDSS.a(1,2)*rr(12);
sysDSS.b(2,1) = sysDSS.b(2,1)*rr(12)*rr(13);
sysDSS.b(1,2) = sysDSS.b(1,2)*rr(14);
sysDSS.b(2,2) = sysDSS.b(2,2)*rr(14)*rr(20);
sysDSS.b(1,3) = sysDSS.b(1,3)*rr(15);
sysDSS.b(2,3) = sysDSS.b(2,3)*rr(15)*rr(19);
sysDSS.b(1,4) = sysDSS.b(1,4)*rr(16);
sysDSS.b(2,4) = sysDSS.b(2,4)*rr(16)*rr(17);
sysDSS.b(1,1) = 0.015*rr(18);
%building augmented state space
Cm = sysDSS.c;
Am = sysDSS.a;
Bm = sysDSS.b;
[m1,n1]=size(Cm);
A = [Am,linspace(0,0,n1)';Cm*Am,1];
B = [Bm;Cm*Bm];
C = [linspace(0,0,n1),1];
D = [0,0,0,0];

%observer
N = 2;
alpha = 0.1;
dhh = (XSteam("h_pT",8.7,512)-XSteam("h_pT",8.7,510))*10^3;
P=0.5;
Po = ones(N+1,N+1)*P;
temp = linspace(dhh,dhh,N+3);
thet = temp(2:N+2);
lamb = dhh;

for II = 0:50
    Pp = A*alpha*(Po -
Po*C'*alpha*inv(lamb+C*alpha*Po*C'*alpha)*C*alpha*Po)*A'*alpha + thet;
    Po = Pp;
    P = [P,Pp(2,2)];
endfor

```


Appendix B Simulation Code

```

Kob = A*alpha*Pp*C'*alpha*inv(lamb+C*alpha*Pp*C'*alpha);

A(:,3) = A(:,3)-Kob;
B = [B,Kob];
D = [0,0,0,0,0];

sys =
dss(A,B,C,D,[],FastestSample,'STNAME',{'dH2','dH1','Hout'},'INNAME',{'Hin','Fire','Fire
dot','Pdot','Yact'},'OUTNAME','Hout');

g = 1:38;
errfeedback = [];
errsqsun = 0;
for l = g

    load("-binary", ["data", int2str(l)])

    Datasize = length(TDSTMFL);

    mlAFact = arrayfun (@(x) min(1.0,max(0.0,(x/100.0-cutoff)*top)),TDMLALVL);
    mlBFact = arrayfun (@(x) min(1.0,max(0.0,(x/100.0-cutoff)*top)),TDMLBLVL);
    mlCFact = arrayfun (@(x) min(1.0,max(0.0,(x/100.0-cutoff)*top)),TDMLCLVL);

    fireA = arrayfun (@(x,z) MA*(x+ F*z),TDMLALOAD.*mlAFact,TDBRNSONA);
    fireB = arrayfun (@(x,z) MB*(x+ F*z),TDMLBLOAD.*mlBFact,TDBRNSONB);
    fireC = arrayfun (@(x,z) MC*(x+ F*z),TDMLCLOAD.*mlCFact,TDBRNSONC);

    for i = 2:Datasize
        fireA(i)= max(min(fireA(i),fireA(i-1)+r),fireA(i-1)-r);
        fireB(i)= max(min(fireB(i),fireB(i-1)+r),fireB(i-1)-r);
        fireC(i)= max(min(fireC(i),fireC(i-1)+r),fireC(i-1)-r);
    endfor

    fireNow = (fireA+fireB+fireC).*1000000;
    fire = fireNow;
    for i = 2:Datasize
        fire(i) = fire(i-1)*(1-rate) +fire(i)*(rate);
    endfor
    %model inputs from Data
    U = zeros(Datasize,4);
    U(:,1) =arrayfun(@(x,y) XSteam("h_pT",x.*10,y)*1000,TDSTMPR, TDSUPIN);
    U(:,2) = fire./TDSTMFL;
    U(:,3) = arrayfun(@(x,y) (x-y),fire,[fire(1);fire(1:Datasize-1)].)/900;
    U(:,4) = arrayfun(@(x,y) (x-y),TDSTMPR,[TDSTMPR(1);TDSTMPR(1:Datasize-
1)])*10^6./900;
    %model Initial Values
    X0 = 1000*XSteam("h_pT",TDSTMPR(1).*10,TDBLROUT(1));
    X0 = [zeros(2,1);X0];
    %delta of inputs
    U = arrayfun(@(x,y) x-y, U, [U(1,:);U(1:Datasize-1,)]);
    U = [U,arrayfun(@(x,y) 1000*XSteam("h_pT",x.*10,y),TDSTMPR,TDBLROUT)];
    %Simulated Outputs
    Out = lsim(sys,U,[],X0);
    %Cost Function
    err = TDBLROUT-arrayfun(@(x,y) XSteam("T_ph",x,y),TDSTMPR.*10,Out/1000);
    errsqsun =sum(err.^2);
    errsqsun = errsqsun + errsqsun;
    errfeedback = [errfeedback;l,errsqsun];

endfor

errsqsun

```

```
endfor
```

Appendix B.3 Iterative Tuning of Fuzzy Control Steam Flow Acceleration Feedback Gains

```
clear all
load -binary saved2

%state space representation used for state observer calculation
sys1= sysDSS;
Cm = sys1.c;
Am = sys1.a;
Bm = sys1.b;
[m1,n1]=size(Cm);
A = [Am, linspace(0,0,n1)'; Cm*Am, 1];
B = [Bm; Cm*Bm];
C = [linspace(0,0,n1), 1];
D = [0,0,0,0];
sys1 =
dss(A,B,C,D,[],15,'STNAME',{'dh2','dh1','Hout'},'INNAME',{'Hin','Fire','Firedo
t','Pdot'},'OUTNAME','Hout');

sys2= sysDSS;
sys2.T = 90;
sys2 = d2d(sys2,15);
Cm = sys2.c;
Am = sys2.a;
Bm = sys2.b;
[m1,n1]=size(Cm);
A = [Am, linspace(0,0,n1)'; Cm*Am, 1];
B = [Bm; Cm*Bm];
C = [linspace(0,0,n1), 1];
D = [0,0,0,0];
sys2 =
dss(A,B,C,D,[],15,'STNAME',{'dh2','dh1','Hout'},'INNAME',{'Hin','Fire','Firedo
t','Pdot'},'OUTNAME','Hout');

load -binary ctrlparam

offs = zeros(50,1);
setp = ones(50,1)*505;
statof = ones(50,1)*500;

statessave = [];
savestats = [];

for itr = 1:100

    sum = zeros(1,5);

    %load last saved best cost function results and tuning parameters
    list = ls ("comparetoparamstestnn*", "/A:-D", "/B", "/O:-N");
```

Appendix B Simulation Code

```

load ("-binary", strsplit (list){1})

rand1 = (rand()-0.5)/10 +1;
rand2 = (rand()-0.5)/10 +1;
rand3 = (rand()-0.5)/10 +1;
rand4 = (rand()-0.5)/10 +1;

gn1 = tweak1*rand1;
gn2 = tweak2*rand2;
gn3 = tweak3*rand3;
gn4 = tweak4*rand4;

close all
g = [1:38];
for l = g

    load( "-binary", ["data", int2str(l)])

    Datasize = length(TDSTMFL);
    top = 1/(fullmill-cutoff);
    mlAFact = arrayfun (@(x) min(1.0,max(0.0,(x/100.0-
cutoff)*top)),TDMLALVL);
    mlBFact = arrayfun (@(x) min(1.0,max(0.0,(x/100.0-
cutoff)*top)),TDMLBLVL);
    mlCFact = arrayfun (@(x) min(1.0,max(0.0,(x/100.0-
cutoff)*top)),TDMLCLVL);

    fireA = arrayfun (@(x,z) MA*(x+ F*z),TDMLALOAD.*mlAFact,TDBRNSONA);
    fireB = arrayfun (@(x,z) MB*(x+ F*z),TDMLBLOAD.*mlBFact,TDBRNSONB);
    fireC = arrayfun (@(x,z) MC*(x+ F*z),TDMLCLOAD.*mlCFact,TDBRNSONC);

    for i = 2:Datasize
        fireA(i)= max(min(fireA(i),fireA(i-1)+r),fireA(i-1)-r);
        fireB(i)= max(min(fireB(i),fireB(i-1)+r),fireB(i-1)-r);
        fireC(i)= max(min(fireC(i),fireC(i-1)+r),fireC(i-1)-r);
    endfor

    fireNow = (fireA+fireB+fireC).*1000000;
    fire = fireNow;
    for i = 2:Datasize
        fire(i) = fire(i-1)*(1-rate) +fire(i)*(rate);
    endfor

    U = zeros (Datasize,4);

    U(:,1) =arrayfun(@(x,y) XSteam("h_pT",x.*10,y)*1000,TDSTMPR, TDSUPIN);
    U(:,2) = fire./TDSTMFL;
    U(:,3) = arrayfun(@(x,y) (x-y),fire,[fire(1);fire(1:Datasize-
1)])./TDDATASAMPLET./TDSTMFL;
    U(:,4) = arrayfun(@(x,y) (x-y),TDSTMPR,[TDSTMPR(1);TDSTMPR(1:Datasize-
1)]).*10^6./TDDATASAMPLET./TDSTMFL;

    X0 = 1000*XSteam("h_pT",TDSTMPR(1).*10,TDBLR0UT(1));
    X0 = [zeros(2,1);X0];

    U = arrayfun(@(x,y) x-y, U, [U(1,:);U(1:Datasize-1,:)]);

```

Appendix B Simulation Code

```

Xappend=X0';
Yappend=X0(3);

Xerrap = Xappend;
Yerrap = Yappend;

Xappendmod = Xappend;
Yappendmod = Yappend;

errApp = [];
dU = [];
refrT = [];

dH_1 = 0;
inputh = 1000*XSteam("h_pT",TDSTMPR(1).*10,TDSUPIN(1));
for i = 1:Datasize-1

    %calculate model error and work out a disturbance input to
duplicate model error
    sys= sysDSS;
    sys.T = 900/TDSTMFL(i);
    sys = d2d(sys,15,"tustin");
    Cm = sys.c;
    Am = sys.a;
    Bm = sys.b;
    [m,n]=size(Cm);
    A = [Am,linspace(0,0,n)';Cm*Am,1];
    B = [Bm;Cm*Bm];
    C = [linspace(0,0,n),1];
    D = [0,0,0,0];
    sys =
dss(A,B,C,D,[],15,'STNAME',{ 'dH2', 'dH1', 'Hout'}, 'INNAME',{ 'Hin', 'Fire', 'Firedo
t', 'Pdot', }, 'OUTNAME', 'Hout');

    %only used to check model
    [Ymod,Tmod,Xmod] = lsim(sys,[U(i,:);0,0,0,0],[],Xappendmod(i,:));
    Xappendmod = [Xappendmod;Xmod(2,:)];
    Yappendmod = [Yappendmod;Ymod(2,:)];
    errout = XSteam("h_pT",TDSTMPR(i+1).*10,TDBLR0UT(i+1))*1000-
Ymod(2,1);

    %calculate model firing error input
    syserr =
dss(sys.A,[sys.B,sys.B(:,2)],sys.C,[sys.D,0],[],15,'STNAME',{ 'dH2', 'dH1', 'Hout
'}, 'INNAME',{ 'Hin', 'Fire', 'Firedot', 'Pdot', 'err'}, 'OUTNAME', 'Hout');
    [Yerr,Terr,Xerr] =
lsim(syserr,[U(i,:),0;0,0,0,0,0],[],Xerrap(i,:));
    errmodout = XSteam("h_pT",TDSTMPR(i+1).*10,TDBLR0UT(i+1))*1000-
Yerr(2,1);
    errApp = [errApp;errmodout/syserr.b(1,5)];
    [Yerr,Terr,Xerr] =
lsim(syserr,[U(i,:),errApp(i);0,0,0,0,0],[],Xerrap(i,:));
    Xerrap = [Xerrap;Xerr(2,:)];
    Yerrap = [Yerrap;Yerr(2,:)];

    %Membership

```

Appendix B Simulation Code

```

Ar1 = (max(10, min(60, TDSTMFL(i))) - 10) / 50;
Ar2 = 1 - Ar1;
Arh = Ar1;
Arl = Ar2;

dM = 0;
if(i == 1)
    Arp = 0;
    Arz = 1;
    Arn = 0;
else
    dM = (TDSTMFL(i) - TDSTMFL(i-1)) / 15;
    Arp = (max(0, min(0.193, (TDSTMFL(i) - TDSTMFL(i-1)) / 15))) / (0.193);
    Arn = (max(0, min(0.193, (TDSTMFL(i-1) - TDSTMFL(i)) / 15))) / (0.193);
    Arz = 1 - Arp - Arn;
endif

refrT = [refrT; 1000 * XSteam("h_pT", TDSTMPR(i) * 10, setp(1))];
dHhat2 = 0;
if(i > 1)
    dHhat2 = Yappend(i) - Yappend(i-1);
endif

%observer gains
m1 = 1;
m2 = 1;

states = [dHhat2; dH_1(i) + m1 * dHhat2; Yappend(i)];
statessave = [statessave, states];

%Calculate all rule control laws
U1 = refrT(i) * Ky1 - KTSK1 * states - Kff1 * U(i, 2:4) + dM * gn3;
U2 = refrT(i) * Ky2 - KTSK2 * states - Kff2 * U(i, 2:4) + dM * gn4;
Uhp = refrT(i) * Kyhp - KTSKhp * states - Kffhp * U(i, 2:4) + dM * gn1;
Uhn = refrT(i) * Kyhn - KTSKhn * states - Kffhn * U(i, 2:4) + dM * gn1;
Ulp = refrT(i) * Kylp - KTSKlp * states - Kfflp * U(i, 2:4) + dM * gn2;
Uln = refrT(i) * Kyln - KTSKln * states - Kffln * U(i, 2:4) + dM * gn2;

%UT = weighted average defuzification
UT = (Uhp * (Arh * Arp) + Uhn * (Arh * Arn) + Ulp * (Arl * Arp) + Uln * (Arl * Arn) +
U1 * Arh * Arz + U2 * Arl * Arz) ./ (Arh * Arp + Arh * Arn + Arl * Arp + Arl * Arn + Arh * Arz + Arl * Arz);

%cap control law at saturation limit if present
maxxval = 1000 * XSteam("h_pT", TDSTMPR(i+1) * 10, TDSPRIN1(i+1) - 10);
UT = min(UT, maxxval - inputh(i));

inputh = [inputh; inputh(i) + UT];
dU = [dU; UT];

%Calculate states based on membership
dH_1kpo1 = (dH_1(i) + m1 * dHhat2) * (sys1.A(2,2) - m1 * sys1.A(1,2)) -
m1 * sys1.A(1,1) * dHhat2 + (sys1.B(2,:) - m1 * sys1.B(1,:)) * [dU(i), U(i, 2:4)]';
dH_1kpo2 = (dH_1(i) + m2 * dHhat2) * (sys2.A(2,2) - m2 * sys2.A(1,2)) -
m2 * sys2.A(1,1) * dHhat2 + (sys2.B(2,:) - m2 * sys2.B(1,:)) * [dU(i), U(i, 2:4)]';
dH_1 = [dH_1; dH_1kpo1 * Ar1 + dH_1kpo2 * Ar2];

%%%%%%%%%% Plant Simulation %%%%%%%%%%%

```

Appendix B Simulation Code

```

        %apply to model to get real output
        [Yout,Tout,Xout] =
lsim(syserr,[dU(i),U(i,2:4),errApp(i);0,0,0,0,0],[],Xappend(i,:));
        Xappend = [Xappend;Xout(2,:)];
        Yappend = [Yappend;Yout(2,:)];

endfor

outcon = arrayfun(@(x,y) XSteam("T_ph",x,y),TDSTMPR.*10,Yappend/1000);
outcon2 = arrayfun(@(x,y)
XSteam("T_ph",x,y),TDSTMPR.*10,Yappendmod/1000);

Wi = 900;
Ln = 450;

offset = offs(1);

initsetT = 1;

while (TDTIMESTAMP(initsetT)<statof(1))
    initsetT = initsetT+1;
endwhile

input = arrayfun(@(x,y) XSteam("T_ph",x,y),TDSTMPR.*10,inputh/1000);

%compute performance stats
[ITSKmax,IWTSKmax] = max(outcon(initsetT:Datasize));
[ITSKmin,IWTSKmin] = min(outcon(initsetT:Datasize));

[Imax,IWmax] = max(TDBLROUT(initsetT:Datasize));
[Imin,IWmin] = min(TDBLROUT(initsetT:Datasize));

[I2TSKmax,I2WTSKmax] = max(input(initsetT:Datasize));
[I2TSKmin,I2WTSKmin] = min(input(initsetT:Datasize));

[I2max,I2Wmax] = max(TDSUPIN(initsetT:Datasize));
[I2min,I2Wmin] = min(TDSUPIN(initsetT:Datasize));

PISTD = std((TDBLROUT-setp(1))(initsetT:Datasize));
TSKSTD = std((outcon-setp(1))(initsetT:Datasize));
PIMN = mean((TDBLROUT-setp(1))(initsetT:Datasize));
TSKMN = mean((outcon-setp(1))(initsetT:Datasize));

stats1 = [TSKSTD,TSKMN,ITSKmax,ITSKmin,ITSKmax-ITSKmin];
sum = sum+[TSKSTD,TSKMN,ITSKmax,ITSKmin,ITSKmax-ITSKmin];

endfor

avgg = sum./length(g);
newinvcost = 0.84/avgg(1) + 6/avgg(5)
if(newinvcost>invcost)
    tweak1 = tweak1*rand1
    tweak2 = tweak2*rand2
    tweak3 = tweak3*rand3
    tweak4 = tweak4*rand4
    compareto = avgg

```

Appendix B Simulation Code

```

    invcost = newinvcost;
    invcoststr = sprintf ("%0.8f",invcost);
    save ("-binary",
["comparetoparamstestnn",invcoststr],"tweak*","compareto","cost")
    endif
endfor

```

Appendix B.4 MPC Controller Simulation

```

%Load Model From Saved2
load -binary saved2
sys1= sysDSS;
Cm = sys1.c;
Am = sys1.a;
Bm = sys1.b;
[m1,n1]=size(Cm);
%Augment Model
A = [Am,linspace(0,0,n1)';Cm*Am,1];
B = [Bm;Cm*Bm];
C = [linspace(0,0,n1),1];
D = [0,0,0,0];
sys1 =
dss(A,B,C,D,[],15,'STNAME',{'dH2','dH1','Hout'],'INNAME',{'Hin','Fire','Firedot','Pdot'},
,'OUTNAME','Hout');

skip = 5;
Np = 15;
Nc = 1;

savestats = [];
summ = zeros(1,5);

%Compute Cost Function matrixes
Ff=[];
for n = (1+skip):(Np+skip)
    Ff(n-skip,:) = C*(A^n);
endfor

for l = 1:4
    phi{l} = zeros(Np,Nc);
    for ci = 1:Nc
        for ri = (1+skip):(Np+skip)
            if(ri-ci)<0
                phi{l}(ri-skip,ci) = 0;
            else
                phi{l}(ri-skip,ci) = C*(A^(ri-ci))*B(:,l);
            endif
        endfor
    endfor
endfor

%Compute Gains
racc=r;
rw = 1;%0.12
R = eye(Nc).*rw;
Rs = ones(Np,1);
pre = inv(phi{1}'*phi{1} + R)*phi{1}';
Ky = pre(1,:)*Rs
Kmpc = pre(1,:)*Ff
Kff = pre(1,:)*[phi{2}(:,1),phi{3}(:,1),phi{4}(:,1)]

```

Appendix B Simulation Code

```

%Observer Gains
mobs = 1;

offs = zeros(50,1);
setp = ones(50,1)*505;
statof = ones(50,1)*500;
savestats = [];

g = [1:38];
for l = g
    load("-binary", ["data", int2str(l)])
    Datasize = length(TDSTMFL);
    top = 1/(fullmill-cutoff);
    mlAFact = arrayfun (@(x) min(1.0,max(0.0,(x/100.0-cutoff)*top)), TDMLALVL);
    mlBFact = arrayfun (@(x) min(1.0,max(0.0,(x/100.0-cutoff)*top)), TDMLBLVL);
    mlCFact = arrayfun (@(x) min(1.0,max(0.0,(x/100.0-cutoff)*top)), TDMLCLVL);

    fireA = arrayfun (@(x,z) MA*(x+ F*z), TDMLALOAD.*mlAFact, TDBRNSONA);
    fireB = arrayfun (@(x,z) MB*(x+ F*z), TDMLBLOAD.*mlBFact, TDBRNSONB);
    fireC = arrayfun (@(x,z) MC*(x+ F*z), TDMLCLOAD.*mlCFact, TDBRNSONC);

    for i = 2:Datasize
        r = racc/TDSTMFL(i)*60;
        fireA(i) = max(min(fireA(i), fireA(i-1)+r), fireA(i-1)-r);
        fireB(i) = max(min(fireB(i), fireB(i-1)+r), fireB(i-1)-r);
        fireC(i) = max(min(fireC(i), fireC(i-1)+r), fireC(i-1)-r);
    endfor

    fireNow = (fireA+fireB+fireC).*1000000;
    fire = fireNow;
    for i = 2:Datasize
        rate2 = d2d(dss([1-rate], [rate], [1], [0], [], 15), 900/TDSTMFL(i)).b;
        fire(i) = fire(i-1)*(1-rate2) +fire(i)*(rate2);
    endfor

    %inputs to the system
    U = zeros(Datasize,4);
    %PID spraywater still simulated alongside the MPC controller
    U(:,1) = arrayfun(@(x,y) XSteam("h_pT", x.*10,y)*1000, TDSTMPR, TDSUPIN);
    U(:,2) = fire./TDSTMFL;
    U(:,3) = arrayfun(@(x,y) (x-y), fire, [fire(1); fire(1:Datasize-
1)])./TDDATASAMPLET./TDSTMFL;
    U(:,4) = arrayfun(@(x,y) (x-y), TDSTMPR, [TDSTMPR(1); TDSTMPR(1:Datasize-
1)]).*10^6./TDDATASAMPLET./TDSTMFL;

    X0 = 1000*XSteam("h_pT", TDSTMPR(1).*10, TDBLROUT(1));
    X0 = [zeros(2,1); X0];

    U = arrayfun(@(x,y) x-y, U, [U(1,:); U(1:Datasize-1,:)]);

    Xappend=X0';
    Yappend=X0(3);
    Xerrap = Xappend;
    Yerrap = Yappend;
    Xappendmod = Xappend;
    Yappendmod = Yappend;
    errApp = [];
    dU = [];
    refrT = [];

    dH_1 = 0;
    inpuh = 1000*XSteam("h_pT", TDSTMPR(1).*10, TDSUPIN(1));

```


Appendix B Simulation Code

```

for i = 1:Datasize-1

    sys= sysDSS;
    Cm = sys.c;
    Am = sys.a;
    Bm = sys.b;
    [ms,n]=size(Cm);
    A = [Am,linspace(0,0,n)';Cm*Am,1];
    B = [Bm;Cm*Bm];
    C = [linspace(0,0,n),1];
    D = [0,0,0,0];
    sys =
dss(A,B,C,D,[],15,'STNAME',{ 'dH2','dH1','Hout'},'INNAME',{ 'Hin','Fire','Firedot','Pdot'
,},'OUTNAME','Hout');

    %only used to check model
    [Ymod,Tmod,Xmod] = lsim(sys,[U(i,:);0,0,0,0],[],Xappendmod(i,:));
    Xappendmod = [Xappendmod;Xmod(2,:)];
    Yappendmod = [Yappendmod;Ymod(2,:)];
    errout = XSteam("h_pT",TDSTMPR(i+1).*10,TDBLROUT(i+1))*1000-Ymod(2,1);

    %calculate model firing error input
    syserr =
dss(sys.A,[sys.B,sys.B(:,2)],sys.C,[sys.D,0],[],15,'STNAME',{ 'dH2','dH1','Hout'},'INNAM
E',{ 'Hin','Fire','Firedot','Pdot','err'},'OUTNAME','Hout');
    [Yerr,Terr,Xerr] = lsim(syserr,[U(i,:);0;0,0,0,0,0],[],Xerrap(i,:));
    errmodout = XSteam("h_pT",TDSTMPR(i+1).*10,TDBLROUT(i+1))*1000-Yerr(2,1);
    errApp = [errApp;errmodout/syserr.b(1,5)];
    [Yerr,Terr,Xerr] = lsim(syserr,[U(i,:),errApp(i);0,0,0,0,0],[],Xerrap(i,:));
    Xerrap = [Xerrap;Xerr(2,:)];
    Yerrap = [Yerrap;Yerr(2,:)];

    m = mobs;
    refrT = [refrT;1000*XSteam("h_pT",TDSTMPR(i)*10,setp(1))];
    dHhat2 = 0;
    if(i>1)
        dHhat2 = Yappend(i)-Yappend(i-1);
    endif
    states = [dHhat2;dH_1(i) + m*dHhat2;Yappend(i)];

    %Calculate U for next cycle
    U1 = refrT(i)*Ky - Kmpc*states - Kff*U(i,2:4)';
    maxxval = 1000*XSteam("h_pT",TDSTMPR(i+1).*10,TDSPRIN1(i+1)-10);
    %place hard constraint on saturation limit
    U1 = min(U1,maxxval-inputh(i));
    inputh = [inputh;inputh(i)+U1];
    dU = [dU;U1];

    %Calculate state
    dH_1kpol = (dH_1(i) + m*dHhat2)*(sys1.A(2,2)-m*sys1.A(1,2)) -
m*sys1.A(1,1)*dHhat2 + (sys1.B(2,:)-m*sys1.B(1,:))*[dU(i),U(i,2:4)]';
    dH_1 = [dH_1;dH_1kpol];
    %%%%%%%%%%% Plant Simulation %%%%%%%%%%%
    %apply to model to get real output
    [Yout,Tout,Xout] =
lsim(syserr,[dU(i),U(i,2:4),errApp(i);0,0,0,0,0],[],Xappend(i,:));
    Xappend = [Xappend;Xout(2,:)];
    Yappend = [Yappend;Yout(2,:)];

endfor

outcon = arrayfun(@(x,y) XSteam("T_ph",x,y),TDSTMPR.*10,Yappend/1000);
outcon2 = arrayfun(@(x,y) XSteam("T_ph",x,y),TDSTMPR.*10,Yappendmod/1000);

```

Appendix B Simulation Code

```

Wi = 900;
Ln = 450;

offset = offs(1);

initsetT = 1;

while (TDTIMESTAMP(initsetT)<statof(1))
    initsetT = initsetT+1;
endwhile

TDTIMESTAMP = TDTIMESTAMP./60 - offset;
input = arrayfun(@(x,y) XSteam("T_ph",x,y),TDSTMPR.*10,inputh/1000);
plottrue = false;

H = figure('Position',[50,50,Wi,Ln]);
subplot(2,1,1)
hold on

plot(TDTIMESTAMP,outcon,['b ;MPC Model Responce [",char(176),"C];"])
plot(TDTIMESTAMP,TDBLROUT,['r ;PID Actual Responce [",char(176),"C];"])
plot([0,TDTIMESTAMP(Datasize)],[setp(1),setp(1)],["g-- ;Setpoint
[",char(176),"C];"])
legend boxoff
legend ("location", "northeastoutside")
xlabel ("Time [min]")
xlim([0,max(TDTIMESTAMP)])

subplot(2,1,2)
hold on
plot(TDTIMESTAMP,input,['m ;MPC Control Inlet [",char(176),"C";"])
plot(TDTIMESTAMP,TDSUPIN,['k ;PID Control Inlet [",char(176),"C];"])
legend boxoff
legend ("location", "northeastoutside")
xlabel ("Time [min]")
xlim([0,max(TDTIMESTAMP)])
print(H, ["MPCCLResulto",int2str(1)], "-demf",["-
S",int2str(Wi),",",int2str(Ln),"])
print(H, ["MPCCLResulto",int2str(1)], "-dpdf",["-
S",int2str(Wi),",",int2str(Ln),"])

[IMPCmax,IWMPmax] = max(outcon(initsetT:Datasize));
[IMPCmin,IWMPmin] = min(outcon(initsetT:Datasize));

[Imax,IWmax] = max(TDBLROUT(initsetT:Datasize));
[Imin,IWmin] = min(TDBLROUT(initsetT:Datasize));

[I2MPCmax,I2WMPmax] = max(input(initsetT:Datasize));
[I2MPCmin,I2WMPmin] = min(input(initsetT:Datasize));

[I2max,I2Wmax] = max(TDSUPIN(initsetT:Datasize));
[I2min,I2Wmin] = min(TDSUPIN(initsetT:Datasize));

PISTD = std((TDBLROUT-setp(1))(initsetT:Datasize));
MPCSTD = std((outcon-setp(1))(initsetT:Datasize));
PIMN = mean((TDBLROUT-setp(1))(initsetT:Datasize));
MPCMN = mean((outcon-setp(1))(initsetT:Datasize));

stats1 = [MPCSTD,MPCMN,IMPCmax,IMPCmin,IMPCmax-IMPCmin];
summ = summ+[MPCSTD,MPCMN,IMPCmax,IMPCmin,IMPCmax-IMPCmin];
savestats = [savestats;stats1];

```

Appendix B Simulation Code

```
endfor
summ/38
save -text stats2 savestats
```

Appendix B.5 Fuzzy Controller Performance

```
load -binary saved2

sys1= sysDSS;
Cm = sys1.c;
Am = sys1.a;
Bm = sys1.b;
[m1,n1]=size(Cm);
A = [Am,linspace(0,0,n1)';Cm*Am,1];
B = [Bm;Cm*Bm];
C = [linspace(0,0,n1),1];
D = [0,0,0,0];
sys1 =
dss(A,B,C,D,[],15,'STNAME',{'dH2','dH1','Hout'},'INNAME',{'Hin','Fire','Firedot','Pdot'},
,'OUTNAME','Hout');
m1=1;

sys2= sysDSS;
sys2.T = 90;
sys2 = d2d(sys2,15);
Cm = sys2.c;
Am = sys2.a;
Bm = sys2.b;
[m1,n1]=size(Cm);
A = [Am,linspace(0,0,n1)';Cm*Am,1];
B = [Bm;Cm*Bm];
C = [linspace(0,0,n1),1];
D = [0,0,0,0];
sys2 =
dss(A,B,C,D,[],15,'STNAME',{'dH2','dH1','Hout'},'INNAME',{'Hin','Fire','Firedot','Pdot'},
,'OUTNAME','Hout');
m2=1;
racc=r;

load -binary ctrlparam

offs = zeros(50,1);
setp = ones(50,1)*505;
statof = ones(50,1)*500;

savstats = [];

for itr = 1:1
    itr
    sum = zeros(1,5);

    list = ls ("comparetoparamstestnn*", "/A:-D", "/B", "/O:-N")
    load ("-binary", strsplit (list){1})

    gn1 = tweak1;
    gn2 = tweak2;
    gn3 = tweak3;
    gn4 = tweak4;
    fflush(stdout);
    g = [1:38];
```

Appendix B Simulation Code

```

for l = g

    See Appendix B.3. Identical inner loop code.

    Wi = 900;
    Ln = 450;
    offset = offs(l);
    initsetT = 1;

    while (TDTIMESTAMP(initsetT)<statof(l))
        initsetT = initsetT+1;
    endwhile

    input = arrayfun(@(x,y) XSteam("T_ph",x,y),TDSTMPR.*10,inputh/1000);

    TDTIMESTAMP = TDTIMESTAMP./60 - offset;

    H = figure('Position',[50,50,Wi,Ln]);
    subplot(2,1,1)
    hold on
    plot(TDTIMESTAMP,outcon,["b ;TSK Model Response [",char(176),"C];"])
    plot(TDTIMESTAMP,TDBLR0UT,["r ;PID Actual Response [",char(176),"C];"])
    plot([0,TDTIMESTAMP(Datasize)],[setp(1),setp(1)],["g-- ;Setpoint
[",char(176),"C];"])
    legend boxoff
    legend ("location", "northeastoutside")
    xlabel ("Time [min]")
    xlim([0,max(TDTIMESTAMP)])

    subplot(2,1,2)
    hold on
    plot(TDTIMESTAMP,input,["m ;TSK Control Inlet [",char(176),"C]          ;"])
    plot(TDTIMESTAMP,TDSUPIN,["k ;PID Control Inlet [",char(176),"C];"])
    legend boxoff
    legend ("location", "northeastoutside")
    xlabel ("Time [min]")
    xlim([0,max(TDTIMESTAMP)])
    print(H, ["TSKCLResultTest",int2str(l)], "-demf",["-
S",int2str(Wi),",",int2str(Ln),""])
    print(H, ["TSKCLResultTest",int2str(l)], "-dpdf",["-
S",int2str(Wi),",",int2str(Ln),""])

endfor
endfor

```